Fretting and Plain Fatigue Competition Mechanism and Prediction in Spline Shaft-Hub Connection

Dissertation

to be awarded the degree

Doctor of Engineering (Dr.-Ing.)

Submitted by

M.Sc. Longjiang Shen

from Liuyang, China

approved by the Faculty of

Mathematic/Computer Science and Mechanical Engineering

Clausthal University of Technology

Date of oral examination

5 March 2012

Bibliografische Information Der Deutschen Bibliothek
Die Deutsche Bibliothek verzeichnet diese Publikation in der Deutschen Nationalbibliografie; detaillierte bibliografische Daten sind im Internet über http://dnb.ddb.de abrufbar.

Vorsitzender der Promotionskommission: Prof. Dr.-Ing. Norbert Müller

Hauptberichterstatter: Prof. Dr.-Ing. Armin Lohrengel

Mitberichterstatter: Prof. Dr.-Ing. Alfons Esderts

D104

Telemannstraße 1 · 38678 Clausthal-Zellerfeld
www.papierflieger-verlag.de

1. Auflage, 2012

ISBN 978-3-86948-206-4

Abstract

The dynamic loaded spline shaft-connections that without macro relative movement between shaft and hub is exposed to the danger of fretting fatigue in the contact zone of teeth flank and the danger of plain fatigue at the teeth fillet out of contact zone at the same time. It makes great sense to the fatigue life prediction and structure optimization that which mechanism dominates the failure of it in these fretting and plain fatigue co-existed situations such as spline shaft-hub connection and railway axles.

A fretting and plain fatigue unified prediction model is suggested in this study. It inherited the successful characteristic of existing pure fretting fatigue prediction FFDP/exFFDP models and pure plain fatigue prediction SWT/FS models, developed a fretting and plain fatigue unified prediction parameter K_{FDP}SWT and K_{FDP}FS. Which applied to tensile mode crack dominated and shear mode crack dominated fretting and plain fatigue respectively. Considering different microscopic crack mechanism and choose corresponding macro prediction model will improve the accuracy of fretting and plain fatigue prediction. Outside of the contact interface, above parameters will degenerate to the pure plain fatigue prediction parameter SWT and FS. The failure of involute spline shaft teeth predicted by this model is plain fatigue at teeth fillet dominated.

Corresponding to the modeling efforts implemented in the representative involute spline teeth, this study developed a fretting and plain fatigue test apparatus of spline teeth. Combined with a resonant fatigue test machine or a standard fatigue test machine, the fretting and plain fatigue behavior of spline teeth can be investigated more deeply and microscopically. The experimental results of the investigated DIN5480 involute spline teeth showed that the failure of it is plain fatigue at teeth fillet dominated, which is consistent with the location predicted by the newly suggested model above. The crack growth orientations at teeth fillet agree with the direction predicted by the SWT parameter. Compared to the crack initiation and propagation recorded by the resonant frequency, the crack initiation life predicted by the averaged SWT or FS within the characteristic length 0.2mm is acceptable.

To look for a better shaft-hub connection profile with better plain and fretting fatigue performance, an IMW complex cycloid profile is introduced in this study. The fretting and plain fatigue performances of the newly developed IMW profiles are evaluated and optimized using the unified prediction parameters. Following this method and referring to DIN5480 standard, the IMW profiles that with better fatigue performances can be standardized conveniently.

Keywords: Fretting fatigue, plain fatigue, competition mechanism, unified prediction model, spline shaft-hub connection, IMW complex cycloid profile

Acknowledgement

I would like to extend all my sincere thanks to all the people who once brought up me, educated me, supported me, and accompanied me.

Institute of Mechanical Engineering in Clausthal University of Technology opened the door for a Chinese student again, great thanks to Prof. Dr.-Ing. A. Lohrengel and Dr.-Ing. G. Schäfer, they offered me the opportunity to study in this famous institute. They are patient and magnanimous to a mischievous and anxious young Chinese and guide him to the right track step by step. Though the theme of my dissertation-fretting fatigue deviates a little bit from their original advice, they still supported my study. Their great knowledge and wisdom let me know the profound of German mechanical engineering science. Their finance support of my third year study in Germany, the finance support from International center of TU Clausthal as well as DAAD and the scholarship from China Scholarship Council are also greatly appreciated.

During the period of my master's study, Prof. Dr. Bingyan Jiang (Central South University of China) gave me some good training about how to do research independently and provided me exciting environment to do my research in the field of 'micro injection molding' in that time. My interest of research and ambition were also motivated in that time. It is also one of the most important reason that why I continue to pursue a PhD degree but not go back to work in Zhuzhou Electric Locomotive Co., Ltd as I originally planned. His guidance and support to me and my family are always appreciated. At the same time, the support and understand from Zhuzhou Electric Locomotive Co., Ltd and deputy general manager Mr. Zhou are also greatly appreciated.

I must also extend my thanks to all the other colleges in Institute of Machine Engineering. Despite of my bad language, they showed great understanding to me and are very friendly to me. Special thanks to our IT expert-Dipl.-Ing. H.-J. Jach-Reinke for his precious and timely technology support of computer and softwares. Special thanks to Dipl.-Ing. Radoslaw Kruk, Dipl.-Ing. Tobias Mänz, Dipl.-Ing. Miaomiao Leng, Dipl.-Ing. Eli Nsenga Biasompa, Dipl.-Ing.Daniel Thoden, Dipl.-Ing.Martina Wächter, Dipl.-Ing.Rico Schmelter, Dipl.-Ing. Joachim Langenbach, Dr.-Ing. Andreas Miehe and Dr.-Ing. W.Rolshofen for their kindly help and encouragement, and I'm always greatly benefited from the discussions and talks with them. Great thanks to Mr. Schumann, J. and M.E. Yang, Shan in Institute of Material Sciences and Engineering for their help in metallographic analysis. I'd also like to thank the colleges of the workshop for their high professional spirit showed in the manufacture of my experiment apparatus.

Last but not least, I'd like to extend my thanks and apology to my kind grandmother, hardworking mother and father for their always support and understanding. Special thanks to my sweet wife Lou, Jing for her loving support and understanding.

Contents

Abstract ....

Acknowledgement ....

Contents .... **I**

List of Figures .... **III**

List of Symbols and Abbreviations .... **IX**

1 Introduction **1**
1.1 Fretting/plain fatigue competition in industry applications 1
1.2 Fretting fatigue prediction models 6
1.3 Fretting/plain fatigue crack initiation mechanism 13
1.4 Aims of this research 16

2 Potential location of fatigue crack in spline shaft-hub connections **18**
2.1 Introduction 18
2.2 FE simulation of spline shaft-hub connections under dynamic torque 20
2.2.1 FE model of spline shaft-hub connections 20
2.2.2 Post processing of FE analysis results 24
2.2.3 Numerical simulation results and analysis 25
2.3 Potential fretting fatigue locations predicted by FFDP 33
2.4 Potential plain fatigue location predicted by SWT parameter 37
2.5 Conclusion 41

3 Fretting and plain fatigue unified prediction model **42**
3.1 Introduction 42
3.2 FE model of the representative tooth pair and results post processing 43
3.3 Fretting/plain fatigue unified prediction model 49
3.3.1 Two fretting fatigue crack initiation processes 49
3.3.2 Fretting/plain fatigue unified prediction parameter and location of crack initiation 52
3.3.3 Crack orientation prediction 63
3.3.4 Fatigue life prediction 67
3.4 Conclusion 72

4 Development of fretting/plain fatigue test apparatus **74**
4.1 Introduction 74
4.2 Concept of the representative specimen test apparatus 74

4.3 In situ detection of fretting/plain fatigue cracks 76
4.4 Structure design of the test apparatus 80
4.5 Conclusion 83

5 Fatigue experiments 85
5.1 Introduction 85
5.2 Experiment design and specimen preparation 85
5.3 Analysis of experimental results 89
5.4 Conclusion 95

6 Palliative measurements by structure optimization 96
6.1 Introduction 96
6.2 Optimization efforts in involute spline teeth 98
6.3 Complex cycloid profiles 101
6.3.1 Complex cycloid profile developed by Ziaei, M. 101
6.3.2 IMW complex cycloid profiles 112
6.4 Conclusion 119

7 Conclusion 121
7.1 Summary 121
7.2 Future works 122

Bibliography 124

Appendix A: Details of different fretting fatigue prediction models 130

Appendix B: Standardization of IMW01 profile 137

Curriculum Vitae 141

List of Figures

Figure 1-1: Fretting fatigue crack in dovetail joint of gas turbine. After http://mms2.ensmp.fr/tribo_paris/practic/Fretting.pdf 1
Figure 1-2: Possible locations of fatigue crack initiation in railway axle [Ekb-04] 2
Figure 1-3: Fatigue fracture of spline teeth [Die-93].. 2
Figure 1-4: Fretting mark on the teeth flank near the start of shaft-hub connection [Hua-07].. 3
Figure 1-5: Typical fatigue cracks in representative specimen of spline teeth: (a) bending-induced fillet cracking on an externally splined tooth, (b) a long fretting-induced crack at an internally-splined teeth flank and (c) a short fretting-induced crack on an internally-splined teeth flank. [HYD-05].................. 3
Figure 1-6: Spline cross section showing common failure locations [Mad-08b].............. 4
Figure 1-7: Competition of fretting fatigue near contact edge and plain fatigue at fillet in practical applications 4
Figure 1-8: Fretting fatigue cracks near the start of engagement along axial direction of involute spline shaft-hub connection [Din-07] 5
Figure 1-9: Plain fatigue cracks initiated close to end of engagement along axial direction of involute spline shaft-hub connection [Sum-04] 6
Figure 1-10: Different spline shaft design in axial direction, (a) with spline run-out; (b) with shaft shoulder: after [FVA-08].. 6
Figure 1-11: Progression of the damage criteria at standardized P3G-connections [Gro-07] 7
Figure 1-12: Stress and fretting parameters along the key groove radius edge [Vid-07]. 8
Figure 1-13: Axial distributions of the modified SWT parameters in comparison with those of SWT parameters for (a) Test 1 and (b) Test 2,(a1-spline axial direction contact width ; a2 -spline tooth-flank or involute profile direction contact width) [Din-07] 10
Figure 1-14: MSSR parameter vs. Fatigue life relationships for fretting fatigue from five-pad geometries and plain fatigue [Nam-02]... 11
Figure 1-15: Development history of frictional energy and critical-plane fatigue based models 12
Figure 1-16: Schematic of stage I (shear mode) and stage II (tensile mode) microscopic fatigue crack growth [Lee-05b]. 13
Figure 1-17: Schematic of the various stages of fretting fatigue crack growth [Lau-01] 14
Figure 1-18: Subsurface SEM image of Ti–6Al–4V fretting fatigue specimen at trailing edge region of slip [Goh-01]... 14
Figure 1-19: Optical micrograph of the cross-section below the 2024T351 (aluminum copper magnesium alloy) fretting fatigue specimen [Pro-05]........... 14
Figure 1-20: Primary crack growth path in specimen tested with 101.6 mm cylindrical pad (Material: Ti–6Al–4V). [LYK-01] 14
Figure 1-21: SEM micrograph of crack initiation angle at the pad contact edge (Material: 7075-T6 aluminium alloy) [Jac-07] 14
Figure 1-22: Different scenarios of fatigue crack growth [Sch-09] 15
Figure 1-23: Cross section of fractured specimen [Lee-05] 16

Figure 1-24: Fatigue parameter evaluation [Lei-07] 16

Figure 2-1: Typical relationship between fatigue life and wear rate as a function of slip amplitude (after Vingsbo and Soderberg [Vin-88]). 18

Figure 2-2: Fretting regimes and their corresponding fretting cycles (after Gallego, L. etc [Gal-06]). 18

Figure 2-3: Cyclic symmetry FE model of spline SHC under dynamic torque 20

Figure 2-4: Coulomb friction model in ANSYS ($\tau_{\lim}$ = limit frictional stress, $\tau_{\max}$ = maximum equivalent frictional stress, μ = coefficient of friction, p=contact normal pressure, b=contact cohesion) [ANS-10] 21

Figure 2-5: Coefficient of friction in fretting tests of a round-against-flat configuration Curve A: without added lubrication; curves B and D: upper and lower bounds for light lubrication; and curve C: typical for light lubrication. Contact load = 500 N, stroke = 50μm, Material: CrMoV alloy steel [Rat-04] 22

Figure 2-6: Time history of dynamic torque 23

Figure 2-7: Change of the angular deflection with the increase of torque [Wes-96] 23

Figure 2-8: Loading sequence applied to the FE model 24

Figure 2-9: Map of FE analysis results from the curved flank surface to a plane 25

Figure 2-10: Distribution of contact pressure under load T_o=560Nm 26

Figure 2-11: Distribution of contact pressure under load T_o=1680Nm 26

Figure 2-12: Distribution of contact pressure under load T_o=2800Nm 27

Figure 2-13: Distribution of total sliding distance on flank surface in a load cycle (from time step 5 to 9), T_o=560Nm, R=0.2 28

Figure 2-14: Distribution of total sliding distance on flank surface in a load cycle (from time step 5 to 9), T_o=1680Nm, R=0.2 29

Figure 2-15: Distribution of total sliding distance on flank surface in a load cycle (from time step 5 to 9), T_o=2800Nm, R=0.8 30

Figure 2-16: Distribution of total sliding distance on flank surface in a load cycle (from time step 5 to 9), T_o=2800Nm, R=0.2 31

Figure 2-17: Distribution of maximal principal stress on flank surface under load T_o=2800Nm 32

Figure 2-18: Distribution of Von-mises stress on flank surface under load T_o=2800Nm 32

Figure 2-19: Definition of local tangential stress on the contact surface of spline flank 34

Figure 2-20: Distribution of FFDP on teeth flank (T_o=560Nm, R=0.2) 34

Figure 2-21: Distribution of FFDP on teeth flank (T_o=1680Nm, R=0.2) 35

Figure 2-22: Distribution of FFDP on teeth flank (T_o=2800Nm, R=0.2) 35

Figure 2-23: Distribution of FFDP on teeth flank (T_o=2800Nm, R=0.8) 36

Figure 2-24: Fretting mark on the teeth flank near the start of shaft-hub connection [Hua-07] 37

Figure 2-25: Position of point P on a unit sphere, orientation of unit normal n is defined by angles θ_v and θ_h [Sum-04] 38

Figure 2-26: Distribution of SWT on teeth flank (T_o=2800Nm, R=0.8) 39

Figure 2-27: Distribution of SWT on teeth flank (T_o=2800Nm, R=0.2) 40

Figure 2-28: Fatigue facture of spline teeth in involute spline shaft-hub connection [Die-93] 40

Figure 3-1: Maximal loaded slice extracted from one tooth pair of involute spline shaft-hub connection 43

Figure 3-2: FE model of the representative teeth pair 44
Figure 3-3: Calculation of equivalent load F for quasi-2D representative teeth pair 45
Figure 3-4: Global and local coordinate system of the involute spline teeth 47
Figure 3-5: Distribution of maximal principal stress and Von-mises stress (normalized by dividing respective maximal value) along shaft teeth flank, F=8667.5N (5183.3+3484.2) 48
Figure 3-6: Distribution of normal stresses in tangential and normal direction of shaft teeth flank (normalized) along shaft teeth flank, F=8667.5N 49
Figure 3-7: Assumptions of fretting fatigue crack initiation situation 50
Figure 3-8: Change in the quasi-COF (Q/P) with increasing applied relative slip range [Jin-04] 51
Figure 3-9: Distribution of σ_t, $(\tau\delta)$ and $(\sigma_t\tau\delta)$ along the interface of blade/disk contact of a dovetail joint under 40KN biaxial load [Lin-97]. 53
Figure 3-10: Schematic configuration of fretting fatigue tests [Ara-04]. 54
Figure 3-11: Distribution of FDP and FFDP (normalized by dividing respective maximal values) along shaft teeth flank, F_m=5183.3N; R_F=0.2. 55
Figure 3-12: Relative fretting damage related to sliding distance and contact pressure [Old-01] 57
Figure 3-13: Fretting damage factor related to sliding distance and contact pressure [Old-01] 58
Figure 3-14: Modeling strategy of the fretting/plain fatigue unified prediction parameter 59
Figure 3-15: Distribution of SWT, K_{FDP}SWT parameter along shaft teeth flank (normalized by dividing respective maximal values), F_m=1040.9N; R_F=0.2. 60
Figure 3-16: Distribution of SWT, K_{FDP}SWT parameter along shaft teeth flank (normalized by dividing respective maximal values), F_m=3113.5N; R_F=0.2. 60
Figure 3-17: Distribution of SWT, K_{FDP}SWT parameter along shaft teeth flank (normalized by dividing respective maximal values), F_m=5183.3N; R_F=0.2. 61
Figure 3-18: Distribution of FS, K_{FDP}FS parameter along shaft teeth flank (normalized by dividing respective maximal values), F_m=1040.9N; R_F=0.2. 61
Figure 3-19: Distribution of FS, K_{FDP}FS parameter along shaft teeth flank (normalized by dividing respective maximal values), F_m=3113.5N; R_F=0.2. 62
Figure 3-20: Distribution of FS, K_{FDP}FS parameter along shaft teeth flank (normalized by dividing respective maximal values), F_m=5183.3N; R_F=0.2. 62
Figure 3-21: Definition of crack orientation 63
Figure 3-22: Crack orientation predicted by SWT parameter, F_m=5183.3N; R_F=0.2. 65
Figure 3-23: Crack orientation predicted by FS parameter, F_m=1040.9N; R_F=0.2. 65
Figure 3-24: Crack orientation predicted by FS parameter, F_m=3113.5N; R_F=0.2. 66
Figure 3-25: Crack orientation predicted by FS parameter, F_m=5183.3N; R_F=0.2. 66
Figure 3-26: Characteristic length l_c along crack orientation 67
Figure 3-27: FS-N_f diagram of 25MoCr4 according to equation (3-27) 72
Figure 4-1: Concept of the representative teeth pair test apparatus 74
Figure 4-2: Force analysis of the load arm (together with the shaft teeth specimen fixed with it) 76
Figure 4-3: In situ detection of fretting fatigue crack using surface acoustic wave in bolt jointed aluminum alloy plates [Wag-09] 77
Figure 4-4: Mechanical schematic diagram of a two mass resonant testing machine 78

Figure 4-5: Mechanical schematic diagram of spline shaft-hub connection [Dietz-78] 79
Figure 4-6: Global stiffness and local stiffness model of representative teeth pair specimen under pure torque..... 80
Figure 4-7: Solid model of the representative teeth pair test apparatus 81
Figure 4-8: Alignment of shaft teeth and hub teeth specimens..... 82
Figure 4-9: Assembly of the fretting/plain fatigue test apparatus and the resonant fatigue test machine 83
Figure 5-1: Dimension of representative specimens cut from spline shaft-hub connection DIN5480 45x2x21 86
Figure 5-2: Photograph of the representative teeth pair 87
Figure 5-3: Microstructure of the surface hardened shaft teeth specimen..... 87
Figure 5-4: Microstructures of induction surface hardened carbon steel and alloy steel gears [Can-08] 88
Figure 5-5: Microstructure of the surface coated spline hub teeth specimen..... 88
Figure 5-6: Resonance frequency history and crack growth (normalized shaft teeth+normalized hub teeth, F_m=5215.2, F_a=3506.3)..... 90
Figure 5-7: Crack at the fillet of shaft teeth specimen (normalized shaft teeth+normalized hub teeth, F_m=5215.2, F_a=3506.3)..... 90
Figure 5-8: Fretted flank surface of hub teeth (normalized shaft teeth+normalized hub teeth, F_m=5215.2, F_a=3506.3)..... 91
Figure 5-9: Resonance frequency history and crack initiation (surface hardened shaft teeth+normalized hub teeth, F_m=8682, F_a=5836) 92
Figure 5-10: Crack at the fillet of shaft teeth specimen (surface hardened shaft teeth+normalized hub teeth, F_m=5215.2, F_a=3506.3)..... 93
Figure 5-11: Fretted flank surface of hub teeth (surface hardened shaft teeth+normalized hub teeth, F_m=8682N, F_a=5836N)..... 93
Figure 5-12: Crack near the contact edge out of contact zone in shaft teeth specimen (surface hardened shaft teeth+normalized hub teeth, F_m=10452, F_a=6968)..... 94
Figure 6-1: Fretting fatigue crack in P3G polygon shaft-hub connection under dynamic torsion, (a) fretting fatigue cracks in P3G shaft with different profile shapes (b) Angular ranges of the initial crack location at standardized P3G shaft. After [Gro-07] 97
Figure 6-2: Fretting fatigue fracture of P4C polygon shaft-hub connection under dynamic torsion, (a) fretting fatigue fractured P4C shaft; (b) schematic diagram of the fretting fatigue crack initiation location. After [Win-01]..... 98
Figure 6-3: Distribution of contact pressure (normalized by dividing respective maximal values) along teeth flank with different fillet and chamfer structure, $F=F_m+F_a$=8667.5N. 99
Figure 6-4: Distribution of K_{FDP}SWT parameter (normalized by dividing respective maximal values) along the flank of spline teeth with different fillet radius, F_m=5183.3N; R_F=0.2. 100
Figure 6-5: Distribution of K_{FDP}FS parameter (normalized by dividing respective maximal values) along the flank of spline teeth with different fillet radius, F_m=5183.3N; R_F=0.2. 100
Figure 6-6: Basic parameters of epitrochoid 102
Figure 6-7: Basic parameters of a complex epitrochoid (T00) 102

Figure 6-8: Four different T00 type profiles referred to DIN5480 45x2x21 (r_{f1}=20.2, r_{a1}=22.3, $r_m = \left(r_{a1} + r_{f1}\right)/2$ =21.25) 104

Figure 6-9: FE model of a complex cycloid profile representative teeth pair 105

Figure 6-10: Distribution of maximal principal stress and Von-mises stress along teeth flank of T00-A (normalized by dividing respective maximal value), F=8667.5N 106

Figure 6-11: Distribution of normal stresses in tangential and normal direction of teeth flank T00-A (normalized by dividing respective maximal value), F=8667.5N 107

Figure 6-12 Distribution of SWT and K_{FDP}SWT parameter along teeth flank of T00-A (refer to DIN5480 45x2x21), F_m=5183.3N; R_F=0.2. 108

Figure 6-13: Distribution of FS and K_{FDP}FS parameter along teeth flank of T00-A (refer to DIN5480 45x2x21), F_m=5183.3N; R_F=0.2. 108

Figure 6-14: Distribution of SWT and K_{FDP}SWT parameter along teeth flank of T00-B (refer to DIN5480 45x2x21), F_m=5183.3N; R_F=0.2. 109

Figure 6-15: Distribution of FS and K_{FDP}FS parameter along teeth flank of T00-B (refer to DIN5480 45x2x21), F_m=5183.3N; R_F=0.2. 109

Figure 6-16: Distribution of SWT and K_{FDP}SWT parameter along teeth flank of T00-C (refer to DIN5480 45x2x21), F_m=5183.3N; R_F=0.2. 110

Figure 6-17: Distribution of FS and K_{FDP}FS parameter along teeth flank of T00-C (refer to DIN5480 45x2x21), F_m=5183.3N; R_F=0.2. 110

Figure 6-18: Distribution of SWT and K_{FDP}SWT parameter along teeth flank of T00-D (refer to DIN5480 45x2x21), F_m=5183.3N; R_F=0.2. 111

Figure 6-19: Distribution of FS and K_{FDP}FS parameter along teeth flank of T00-D (refer to DIN5480 45x2x21), F_m=5183.3N; R_F=0.2. 111

Figure 6-20: Four different IMW01 profiles referred to DIN5480 45x2x21 (r_{f1}=20.2, r_{a1}=22.3, $r_m = \left(r_{a1} + r_{f1}\right)/2$ =21.25) 113

Figure 6-21: Distribution of maximal principal stress and Von-mises stress along teeth flank of IMW01-A (normalized by dividing respective maximal value), F=8667.5N 114

Figure 6-22: Distribution of normal stresses in tangential and normal direction of teeth flank IMW01-A (normalized by dividing respective maximal value), F=8667.5N 115

Figure 6-23: Distribution of SWT and K_{FDP}SWT parameter along teeth flank of IMW01-A (refer to DIN5480 45x2x21), F_m=5183.3N; R_F=0.2. 115

Figure 6-24: Distribution of FS and K_{FDP}FS parameter along teeth flank of IMW01-A (refer to DIN5480 45x2x21), F_m=5183.3N; R_F=0.2. 116

Figure 6-25: Distribution of SWT and K_{FDP}SWT parameter along teeth flank of IMW01-B (refer to DIN5480 45x2x21), F_m=5183.3N; R_F=0.2. 116

Figure 6-26: Distribution of FS and K_{FDP}FS parameter along teeth flank of IMW01-B (refer to DIN5480 45x2x21), F_m=5183.3N; R_F=0.2. 117

Figure 6-27: Distribution of SWT and K_{FDP}SWT parameter along teeth flank of IMW01-C (refer to DIN5480 45x2x21), F_m=5183.3N; R_F=0.2. 117

Figure 6-28: Distribution of FS and K_{FDP}FS parameter along teeth flank of IMW01-C (refer to DIN5480 45x2x21), F_m=5183.3N; R_F=0.2. 118

Figure 6-29: Distribution of SWT and K_{FDP}SWT parameter along teeth flank of IMW01-D (refer to DIN5480 45x2x21), F_m=5183.3N; R_F=0.2. 118

Figure 6-30: Distribution of FS and $K_{FDP}FS$ parameter along teeth flank of IMW01-D (refer to DIN5480 45x2x21), F_m=5183.3N; R_F=0.2. 119

List of Symbols and Abbreviations

b	Thickness of the specimen (in axial direction)	mm
b	Fatigue strength exponent	-
b_0	Shear fatigue strength exponent	-
c	Fatigue ductility exponent	-
c_0	Shear fatigue ductility exponent	-
C_{em}	Equivalent stiffness of electro-magnet	N/mm
C_{pr}	Stiffness of preload spring	N/mm
C_{sp}	Stiffness of the specimen	N/mm
C_2	Stiffness of spring between workbench and basement	N/mm
C_{Lo}	Contact stiffness or ‘local stiffness’	N/mm
C_{Gs},	‘Global stiffness’ of shaft teeth	N/mm
C_{Gh}	‘Global stiffness’ of hub teeth	N/mm
e	eccentricity	mm
E	Young’s modulus	$\mathrm{N/mm^2}$
f_i	Frictional stress at node i on the teeth flank	$\mathrm{N/mm^2}$
F	Load force	N
F_{cx_i} F_{cy_i}	Reaction force resolved in horizontal and vertical direction	N
F_{bx}, F_{by}	Reaction force at the rotation center	N
G	Shear modulus	$\mathrm{N/mm^2}$
K_{FDP}	Relative fretting damage factor	-
k	Material constant in FS parameter	-
l_c	Characteristic length of crack initiation	mm
m_1, m_2	Excite mass and workbench mass of resonant fatigue test machine	Kg
n	Orientation of unit normal	-

N	Number of nodes along teeth flank	-
N_f	Number of cycles to initiate a crack	-
p	Contact normal pressure	N/mm^2
p_i	Contact pressure at node i on the teeth flank	N/mm^2
P	Position of point on a unit sphere	-
r	Radius of rolling circle	mm
r_b	Radius of base circle	mm
r_i	Radius vector at point i	mm
R	Radius of fixed circle	mm
R_i	Radius of node i on teeth flank	mm
R_τ	Shear stress ratio	-
s	Sliding distance	mm
s_1	Basic tooth thickness, circular	mm
T	Torque	Nm
T_o	Maximal torque	Nm
T_u	Minimal torque	Nm
T_m	Mean torque	Nm
x_l	Length of the contact element	mm
x_i , y_i	Axis of the local coordinate system	-
X, Y	Axis of the global coordinate system	-
W_{t1}	Section modulus of torsion	mm^3
x_1	Addendum coefficient	-
z	Number of teeth	-
α	Angle from the starting point to the tangential point of rolling circle and fixed circle	Degree, °
α_i	Pressure angle at node i on teeth flank	Degree, °

β_i	Angle between the normal direction of point i in teeth flank and vertical direction	Degree, °
$\gamma_f^{'}$	Shear fatigue ductility coefficient	-
γ_{xy}	Shear strain in local coordinate system	-
γ_{XY}	Shear strain in global coordinate system system	-
$\varepsilon_f^{'}$	Fatigue ductility coefficient	-
$\varepsilon_x, \varepsilon_y, \varepsilon_z$	Normal strain in local coordinate system	%
$\varepsilon_X, \varepsilon_Y, \varepsilon_Z$	Normal strain in global coordinate system	%
$\Delta\varepsilon$	Normal strain range	%
θ	Rotation angle of the eccentric bearing housing	Degree, °
θ_c	Crack initiation orientation angle	Degree, °
θ_{cc}	Critical angle of crack initiation	Degree, °
θ_{hc}	Crack initiation orientation angle in hub teeth flank	Degree, °
θ_i	Spread angle of involute	Degree, °
θ_{sc}	Crack initiation orientation angle in shaft teeth flank	Degree, °
θ_{sl}	Angle between micro sliding direction and teeth root-teeth tip direction	Degree, °
θ_v, θ_h	Angles to define the orientation of unit normal in sphere coordinate system	Degree, °
μ	Coefficient of friction	-
$\sigma_f^{'}$	Fatigue strength coefficient	N/mm^2
$\sigma_{\max}$	Maximal normal stress	N/mm^2
$\sigma_n^{\max}$	Maximal normal stress on the maximal shear strain plane	N/mm^2
$\sigma_{\tan}$	Tangential stress	N/mm^2
σ_Y^*	Yield stress of material	N/mm^2

σ_x , σ_y , σ_z	Normal stress in local coordinate system	N/mm^2
σ_X , σ_Y , σ_Z	Normal stress in global coordinate system	N/mm^2
τ_{fric}	Frictional stress	N/mm^2
$\tau_f^{'}$	Shear fatigue strength coefficient	N/mm^2
$\tau_{\lim}$	Limit frictional stress	N/mm^2
$\tau_{\max}^{*}$	Maximal equivalent frictional stress	N/mm^2
$\tau_{\max}$	Maximal shear stress	N/mm^2
$\tau_{\min}$	Minimal shear stress	N/mm^2
τ_{tn1}	Nominal shear stress under torque	N/mm^2
τ_{xy}	Shear stress in local coordinate system	N/mm^2
τ_{XY}	Shear stress in global coordinate system	N/mm^2
$\Delta\tau_{\max}$	Maximal shear stress range	N/mm^2
$\Delta\gamma_{\max}$	Maximal shear strain range	-
ϕ	Angle corresponding to half basic tooth thickness $s_1/2$	Degree, $^\circ$
ψ	Compensate coefficient	-
$\omega_{1,2}$	Natural angular frequency the mass-spring oscillator	rad/s

COF	Coefficient of friction
DIN	Deutsches Institut für Normung (German standards)
FEA	Finite Element Analysis
FEM	Finite Element Method
FFDP	Fretting-Fatigue-Damage-Parameter
FS	FATEMI-SOCIE (damage parameter)
HCF	High Cycle Fatigue
HB	Brinell hardness
HRC	Rockwell hardness

$K_{FDP}SWT$	Tensile crack mode fretting/plain fatigue unified prediction parameter
$K_{FDP}FS$	Shear crack mode fretting/plain fatigue unified prediction parameter
S-N	Stress-Cycle diagram (“Wöhler”-diagram)
SEQV	Von Mises equivalent stress
SHC	Shaft-hub connection
SIF	Stress intensity factor
SWT	SMITH-WATSON-TOPPER (damage parameter)

1 Introduction

1.1 Fretting/plain fatigue competition in industry applications

Fretting is a small oscillatory relative movement between contact surfaces that are subjected to vibration or cyclic stresses. It may leads to fretting wear or catastrophic fretting fatigue (FF) crack with the presence of cyclic bulk fatigue loading under one of the contact surfaces. Examples of FF failure can be found in gas turbine parts like dovetail joints, wire ropes, bolted connections, rivet structure, and (press, key, spline) shaft-hub connections, etc. Among them, intense efforts have been devoted to the fretting fatigue research of dovetail joint in gas turbine during the last 50 years because it is always a relevant failure mechanism of it, as shown in Figure 1-1.

Figure 1-1: Fretting fatigue crack in dovetail joint of gas turbine. After http://mms2.ensmp.fr/tribo_paris/practic/Fretting.pdf

Another one that most often concerned about the problem of fretting fatigue is railway axles. The difference is that sometimes occur plain fatigue crack out of the contact interface but not always fretting fatigue crack within the axle-wheel contact interface. Ekberg, A. reviewed possible fatigue crack initiation locations in a railway axle, as shown in Figure 1-2 [Ekb-04].

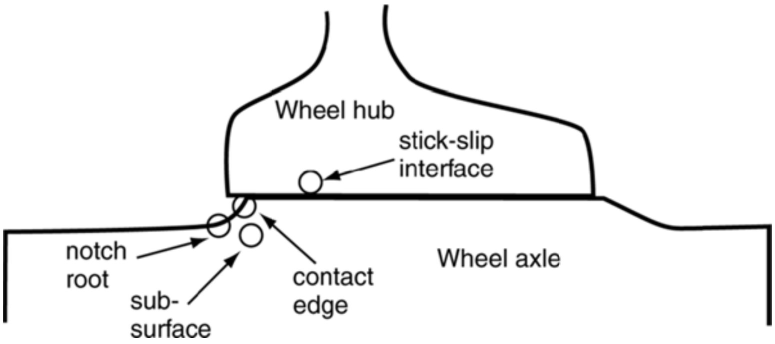

Figure 1-2: Possible locations of fatigue crack initiation in railway axle [Ekb-04]

For the spline shaft hub connections, the teeth fillet out of contact zone is exposed to the danger of plain fatigue due to dynamic bending moment, and the dynamic loaded spline shaft-connections in the running state that without macro relative movement between shaft and hub provide favorable conditions of fretting in the contact interface between teeth flank, and therefore is exposed to the danger of fretting fatigue as well as fretting wear. Figure 1-3 and Figure 1-4 show the fatigue fracture of spline teeth and fretting mark on the teeth flank respectively. Hyde, T.R. et al. investigated the fatigue behavior of involute spline teeth with a representative specimen test apparatus, different types of cracks occurred in their study, as shown in Figure 1-5 [HYD-05], Madge, J.J. also mentioned the coexist of plain fatigue failure and fretting fatigue failure in spline shaft-hub connection teeth, as shown in Figure 1-6 [Mad-08b].

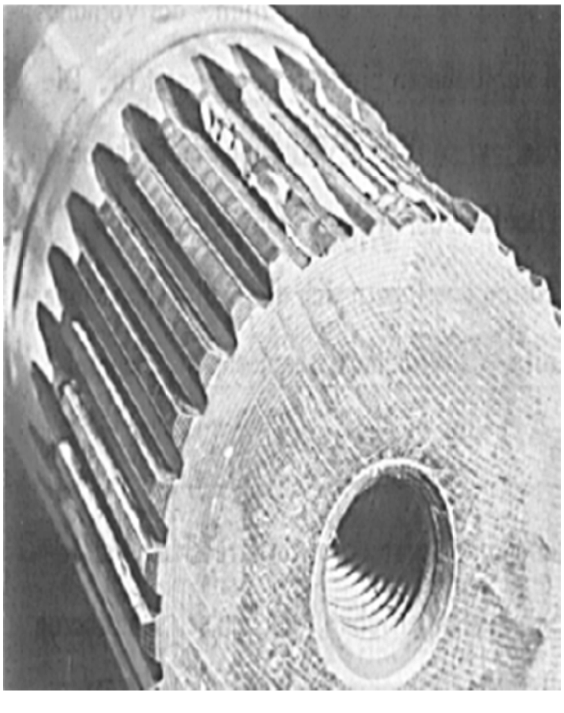

Figure 1-3: Fatigue fracture of spline teeth [Die-93]

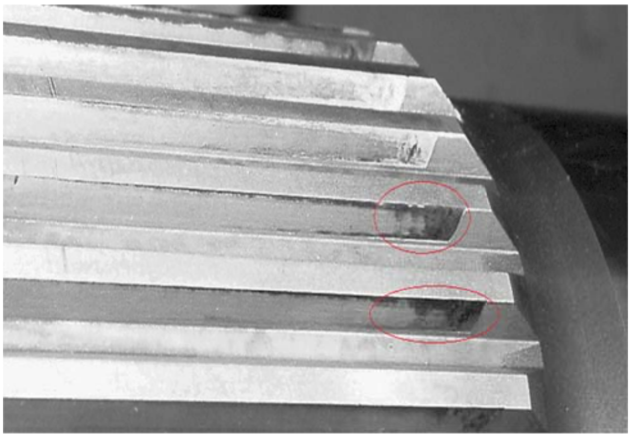

Figure 1-4: Fretting mark on the teeth flank near the start of shaft-hub connection [Hua-07]

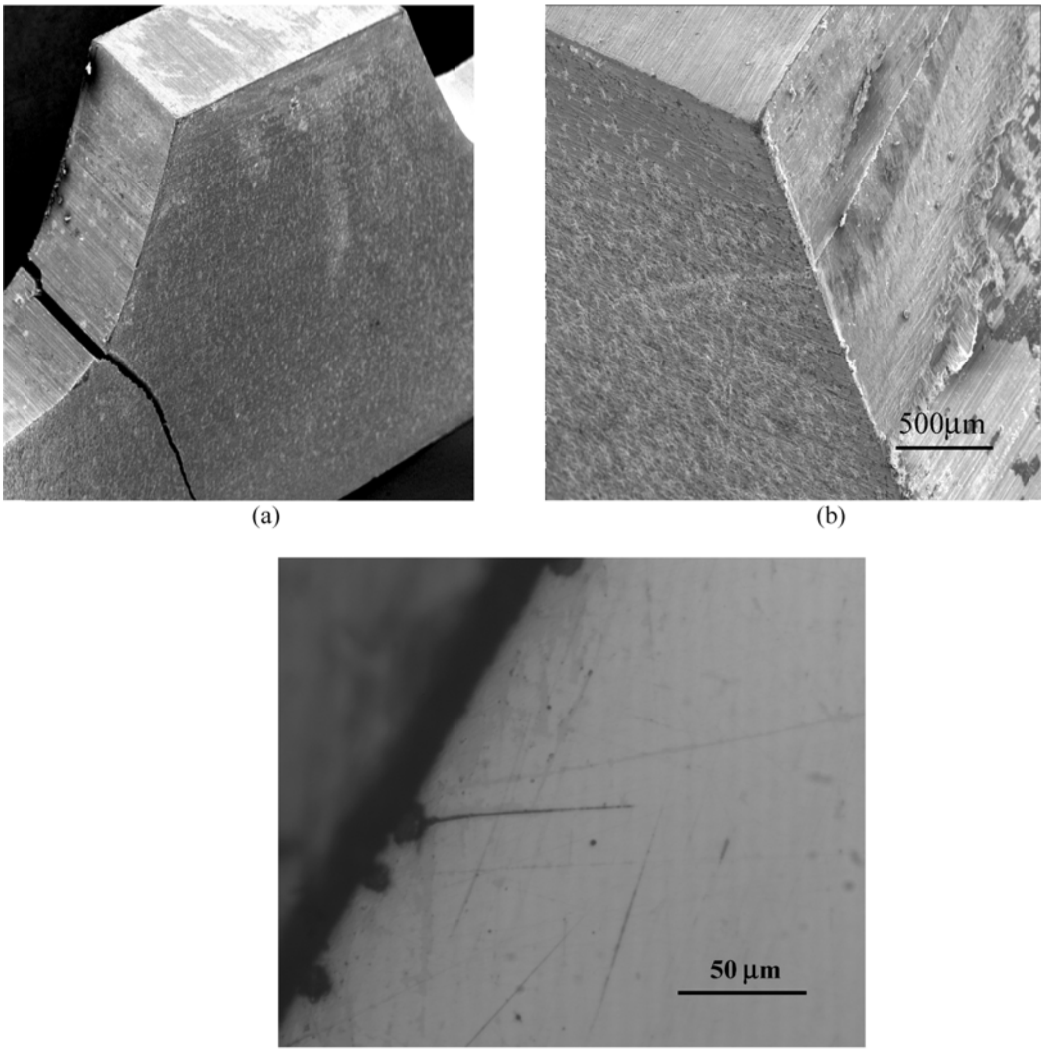

Figure 1-5: Typical fatigue cracks in representative specimen of spline teeth: (a) bending-induced fillet cracking on an externally splined tooth, (b) a long fretting-induced crack at an internally-splined teeth flank and (c) a short fretting-induced crack on an internally-splined teeth flank. [HYD-05]

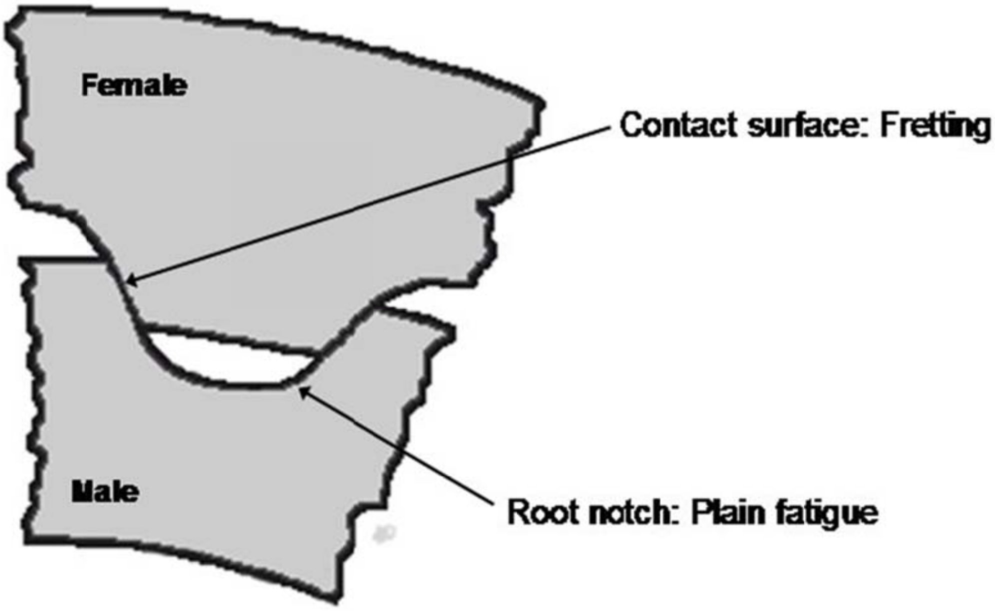

Figure 1-6: Spline cross section showing common failure locations [Mad-08b]

As a matter of fact, above discussed dovetail joint, railway axle (shrink fitted shaft-hub connections) and spline shaft-hub connection teeth shares a similar situation- coexist of fillet and contact edge in structure (as shown in Figure 1-7) and consequently coexist of plain fatigue and fretting fatigue/wear.

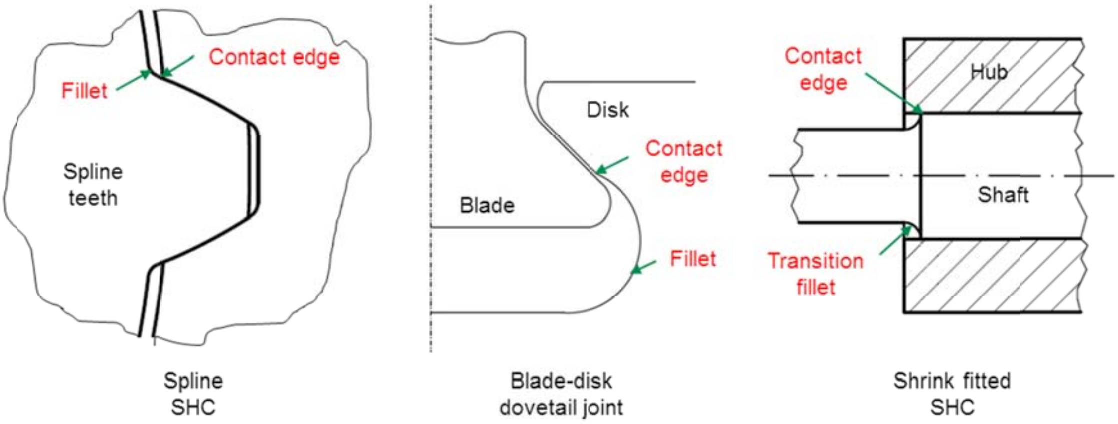

Figure 1-7: Competition of fretting fatigue near contact edge and plain fatigue at fillet in practical applications

It seems that the failure of dovetail joint in gas turbine is always fretting fatigue dominated, but which one leads to the failure of shrink fitted shaft and spline shaft-hub connection teeth depends on the ‘competition’ of plain fatigue at fillet and fretting fatigue/wear at contact edge. Obviously, our purpose is to improve the fatigue life of the whole assembly, that's to say minimize the danger of fretting fatigue near contact edge and plain fatigue in fillet at the same time. But, for example, in the spline shaft-hub connection teeth, the optimization of fillet are believed not only affect the plain fatigue at fillet itself but also affect the fretting behavior near neighbored contact edge. To find the perfect spline shape that with optimum over-all fatigue performance, a unified plain/fretting fatigue prediction parameter is an absolute essential.

It must be mentioned here that there's also competition of plain fatigue (in the spline run-out or the start of engagement out of contact zone) and fretting fatigue near the start of engagement along the axial direction of spline shaft-hub connections, as shown in Figure 1-8 and Figure 1-9. It can be optimized through axial profile modification, change the distance between the spline run-out and the start of engagement in axial direction, or even avoided by a shaft shoulder design, as shown in Figure 1-10. In this study, the fretting/plain fatigue in axial direction of spline shaft will not further discussed.

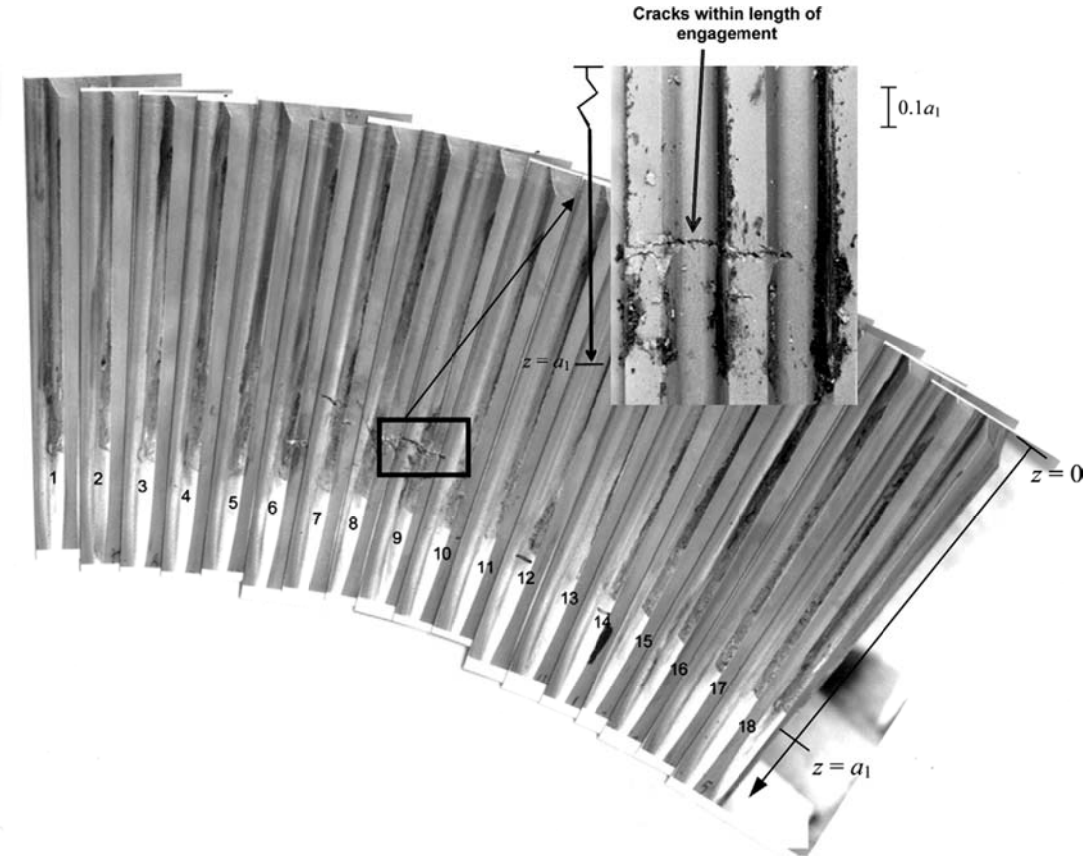

Figure 1-8: Fretting fatigue cracks near the start of engagement along axial direction of involute spline shaft-hub connection [Din-07]

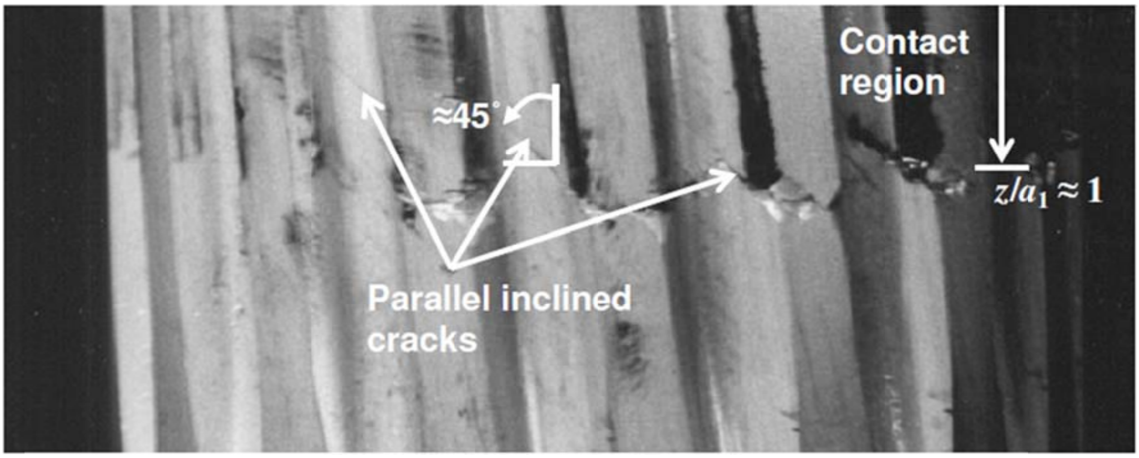

Figure 1-9: Plain fatigue cracks initiated close to end of engagement along axial direction of involute spline shaft-hub connection [Sum-04]

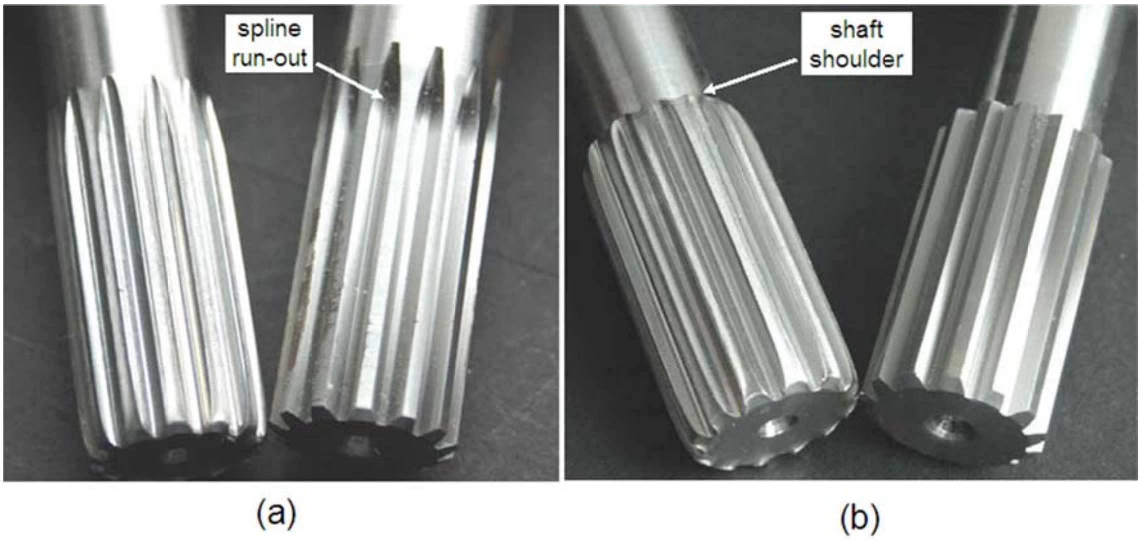

Figure 1-10: Different spline shaft design in axial direction, (a) with spline run-out; (b) with shaft shoulder: after [FVA-08]

1.2 Fretting fatigue prediction models

Numerous parameters have been developed to determine the onset of cracks in a component subjected to plain fatigue and it is too big a topic to discuss here. Actually, the fretting fatigue prediction parameters are in some sense an extension of plain fatigue prediction parameters, especially the group of critical-plane fatigue based models reviewed in following.

The first well known qualitative fretting fatigue prediction model is the fretting fatigue damage parameter (FFDP) introduced by Ruiz C. et al., which multiply the frictional work with the local maximal tangential stress empirically, and was originally used in fretting fatigue life assessment of dovetail joint [Rui-84, He-89]. Glöggler, C. applied Ruiz's FFDP model to predict the crack nucleation location in fretting contact of press fit shaft-hub connections (SHC) [Glö-03]; Großmann, C. studied fretting fatigue of polygon-connections (P3G) and the results showed the use of the FFDP gives the best results within FFDP, SWT, FS and SEQV criterion, as shown in Fig.1-11 [Gro-07].

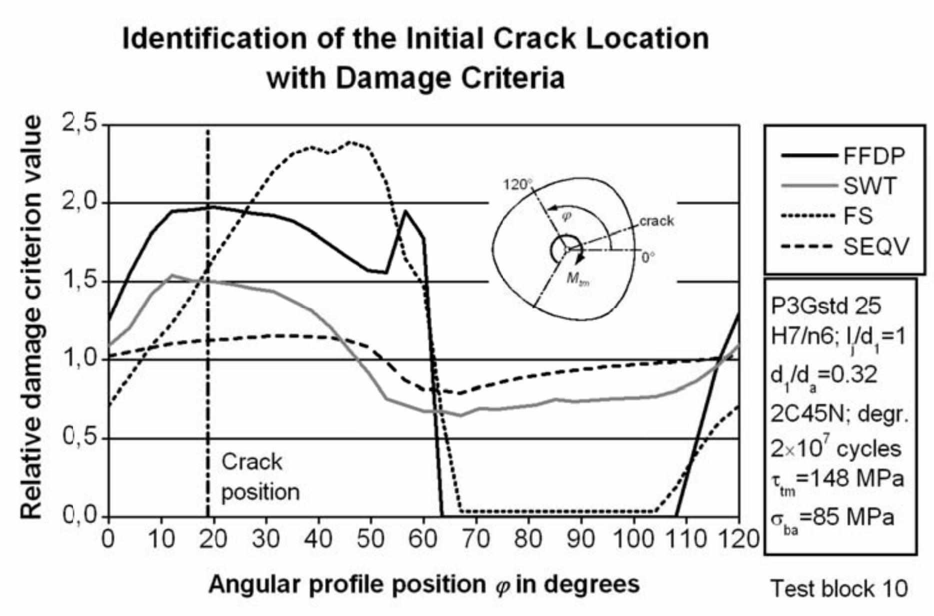

Figure 1-11: Progression of the damage criteria at standardized P3G-connections [Gro-07]

Based on FFDP model, Odendorf, U. introduced an empirical stress concentration factor β_{KC} by fitting experimental results between fretting damage, micro slip and contact pressure to replace the frictional work $\tau_{fric} \cdot s$ in FFDP model, developed an expanded FFDP (exFFDP) and argued that which have good correlation with experimental results in key SHC [Old-99, Old-01]. Ziaei, M. made two fundamental modifications of the Ruiz's FFDP, and developed a modified fatigue-fretting damage parameter (mFFDP), he implemented a physically correct integral description of the specific frictional work and replaced the tangential stress in the Ruiz's formulation with the maximal principal stress in mFFDP, which was able to predict the shaft failure location in finite-element analysis of polygon and shrink-fitted SHC [Zia-97, Zia-02]. After mFFDP model, Vidner and Leidich presented an enhanced Ruiz fretting fatigue damage parameter (eFFDP) model, resulting in a combined frictional energy-multiaxial fatigue eFFDP model, which was shown to successfully predict cracking sites in a key shaft–hub connection under combined torque and bending fatigue (as shown in Fig.1-12) and identified the fretting fatigue limit at 2×10^7 load cycles using FE simulation results and experimental data [Vid-07]. All the above mentioned models are originated from frictional energy based FFDP, which hypothesize that fretting fatigue is a surface damage phenomenon, and developed to the eFFDP model which take into account the effects of multiaxial stress status underlying the contact surface at last.

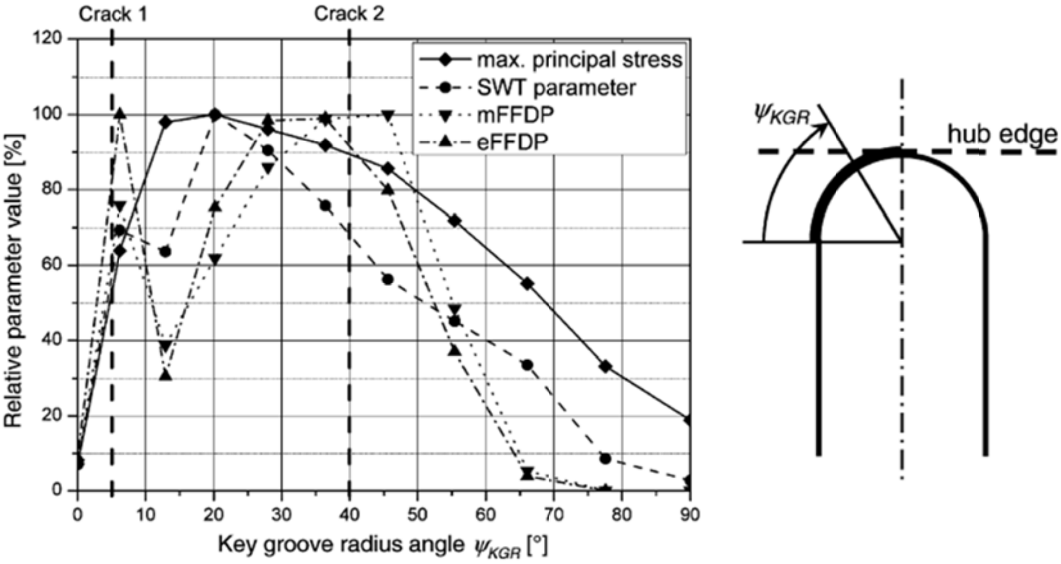

Figure 1-12: Stress and fretting parameters along the key groove radius edge [Vid-07].

Another group is based on the assumption that fretting fatigue is a multiaxial fatigue phenomenon from a stress raiser feature resulting from frictional contact. Lykins, C.D. and Mall, S. et al. evaluated abilities of the critical plane Smith-Watson-Topper (SWT) parameter (critical plane-Mode I crack), the Fatemi-Socie (FS) parameter (critical plane-Mode II crack) and other plain fatigue parameters to predict fretting fatigue crack initiation in titanium alloy Ti–6Al–4V using simple cylinder-on-flat contact configuration. The experimental and numerical results indicated that the maximum strain amplitude at the contact interface was an important parameter for fretting fatigue crack initiation and for Ti–6Al–4V that exposed to the fretting fatigue condition behaved in a manner similar to the plain fatigue condition [Lyk-00, Lyk-01]. These facts lead to the choice of critical plane plain fatigue parameter as fretting fatigue life prediction criterion.

Based on the critical plane SWT parameter, researchers in University of Oxford and University of Nottingham exert continuous efforts in solving the fretting fatigue problem of aero engine spline SHC via experiments as well as numerical simulations. Their fretting fatigue prediction modeling attempts started from Sum, W.S. et al.'s study, they use the critical plane SWT multiaxial fatigue criterion to predict fretting fatigue life of aero engine spline SHC, which has shown to be effective in crack location, orientation and lifetime prediction of spline SHC but insufficient to cause cracking either before spline root cracking or within a realistic number of operating cycles [Sum-04, Sum-05]. After that, Ding developed a modified SWT (mSWT) model, which includes the effect of micro slip. This mSWT model led to more accurate predictions of both life and fretting fatigue locations in spline SHC than SWT model and Ruiz's FFDP, as shown in Fig.1-13[Din-07]. To account for the effects of fretting wear, Madge etc. presented a wear-SWT model, and soon a Wear-Nucleation-Propagation model to address the interaction between crack nucleation, growth and wear effects: But, due to the gradual and progressive wear progress and complexity of crack propagation analysis, therefore computationally intensive, these model only implemented in the simple cylindrical pad-flat fretting contact configuration [Mad-07, Mad-08]. At the same time, Houghton, D. and WAVISH, P. M. et al. developed a simplified representative test rig, which mimics the multiaxial fretting conditions between spline teeth via biaxial loading of specially-designed bridge pads and a fatigue specimen, based on this multiaxial representative specimen, they presented a combined nucleation and propagation life prediction methodology along with a multiaxial critical-plane fatigue parameter for crack nucleation followed by crack growth prediction in the Paris regime using El Haddad small crack correction[Hou-09, Wav-09].

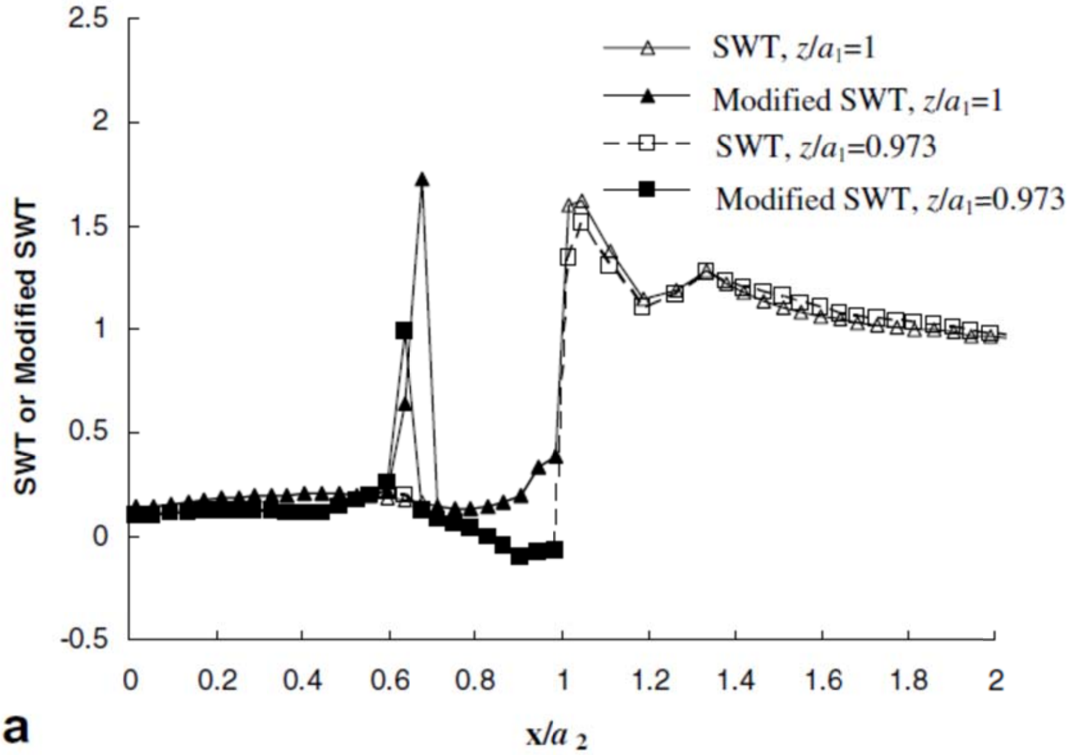

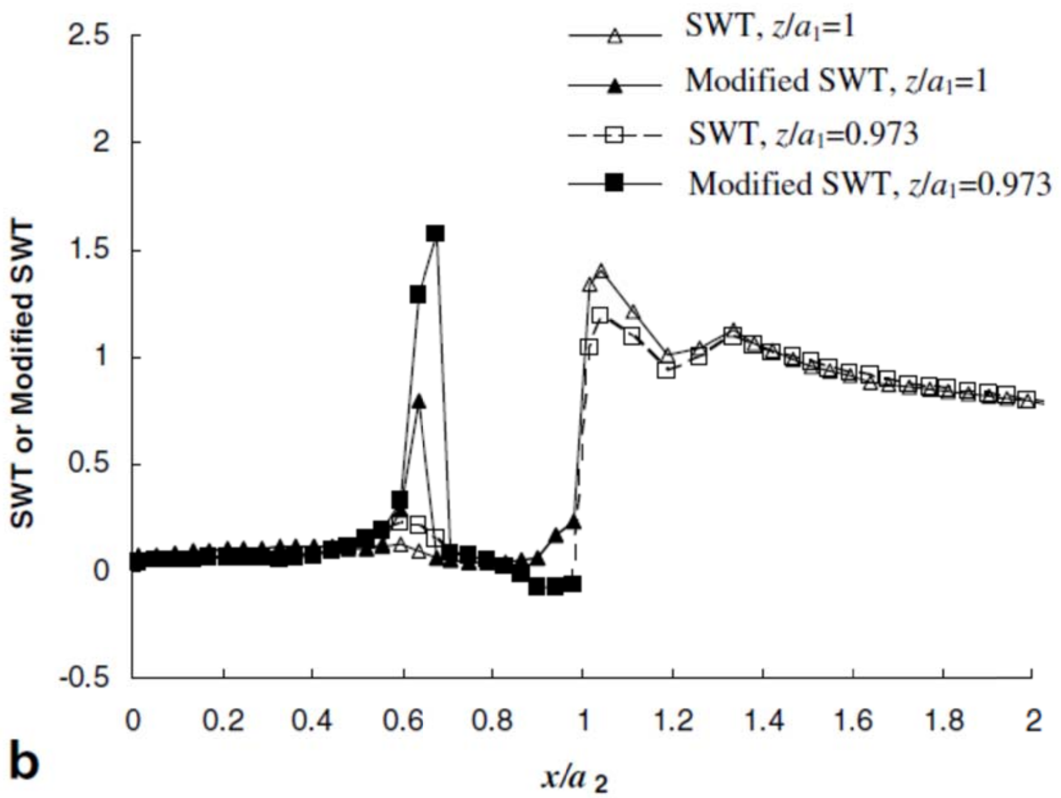

Figure 1-13: Axial distributions of the modified SWT parameters in comparison with those of SWT parameters for (a) Test 1 and (b) Test 2,(a1-spline axial direction contact width ; a2 -spline tooth-flank or involute profile direction contact width) [Din-07]

As a counterpart to the SWT parameter, the critical plane-Mode II crack based FS parameter is also evaluated in the prediction of fretting fatigue [Neu-00, Lyk-00, Lyk-01a]. With the shear mode crack assumption, researchers in Air Force Research Laboratory of Wright Patterson Air Force Base (USA) developed a shear stress range critical plane parameter (SSR) and soon after a modified shear stress range critical plane parameter (MSSR), Figure 1-14 shows the measured fretting fatigue life data as a function of MSSR parameter, for the tested titanium alloy Ti6Al4V, which shows better prediction results than SWT and FS parameters [Lyk-01b, Nam-02].

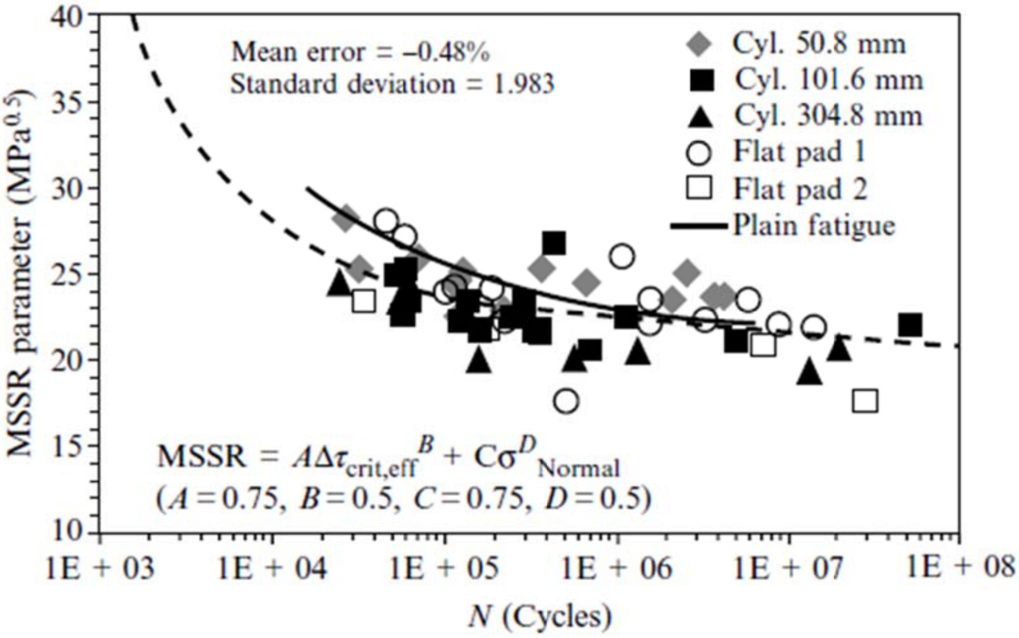

Figure 1-14: MSSR parameter vs. Fatigue life relationships for fretting fatigue from five-pad geometries and plain fatigue [Nam-02]

To make a clear map, the development history of main FF models mentioned above is shown in Figure 1-15, and the details of these models are collected in Appendix A. The above review of fretting fatigue researches showed that though the two fretting fatigue modeling group originated from frictional energy basis and critical-plane fatigue basis respectively, but they come to a common point that the fretting fatigue model should include the effects of slip (frictional energy) between contact surfaces and multiaxial stress state under contact surface at the same time. Combining energetic approach based on the work of Ruiz and critical plane multiaxial fatigue are expected leading to a development of more accurate general fretting fatigue assessment method. In the energetic approach and critical plane multiaxial fatigue approach combined fretting fatigue prediction model, there’s already plain fatigue prediction parameter. In order to be compatible to plain fatigue prediction, it should be able to degenerate to a pure plain fatigue prediction parameter outside of contact interface (or at fillet in this study).

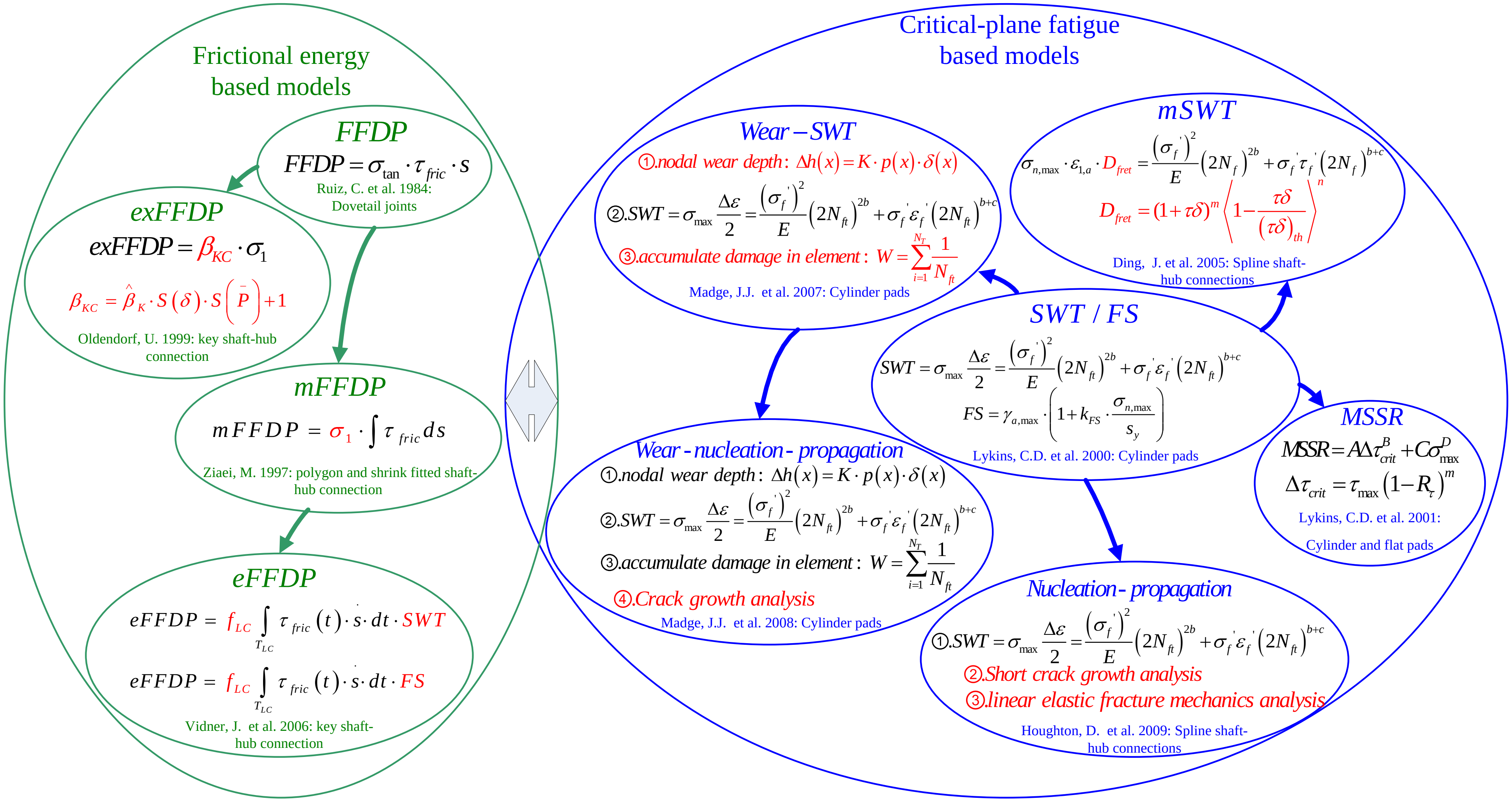

Figure 1-15: Development history of frictional energy and critical-plane fatigue based models

1.3 Fretting/plain fatigue crack initiation mechanism

In microscopic, the growth of plain fatigue crack initiated from surface is divided to the shear mode “stage I” and tensile mode “stage II”, as shown in Figure1-16 [Ste-01, Lee-05a].

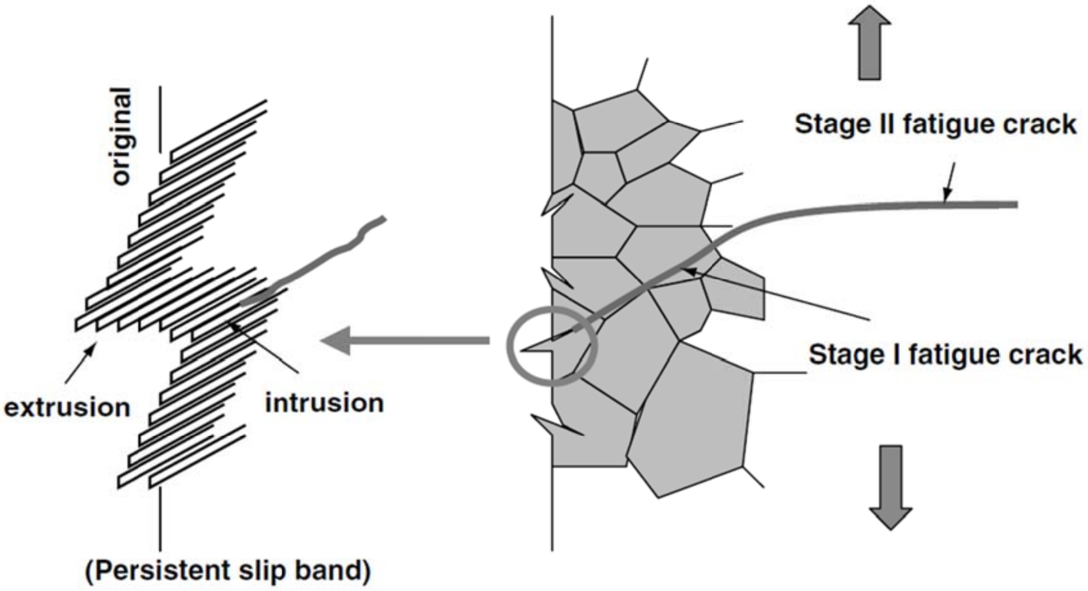

Figure 1-16: Schematic of stage I (shear mode) and stage II (tensile mode) microscopic fatigue crack growth [Lee-05b].

The fretting fatigue crack process is divided in four stages, as shown in Fig.1-17 [Lau-01 , Bre-02]. Fretting tests of a low carbon content martensitic PH13-8 Mo stainless steel conducted by Neu et al. clearly showed three main regimes of crack growth: the first regime was within about 50μm of the surface and the crack angle was near 55^o as measured from a line perpendicular to the surface; the second regime was between 50μm and 200μm from the surface, the crack angle was near 27^o during this regime; the third regime was between 200μm and 800μm, the crack angle gradually reduced to 0^o [Neu-00]. Similar cracks also observed in many other fretting fatigue tests performed under pad-on-flat contact configuration, as shown in Fig.1-18~Fig.1-21 [Goh-01, Pro-05, LYK-01 and Jac-07]. Refer to the plain fatigue crack growth process, the stage I and stage II of fretting fatigue is more shear mode dominated, the stage III is more tensile mode dominated. To be comparable to plain fatigue crack process, the fretting fatigue crack will roughly divided to shear mode stage (including stage I and stage II) and tensile mode stage (including stage III).

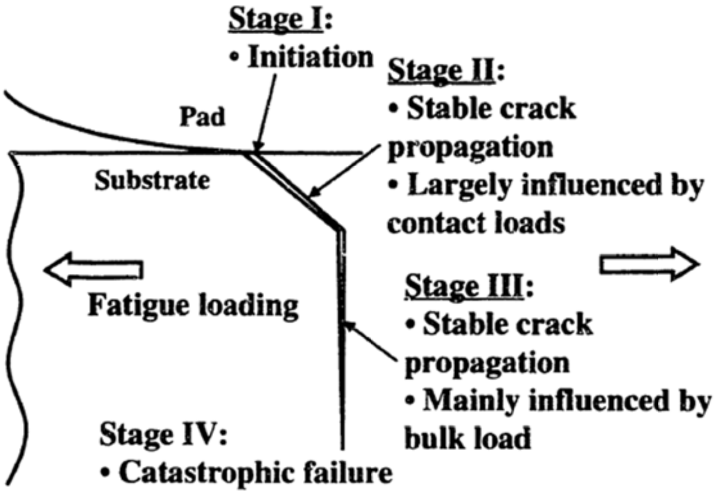

Figure 1-17: Schematic of the various stages of fretting fatigue crack growth [Lau-01]

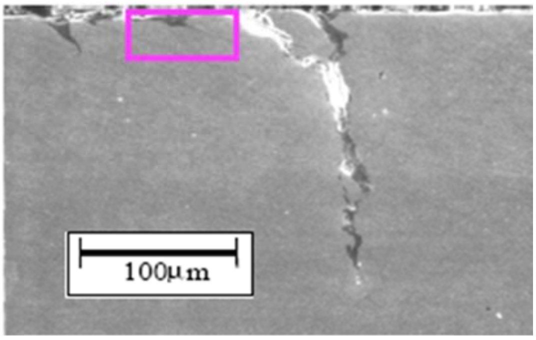

Figure 1-18: Subsurface SEM image of Ti–6Al–4V fretting fatigue specimen at trailing edge region of slip [Goh-01]

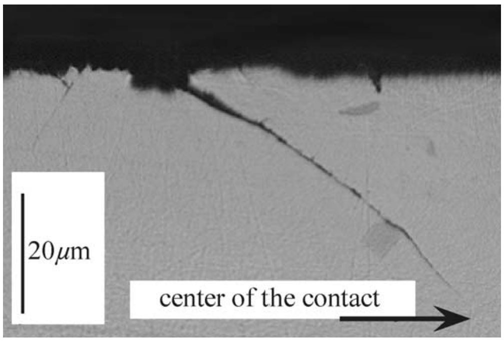

Figure 1-19: Optical micrograph of the cross-section below the 2024T351 (aluminum copper magnesium alloy) fretting fatigue specimen [Pro-05]

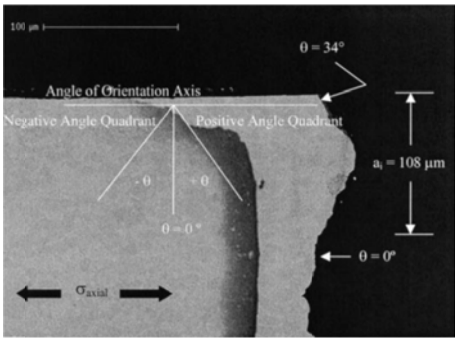

Figure 1-20: Primary crack growth path in specimen tested with 101.6 mm cylindrical pad (Material: Ti–6Al–4V). [LYK-01]

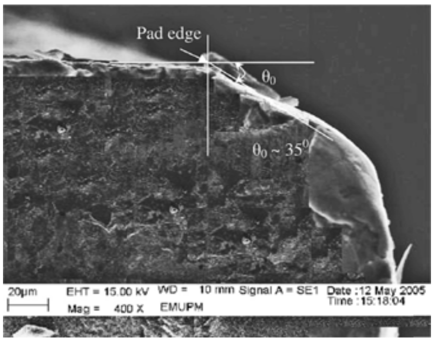

Figure 1-21: SEM micrograph of crack initiation angle at the pad contact edge (Material: 7075-T6 aluminium alloy) [Jac-07]

Which one-the shear mode stage (crack initiation period) or the tensile mode stage (crack propagation period) is dominant in the whole fatigue crack process determined the validity of a certain macro fatigue prediction parameter. In plain fatigue, the crack initiation period may cover a significant part of the fatigue life, but it is also greatly affected by the surface condition and depends on the scale definition. As shown in Figure 1-22, the major part of the fatigue life is spent within a crack size below 1mm [Sch-09]. For fretting fatigue crack, as reviewed by Nicholas, T., there’s contention between different researchers and no definitive conclusion can be drawn from present researches. He also notes that “the crack initiation and propagation life can be sensitive to the material and it’s COF, the assumed initial flaw size that separates the initiation from the crack propagation phases, and the geometry of the test fixture or component [Nic-06].”

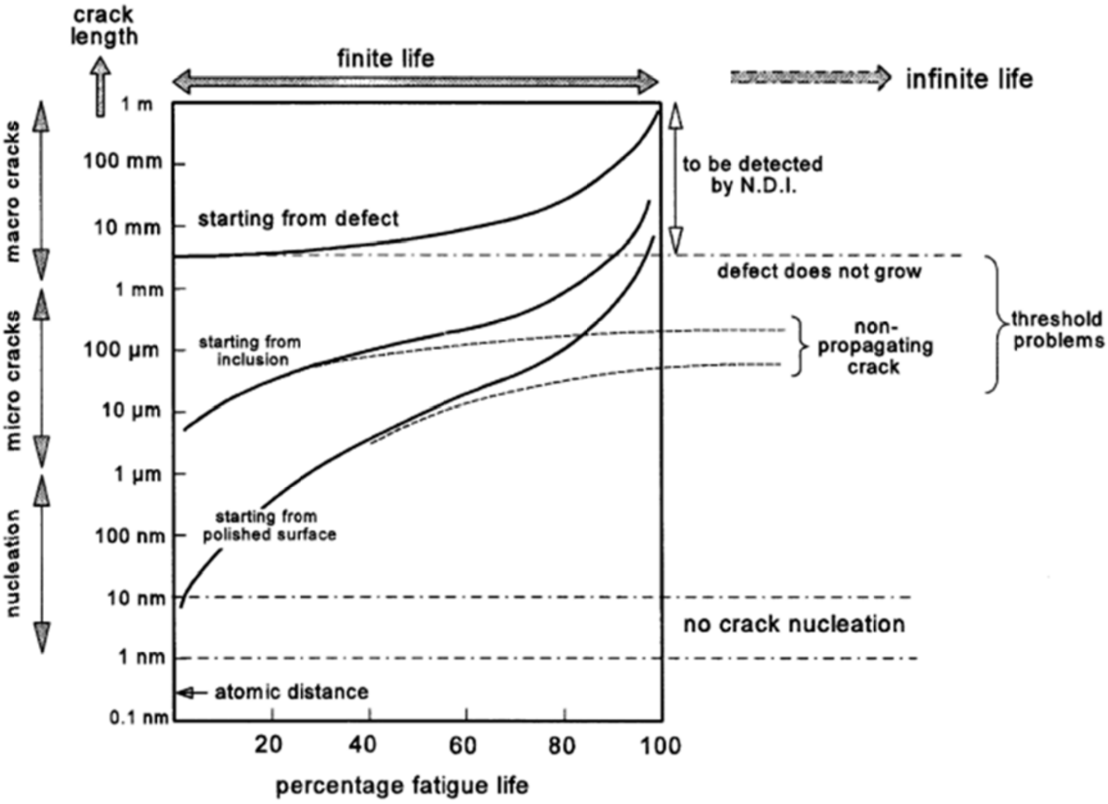

Figure 1-22: Different scenarios of fatigue crack growth [Sch-09]

In fact, all the fretting fatigue prediction models reviewed in section 1.2 do not distinguish different stages of crack growth and pay little attention to the crack initiation mechanism of fretting fatigue. So, it is reasonable that most of them are only valid or partly valid in some special cases. Inconsistent conclusions in different application cases are often appeared in literatures. For example, recent work of Lee, D. H. et al. showed that the predicted crack nucleation angle by SWT parameter is in a good agreement with the experimental results in press-fitted shafts (material: shaft- carbon steel KS SFA60, hub- high carbon steel KS RSW1), which is between 68°and 72° from the contact surface (see Fig.1-22), but the predicted locations for crack initiation by critical plane SWT and FS parameters are different from the experimental results [Lee-05b]. At the same time, Leidich, E.; et al. evaluated the critical plane fatigue parameters SWT and FS for endurance limit evaluation on shrink-fitted shaft-hub connection (material: shaft-AISI 1045, hub-AISI 1045) subjected to rotation bending as well as to dynamic torque loading, and find that the FS parameter have a good compliance for both loading cases, which can estimate both failure modes of the shrink-fitted shaft, see Fig.1-23 [Lei-09]. But, his former study showed that this parameter is not effective for fretting fatigue prediction in key SHC [Lei-07]. Above used SWT and FS is Mode I (tensile mode) and Mode II (shear mode) crack based plain fatigue prediction parameter respectively. Without considering the crack initiation mechanism in a special application case will lead to the incorrect results both in plain fatigue and fretting fatigue prediction.

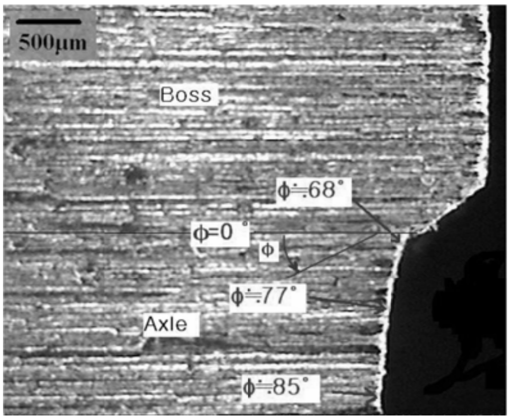

Figure 1-23: Cross section of fractured specimen [Lee-05]

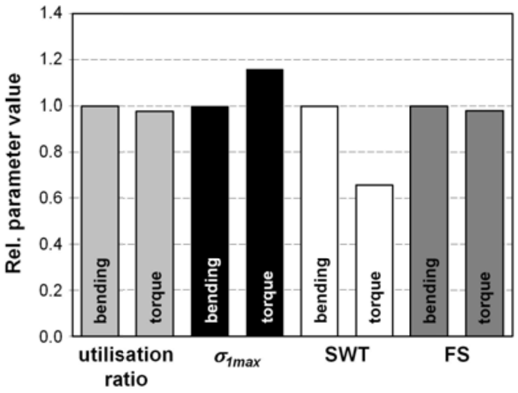

Figure 1-24: Fatigue parameter evaluation [Lei-07]

1.4 Aims of this research

The aims of this research are:

(1) Develop a fretting and plain fatigue unified prediction parameter considering the fatigue crack initiation mechanism;

(2) Investigate the fretting and plain fatigue performances of spline shaft-hub connection teeth by experiment;

(3) Based on the newly developed fretting and plain unified fatigue prediction parameter, looking for an alternative shaft-hub connection profile that with overall optimum fatigue performances.

2 Potential location of fatigue crack in spline shaft-hub connections

2.1 Introduction

Many studies have verified that fretting fatigue cracks will occur in the mixed stick-slip regime in fretted area. Gross slip gives high energy dissipation and high wear volumes but tends to lead to infinite or longer fatigue life (namely fretting wear in the absence of the bulk stress in the components), whereas partial slip produces less energy dissipation and smaller wear volumes but tends to lead to shorter fatigue life and come to fretting fatigue with the presence of cyclic bulk stresses superimposed on one or both of the contacting components [Vin-88, Fou-04]. The relationship between fatigue life and wear rate as a function of slip amplitude set up by Vingsbo and Soderberg clearly reveals this phenomenon (Figure.2-1) [Vin-88] .Gallego, L. etc also presented a similar tangential force-tangential displacement curve, showed in Figure 2-2, three different regimes are distinguished by function of the normal load and the tangential displacement: the stick regime, corresponding to very limited surface damage; the mixed stick-slip regime, corresponding to cracks; and the gross slip regimes corresponding to wear [Gal-06].

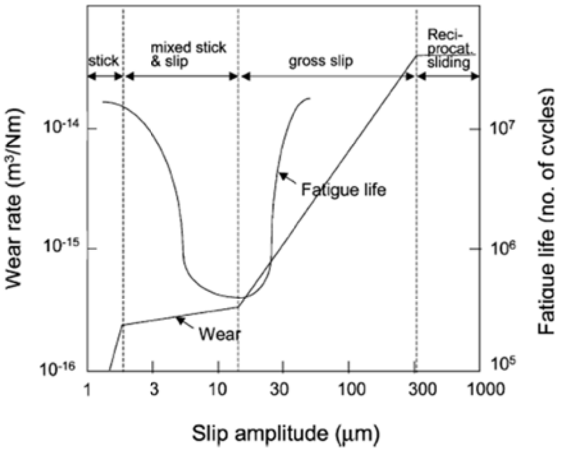

Figure 2-1: Typical relationship between fatigue life and wear rate as a function of slip amplitude (after Vingsbo and Soderberg [Vin-88]).

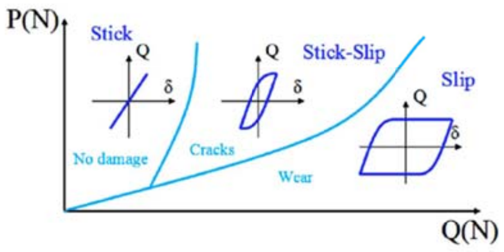

Figure 2-2: Fretting regimes and their corresponding fretting cycles (after Gallego, L. etc [Gal-06]).

According to the analysis of spline shaft-hub load conditions, [Wes-96, DIN 5466], there will be no macro relative movement or very small relative movement between teeth flank under torque predominant load conditions in side fitted spline shaft-hub connections (flankenzentrierter Verbindungen) and there will be no macro relative movement or very small relative movement between teeth flank under all load conditions in diameter fitted spline shaft-hub connections (durchmesserzentrierter Verbindungen). These kind of 'no macro relative movement' running state avoid the sliding wear of teeth flank, but which also provide favarable conditions of fretting fatigue as well as fretting wear at the same time, as shown in Table 2-1. There will be stick-slip regimes in the contact trailling edges of teeth flanks under dynamic torque predominant loads. This chapter will carry out FE simulation of spline shaft-hub connections under dynamic torque to investigate the potential location of fretting fatigue crack as well as plain fatigue crack in it.

Table 2-1: Running states and damage mechanism of profile shaft-hub connection (referred to [Wes-96, DIN 5466])

	Boundary conditions	Running state	Damage mechanism
Side fitted profile shaft-hub connection	I.Predominent or pure transverse force/bending moment	Large relative movement	Plain fatigue Sliding wear
	II.Predominent torque	Small relative movement	Plain fatigue Sliding wear/fretting wear
	III.Predominent torque	No macro relative movement	Plain fatigue Fretting fatigue/wear
Diameter fitted profile shaft-hub connection	I. Transverse force/ bending moment carried by centered diameter	No macro relative movement	Plain fatigue Fretting fatigue/wear
	II.Transverse force/bending moment partly carried by teeth flank	Small relative movement	Plain fatigue Sliding wear/fretting wear
	III. Transverse force/ bending moment partly carried by teeth flank	No relative movement	Plain fatigue Fretting fatigue/wear

2.2 FE simulation of spline shaft-hub connections under dynamic torque

2.2.1 FE model of spline shaft-hub connections

For the spline shaft-hub connections (side fitted or diameter fitted) under dynamic torque, it is cyclic symmetry about the axis. All FE simulations are carried out with FE software ANSYS. The cyclic symmetry FE model of a DIN5480 45x2x21 spline shaft-hub connection is shown in Figure 2-3. Eight-node linear brick elements SOLID45 are used throughout the whole model. The surface layer of teeth flank and the zone near begin of shaft-hub contact are very fine meshed in order to improve the analysis accuracy of potential fretting fatigue regimes.

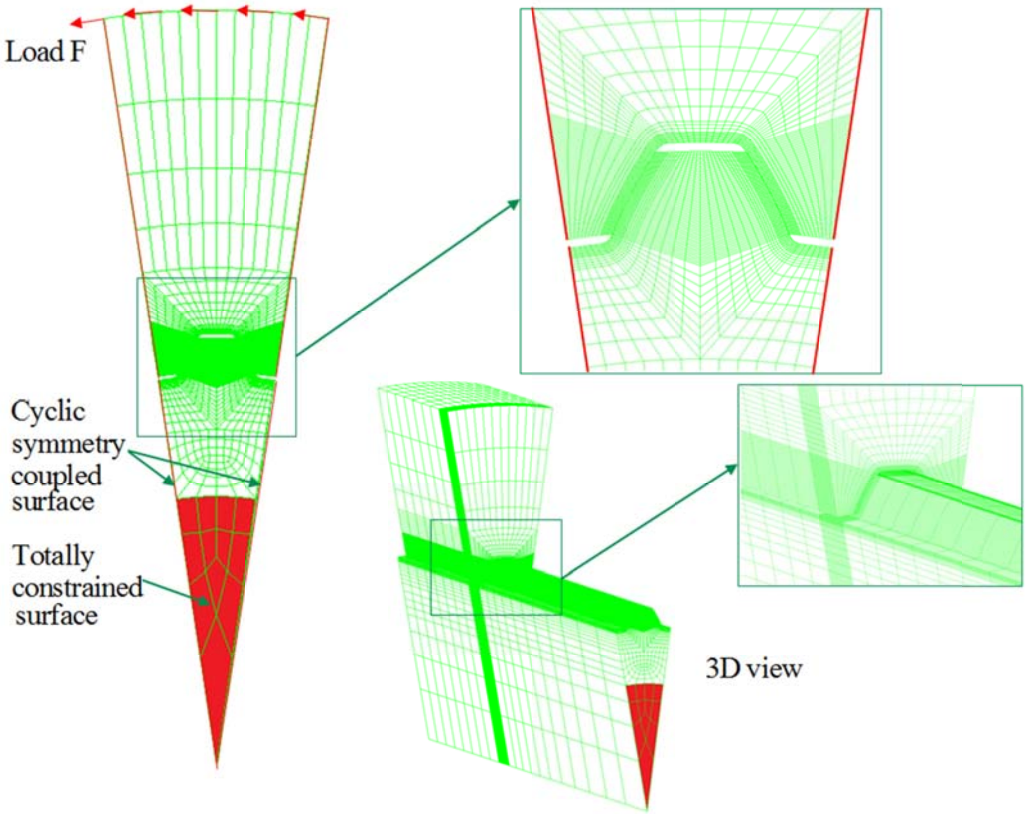

Figure 2-3: Cyclic symmetry FE model of spline SHC under dynamic torque

For the contact between flanks of shaft and hub, CONTA174 element is used to represent contact and sliding between the “target” surfaces (flank surface of hub) and the deformable surface (flank surface of shaft) which defined by this element. Contact occurs when the contact element penetrates the target segment elements, represented by TARGE170 covered on the target surface. The basic Coulomb friction model (as shown in Figure 2-4) with isotropic friction is employed and Frictional contact conditions are determined via the augmented Lagrange method in the FE model [ANS-10, Wri-06]. When the equivalent shear stress is less than the limit frictional stress $\tau_{\lim}$, there will be no motion between the two surfaces, this state is known as 'closed and sticking'; when the equivalent frictional stress exceeds $\tau_{\lim}$, the contact and target surfaces will slide relative to each other, this state is known as 'closed and sliding'. Sliding will also occur if the equivalent frictional stress reaches the maximum equivalent frictional stress $\tau_{\max}$ regardless of the contact pressure magnitude, the value of $\tau_{\max}$ is recommended to $\sigma_y / \sqrt{3}$, σ_y is the yield stress of material (hub-C35 surface harded HRC50, $\sigma_y \approx 1700$MPa; shaft-25MoCr4, surface harded HRC60 $\sigma_y \approx 2250$MPa). After the researches of S. Medina et al. [Med-02], C.H.H. Ratsimba et al. [Rat-04] and Ding, J. et al. [Din-07], a median coefficient of friction (COF) value 0.3 is used in this study at first.

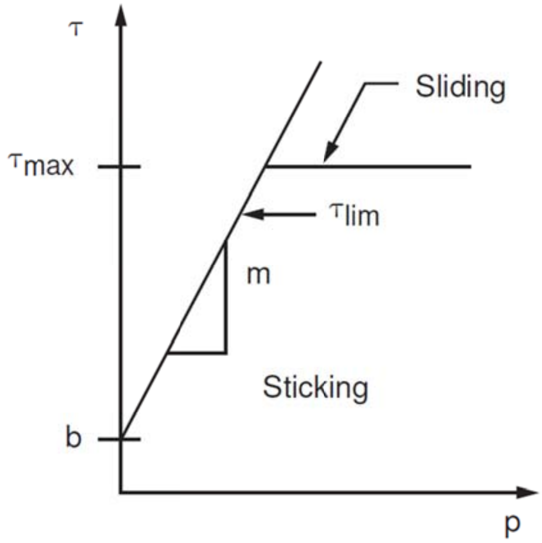

Figure 2-4: Coulomb friction model in ANSYS ($\tau_{\lim}$ = limit frictional stress, $\tau_{\max}$ = maximum equivalent frictional stress, μ = coefficient of friction, p=contact normal pressure, b=contact cohesion) [ANS-10]

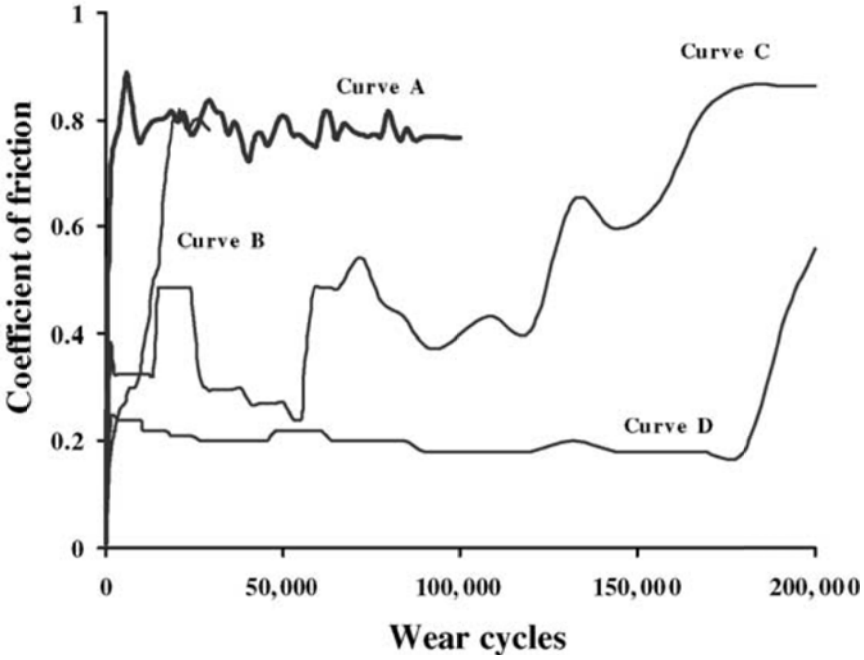

Figure 2-5: Coefficient of friction in fretting tests of a round-against-flat configuration Curve A: without added lubrication; curves B and D: upper and lower bounds for light lubrication; and curve C: typical for light lubrication. Contact load = 500 N, stroke = 50µm, Material: CrMoV alloy steel [Rat-04]

The time history of the dynamic torque applied to the shaft-hub connection will be a sine curve with constant amplitude, as shown in Figure 2-6. The experimental investigation of DIN5480 45x2x30x21 shaft-hub connection (material: 25CrMo4) under static torque loading showed that large plastic deformation in shaft-hub connection begin at about T=3000Nm, as shown in Figure 2-7 [Wes-96]. Here, fretting fatigue, the problem we are focused on, is a typical high cycle fatigue problem [Nic-06], large plastic deformation are not expected to occur. So, the maximal torque of three levels of torque will be 560Nm, 1680Nm and 2800 respectively. Corresponding to these torques, the nominal shear stresses (according to DIN5466) will be 40MPa, 120MPa and 200MPa respectively. With the same maximal torque, the ratio between minimal torque and maximal torque($R=T_u/T_o$) will change from 0.8 to 0.2, the parameter of dynamic torques are shown in table 2-2.

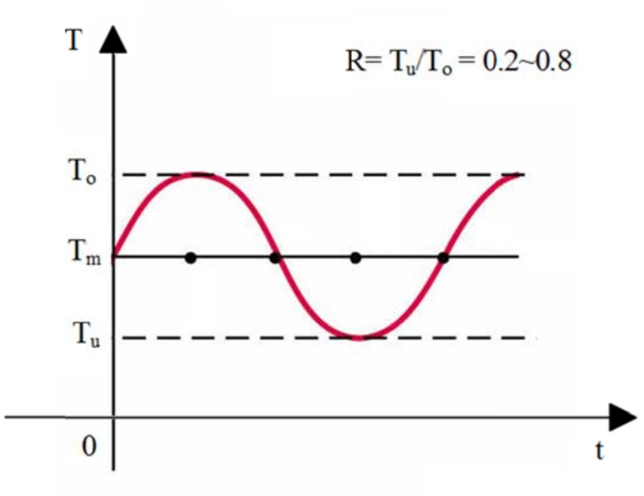

Figure 2-6: Time history of dynamic torque

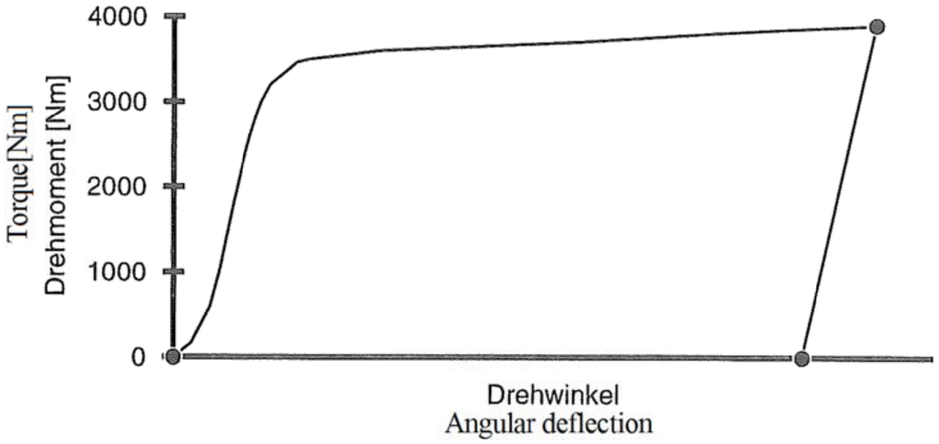

Figure 2-7: Change of the angular deflection with the increase of torque [Wes-96]

Table 2-2: Dynamic torques

$R=T_u/T_o$ τ_{tn1} (MPa)		0,8	0,7	0,6	0,5	0,4	0,3	0,2
40,096	T_o	560	560	560	560	560	560	560
	T_a	56	84	112	140	168	196	224
120,288	T_o	1680	1680	1680	1680	1680	1680	1680
	T_a	168	252	336	420	504	588	672
200,48	T_o	2800	2800	2800	2800	2800	2800	2800
	T_a	280	420	560	700	840	980	1120

Notes: 1. Spline shaft-hub connection DIN5480 45x2x21; 2. τ_{tn1} =T/W_{t1} according to DIN5466;
3.Material: hub-C35, shaft-25MoCr4 μ=0.3 FKN=10 FTOLN=0.01

In the FE model, the above torques will be converted to forces and applied on the cylindrical surface of the hub; the sine load history will be simplified to triangular wave load history and every cycle will be discrete to 5 time steps. Figure 2-8 shows the load sequence of the FE model, at 1st step, torque is applied by ramping up linearly from zero to the begin values in cycle, and the rest steps are cycle loading.

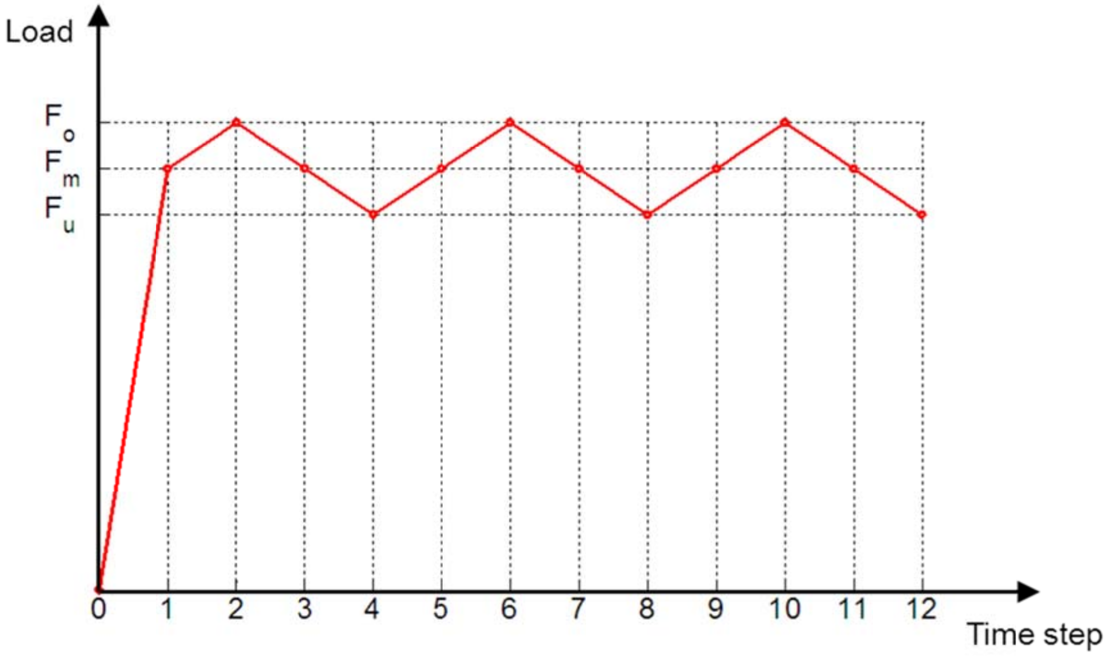

Figure 2-8: Loading sequence applied to the FE model

2.2.2 Post processing of FE analysis results

For the convenience of post processing and results comparison, all the nodal results along surface of spline flank are read out from ANSYS and post processed in software package MATLAB version 2009b. The outputted results are mapped to a two-dimensional coordinate system, as shown in Figure 2-9; the horizontal and vertical coordinates are normalized by dividing lengths along axial direction and involutes profile respectively.

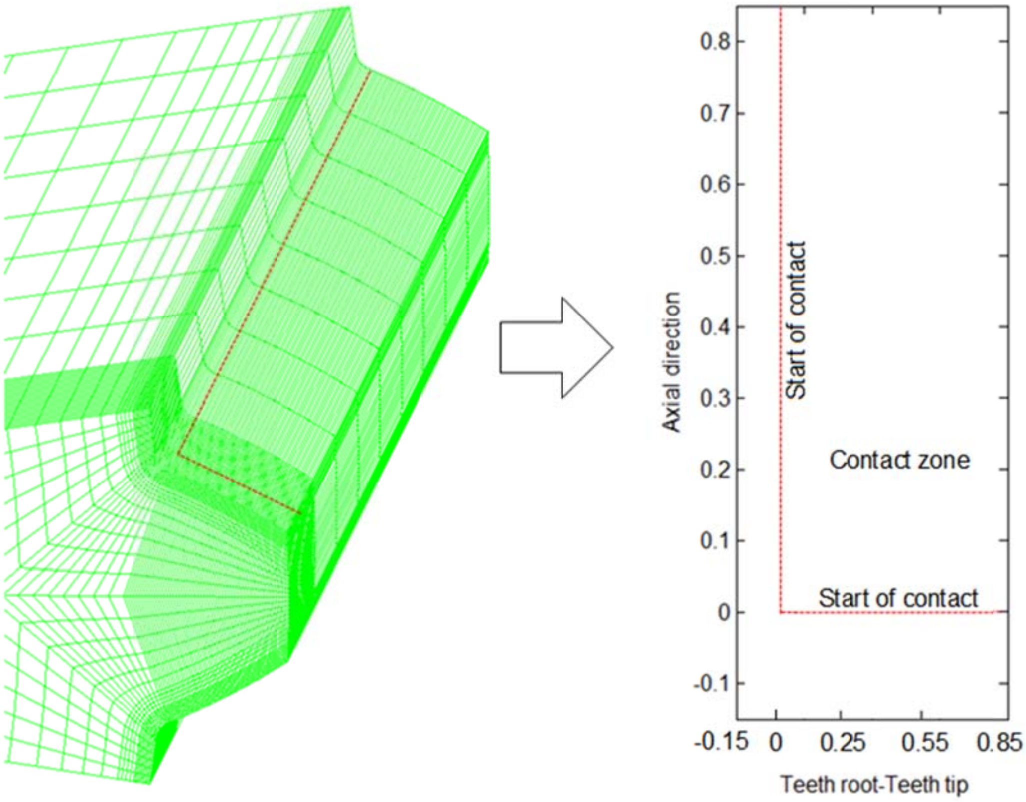

Figure 2-9: Map of FE analysis results from the curved flank surface to a plane

2.2.3 Numerical simulation results and analysis

2.2.3.1 Distribution of contact pressure on teeth flank

Due to the abrupt change of stiffness, most of the fracture failures are started from the area near the start of connection in shaft-hub connections. Here, 6mm length (in axial direction) flank near the start of connection (1mm out of contact flank and 5mm in contact flank) will be focused on. Figure 2-10 to Figure 2-12 showed the distribution of contact pressure on the concerned teeth flank under torque 560Nm, 1680Nm and 2800Nm (maximal torque of three levels dynamic torque as listed in Table 2-2.).The contact pressure on the teeth flank under different torque showed similar distribution, a ‘U’ shape distribution along the teeth root-teeth tip direction, the peak value occurred at the teeth tip of shaft (corresponding to the contact edge near teeth root of hub in contact pair), the second peak value occurred at the contact edge near the teeth root (corresponding to the teeth tip of hub in contact pair) and the altitude of ‘U’ shape decreased along axial direction from the start of contact.

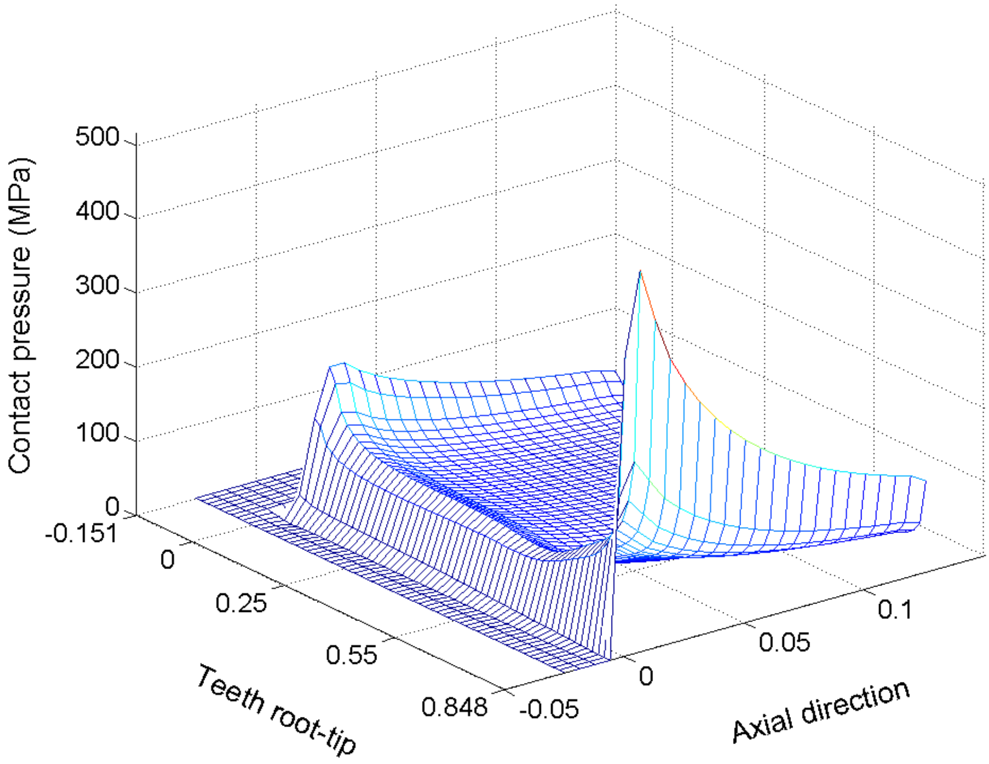

Figure 2-10: Distribution of contact pressure under load T_o=560Nm

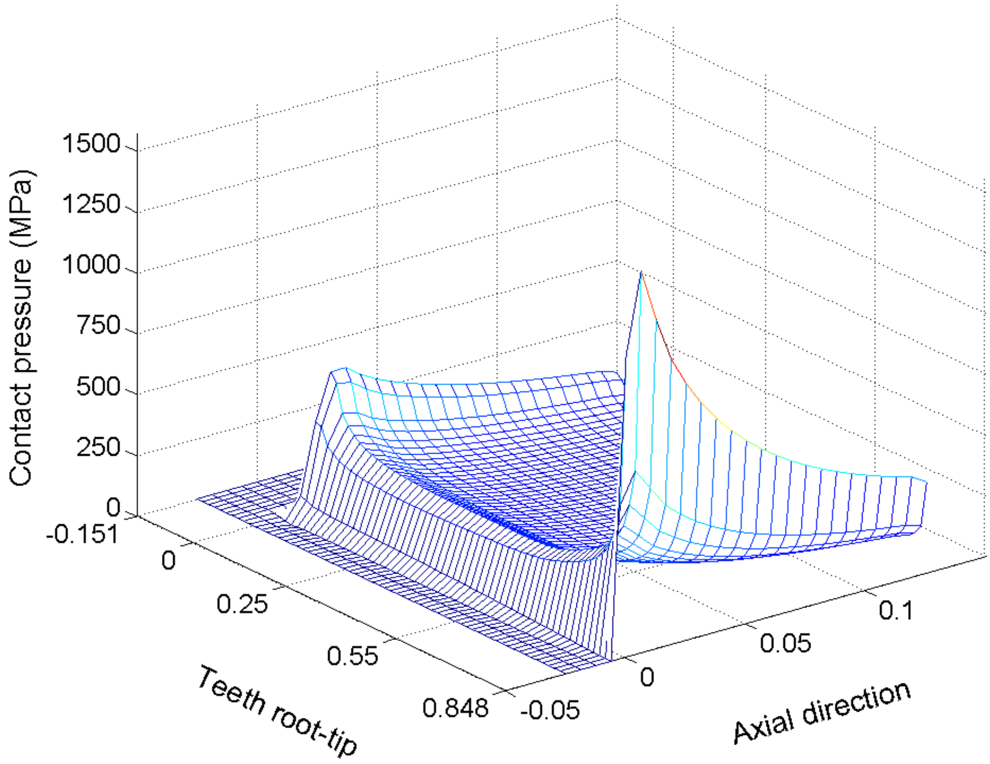

Figure 2-11: Distribution of contact pressure under load T_o=1680Nm

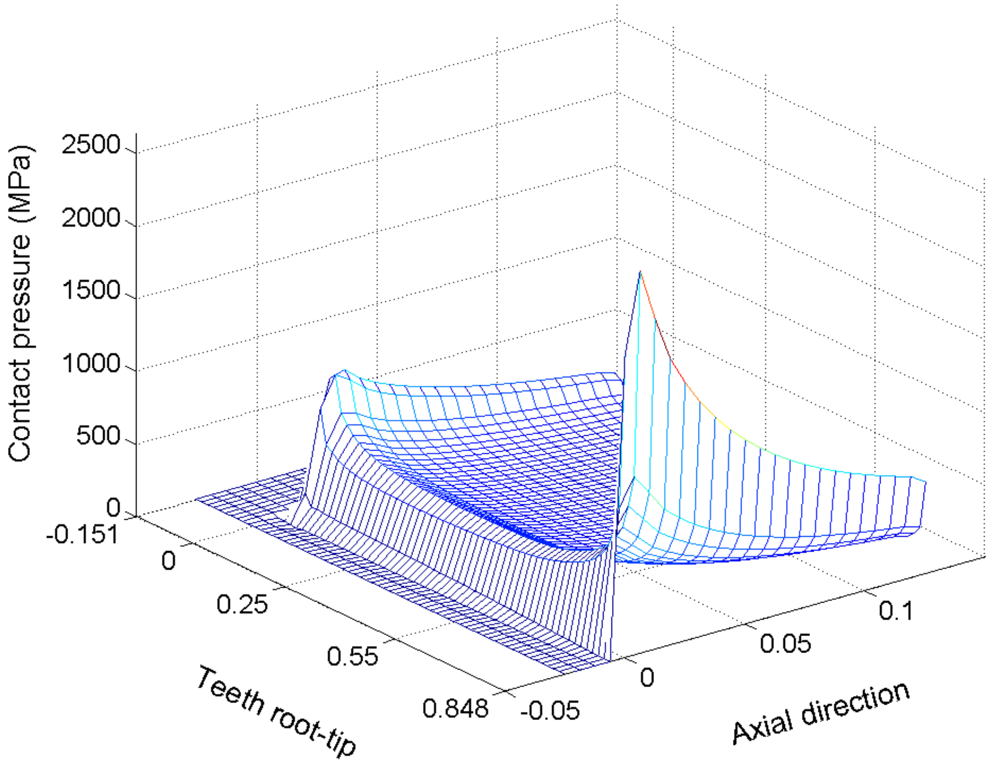

Figure 2-12: Distribution of contact pressure under load T_o=2800Nm

2.2.3.2 Distribution of total contact sliding distance

Figure 2-13 to Figure 2-16 showed the distribution of total contact sliding distance (total contact sliding distance is the value relative to the initial state of loading [ANS-10]) on the concerned teeth flank under dynamic loadings listed in Table 2-2.(only several representatives are laid out due to the similarity) The total contact sliding distance on the teeth flank under different torque loading magnitudes showed similar distribution, the peak edge of contact sliding distance value occurred near the start line of shaft-hub contact and decreased along the axial direction. The magnitude of total contact sliding distance reached $8x10^{-3}$ mm when T_o=2800Nm, which increase with the increase of loading. The range of sliding distance (the difference between maximal sliding distance and minimal distance in a cycle) depends on the load ratio R, namely the vibration amplitude of load, greater vibration amplitude create greater range of sliding distance. As a matter of fact, the sliding distance here includes the elastic deformation of the contact pair in tangential direction of the contact surface. The accuracy is greatly dependent on the friction model, for the problem of fretting, there’s still much room for improvement.

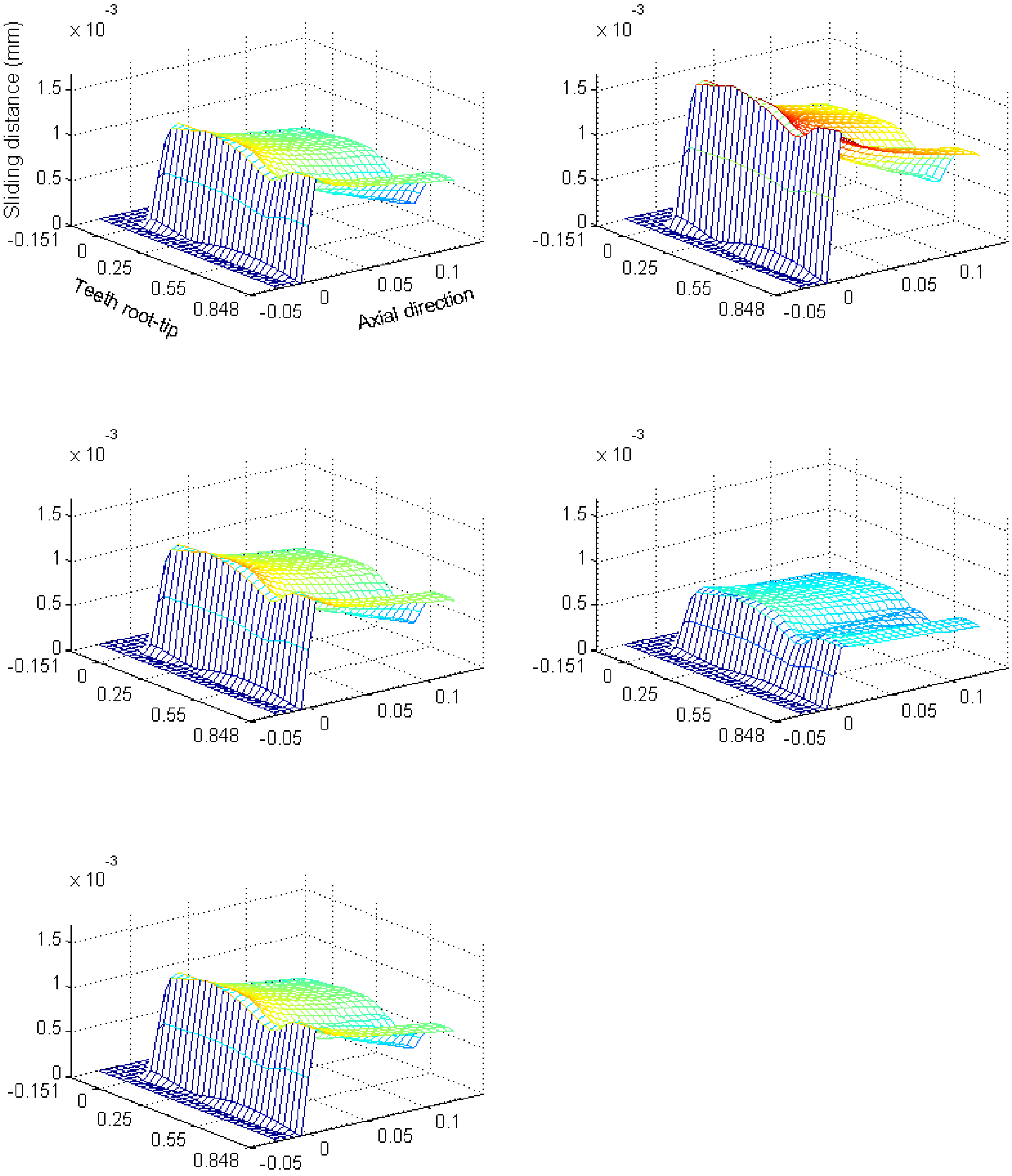

Figure 2-13: Distribution of total sliding distance on flank surface in a load cycle (from time step 5 to 9), T_o=560Nm, R=0.2

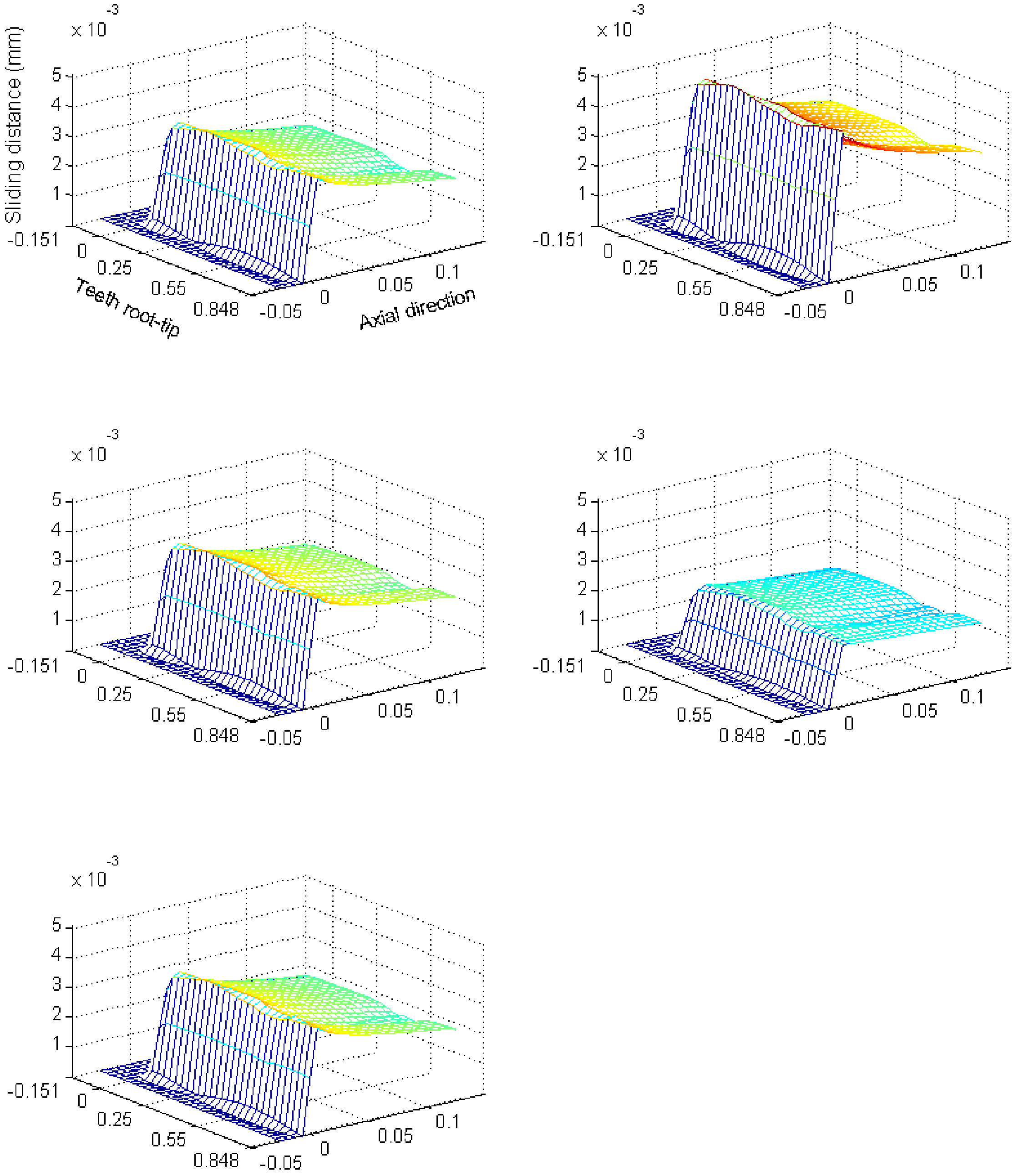

Figure 2-14: Distribution of total sliding distance on flank surface in a load cycle (from time step 5 to 9), T_o=1680Nm, R=0.2

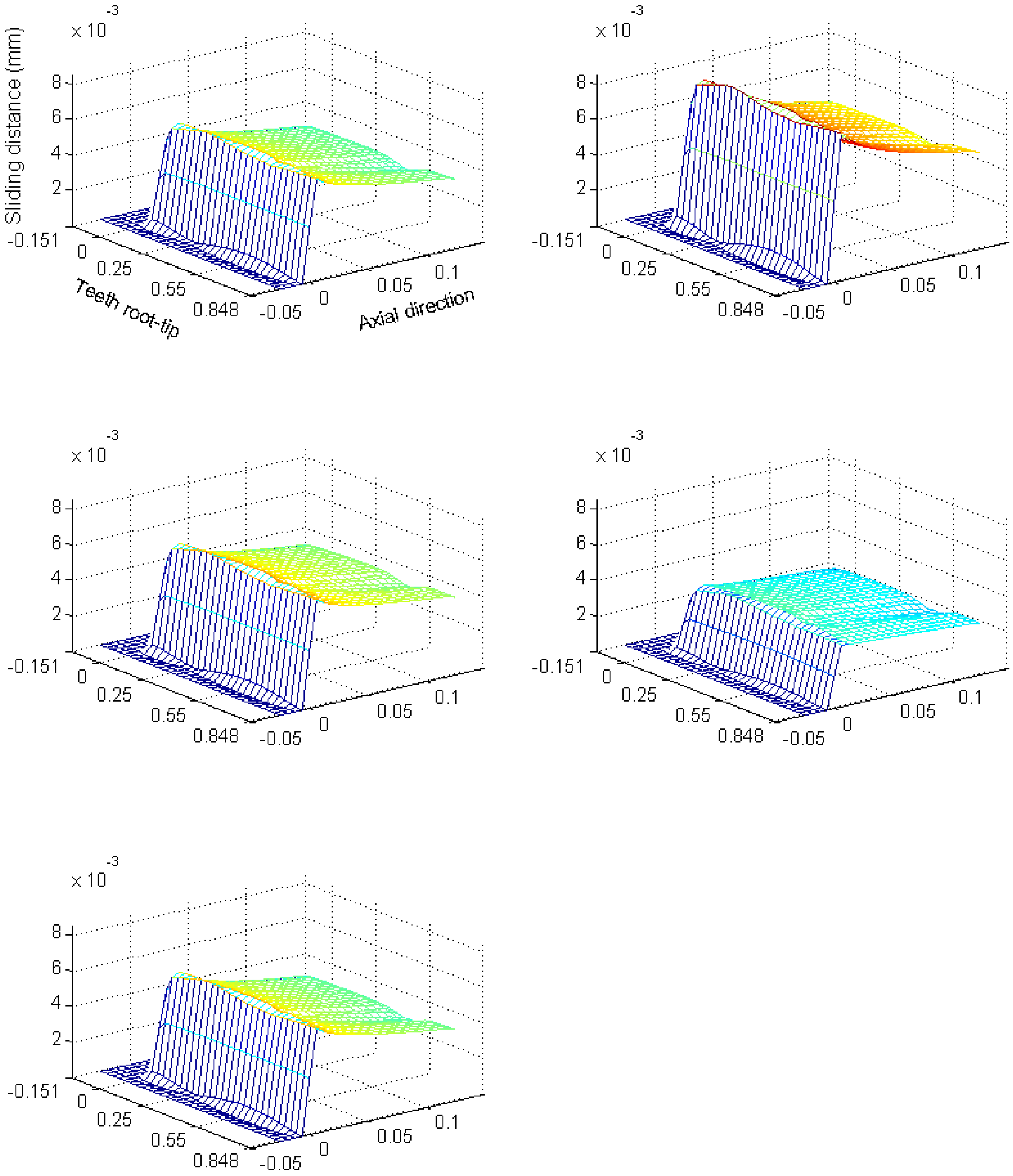

Figure 2-15: Distribution of total sliding distance on flank surface in a load cycle (from time step 5 to 9), T_o=2800Nm, R=0.8

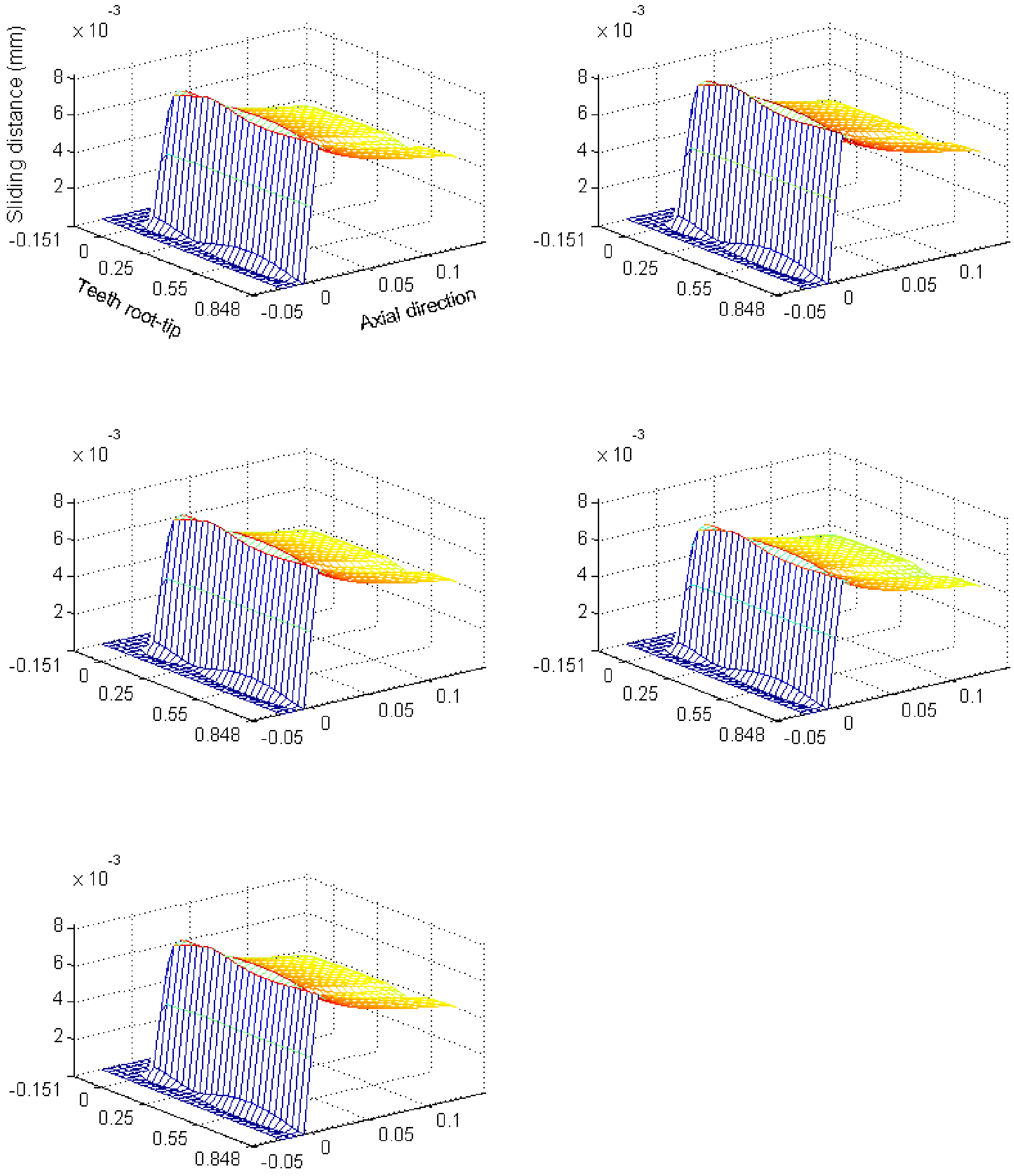

Figure 2-16: Distribution of total sliding distance on flank surface in a load cycle (from time step 5 to 9), T_o=2800Nm, R=0.2

2.2.3.3 Distribution of maximal principal stress and Von-mises stress on teeth flank

Figure 2-17 showed the distribution of maximal principal stress on the concerned teeth flank, the first peak value of maximal principal stress occurred in the teeth root (out of contact zone) and decreased along the axial direction. Figure 2-18 showed the distribution of Von-mises stress on the concerned teeth

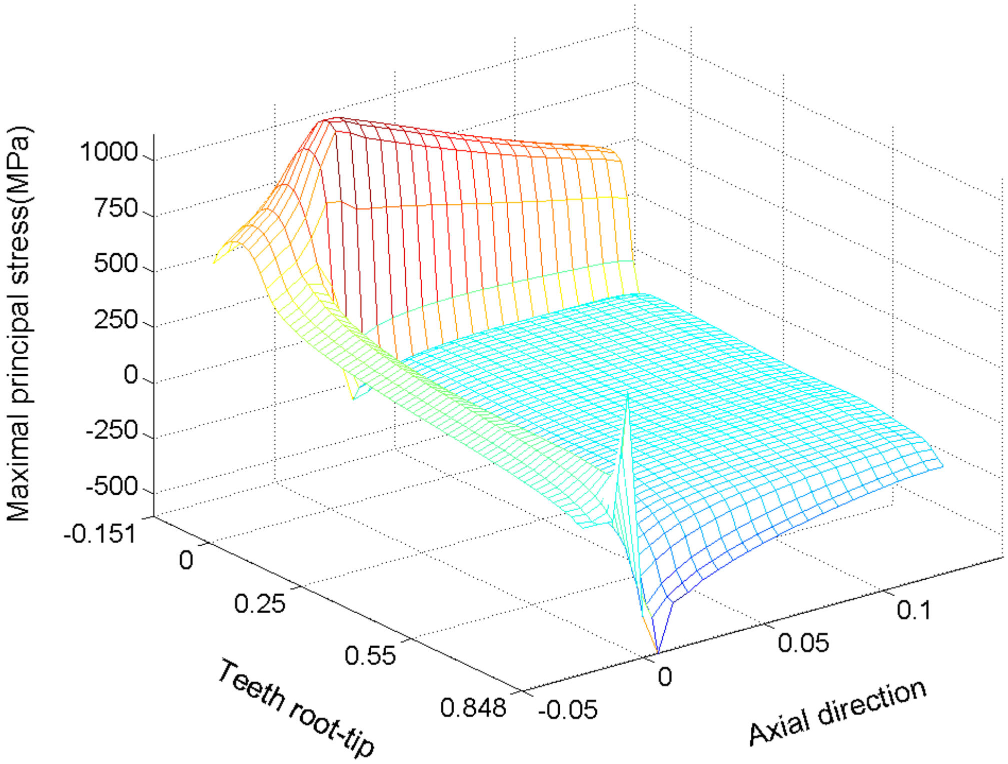

Figure 2-17: Distribution of maximal principal stress on flank surface under load T_o=2800Nm

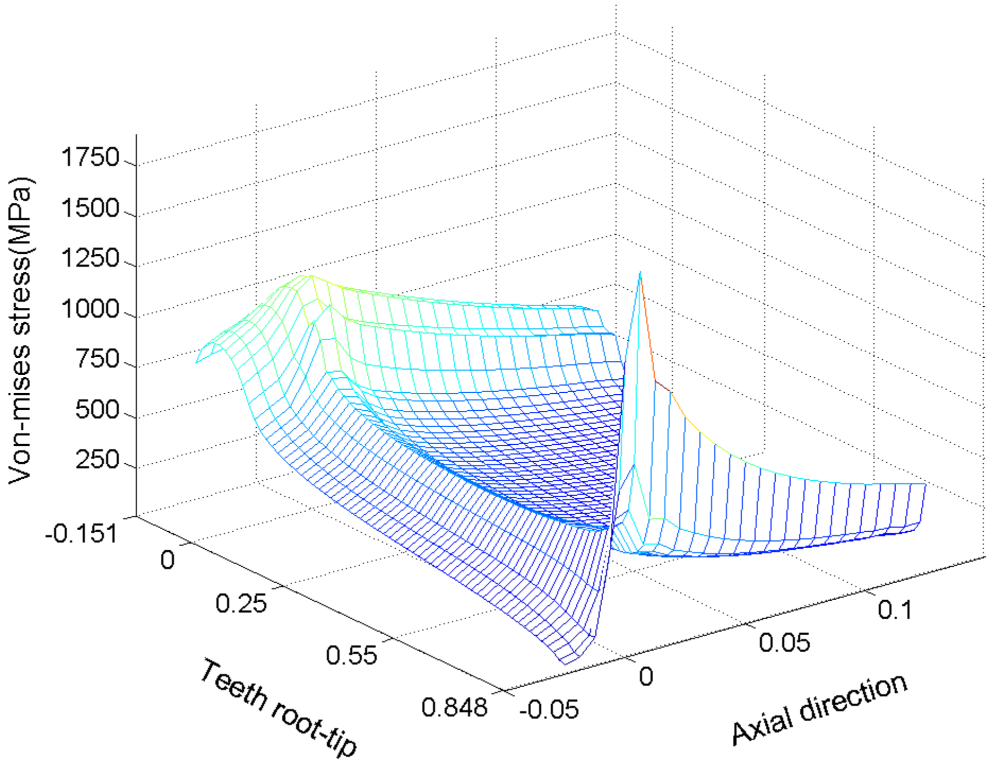

Figure 2-18: Distribution of Von-mises stress on flank surface under load T_o=2800Nm

flank, the first peak value of Von-mises stress occurred at the teeth tip and the second peak value occurred at the teeth root (out of contact zone) and both of them decreased along the axial direction.

2.3 Potential fretting fatigue locations predicted by FFDP

It is verified by some researches that the fretting fatigue damage parameter (FFDP) model gives reasonable results in predict of fretting fatigue crack nucleation location, and often used in practice due to its simplicity [Rui-84, He-89, Glö-03, Gro-07]. The FFDP model multiplies the frictional work $\tau_{fric} \cdot s$ with the local tangential stress $\sigma_{\tan}$ empirically:

$$FFDP = \sigma_{\tan} \cdot \tau_{fric} \cdot s \tag{2-1}$$

FFDP model was originally developed in a biaxial stress condition, in the spline shaft –hub connection, the teeth undergoes three dimensional stress conditions. The friction force τ_{fric} and the range of total sliding distance s keep in the same direction. Here we define the local tangential stress on the contact surface of spline flank:

$$\sigma_{\tan} = \sqrt{\sigma_x^{\ 2} + \sigma_z^{\ 2}} \tag{2-2}$$

as shown in Figure 2-19, σ_x , σ_y and σ_z are three local normal stresses at a certain point on the contact surface of teeth flank, σ_x is tangential to the involute spline, σ_y is perpendicular to the teeth flank and σ_z parellel to the axial direction. And , we assum that the direction of $\sigma_{\tan}$ is the same with τ_{fric} and s . Based on above definition and assumption, the FFDP model will be implemented to the spline teeth under dynamic torque. The distribution of FFDP on concerned teeth flank are shown in Figure 2-20 to Figure 2-23.

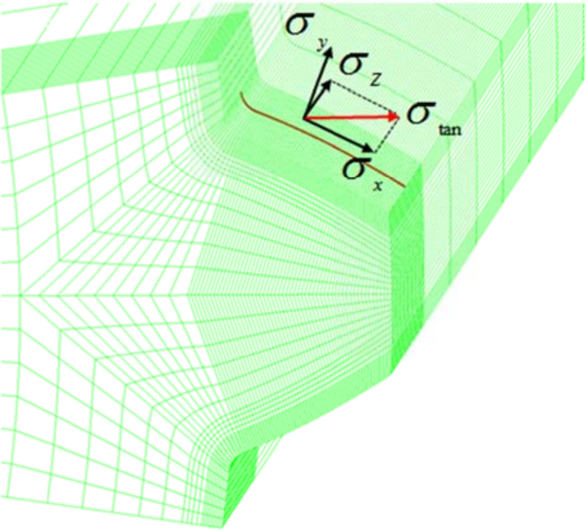

Figure 2-19: Definition of local tangential stress on the contact surface of spline flank

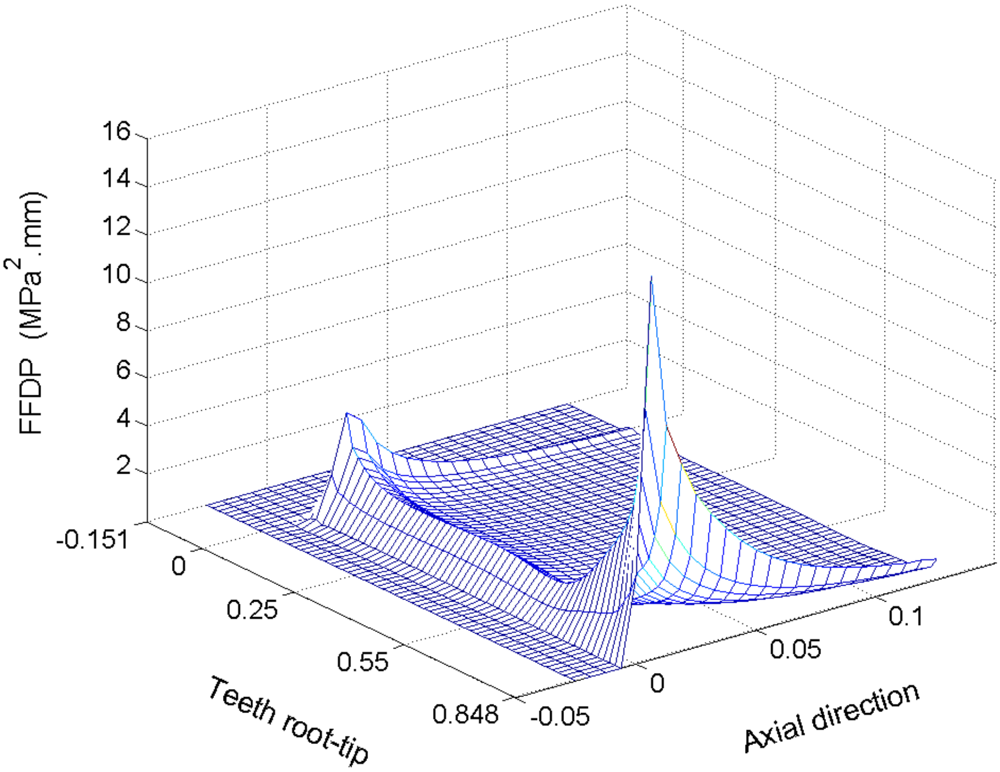

Figure 2-20: Distribution of FFDP on teeth flank (T_o=560Nm, R=0.2)

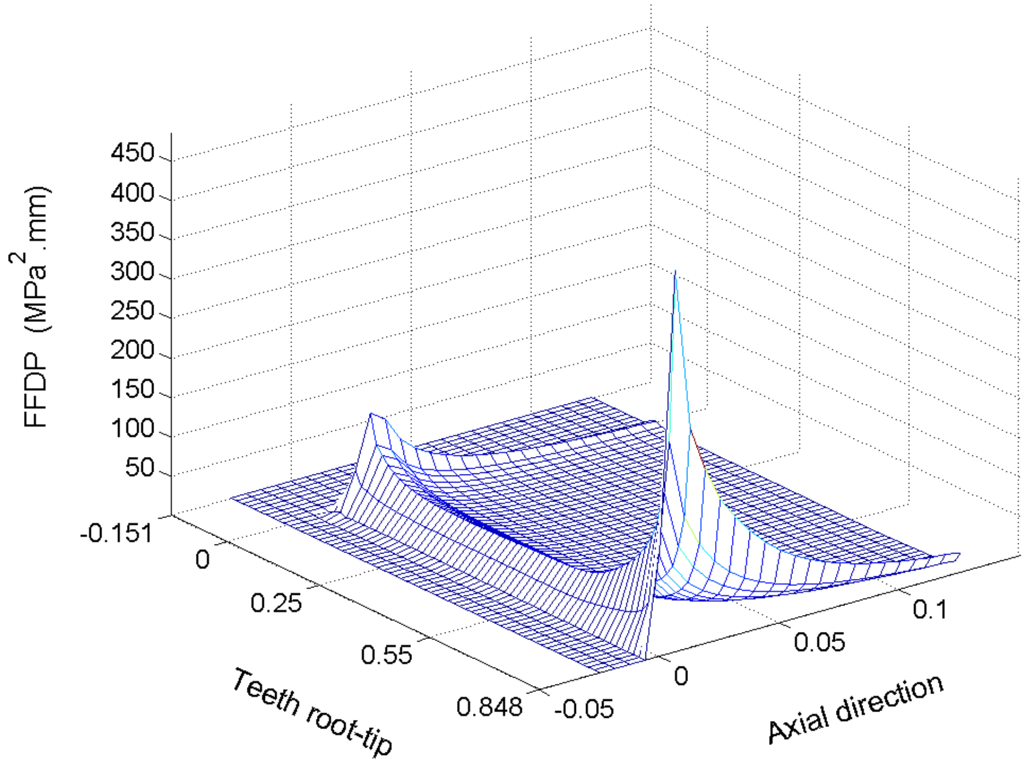

Figure 2-21: Distribution of FFDP on teeth flank (T_o=1680Nm, R=0.2)

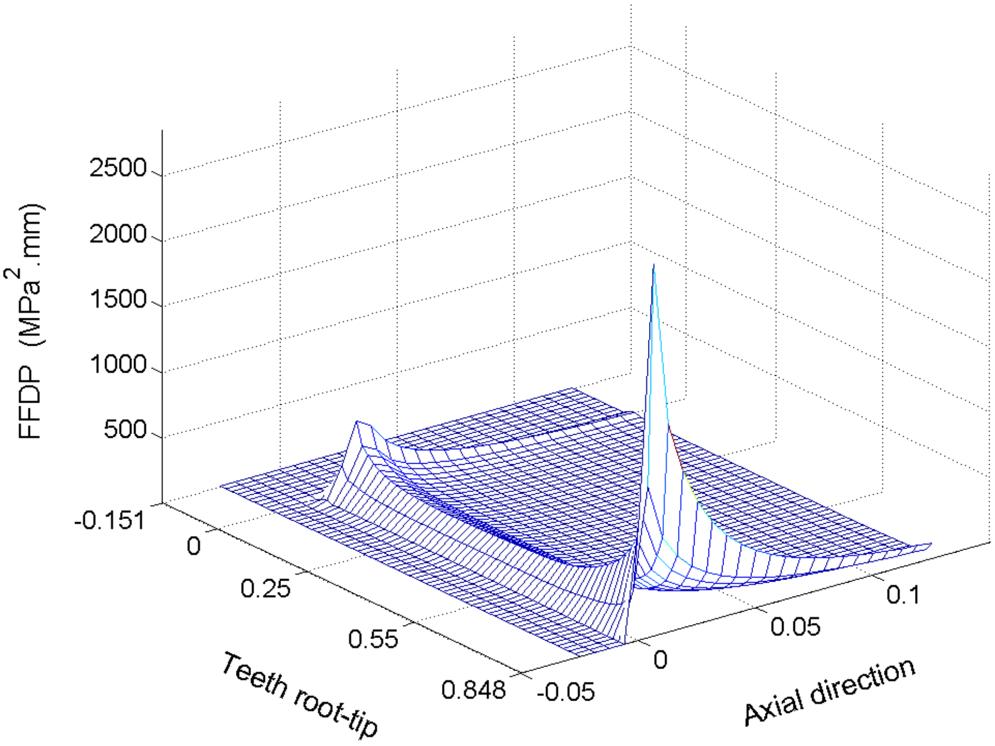

Figure 2-22: Distribution of FFDP on teeth flank (T_o=2800Nm, R=0.2)

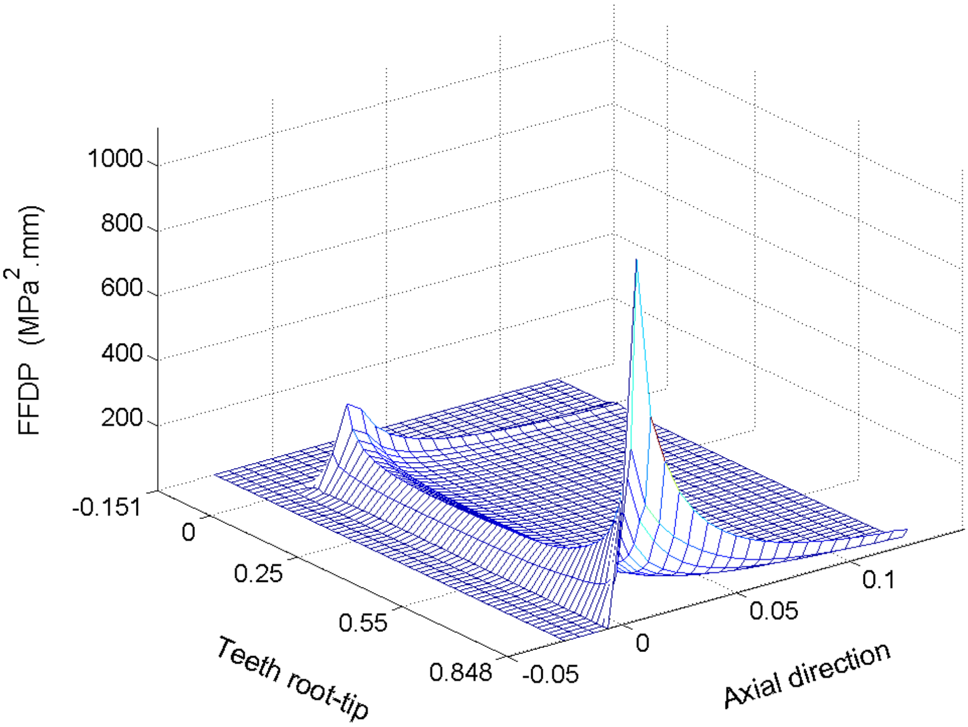

Figure 2-23: Distribution of FFDP on teeth flank (T_o=2800Nm, R=0.8)

As shown in above figures, the distribution of FFDP on teeth flank showed similar characteristic compared with contact pressure distribution, the first peak value occurred at the teeth tip inside the start of contact line, the second peak value occurred inside the start of contact line near the teeth root (corresponding to the teeth tip of hub in contact pair), and the altitude of ‘U’ shape decreased along axial direction from the start of contact. The value of FFDP increased dramatically with the increase of maximal torque and vibration amplitude of torque. Figure 2-25 clearly shows the fretting marks on the teeth flank near the start of shaft-hub connection, and the fretting marks near teeth tip is darker than that near teeth root, which is consistent with the distribution of FFDP and contact pressure on teeth flank qualitatively.

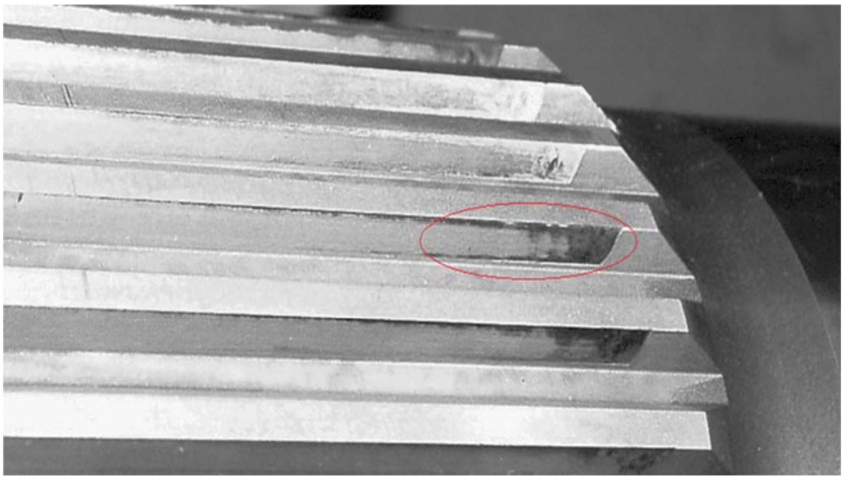

Figure 2-24: Fretting mark on the teeth flank near the start of shaft-hub connection [Hua-07]

It have been discussed by some researchers that frictional slip may accelerate crack initiation and produce fretting fatigue combined with cyclic bulk stresses or worn away microcracks below the surface before propagation and produce fretting wear, namely, the accelerating effect and the arresting effect of frictional slip [Fou-09]. That's to say that both peak value of frictional slip based FFDP model means only the potential location of fretting fatigue. The square root definition of $\sigma_{\tan}$ missed the information of stress direction (tension or compression), consequently the value of FFDP is always positive and missed some information of indication. Actually, the situation at the teeth tip is not benefit for the propagation of a fretting fatigue crack though the first peak value occurred here, the micro cracks will be quickly worn away by frictional slip, the sharp edge of teeth tip will be soon rounded. So, the potential locations of fretting fatigue reduced to the intersection point of start contact line near teeth root.

2.4 Potential plain fatigue location predicted by SWT parameter

Considering the distribution of maximal principal stress showed in Figure 2-17 and Von-mises stress showed in Figure 2-18, the maximum occurred at the teeth root outside of contact zone, this indicated the possibility of plain fatigue rather than fretting fatigue at teeth root. As a comparison of FFDP distribution on teeth flank, the critical plane SWT multiaxial plain fatigue criterion is also implemented to the dynamically loaded spline teeth flank.

$$SWT = \sigma_{\max}\frac{\Delta\varepsilon}{2} = \frac{\left(\sigma_f^{'}\right)^2}{E}\left(2N_f\right)^{2b} + \sigma_f^{'}\varepsilon_f^{'}\left(2N_f\right)^{b+c} \qquad (2\text{-}3)$$

where $\sigma_{\max}$ is the maximal normal stress, $\Delta\varepsilon$ is normal strain range, $\sigma_f^{'}$ and b are the fatigue strength coefficient and exponent, $\varepsilon_f^{'}$ and c are the fatigue ductility coefficient and exponent, N_f is the number of cycles to initiate a crack [Neu-00, Ara-04]. In three-dimensional critical plane implementation, the position of a candidate critical plane is defined by two angles, θ_v and θ_h, illustrated in Figure 2-25. There will be 5184 candidate critical plane for every integration points (or nodes) in increment of 5^0, the maximal SWT value of a node will be picked out by comparison of the SWT value in every candidate critical plane.

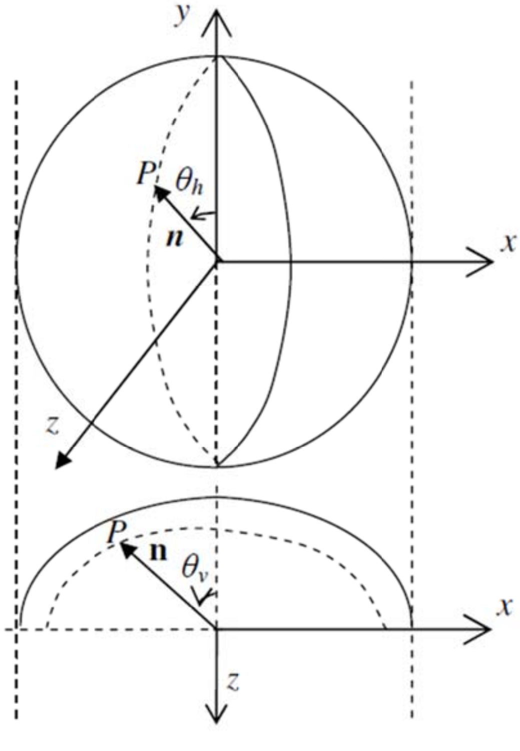

Figure 2-25: Position of point P on a unit sphere, orientation of unit normal n is defined by angles θ_v and θ_h [Sum-04].

Figure 2-26 and Figure 2-27 show the distribution of SWT parameter on the concerned teeth flank, under the dynamic load with smaller vibration amplitude and the dynamic load with greater vibration amplitude, both the first peak values occur at the teeth root outside contact zone. It is easy to understand the teeth root outside contact zone suffered from the danger of plain fatigue. Which one, fretting fatigue inside the contact zone near teeth root or the plain fatigue at teeth root outside the contact zone will leads to the fracture of the spline teeth and consequently the whole spline shaft depends on the 'competition' of these two fatigue mechanism. Figure 2-28 shows the fatigue fracture at teeth root of a spline shaft-hub connection, it have not been distinguished which fatigue mechanism-fretting fatigue or plain fatigue leads to the fracture of the spline tooth.

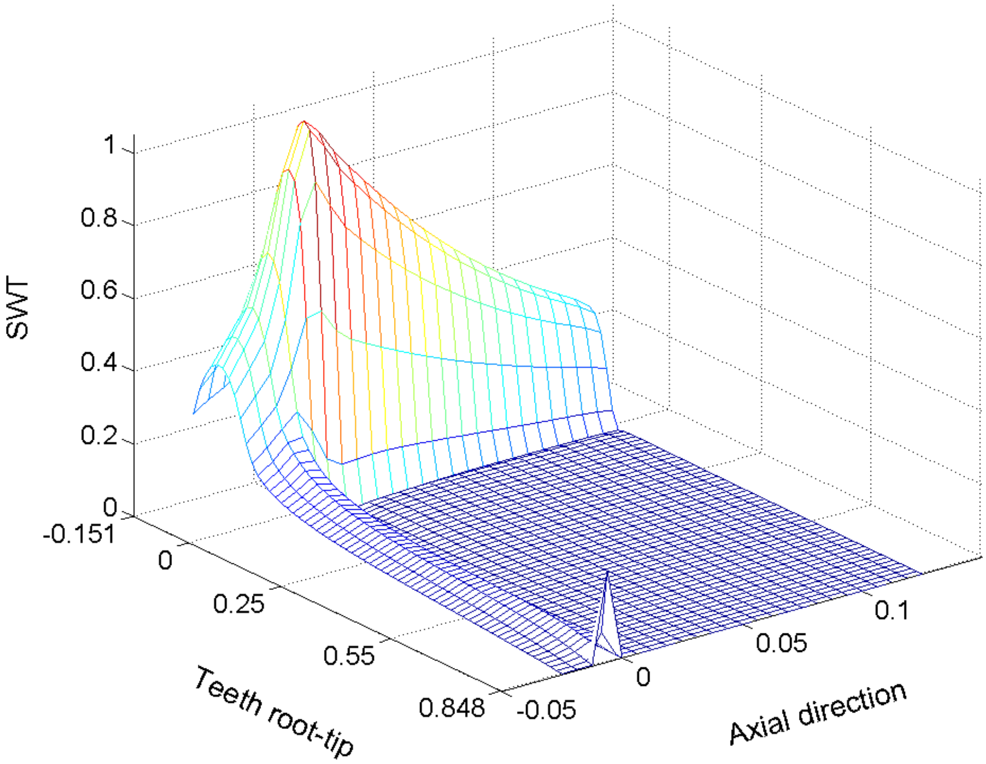

Figure 2-26: Distribution of SWT on teeth flank (T_o=2800Nm, R=0.8)

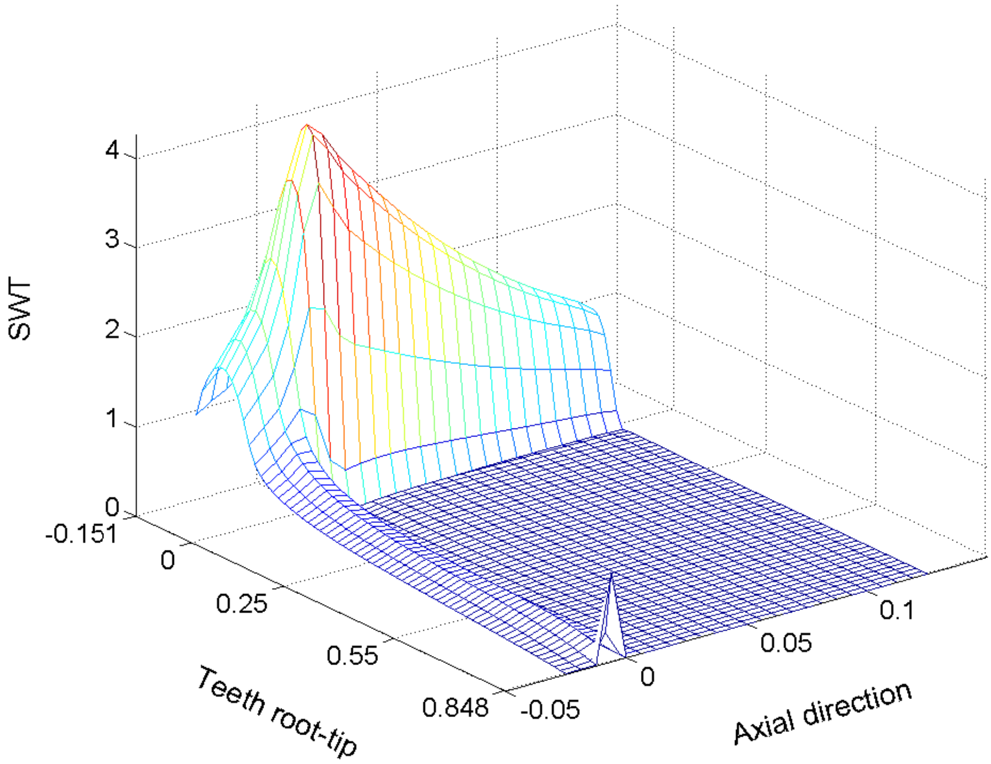

Figure 2-27: Distribution of SWT on teeth flank (T_o=2800Nm, R=0.2)

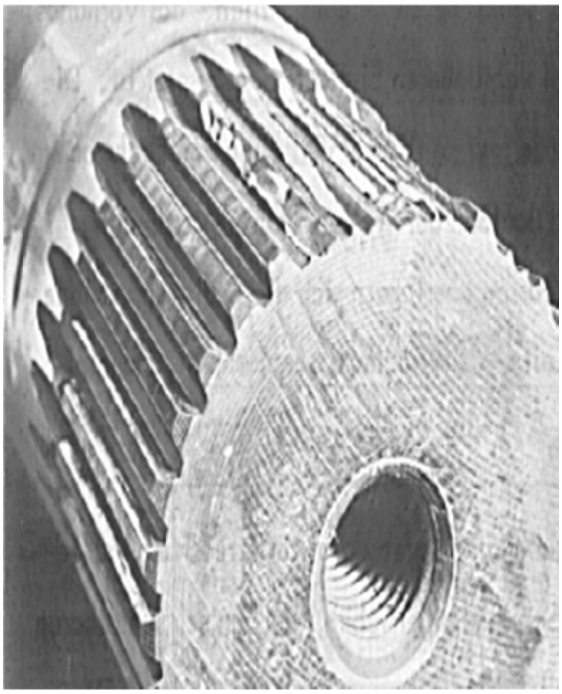

Figure 2-28: Fatigue facture of spline teeth in involute spline shaft-hub connection [Die-93]

2.5 Conclusion

Numerous models are developed to predict plain fatigue and fretting fatigue independently. The potential location of fretting fatigue predicted by FFDP is near the contact edge of spline teeth and the potential location of plain fatigue predicted by SWT is at fillet of spline teeth. Usually, the value of fretting fatigue prediction parameter and plain fatigue prediction parameter are not comparable, so it’s remains unclear which fatigue mechanism will dominate the failure of the whole assembly. A fretting and plain fatigue unified prediction model is waited for in this fretting and plain fatigue coexisted situation.

3 Fretting and plain fatigue unified prediction model

3.1 Introduction

As analyzed above, the potential location of fretting fatigue predicted by FFDP is at contact edge near the teeth root, the potential location of plain fatigue predicted by the plain fatigue prediction parameter SWT is at the teeth fillet outside of contact zone. But, the value of fretting fatigue prediction parameter and pure plain fatigue prediction parameter is not comparable, so it is still unclear that which one will lead to the failure of spline shaft-hub connection at first. To evaluate the competition of plain fatigue at teeth fillet and fretting fatigue near contact edge, this chapter will develop a fretting/plain fatigue unified prediction model. And for the optimization of shaft-hub connection spline with overall better fatigue performance, a fretting/plain fatigue unified prediction parameter is an absolute essential.

In this study, we focus on the fretting/plain fatigue competition in teeth root-teeth tip direction. Refer to the study of Hyde T.R. et al [HYD-05, DEA-09], a maximal loaded slice vertical to axial direction will be extracted from one teeth pair of spline shaft-hub connection (as shown in Figure 3-1). Neglecting the effects in axial direction, the spline shaft-hub connection (DIN5480 45x2x30x21) is simplified to a quasi-two dimensional one tooth pair representative model. Following analysis and modeling efforts are implemented in this two dimensional one teeth pair representative model.

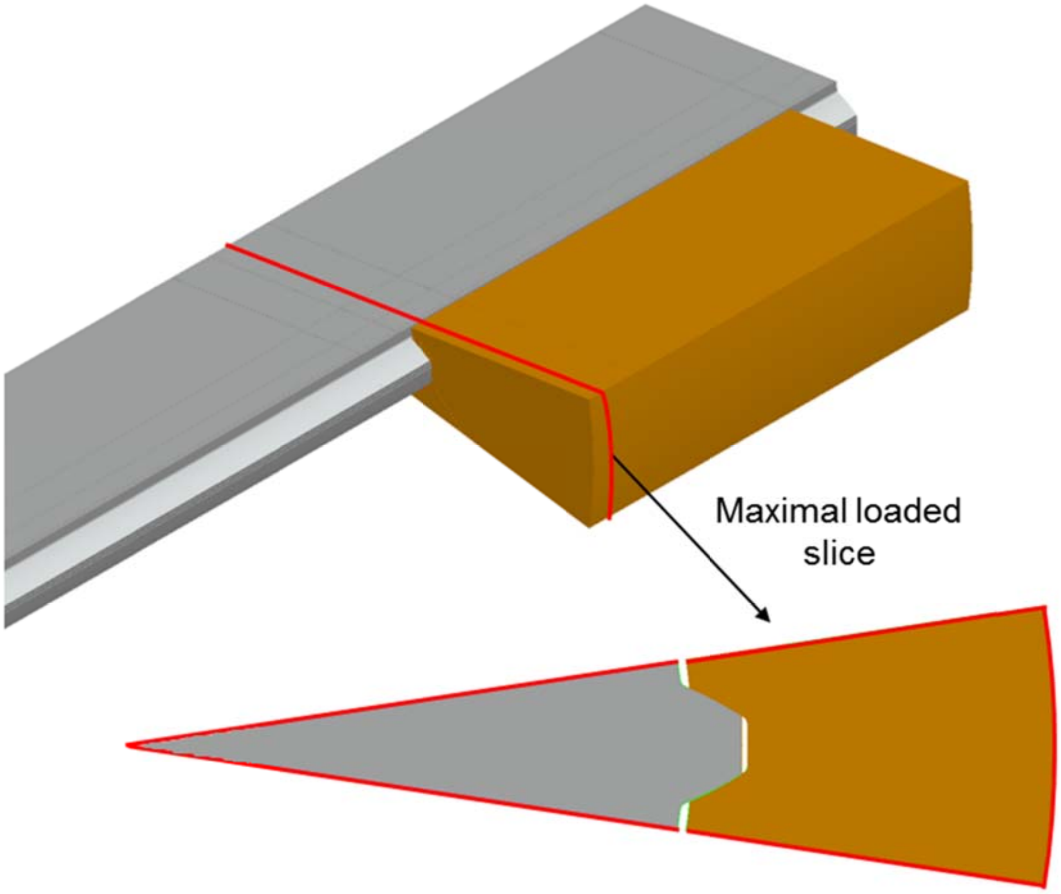

Figure 3-1: Maximal loaded slice extracted from one tooth pair of involute spline shaft-hub connection

3.2 FE model of the representative tooth pair and results post processing

Figure 3-2 shows the FE model of the quasi two dimensional representative teeth pair. As introduced in section 3.1, the representative teeth pair is a maximal loaded slice extracted from one tooth pair of spline shaft-hub connection. The equivalent load F that equally applied on the external surface of hub can be calculated out according following equation (referred and modified from the equation (2) and (3) in [HYD-05]):

$$F = \frac{1}{R} b x_l \psi \sum_{i=1}^{n-1} \left(\frac{R_i + R_{i+1}}{2}\right) \left(\frac{p_i + p_{i+1}}{2} \cos\left(\frac{\alpha_i + \alpha_{i+1}}{2}\right) + \frac{f_i + f_{i+1}}{2} \sin\left(\frac{\alpha_i + \alpha_{i+1}}{2}\right) \right) \tag{3-1}$$

F: equivalent load ; R: external radius of hub tooth (here, R=33.5mm); b: thickness of the teeth (in axial direction, here b=12mm); x_l:length of the contact element; ψ:compensate coefficient for slight variation in contact pressure and frictional stress across the thickness b; n: number of nodes along teeth flank in contact line; R_i: radius of node i on teeth flank; α_i: pressure angle of at node i on teeth flank; μ: coefficient of friction (0.3 in this study); p_i: contact pressure at node i on the teeth flank; f_i: frictional stress at node i on the teeth flank. R_i, α_i, f_i and p_i are shown in Figure 3-3, the contact pressure p_i and frictional stress f_i of the maximal loaded slice are output from the results of FE analysis carried out in chapter 2. Corresponding to dynamic torques listed in Table 2-2, the equivalent loads of the quasi two dimensional representative tooth pair are calculated using equation (3-1) and listed in Table 3-1.

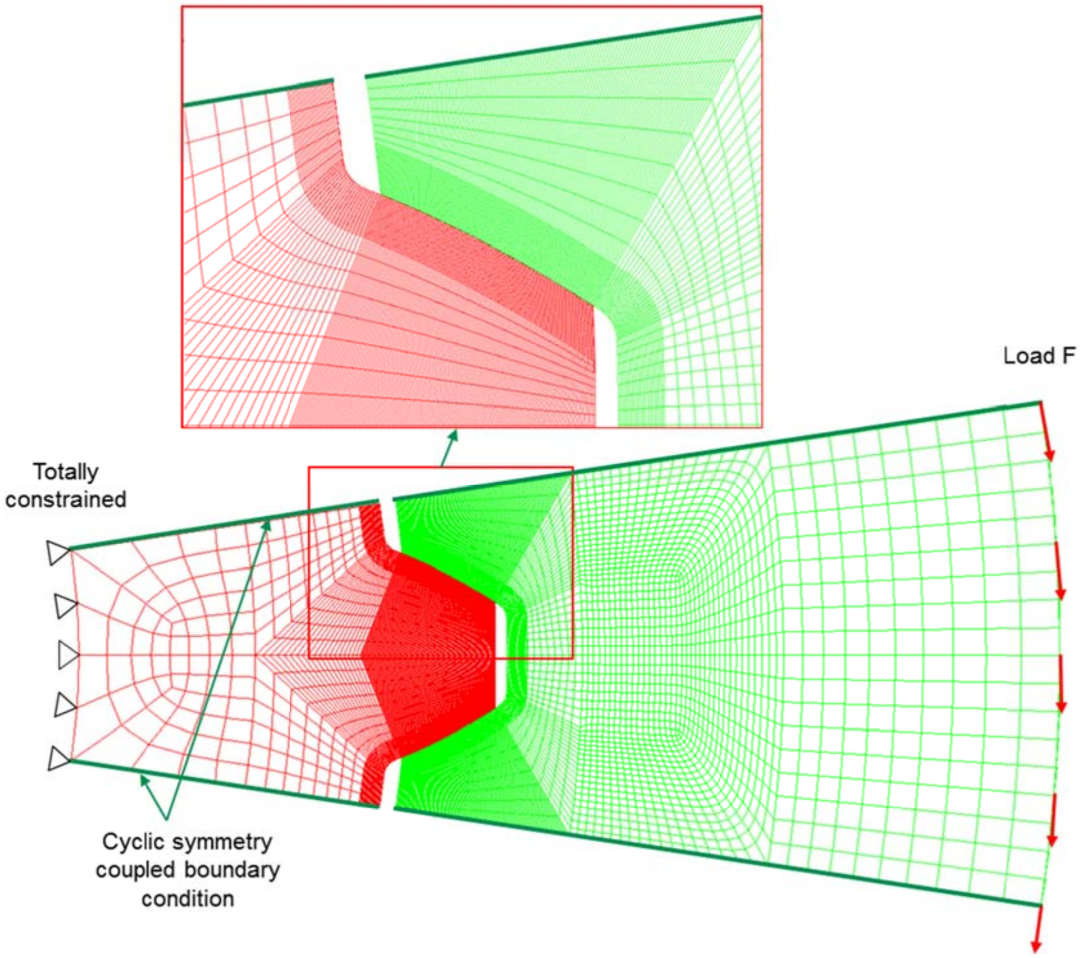

Figure 3-2: FE model of the representative teeth pair

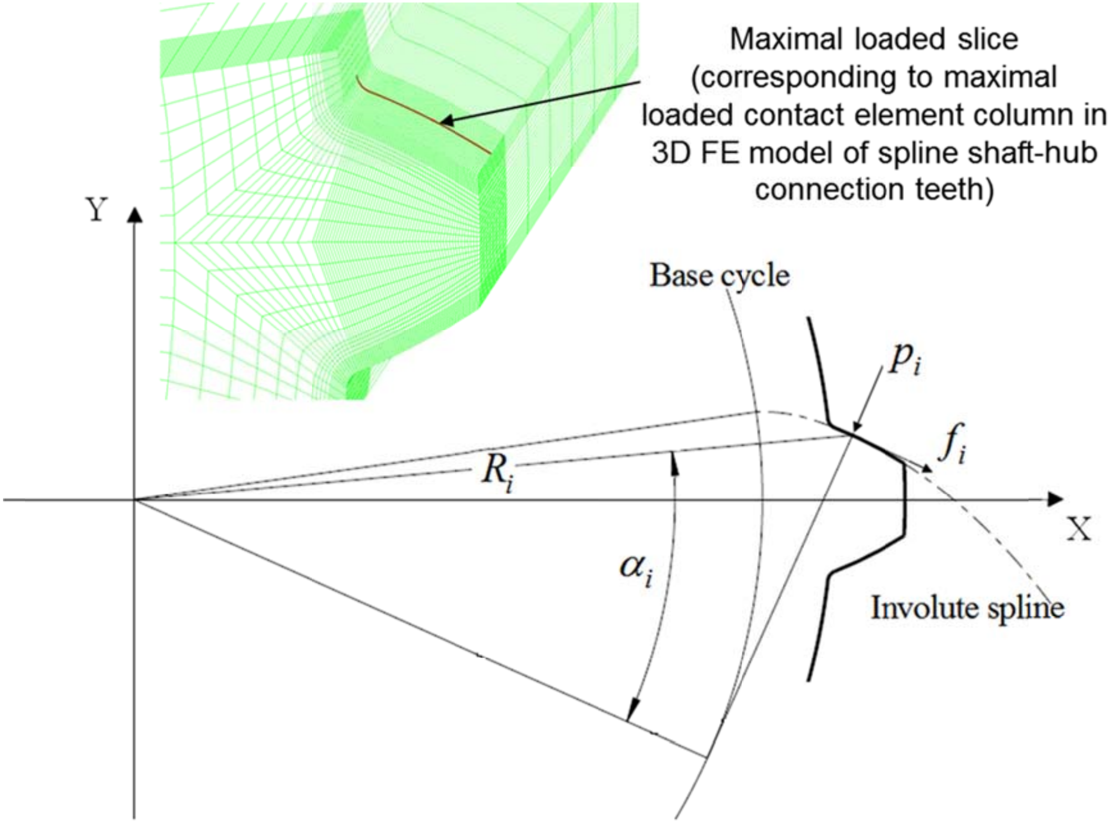

Figure 3-3: Calculation of equivalent load F for quasi-2D representative teeth pair

Table 3-1: Dynamic load F of 2D FE model

$R_F=F_u/F_o$ τ_t (MPa)		0,8	0,7	0,6	0,5	0,4	0,3	0,2
40,096	F_m(N)	1563,3	1476,1	1388,9	1301,7	1214,6	1127,5	1040,9
	F_a(N)	175,2	262,9	350,6	438,2	525,9	613,6	701
120,288	F_m(N)	4673,9	4413,3	4152,7	3892	3631,5	3371	3113,5
	F_a(N)	522,9	784,7	1046,7	1308,8	1571	1833,1	2093,3
200,48	F_m(N)	7763,6	7331,3	6898,5	6465,7	6032,2	5598,8	5183,3
	F_a(N)	865,7	1299,7	1734,3	2169,5	2605,4	3040,6	3484,2

Notes: 1. Spline shaft-hub connection DIN5480 45x2x30x21; 2. F_u: minimal load F, F_o: maximal load F, τ_t =T/W_t according to DIN5466 for corresponding spline shaft hub connection; 3.Material: hub-C35, shaft-25MoCr4

For the convenience of post processing and results comparison, all the concerned nodal results (especially along surface of spline flank) are read out from ANSYS and post processed in software package MATLAB. The direction of stress and strain exported from ANSYS are expressed in global coordinate system of FE model, but not related to the direction of spline teeth flank surface. In fatigue prediction model, especially the direction of critical plane and the direction of crack initiation must be expressed in the local coordinate system of a certain point along the teeth flank. Figure 3-4 shows the global coordinate and local coordinate system established for the spline teeth pair. The origin of the global coordinate system XOY is set to the center of spline shaft, the X axis match together with the bisector of the spline tooth. The origin of local coordinate system xoy lies on the surface of spline flank. The y_1 as well as y_2 axis of the local systems are vertical to the surface of the spline flank, their angle to the Y axis of the global coordinate system are β_1 and β_2 respectively. β_1 and β_2 will be calculated according to formula (3-2) ~(3-7), in these formulas, α_i is the pressure angle, r_i is radius vector at point i, r_b is radius of base circle, m is modulus, z is number of teeth, θ_i is the spread angle of involute spline, s_1 is tooth thickness along the pitch circle, x_1 is addendum coefficient, ϕ is the angle corresponding to half tooth thickness $s_1/2$. With angle β_i, the stress and strain status of a certain point on the spline teeth flank can be transferred from global coordinate system to their respective local coordinate system using formula (3-8) and (3-9).

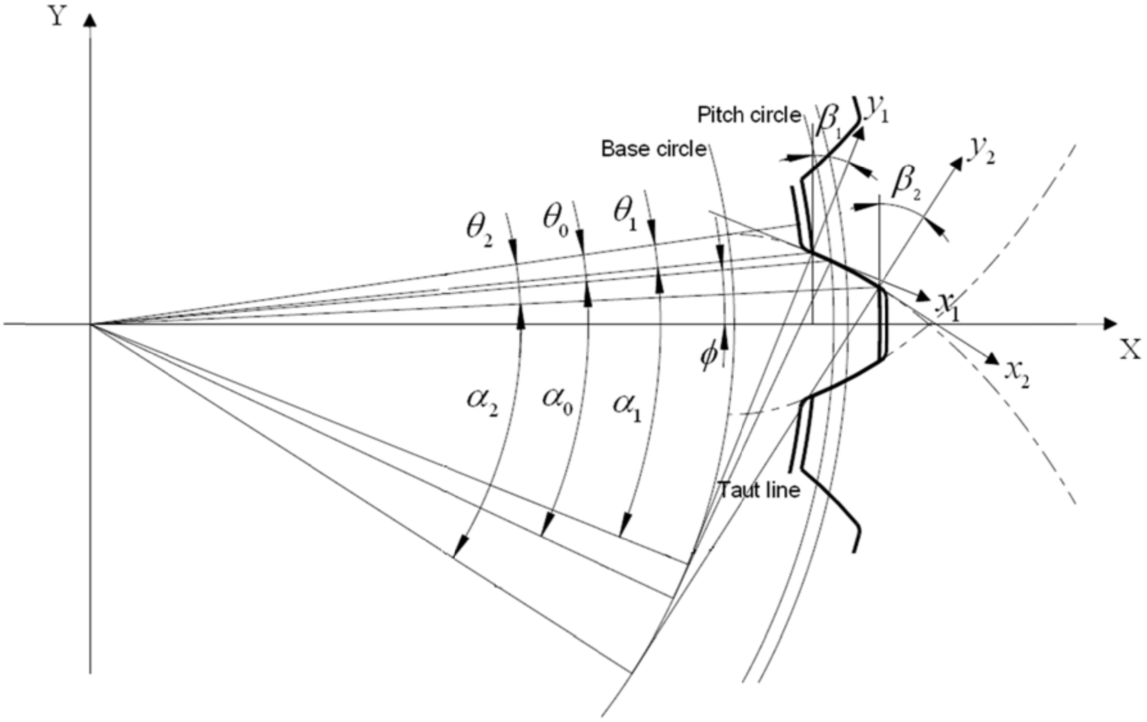

Figure 3-4: Global and local coordinate system of the involute spline teeth

$$\alpha_0 = 30^\circ \times \pi / 180^\circ \tag{3-2}$$

$$\alpha_i = arc\cos(r_b / r_i) = arc\cos(mz\cos\alpha_0 / 2r_i),\ i = 1, 2 \tag{3-3}$$

$$\theta_i = inv\alpha_i = \tan\alpha_i - \alpha_i\ ,\ i = 1, 2 \tag{3-4}$$

$$\theta_0 = inv\alpha_0 \tag{3-5}$$

$$\phi = s_1 / mz = (\pi / 2 + 2x_1 \tan\alpha_0) / z \tag{3-6}$$

$$\beta_i = \left[(\alpha_i + \theta_i) - (\phi + \theta_0)\right] \times 180 / \pi\ ,\ i = 1, 2 \tag{3-7}$$

$$\begin{bmatrix} \sigma_{x_i} & \tau_{x_i y_i} \\ \tau_{y_i x_i} & \sigma_{y_i} \end{bmatrix} = \begin{bmatrix} \cos\beta_i & -\sin\beta_i \\ \sin\beta_i & \cos\beta_i \end{bmatrix} \begin{bmatrix} \sigma_X & \tau_{XY} \\ \tau_{YX} & \sigma_Y \end{bmatrix} \begin{bmatrix} \cos\beta_i & \sin\beta_i \\ -\sin\beta_i & \cos\beta_i \end{bmatrix} \tag{3-8}$$

$$\begin{bmatrix} \varepsilon_{x_i} & \frac{1}{2}\gamma_{x_i y_i} \\ \frac{1}{2}\gamma_{y_i x_i} & \varepsilon_{y_i} \end{bmatrix} = \begin{bmatrix} \cos\beta_i & -\sin\beta_i \\ \sin\beta_i & \cos\beta_i \end{bmatrix} \begin{bmatrix} \varepsilon_X & \frac{1}{2}\gamma_{XY} \\ \frac{1}{2}\gamma_{YX} & \varepsilon_Y \end{bmatrix} \begin{bmatrix} \cos\beta_i & \sin\beta_i \\ -\sin\beta_i & \cos\beta_i \end{bmatrix} \tag{3-9}$$

Figure 3-5 showed the distribution of maximal principal stress and Von-mises stress (normalized by dividing the maximal value) along the shaft tooth flank under static load (positive value means tension stress and negative value means compression stress). The distribution of contact pressure indicates the start and end of contact zone along teeth flank. The value of Von-mises stress is always positive but lost the direction information and without distinguishing tension or compression. The value of maximal principal stress is positive at teeth fillet and changes to negative suddenly near the start of contact inside the contact zone, but it is still lack of relation to the direction of spline flank.

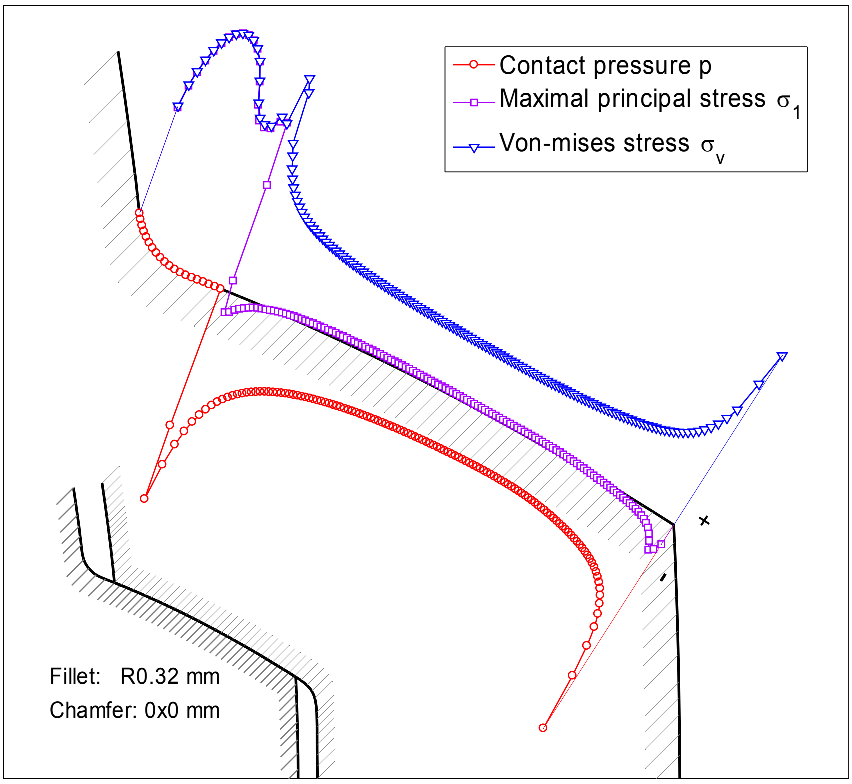

Figure 3-5: Distribution of maximal principal stress and Von-mises stress (normalized by dividing respective maximal value) along shaft teeth flank, F=8667.5N (5183.3+3484.2)

In order to catch the direction information of stresses and relate them to the direction of contact surface, stresses of every node along tooth flank are transformed in their respective local coordinate systems. Figure 3-6 showed the distribution of normal stress in tangential direction of teeth flank and normal stress in normal direction of teeth flank (normalized by dividing their respective maximal value) along shaft tooth flank. The normal stress in tangential direction of teeth flank is tension stress at tooth fillet; it changes to compression stress suddenly near the start of contact inside the contact zone, and then changes near to zero in the middle part of contact zone. The normal stress in normal direction of teeth flank should be equal to contact pressure distribution, small deviation showed in the figure is due to the error of numerical calculation.

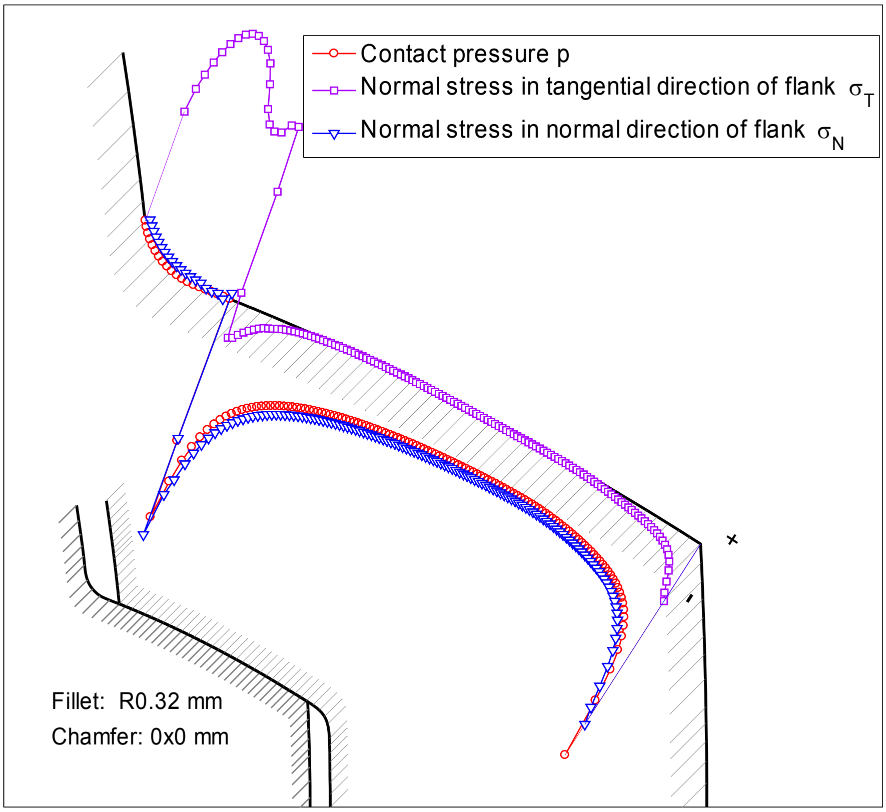

Figure 3-6: Distribution of normal stresses in tangential and normal direction of shaft teeth flank (normalized) along shaft teeth flank, F=8667.5N

3.3 Fretting/plain fatigue unified prediction model

3.3.1 Two fretting fatigue crack initiation processes

As reviewed in section 1.2, two crack initiation mechanisms of fretting fatigue are identified and assumed in existing fretting fatigue prediction models, especially the critical plane multiaxial fatigue based models: normal stresses governed tensile crack mechanism and shear stress governed extrusion-intrusion crack mechanism. The SWT model and its variants are based on the assumption that crack initiation is normal stresses governed, on the contrary, the FS model, SSR model, Dang Van model (mesoscopic) and their variants are based on the assumption that crack initiation is shear stress governed. But they still treated the fretting fatigue crack initiation mechanism as the same with plain fatigue crack initiation mechanism. The frictional energy based FFDP model and its variants, are more empirical and without considering the crack initiation mechanism, but which hypothesize that fretting fatigue is mainly a surface damage phenomenon. Early in 1980, based on the metallographic observation of fretted 4130 steel specimen, Gaul, D.J. and Duquette, D.J. described the process of fretting fatigue crack initiation as followings: “(1) subsurface cracking associated with rubbed surfaces leading to surface connected microcracks and spalling; (2) rougher surfaces in contact lead to deeper subsurface cracking under asperities; (3) link up of subsurface cracks leads to stress concentration and cracks deviate toward interior of alloy to become fatigue cracks” [Gau-80]. Based on this process description and above reviews, here we assumed two ‘situations’ of crack initiation process in fretted surface, as shown in Figure 3-7:

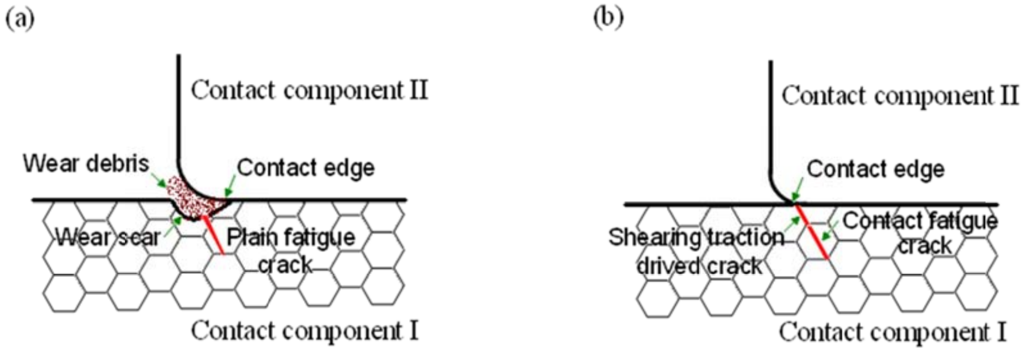

Figure 3-7: Assumptions of fretting fatigue crack initiation situation

(a). At first, the area near the contact edge forms a wear scar due to fretting, because the ‘micro notch‘ effect of this wear scar, the crack will be initiated the same as to the plain fatigue crack initiation mechanism;

The wear-SWT model and the updated wear-nucleation-propagation model from Madge, J.J. et al are based on this so called ‘contact evolution’ assumption [Mad-07a, Mad-07b, Mad-08]. The wear debris may come from particle detachment in gross slip area or sweep of not propagate micro cracks in partial slip area. The wear debris (named as ‘third body’) is discontinuously ejected from the contact interface, accelerate or retard the formation of wear scar [Bla-91]. Due to the ‘micro notch’ effect of the formed wear scar, the crack will initiate in the bottom of wear scar. This kind of situation is more favorable to an open mode (mode I) crack, so the tensile cracking SWT model is often used to predict the crack initiation. Considering the effect of fretting wear, the mSWT model and eFFDP model also try to multiply the frictional energy parameters with SWT parameter in their fretting fatigue models. By comparison, the wear evolution-SWT model seems more physically understandable, though it is very calculation intensive.

(b). Many micro cracks initiated on the slip-stick area of contact surface by the shear traction, when one of then coalesced with the micro crack initiated under the contact surface by the reversing shear stress, then the crack initiation phase finished.

As a contrast to situation a, it is observed that a fretting fatigue crack often initiates at the contact edge without substantial fretting wear in cases of relatively high contact pressure with small relative slip [Kon-04, Val-07]. For this kind of situation, we assumed a coalesced model.

Fretting fatigue is often modeled as an extension of contact problem including partial slip under tangential loading [Hil-94, Bre-02]. Analytical solution of simple geometries indentation showed that the maximal shear stress occurs under contact surface, cyclic contact load will result in reversing shear stress under contact surface and which will initiate crack under contact surface. In view of micromechanics, the subsurface crack will initiate along slip band (transgranular crack) and grain boundary (intergranular crack) propelled by the reversing shearing stresses under contact fatigue [Che-94, Fel-97]. At the same time, many micro cracks initiated in trailing edge of contact by the shear traction. The shear traction is greatly affected by the slip amplitude, as shown in Figure 3-8 [Jin-04], in partial slip zone, the shear traction is not great enough to sweep away the formed micro cracks. After a certain number of cycles, one of surface micro cracks coalesce with the subsurface contact fatigue micro crack, the initiation process of fretting fatigue finished.

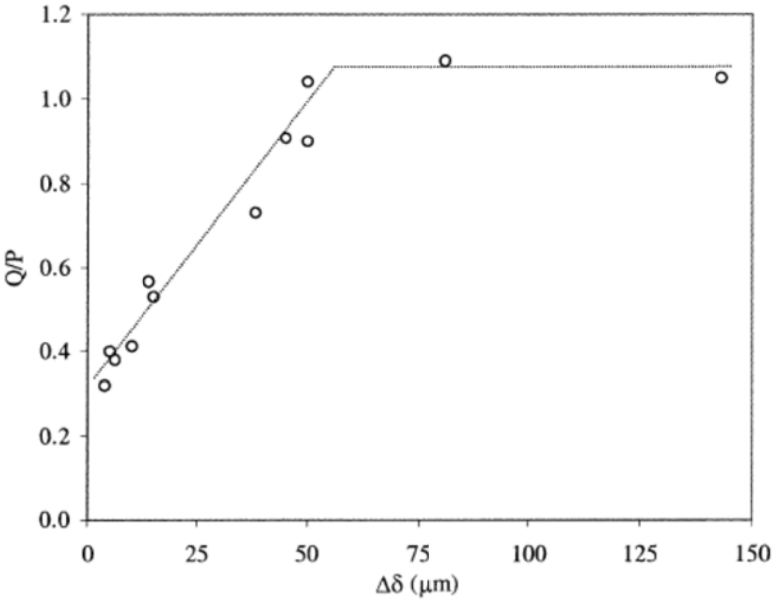

Figure 3-8: Change in the quasi-COF (Q/P) with increasing applied relative slip range [Jin-04]

3.3.2 Fretting/plain fatigue unified prediction parameter and location of crack initiation

Both fretting fatigue and plain fatigue can be roughly classified to the tensile crack mode governed fatigue mechanism and the shear crack mode governed fatigue mechanism. The difference is that the effects of fretting should be added to in fretting fatigue. So, the first requirement of the fretting/plain fatigue unified prediction parameter is that it should include these two fatigue mechanism. In order to be compatible to plain fatigue prediction, in the fretting/plain fatigue unified prediction model, the item of fretting effects should degenerate to 1 outside of contact zone, that's to say, the fretting/plain fatigue unified prediction model should degenerate to a pure plain fatigue prediction parameter outside of contact zone, which is the second requirement of the fretting/plain fatigue unified prediction model. In the existing energetic approach and critical plane multiaxial fatigue approach combined fretting fatigue prediction model like mSWT or eFFDP model, the tensile crack mode based SWT plain fatigue prediction parameter or shear crack mode based FS plain fatigue prediction parameter is already as a multiplier included in them, but unfortunately, none of them can fulfill the two requirements above at the same time.

Among all the fretting fatigue prediction models reviewed in section 1.2, it was verified by many researchers that the FFDP ($FFDP = \sigma_t \cdot \tau \cdot \delta$) model introduced by Ruiz is success in the prediction of fretting fatigue crack location, though it is a more empirical model. As a matter of fact, it also includes the effect of plain stress under contact surface in the tangential normal stress item σ_t and effects of frictional slip between contact surfaces in the rest items $\tau \cdot \delta$. It is based on the assumption that the growth of cracks developed from fretting surface damage is controlled by the tangential stress along the line of contact and crack is more likely to initiate in a region with tensile tangential stress compared to that with compressive tangential stress [Rui-84, He-89, Lin-97]. This assumption in FFDP model also implies that they think fretting fatigue crack initiation complies with the tensile normal stress governed fatigue mechanism. Figure 3-9 showed the distribution of σ_t , $(\tau\delta)$ and $(\sigma_t\tau\delta)$ along the interface of blade/disk contact of a dovetail joint, which showed good agreement between crack position and the maximal value of $(\sigma_t\tau\delta)$. In the exFFDP ($exFFDP = K_{FDP} \cdot \sigma_1$) as well as mFFDP ($mFFDP = \sigma_1 \cdot \int \tau_{fric} ds$) model, the tangential stress σ_t is replaced by the maximal principle stress σ_1 . The access difficult of tangential stress σ_t in some complex contact surfaces may be an explanation to this modification.

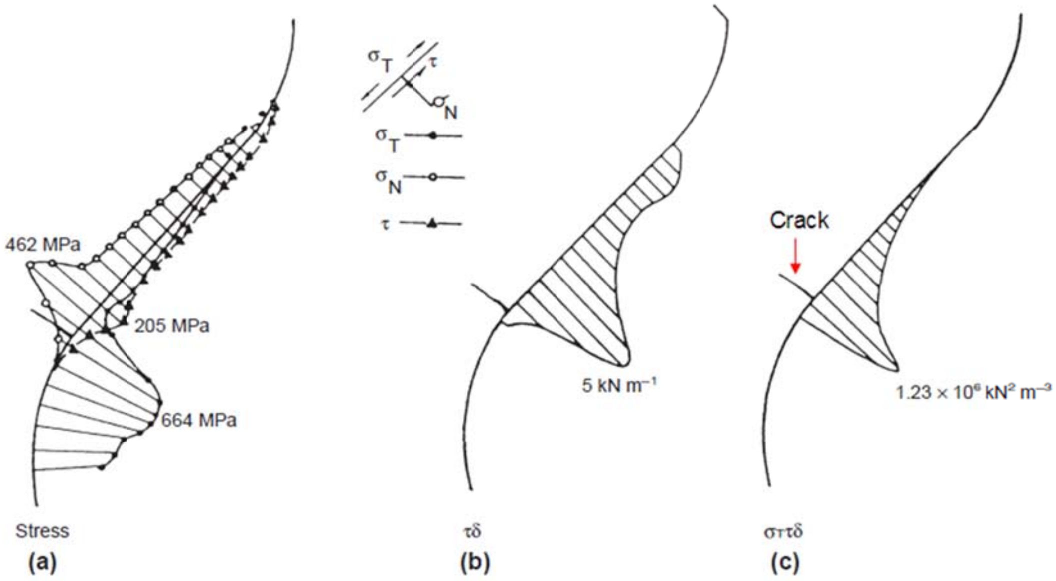

Figure 3-9: Distribution of σ_t , $(\tau\delta)$ and $(\sigma_t\tau\delta)$ along the interface of blade/disk contact of a dovetail joint under 40KN biaxial load [Lin-97].

Many of the fretting fatigue researches are implemented in a fretting pad + uniaxial tensioned specimen experiment configuration (as shown in Figure 3-10) [Hil-94, Ara-04], the normal stress in tangential direction of contact surface keeps in tension stress, so the sign of tangential stress σ_t and consequently FFDP or other prediction parameter in this kind of experiment configuration are rarely mentioned. But, in practical applications such as dovetail joint, spline or shrink fitted shaft hub connections, the tangential stress along the contact surface are generated by the bending of the 'specimen' (dovetail in dovetail joint, teeth in spline shaft-hub connections or shaft in shrink fitted shaft-hub connections) just because of the contact load on the specimen surface, the sign of tangential stress may change from positive to negative or vice versa along the specimen surface.

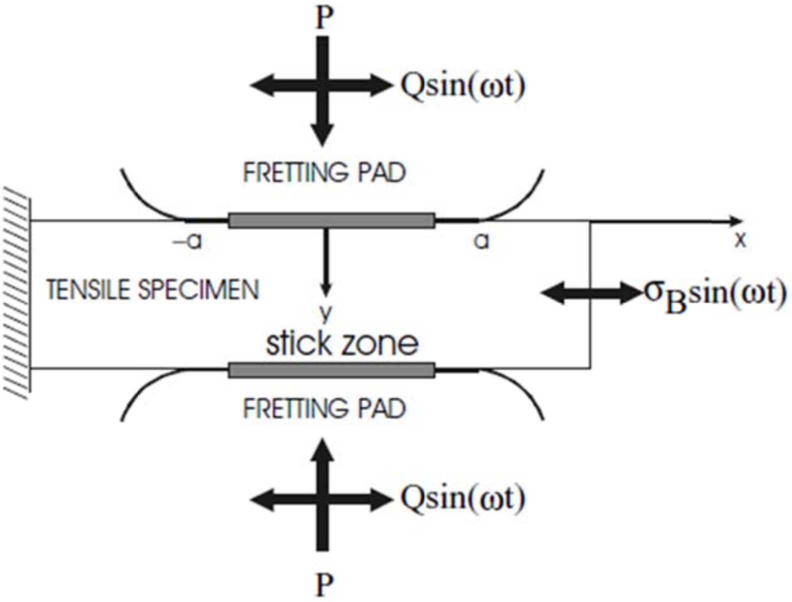

Figure 3-10: Schematic configuration of fretting fatigue tests [Ara-04].

Figure 3-11 showed the distribution of fretting damage parameter (FDP, $FDP = \tau_{fric} \cdot s$) and fretting fatigue damage parameter (FFDP, $FFDP = \sigma_{\tan} \cdot \tau_{fric} \cdot s$) along shaft teeth flank under dynamic load (F_m=5183.3N; R=0.2). The distribution of FDP along teeth flank is similar to the distribution of contact pressure, and without doubt, the value is not smaller than zero. Serious friction at both of the contact edge may leads to serious fretting wear but not bound leading to fatigue crack. The algebraic maximal value of FFDP occurs near the start of contact, and after that, the value of FFDP changed from positive to negative. Because the normal stress in tangential direction of flank $\sigma_{\tan}$ changed from tension to compression stress suddenly near the start of contact inside the contact zone. So, according to the distribution of FFDP along teeth flank, the most possible location of fretting fatigue crack is near the start of contact near teeth fillet. The FFDP under three different levels of load and load ratio predicted the same potential location of fretting fatigue, because the distribution of normal stress in tangential direction of flank remains similar under different levels of load. And it is easy to understand that they increase with the increase of load and load ratio.

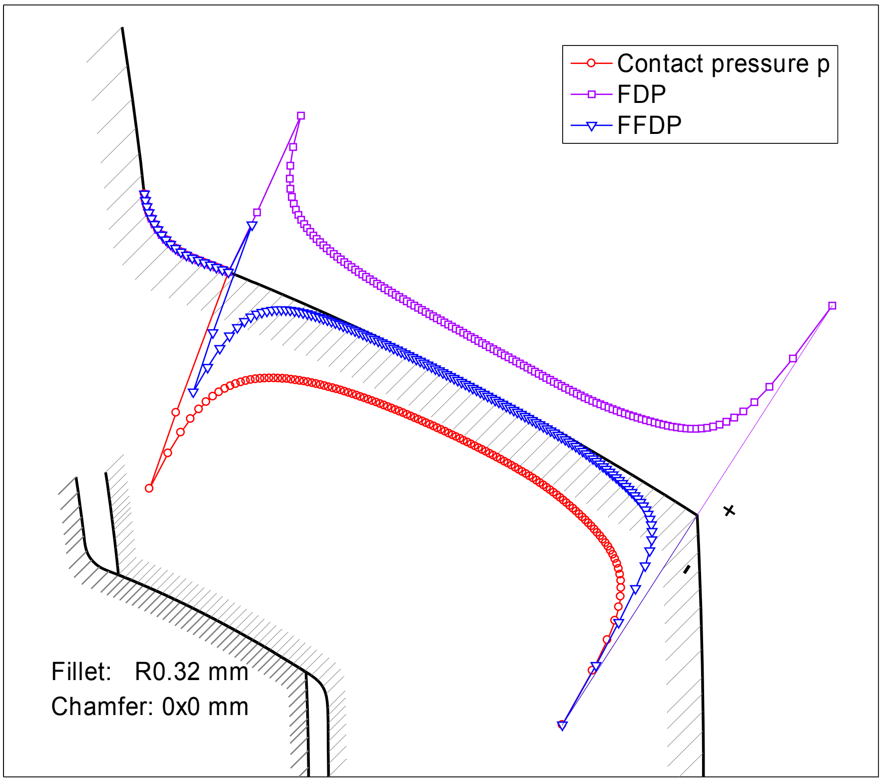

Figure 3-11: Distribution of FDP and FFDP (normalized by dividing respective maximal values) along shaft teeth flank, F_m=5183.3N; R_F=0.2.

The tangential stress σ_t in FFDP is only a static parameter, so the first modification is to replace the tangential stress σ_t in FFDP model with the tensile crack mode based critical plane fatigue prediction parameter SWT or the shear crack mode based critical plane fatigue prediction parameter FS. The SWT parameter uses the product of normal strain amplitude $\Delta\varepsilon/2$ and maximal normal stress $\sigma_{\max}$ in critical plane to determine the initiation life of tensile mode crack governed fatigue [Smi-70]. The most often used form of SWT parameter in the critical plane is the form proposed by Socie [Soc-87]:

$$SWT = \sigma_{\max}\frac{\Delta\varepsilon}{2} = \frac{\left(\sigma_f^{'}\right)^2}{E}\left(2N_f\right)^{2b} + \sigma_f^{'}\varepsilon_f^{'}\left(2N_f\right)^{b+c} \tag{3-10}$$

where, $\Delta\varepsilon$ is the difference between the maximum and the minimum normal strain of the same plane in a cycle, $\sigma_{\max}$ is the maximum normal stress in this plane, the critical plane is the one that experiences the maximal value of the product $\sigma_{\max}\Delta\varepsilon$. $\sigma_f^{'}$ and b are the fatigue strength coefficient and exponent, $\varepsilon_f^{'}$ and c are the fatigue ductility coefficient and exponent, N_f is the number of cycles to initiate a crack of a certain length. The SWT parameter is applied to tensile loading, and is set to zero for compressive stresses, that's to say there's no fatigue when $\sigma_{\max} < 0$. Which agree with the opinion in FFDP model that "crack is more likely to initiate in a region with tensile tangential stress compared to that with compressive tangential stress". The FS parameter is expressed as a function of maximal shear strain amplitude $\Delta\gamma_{\max}/2$ and maximal normal stress $\sigma_n^{\max}$ acting on the maximal shear strain plain in a cycle [Fat-88]:

$$FS = \frac{\Delta\gamma_{\max}}{2} \cdot \left(1 + k \cdot \frac{\sigma_n^{\max}}{\sigma_y}\right) = \frac{\tau_f^{'}}{G}\left(2N_f\right)^{b_0} + \gamma_f^{'}\left(2N_f\right)^{c_0} \tag{3-11}$$

where k is a material constant that approaches 1 for long lives and reduced for shorter lives, σ_y is the yield strength of material. $\tau_f^{'}$ is shear fatigue strength coefficient, G is the shear modulus and, b_0 shear fatigue strength exponent, $\gamma_f^{'}$ is shear fatigue ductility coefficient, c_0 is shear fatigue ductility exponent, N_f is the number of cycles to initiate a crack. In the shear cracking Fatemi & Socie (FS) plain fatigue prediction parameter, the secondary item $\sigma_n^{\max}$ reflects the influence of normal stress on the crack plane. The mathematic form of FS parameter implied that tensile normal stress on the maximum shear plane is more benefit to initiate a crack than a compressive normal stress on the maximum shear plane. Here, we assume that the compressive normal stress on the maximum shear plane have no influence to the initiation of a crack, that's to say the secondary item in FS parameter equal zero when $\sigma_n^{\max} \le 0$ .This is also consistent with the assumption in FFDP model 'the tangential stress along the line of contact and crack is more likely to initiated in a region with tensile tangential stress compared to that with compressive tangential stress'.

Obviously, the items $\tau \cdot \delta$ in FFDP model that include effects of frictional slip between contact surfaces do not degenerate to 1 but equal to zero outside of contact zone. The expanded FFDP model ($exFFDP = K_{FDP} \cdot \sigma_1$) from Odendorf, U [Old-99, Old-01] introduced an empirical fretting effect factor K_{FDP} (it is β_{KC} in original literature, here renamed as K_{FDP} to avoid confuse) by fitting experimental results between fretting damage, micro slip and contact pressure. The fretting factor K_{FDP} happens to have the characteristic that it degenerate to 1 when sliding distance or contact pressure equal to zero. The relative fretting damage curve and corresponding function expression of fretting effect factor by fitting experimental data are shown as following.

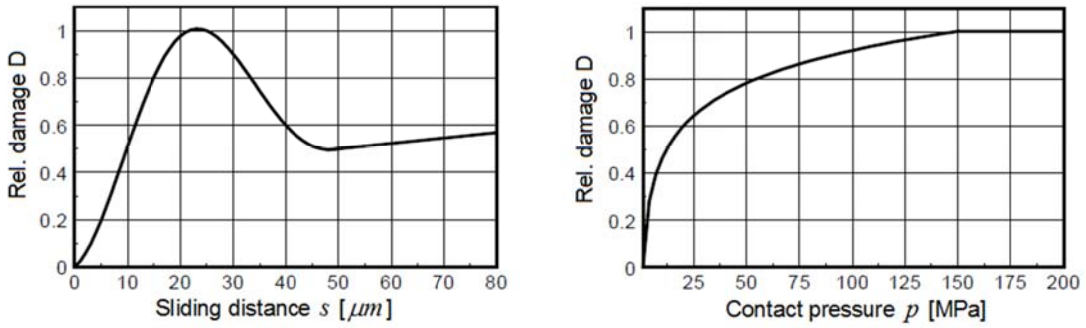

Figure 3-12: Relative fretting damage related to sliding distance and contact pressure [Old-01]

$$\begin{array}{l|l} D(s) = -\frac{2}{3} \cdot e^{-0.0277 \cdot s} \cdot \cos(\frac{2 \cdot \pi}{50} \cdot s) + \frac{2}{3} & 0 \le s \le 50 \\ D(s) = \frac{1}{2} + \frac{3}{1000} \cdot (s - 50) & 50 < s \end{array} \tag{3-12}$$

$$\begin{array}{l|l} D(p) = \frac{2}{10} \cdot \ln(p) & 0 \le p \le 150 \\ D(p) = 1 & 150 < p \end{array} \tag{3-13}$$

$$K_{FDP} = \hat{K}_{FDP} \cdot D(s) \cdot D(p) + 1 \tag{3-14}$$

where D is relative fretting damage related to sliding distance s or contact pressure p, K_{FDP} is the relative fretting damage factor, $\hat{K}_{FDP}$ is the maximal fretting damage factor under the fretting condition that $s = 25\mu m$ and $p \ge 150 MPa$, which dependent on the material characteristics of the contact pair. For the normalized C45 material shaft and cold-drawn key in key shaft-hub connection investigated by Odendorf, U., the change of fretting damage factor K_{FDP} related to the sliding distance and contact pressure is shown in Figure 3-13. So, the second reasonable modification is to replace the frictional slip effect items $\tau \cdot \delta$ in FFDP model with the fretting effect factor K_{FDP}.

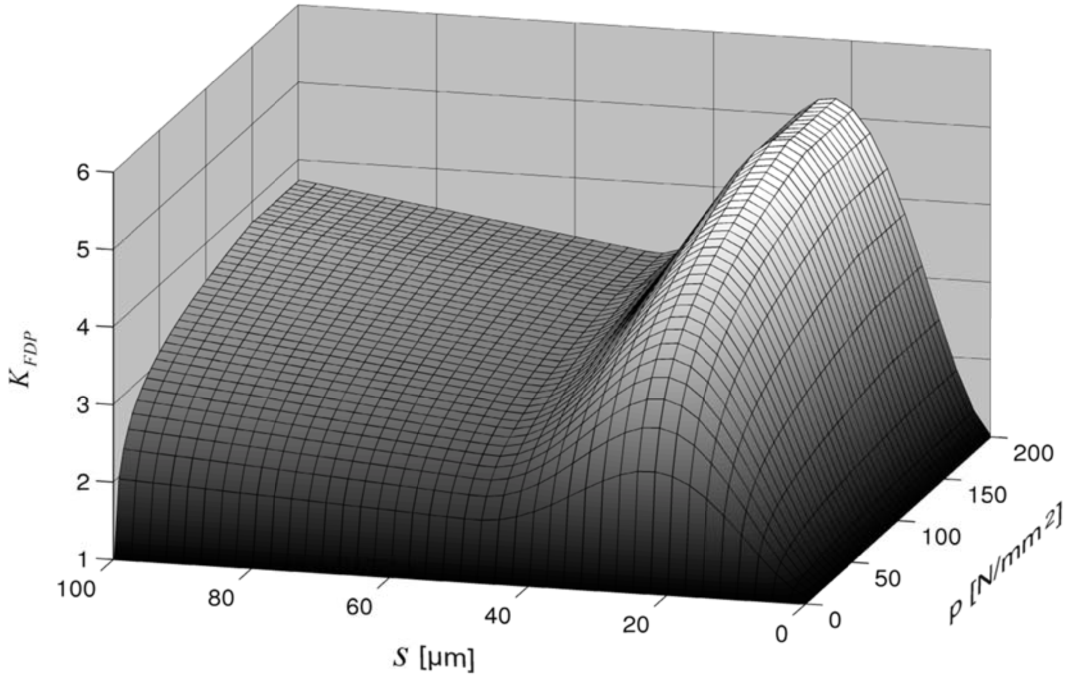

Figure 3-13: Fretting damage factor related to sliding distance and contact pressure [Old-01]

Above two modifications lead to the tensile crack mode fretting/plain fatigue unified prediction parameter $K_{FDP}SWT$:

$$K_{FDP}SWT = K_{FDP}\sigma_{\max}\frac{\Delta\varepsilon}{2} \tag{3-15}$$

and the shear crack mode fretting/plain fatigue unified prediction parameter $K_{FDP}FS$:

$$K_{FDP}FS = K_{FDP}\cdot\frac{\Delta\gamma_{\max}}{2}\cdot\left(1+k\cdot\frac{\sigma_n^{\max}}{\sigma_y}\right) \tag{3-16}$$

The strategy of above modelling efforts is shown as following:

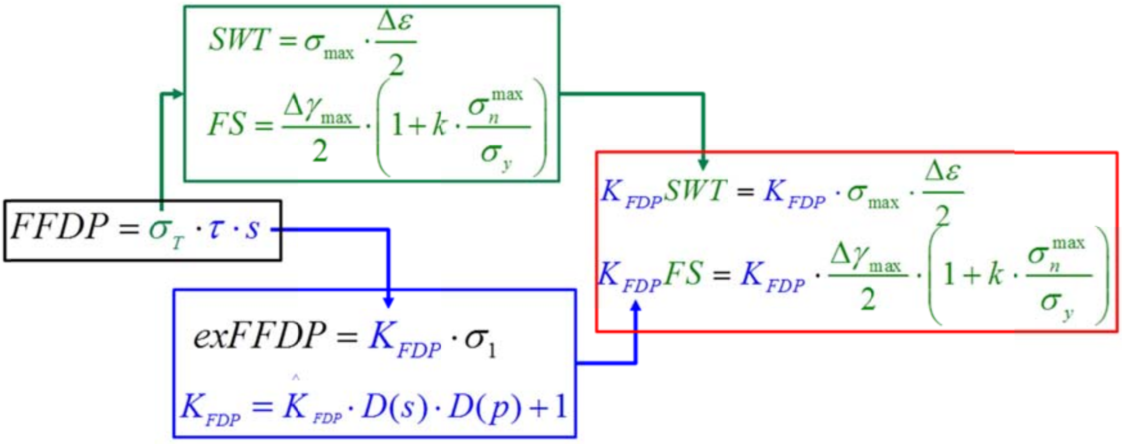

Figure 3-14: Modeling strategy of the fretting/plain fatigue unified prediction parameter

Figure 3-15 to Figure 3-20 show the distribution of $K_{FDP}SWT$ and $K_{FDP}FS$ parameter along shaft teeth flank under different load, as a comparison, the pure plain fatigue prediction SWT and FS parameter along the teeth flank are also calculated out and showed in these figures. The maximum of $K_{FDP}SWT$ as well as SWT parameter occurs at the teeth fillet of shaft teeth, the second peak values occur near the start of contact. Because the maximal normal stress $\sigma_n^{\max}$ in the critical plane in the zone after start of contact is much smaller than that in the teeth fillet, the SWT and $K_{FDP}SWT$ parameter in this zone is near to zero, the danger of tensile crack mode fatigue do not increase due to fretting. On the contrary, the value of shear mode crack unified fatigue parameter $K_{FDP}FS$ increased in the contact zone compared to the pure plain fatigue prediction parameter FS, especially under the load F_m=3113.5N; R_F=0.2.But it is still not great enough to succeed the value at teeth fillet, the most danger location of shear mode fatigue crack is also at tooth fillet under this load case. Under dynamic load with small vibration amplitude, the effects of fretting is very small both for the tensile mode crack unified fatigue parameter $K_{FDP}SWT$ and shear mode crack unified fatigue parameter $K_{FDP}FS$, the predicted locations of fatigue crack both by $K_{FDP}SWT$ and $K_{FDP}FS$ are always at tooth fillet, without great difference to the distribution of pure SWT and FS parameter. Overall, the maximal value of $K_{FDP}SWT$ occurs always at (shaft) teeth fillet; the maximal value of $K_{FDP}FS$ occurs still at teeth fillet though it may be greatly increased near the contact edge due to the effect of fretting under some favorite dynamic loads.

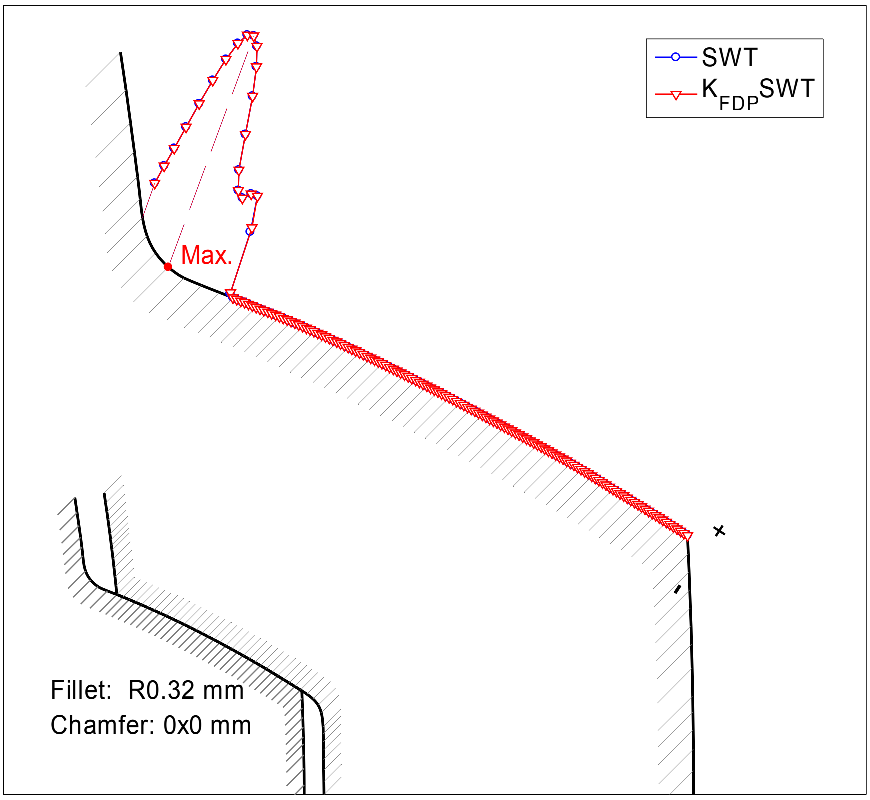

Figure 3-15: Distribution of SWT, K_{FDP}SWT parameter along shaft teeth flank (normalized by dividing respective maximal values), F_m=1040.9N; R_F=0.2.

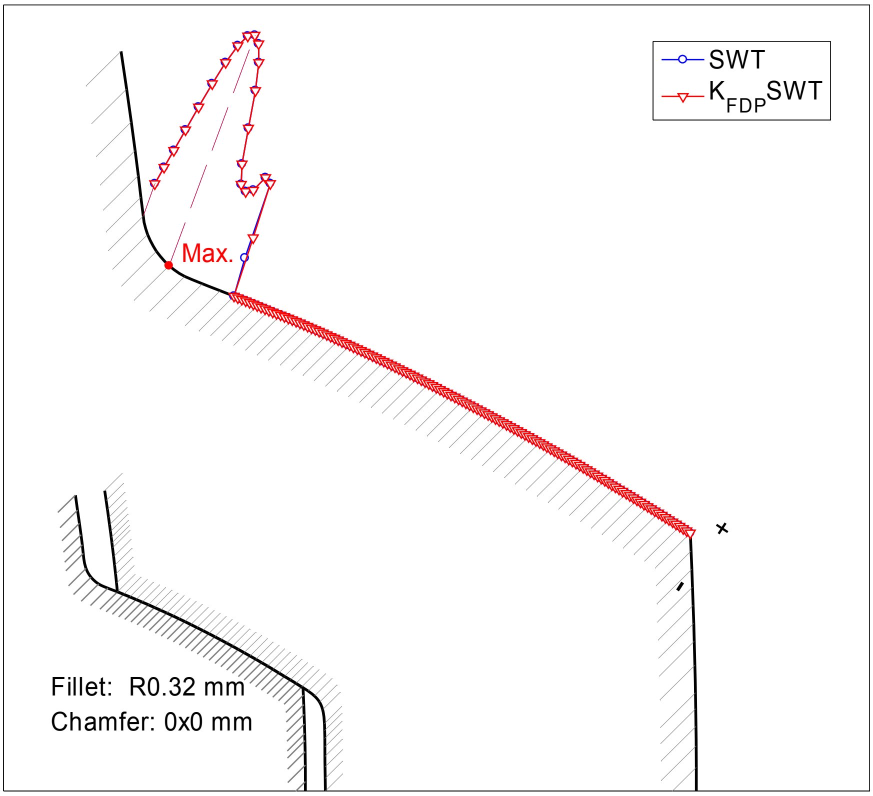

Figure 3-16: Distribution of SWT, K_{FDP}SWT parameter along shaft teeth flank (normalized by dividing respective maximal values), F_m=3113.5N; R_F=0.2.

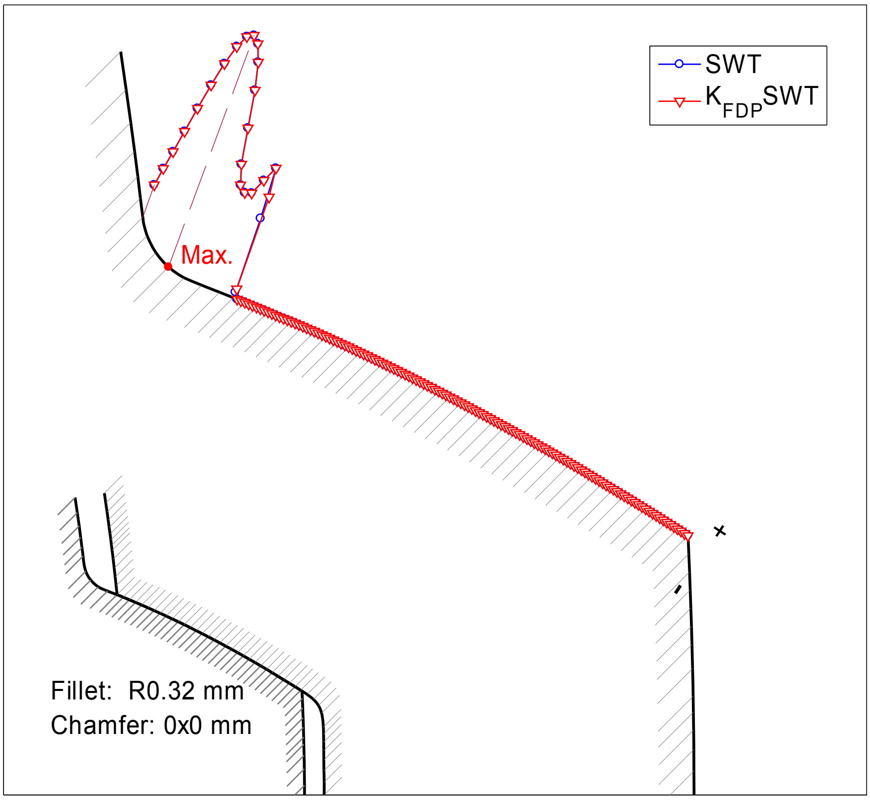

Figure 3-17: Distribution of SWT, K_{FDP}SWT parameter along shaft teeth flank (normalized by dividing respective maximal values), F_m=5183.3N; R_F=0.2.

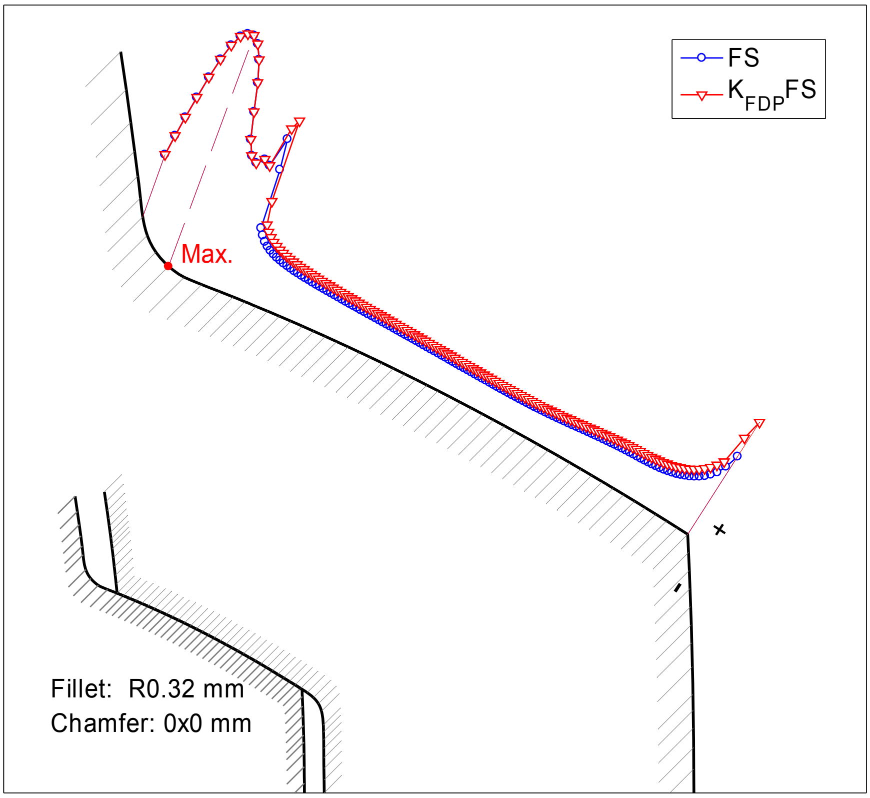

Figure 3-18: Distribution of FS, K_{FDP}FS parameter along shaft teeth flank (normalized by dividing respective maximal values), F_m=1040.9N; R_F=0.2.

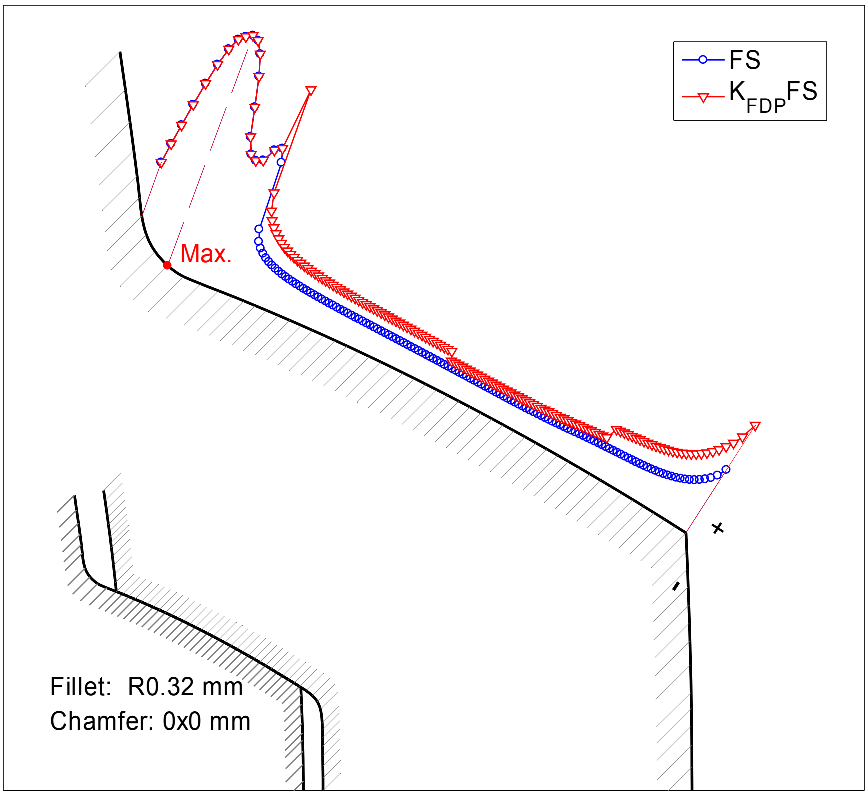

Figure 3-19: Distribution of FS, K_{FDP}FS parameter along shaft teeth flank (normalized by dividing respective maximal values), F_m=3113.5N; R_F=0.2.

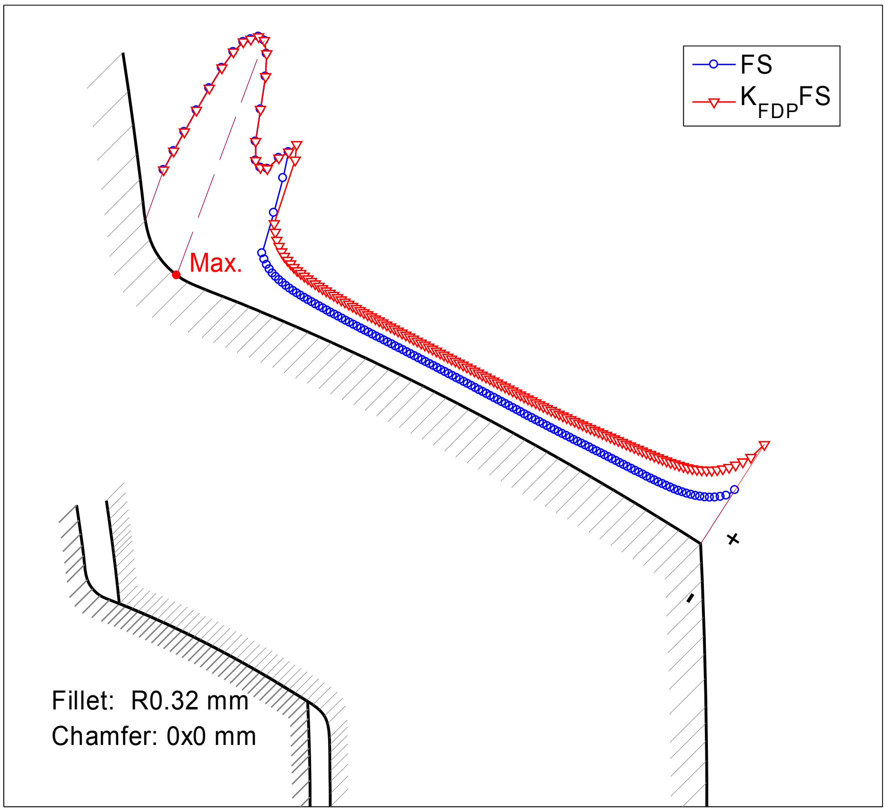

Figure 3-20: Distribution of FS, K_{FDP}FS parameter along shaft teeth flank (normalized by dividing respective maximal values), F_m=5183.3N; R_F=0.2.

3.3.3 Crack orientation prediction

As reviewed in section 1.3, the growth of both plain fatigue crack and fretting fatigue crack is divided to the shear mode stage and tensile mode stage in microscopic. For the shear mode dominated crack, the macroscopically exhibited crack orientation is the shear mode crack initiation orientation, and determined mainly by the shear stress/strain mode parameters. For the tensile mode dominated crack, the crack initiation stage is negligible; the macroscopically exhibited crack orientation is the tensile mode crack growth orientation. Here, we define the angle θ_c as the angle between the crack orientation and the normal of the teeth flank surface, at the location of crack initiation, as showed in Figure 3-21, it is measured counterclockwise.

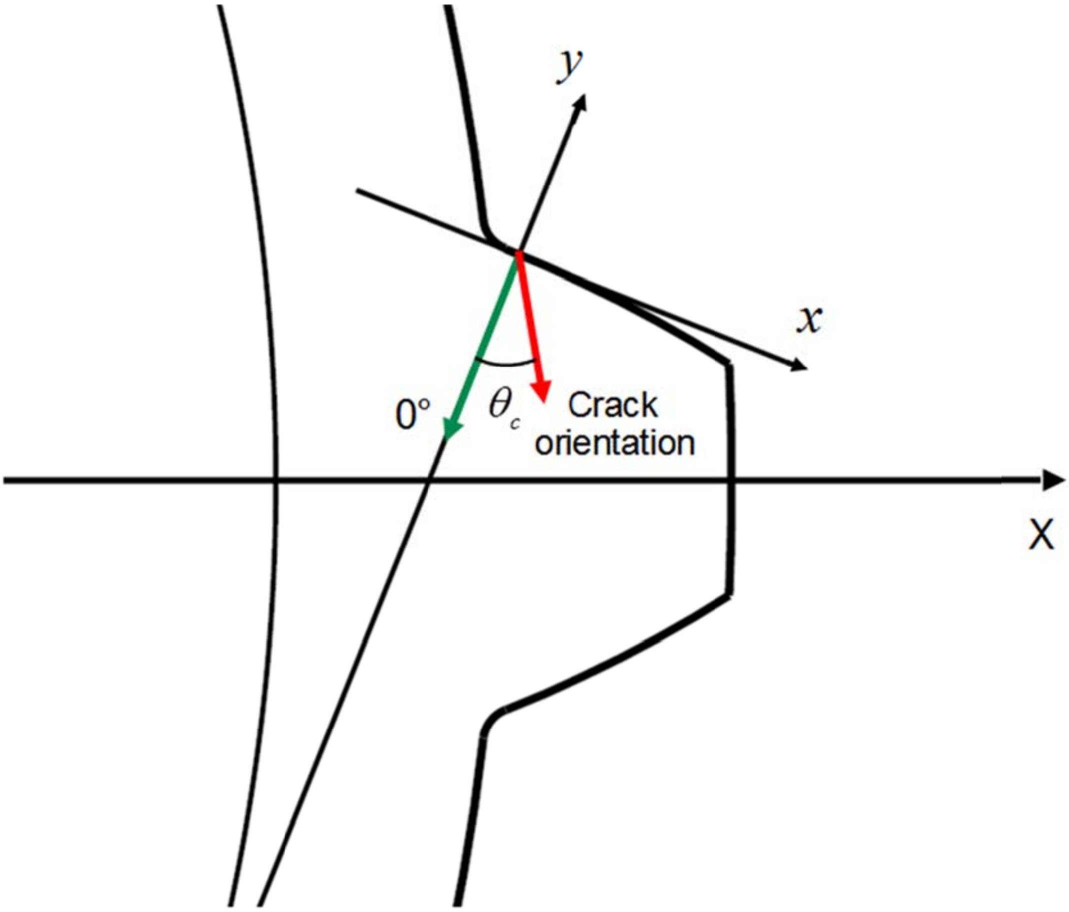

Figure 3-21: Definition of crack orientation

The tensile crack mode SWT parameter and shear crack mode FS parameter are used to determine the orientation of tensile mode dominated fatigue crack and shear mode dominated fatigue crack respectively. Above critical plane based parameters will be calculated in all the direction range from -90^0 to 90^0 (in space of 2.5^0) using the stress and strain data obtained by FE calculations to search the maximal value of these parameters and corresponding critical direction angles θ_c. The stress and strain status on every inclined plane will be transformed using formula (3-17) and (3-18).

$$\begin{bmatrix} \sigma_{x_{\theta_c}} & \tau_{x_{\theta_c} y_{\theta_c}} \\ \tau_{y_{\theta c} x_{\theta_c}} & \sigma_{y_{\theta_c}} \end{bmatrix} = \begin{bmatrix} \cos\theta_c & \sin\theta_c \\ -\sin\theta_c & \cos\theta_c \end{bmatrix} \begin{bmatrix} \sigma_x & \tau_{xy} \\ \tau_{yx} & \sigma_y \end{bmatrix} \begin{bmatrix} \cos\theta_c & -\sin\theta_c \\ \sin\theta_c & \cos\theta_c \end{bmatrix} \tag{3-17}$$

$$\begin{bmatrix} \varepsilon_{x_{\theta_c}} & \frac{1}{2}\gamma_{x_{\theta_c} y_{\theta_c}} \\ \frac{1}{2}\gamma_{y_{\theta_c} x_{\theta}} & \varepsilon_{y_{\theta_c}} \end{bmatrix} = \begin{bmatrix} \cos\theta_c & \sin\theta_c \\ -\sin\theta_c & \cos\theta_c \end{bmatrix} \begin{bmatrix} \varepsilon_x & \frac{1}{2}\gamma_{xy} \\ \frac{1}{2}\gamma_{yx} & \varepsilon_y \end{bmatrix} \begin{bmatrix} \cos\theta_c & -\sin\theta_c \\ \sin\theta_c & \cos\theta_c \end{bmatrix} \tag{3-18}$$

Under most of the dynamic loads, the location of fatigue crack predicted by the fretting/plain fatigue unified prediction parameter in section 3.3.2 is at teeth fillet, the crack is a pure plain fatigue crack. The normal of the fillet surface will be through the fillet centre. Under dynamic load F_m=5183.3N; R_F=0.2, the crack orientation predicted by SWT parameter is 0^0, as shown in Figure 3-22, change the magnitude of dynamic load will not affect the crack orientation predicted by SWT parameter. Both the maximal K_{FDP}SWT and K_{FDP}FS occur at teeth fillet, but usually they do not fall in the same point in the same dynamic load case, the location of maximal K_{FDP}FS is a little bit close to the contact edge. As shown in Figure 3-22 and Figure 3-25, the normal at the location of maximal K_{FDP}SWT is 42^0 to the vertical direction and the normal at the location of maximal K_{FDP}FS is 37^0 to the vertical direction. The crack orientation predicted by FS parameter is 40^0 under dynamic load F_m=1040.9N; R_F=0.2, as shown in Figure 3-23, with the increase of maximal load, the crack orientation predicted by FS parameter will move close to the orientation predicted by SWT parameter, as shown from Figure 3-23 to Figure 3-25, which means the effect of normal stress will exceed the effect of shear stress under heavy load. Keeping the maximal load in constant, the change of load ratio will not affect the crack orientation predicted by both of the two parameters.

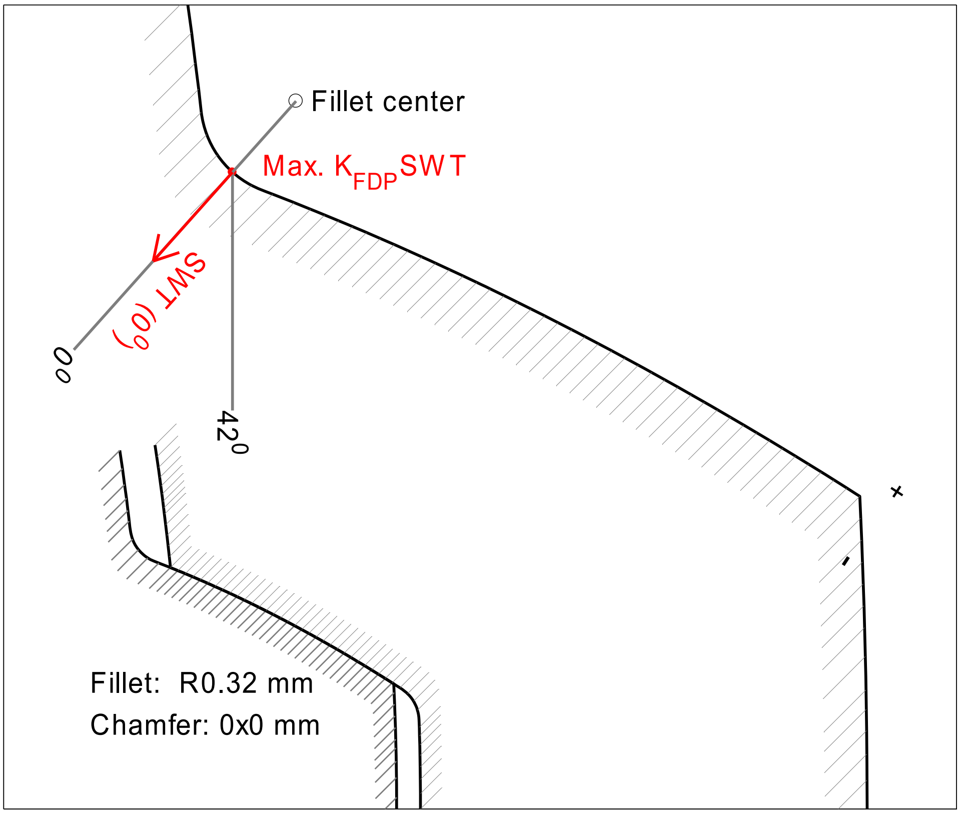

Figure 3-22: Crack orientation predicted by SWT parameter, F_m=5183.3N; R_F=0.2.

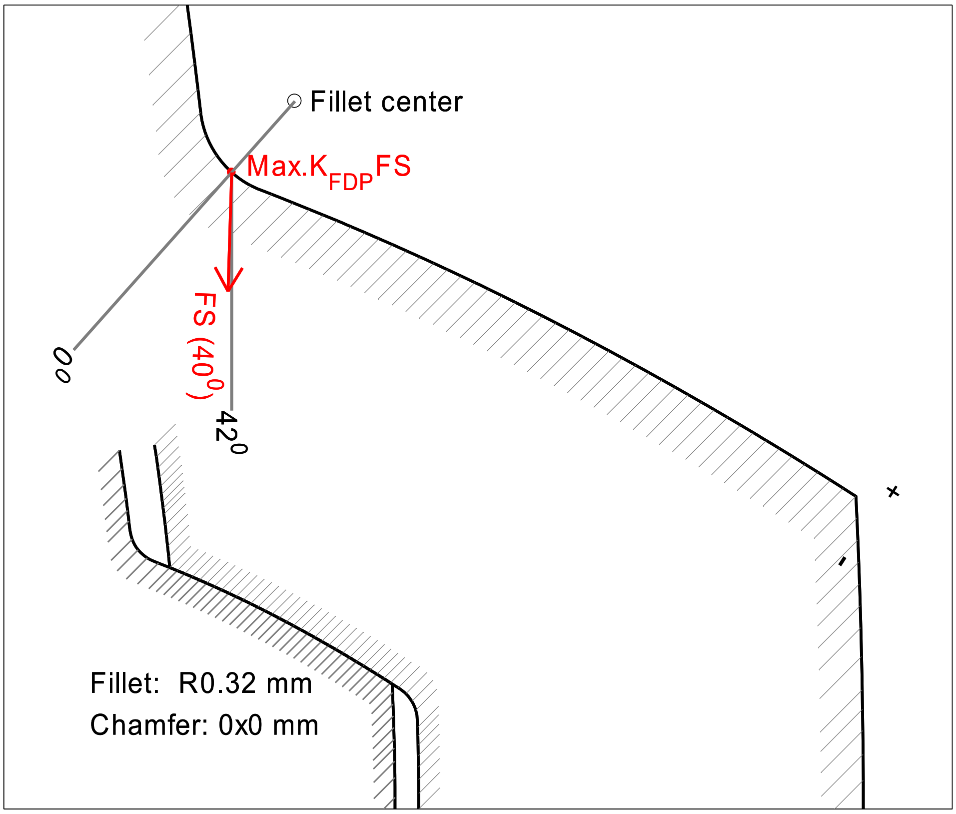

Figure 3-23: Crack orientation predicted by FS parameter, F_m=1040.9N; R_F=0.2.

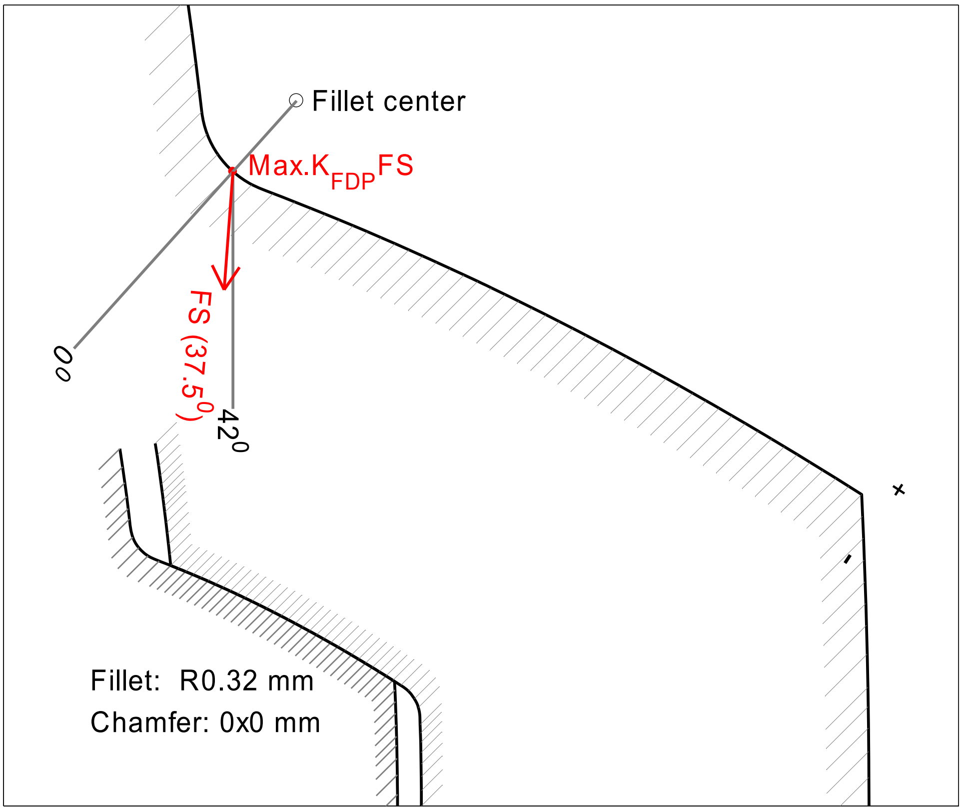

Figure 3-24: Crack orientation predicted by FS parameter, F_m=3113.5N; R_F=0.2.

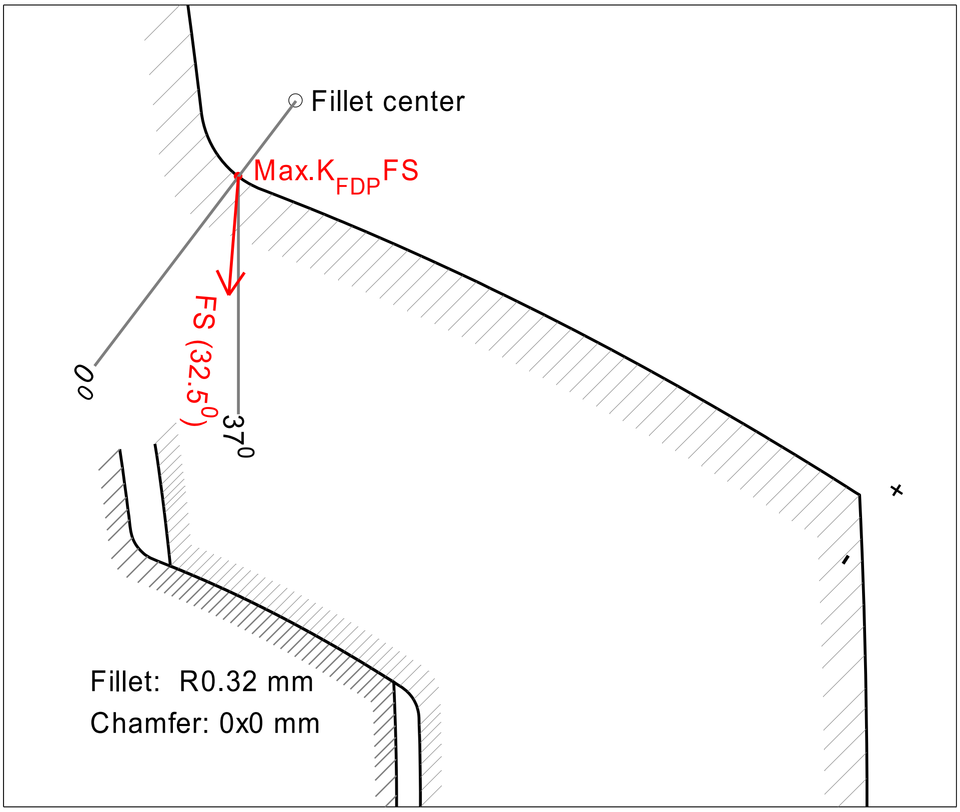

Figure 3-25: Crack orientation predicted by FS parameter, F_m=5183.3N; R_F=0.2.

3.3.4 Fatigue life prediction

In the formulations of SWT and FS parameters (as shown in equation (3-10) and (3-11)) include the strain-life format. We assume this strain-life formulation is still valid for the fretting/plain fatigue unified prediction parameter K_{FDP}SWT and K_{FDP}FS. To include the stress gradient and microstructural effects near the crack initiate surface (so called 'critical layer'), a numerically averaging method introduced by Araùjo, J.A. and Nowell, D. [Ara-02] is also implemented here. The multiaxial critical plane fatigue parameter SWT or FS will be averaged along the crack orientation θ_c determined above over a characteristic length l_c, as shown in Figure 3-26.

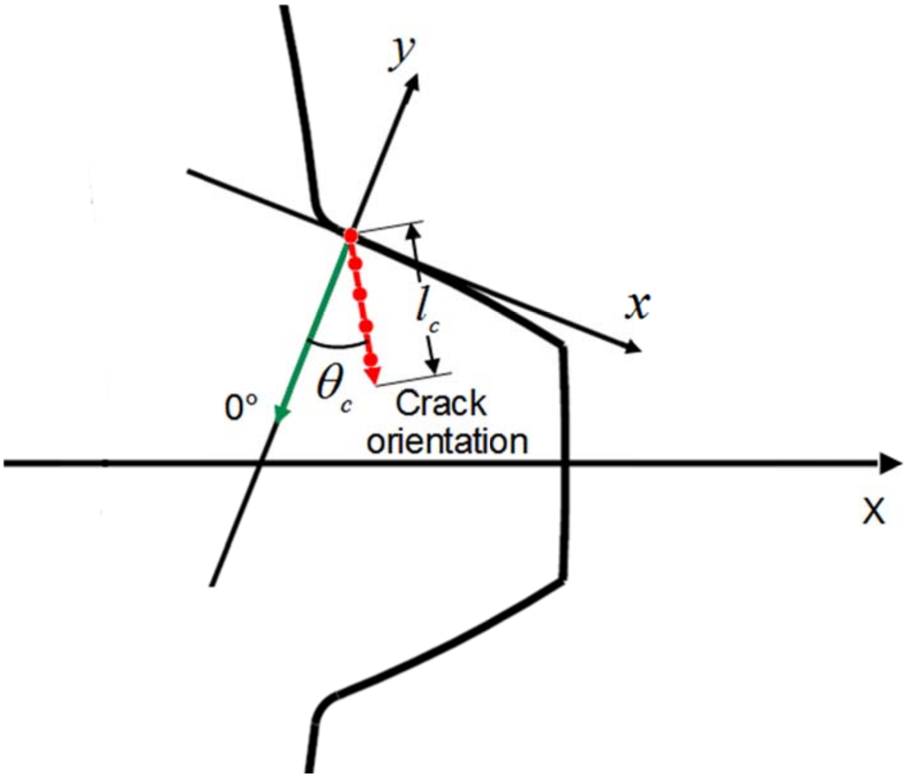

Figure 3-26: Characteristic length l_c along crack orientation

The characteristic length l_c related to the microstructure parameters such as grain size of surface layer. Here we assume that $l_c = 0.2mm$, about size of 3~4 austenite grains according to research of Angelika Brückner-Foit et. al.[Ang-06]. The tensile crack mode fretting/plain fatigue unified prediction parameter will be further formulated as following:

$$SWT_i = \sigma_{\max,i} \frac{\Delta\varepsilon_i}{2} \tag{3-19}$$

$$SWT_m = \frac{1}{n}\sum_{i=1}^{n} SWT_i \tag{3-20}$$

$$K_{FDP} \cdot SWT_m = \frac{\left(\sigma_f^{'}\right)^2}{E}\left(2N_f\right)^{2b} + \sigma_f^{'}\varepsilon_f^{'}\left(2N_f\right)^{b+c} \tag{3-21}$$

where SWT_i is the SWT parameter of node i in the crack path. And the shear crack mode fretting/plain fatigue unified prediction parameter will be further formulated as following:

$$FS_i = \frac{\Delta\gamma_{\max,i}}{2} \cdot \left(1 + k \cdot \frac{\sigma_{n,i}^{\max}}{\sigma_y}\right) \tag{3-22}$$

$$FS_m = \frac{1}{n}\sum_{i=1}^{n} FS_i \tag{3-23}$$

$$K_{FDP} \cdot FS_m = \frac{\tau_f^{'}}{G}\left(2N_f\right)^{b_0} + \gamma_f^{'}\left(2N_f\right)^{c_0} \tag{3-24}$$

where FS_i is the FS parameter of node i in the averaging path.

The fatigue cyclic properties of material 25MoCr4 and C35 that used in this study are not available. Based on the tensile strength and E-modulus, Bäumel, A. Jr. et. al. provide a formula to estimate the fatigue cyclic properties of metal materials[Bäu-90], according to their formula, the fatigue cyclic properties of 25MoCr4 and C35 are calculated in table 3-2. Since the cyclic shear fatigue data were unavailable, the constants were approximated from uniaxial fatigue tests [Mih-09]:

$$\tau_f^{'} = \frac{\sigma_f^{'}}{\sqrt{3}}, \; b_0 = b \tag{3-25}$$

$$\gamma_f^{'} = \sqrt{3}\varepsilon_f^{'}, \; c_0 = c \tag{3-26}$$

Table 3-2: Estimated fatigue cyclic properties of 25MoCr4 and C35

Material Properties	25MoCr4 (DIN 1.7325)	C35 (DIN 1.0501)
Tensile strength R_m (MPa)	980~1370	550~780
Yield strength σ_y (MPa)	540~735	320~430

E-Modulus (MPa)	210000	210000
Fatigue strength coefficient $\sigma_f^{'} = 1.5R_m$ (MPa)	1762.5	997.5
Fatigue strength exponent $b = -0.087$	-0.087	-0.087
Fatigue ductility coefficient $\varepsilon_f^{'} = 0.59\psi$, $\psi = 1.0$ for $R_m \le 630$; $\psi = 1.375 - 125 \cdot R_m / E$ for $R_m > 630$;	0.398	0.578
Fatigue ductility exponent c =-0.58	-0.58	-0.58

Table 3-3: Predicted fatigue life of spline shaft teeth (normalized) under different dynamic loads with same load ratio

Dynamic load	l_c Fatigue life prediction	0.2mm	0.3mm	0.4mm
F$_m$=1743.6N; R$_F$=0.2	SWT_m (θ_c =0°)	0.1754	0.1337	0.1079
	N_{f1}	>10^8	>10^8	>10^8
	FS_m (θ_c = 40°)	0.0013	0.0011	0.00097
	N_{f2}	>10^8	>10^8	>10^8
F$_m$=3113.5N; R$_F$=0.2	SWT_m (θ_c =0°)	1.5822	1.2066	0.9748
	N_{f1}	2.79x10^5	9.02x10^5	3.4432x10^6
	FS_m (θ_c = 37.5°)	0.0045	0.0037	0.0033
	N_{f2}	1.93x10^5	11.0x10^5	3.1923x10^6
F$_m$=5183.3N; R$_F$=0.2	SWT_m (θ_c =0°)	4.3623	3.3283	2.6893
	N_{f1}	0.5430x10^4	1.288x10^4	2.782x10^4
	FS_m (θ_c = 35°)	0.0084	0.0069	0.0061
	N_{f2}	0.6386x10^4	1.254x10^4	2.764x10^4

As predicted by the fretting/plain fatigue unified prediction parameter in section 3.3.2, the plain fatigue at teeth fillet will dominate the failure of the involute spline shaft teeth studied here. At teeth fillet, K_{FDP}=1, the prediction of fatigue life falls to the same with the plain fatigue life prediction. Table 3-3 listed the predicted fatigue life using above method under three different level dynamic loads F_m=1743.6N; R_F=0.2, F_m=3113.5N; R_F=0.2 and F_m=5183.3N; R_F=0.2. The SWT and FS parameters are averaged along the crack orientation within characteristic length l_c=0.2, l_c=0.3 and l_c=0.4 respectively, as we can see, the characteristic length greatly affected the prediction results, to determine a proper value of characteristic length l_c, more experimental investigations are needed. With the same characteristic length, the crack initiation lives predicted by averaged SWT and FS parameter are very close. Under the lowest level dynamic load F_m=1743.6N; R_F=0.2, the fatigue crack initiation life at teeth fillet is greater than 10^8 cycles, with the increase of dynamic load, the fatigue crack initiation life decreased.

Usually, the fatigue data are tested in the normalized condition of material. Different process of heat treatment will change the microstructure of the material, and thus affects the fatigue properties of the material. Table 3-4 listed the fatigue data of material in different hardening processed conditions.

Table 3-4: Fatigue cyclic properties of case or induction hardened materials

Material & hardening Process / Fatigue property	AISI/SAE 8620 [Yin-09]		AISI/SAE 1050 [Sha-09]	
	Case hardened		Quenched and tempered	Induction hardened
	Core	Case		
Fatigue strength coefficient σ_f' (MPa)	5874	3377	1346	4974
Fatigue strength exponent b	-0.183	-0.100	-0.062	-0.152
Fatigue ductility coefficient ε_f'	15.4	0.003	2.01	0.529
Fatigue ductility exponent c	-1.110	-0.269	-0.725	-0.910

For the FS model, Shamsaei, N. and Fatemi, A et. al. proposed an alternative method to calculated the fatigue life based on the Brinell hardness of material in absence of any fatigue data, formulated as following [Yin-09, Sha-09]:

$$FS = \frac{\Delta\gamma_{\max}}{2} \cdot \left(1 + k \cdot \frac{\sigma_n^{\max}}{\sigma_y}\right) = \left[A\left(2N_f\right)^{-0.09} + B\left(2N_f\right)^{-0.56}\right]\left[1 + kC\left(2N_f\right)^{-0.09}\right] \tag{3-27}$$

$$A = \frac{5.53\left(HB\right) + 293}{E} \tag{3-28}$$

$$B = \frac{0.48\left(HB\right)^2 - 731\left(HB\right) + 286500}{E} \tag{3-29}$$

$$C = \frac{1}{0.0022\left(HB\right) + 0.382} \tag{3-30}$$

$$\sigma_y = 0.0044\left(HB\right)^2 + 1.33\left(HB\right) \tag{3-31}$$

This hardness based multiaxial life prediction method is claimed to be valid for the steel within the hardness between 150HB and 700HB in their research. The Rockwell hardness of the surface hardened and normalized shaft teeth flank in this study is 53HRC and 17HRC respectively, converted to Brinell hardness is 532HB and 191HB (calculated by interpolation) respectively. It provided great convenience for the fatigue life prediction of surface hardened specimen, and which will be also implemented in the teeth flank of spline shaft-hub connections to predict the fretting/plain fatigue life similar to the implementation of the classical FS model discussed before, as shown following:

$$K_{FDP} \cdot FS_m = \left[A\left(2N_f\right)^{-0.09} + B\left(2N_f\right)^{-0.56}\right]\left[1 + kC\left(2N_f\right)^{-0.09}\right] \tag{3-32}$$

According to equation (3-27) to (3-31), the correlation between FS parameter and number of cycles N_f of 25MoCr4 in normalized state and hardened state respectively. It clearly showed that the number of cycles to initiate a crack for the hardened specimen is more than that for the normalized specimen in high cycle domain. It’s a pity that there’s no corresponding hardness based multiaxial life prediction formulation for the tensile crack mode SWT parameter. According to above equation, the fatigue crack initiation (at teeth fillet) life of the surface hardened spline shaft teeth under dynamic loads F_m=3113.5N; R_F=0.2 and F_m=5183.3N; R_F=0.2 are calculated and listed in Table 3-5.

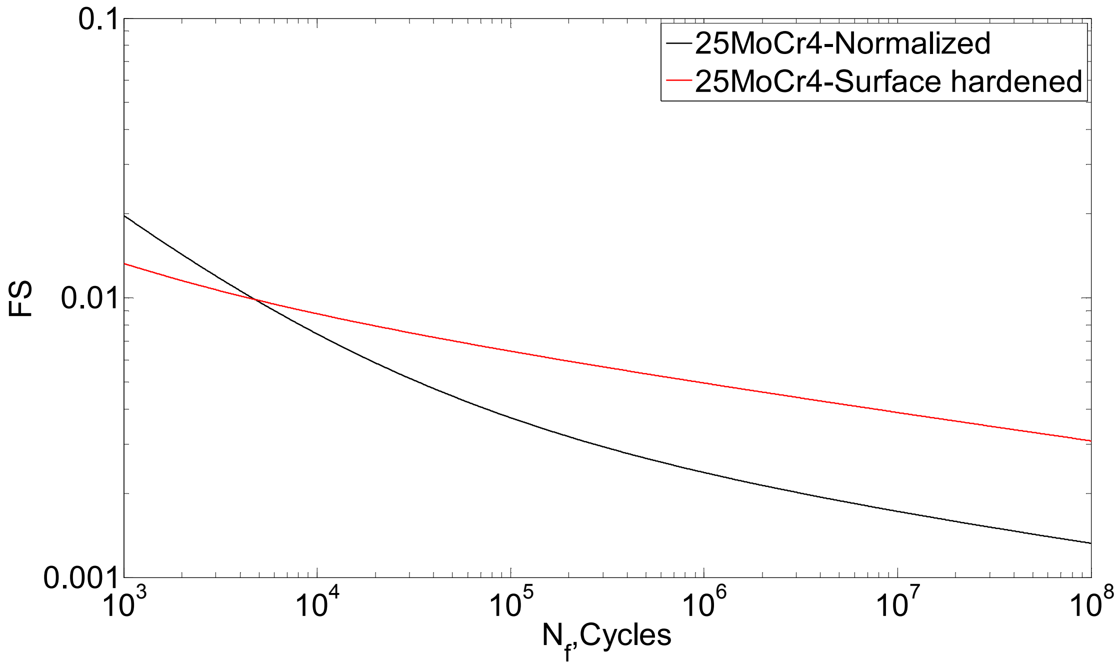

Figure 3-27: FS-N_f diagram of 25MoCr4 according to equation (3-27)

Table 3-5: Predicted fatigue life of spline shaft teeth (surface hardened) under different dynamic loads with same load ratio

Dynamic load	l_c Fatigue life prediction	0.2mm	0.3mm	0.4mm
F_m=3113.5N;	FS_m (θ_c = 37.5°)	0.0045	0.0037	0.0033
R_F=0.2	N_{f2}	2.5744×10^6	1.4902×10^7	5.3822×10^7
F_m=5183.3N;	FS_m (θ_c = 35°)	0.0084	0.0069	0.0061
R_F=0.2	N_{f2}	1.3903×10^4	5.4866×10^4	1.6805×10^4

3.4 Conclusion

To provide a unified evaluation criterion of fretting fatigue and plain fatigue, a fretting and plain fatigue unified prediction model is suggested and implemented in representative teeth pair of involute spline shaft-hub connection. It inherited the successful characteristic of existing pure fretting fatigue prediction FFDP/exFFDP models and pure plain fatigue prediction SWT/FS models, integrated the tensile mode crack governed and shear mode crack governed fretting/plain fatigue mechanism. The newly developed fretting/plain fatigue unified prediction parameter $K_{FDP}SWT$ and $K_{FDP}FS$ will be applied to the tensile mode crack governed and shear mode crack governed fretting/plain fatigue respectively. Following the incremental approach, the fretting/plain fatigue unified prediction model will be divided into 3 steps: i. Determine the location of fatigue crack; ii. Determine the crack orientation; iii. Predict the fatigue life. Only step i or the whole three steps will be implemented to industry applications according to requirements. The fretting relative damage factor $K_{FDP,}$ the governed crack mode and fatigue cyclic properties are material dependent, so more basic standard material test data are needed in order to improve the prediction accuracy.

The failure of involute spline shaft teeth (along teeth root-teeth tip direction) predicted by both $K_{FDP}SWT$ and $K_{FDP}FS$ are plain fatigue at teeth fillet dominated. The crack orientation and fatigue life prediction are implemented at teeth fillet using the degenerated fretting/plain fatigue unified parameter-the SWT or FS parameter. As a matter of fact, besides the competition of plain fatigue at teeth fillet and fretting fatigue near contact edge along teeth flank of shaft teeth or hub teeth, there’s also completion between plain/fretting fatigue of shaft teeth and hub teeth though we are always concerned about the failure of shaft teeth in involute spline shaft-hub connections.

4 Development of fretting/plain fatigue test apparatus

4.1 Introduction

Corresponding to the quasi-two dimensional one teeth pair representative model of spline shaft-hub connection introduced in chapter 3, a representative specimen test apparatus is developed in this chapter. The test apparatus will be fitted to a resonant fatigue test machine and take advantage of its resonant frequency monitoring system to detect the initiation of fretting/plain fatigue cracks. The apparatus can be also combined with a standard fatigue test machine to carry out fatigue tests, but additional fretting and plain fatigue crack detection method are needed when man interested in the life time of fatigue crack initiation and propagation.

4.2 Concept of the representative specimen test apparatus

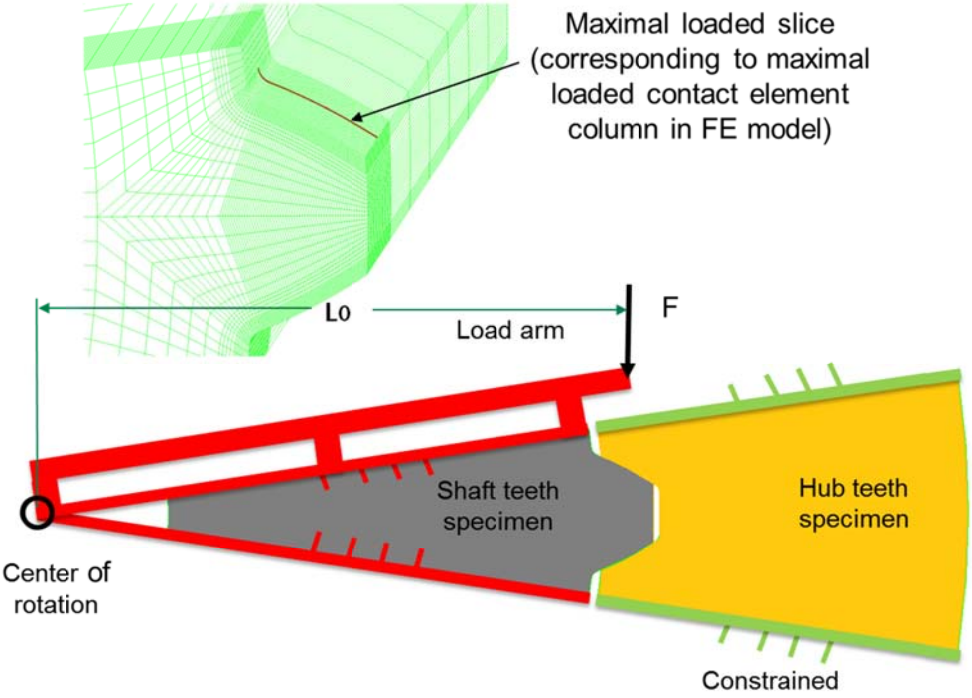

Figure 4-1: Concept of the representative teeth pair test apparatus

In FE model of the representative teeth pair, cyclic symmetry coupled boundary conditions is applied in the cyclic symmetry plane of the teeth pair, the equivalent load F is equally applied on the external surface of hub teeth. In the test apparatus, the virtual ‘cyclic symmetry boundary condition’ cannot realized by a structure design. The concept of the representative specimen test apparatus is shown in Figure 4-1, the hub teeth specimen is fixed, the shaft teeth specimen rotate with the load arm around the geometry center of shaft. The dynamic contact between the teeth pair is created by the equivalent load F through a load arm. Similar to equation (3-1), the equivalent load F is calculated out using equation (4-1), the contact pressure p_i and frictional stress f_i are output from the maximal loaded slice vertical to axial direction in FE analysis carried out in chapter 2.

$$F = \frac{1}{L_o} b x_l \psi \sum_{i=1}^{n-1} (\frac{R_i + R_{i+1}}{2}) \left(\frac{p_i + p_{i+1}}{2} \cos(\frac{\alpha_i + \alpha_{i+1}}{2}) + \frac{f_i + f_{i+1}}{2} \sin(\frac{\alpha_i + \alpha_{i+1}}{2}) \right) \tag{4-1}$$

F: load of the test setup ; L0: length of load arm (as shown in Figure 4-1); b: thickness of the specimen (in axial direction); x_l:length of the contact element; ψ:compensate coefficient for slight variation in contact pressure and frictional stress across the thickness b; n: number of nodes along teeth flank; R_i: radius of node i on teeth flank; α_i: pressure angle of at node i on teeth flank; μ: coefficient of friction (0.3 in this study); p_i: contact pressure at node i on the teeth flank; f_i: frictional stress at node i on the teeth flank,), R_i, α_i, f_i and p_i are shown in figure 4-2. Force analysis of the load arm together with the shaft teeth specimen fixed with it are also shown in this figure, F_{bx} and F_{by} are reaction force at the rotation center, β_i is the angle between the normal direction and vertical direction at point i in teeth flank, F_{cx_i} and F_{cy_i} are the reaction force resolved in horizontal and vertical direction respectively at point i. The force analysis above are carried on the basis that the direction of F is downward compression force, it can be also an upward tension force.

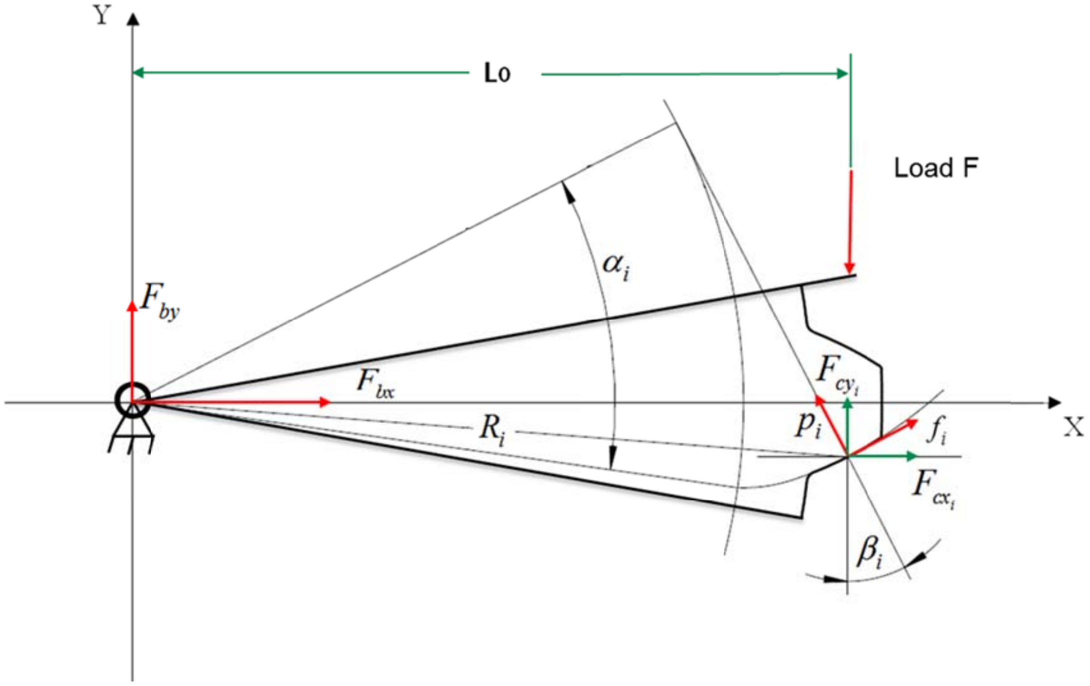

Figure 4-2: Force analysis of the load arm (together with the shaft teeth specimen fixed with it)

4.3 In situ detection of fretting/plain fatigue cracks

In order to monitor the initiation and propagation of fretting or plain fatigue crack, the in developing test apparatus should have the capability of in situ fretting/plain fatigue crack detection. Due to the small scale and the access difficulty of these cracks, especially the fretting fatigue between contact interfaces, detection of these cracks is a critical aspect of the fretting/plain fatigue life prediction effort. Most of the previous researches are post-fracture qualitative analysis, and how long the crack initiation and propagation process will take remains unclear.

Hutson, A.L. et.al. once studied the feasibility of online fretting fatigue crack detection using ultrasonic shear wave in pad-plate fretting fatigue test configuration, the results showed that ‘the shear wave NDI technique was insensitive to small cracks in his study [Hut-05]. Wagle, S. et.al introduced the ultrasonic surface acoustic wave with local immersion method using a water bag to carry out online fretting fatigue crack detection at bolt jointed aluminum alloy plates, as shown in figure 4-3. A fretting fatigue crack of 11.5mm length 2.3mm before the bolt hole edge was detected by the SAW measurement system in his study, but the limitation is that this method is only appropriate for flat specimens [Wag-09, Wal-11]. The fretted surface in this study is an involute spline surface and the length of the profile surface is about 2.5mm. So, it seems that the ultrasonic wave crack detection method is not appropriate to be used in present study due to scale and geometry limitation according to the review above.

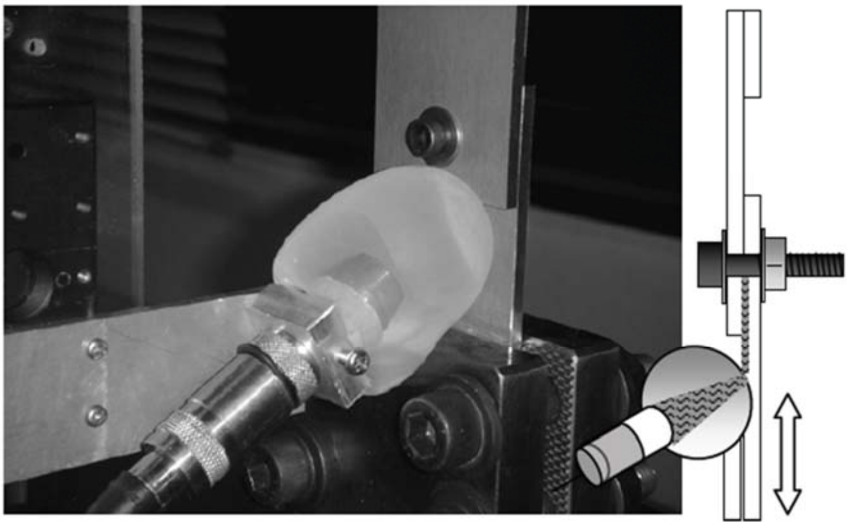

Figure 4-3: In situ detection of fretting fatigue crack using surface acoustic wave in bolt jointed aluminum alloy plates [Wag-09]

Another in situ crack detection method is the resonant fatigue test method. It has been widely used in the plain fatigue tests, and various resonant fatigue testing machines have been available in the market since the first resonant testing machine was invented by Max E. Russenberger in 1938 [Rus-84]. The electromagnet excited resonant fatigue test machines are currently available with the test frequency up to 300Hz and dynamic load up to 1000KN. In resonant testing machine, the dynamic load is generated by a mechanical oscillating system, which consists of masses and springs, the specimen with elasticity is also part of the mechanical oscillating system. The frequency of a particular mode remains constant during the test until a crack occurs, upon the initiation of cracks, the spring constant of the specimen changes and throws the system off resonance, therefore, the initiation of crack will be detected by monitoring the change of resonant frequency [Hug-03, Pöt-04]. Resonant machines are mainly used to characterize the performance of materials under cyclic loading, with specially designed fixtures, different components such as teeth of gear, connecting rod, screws, etc. can be also adapted to resonant fatigue test machines to test their fatigue limits [Klu-08]. The resonant method is a passive detection method, the validation and the resolution to micro crack in fretting fatigue test will be studied in this study.

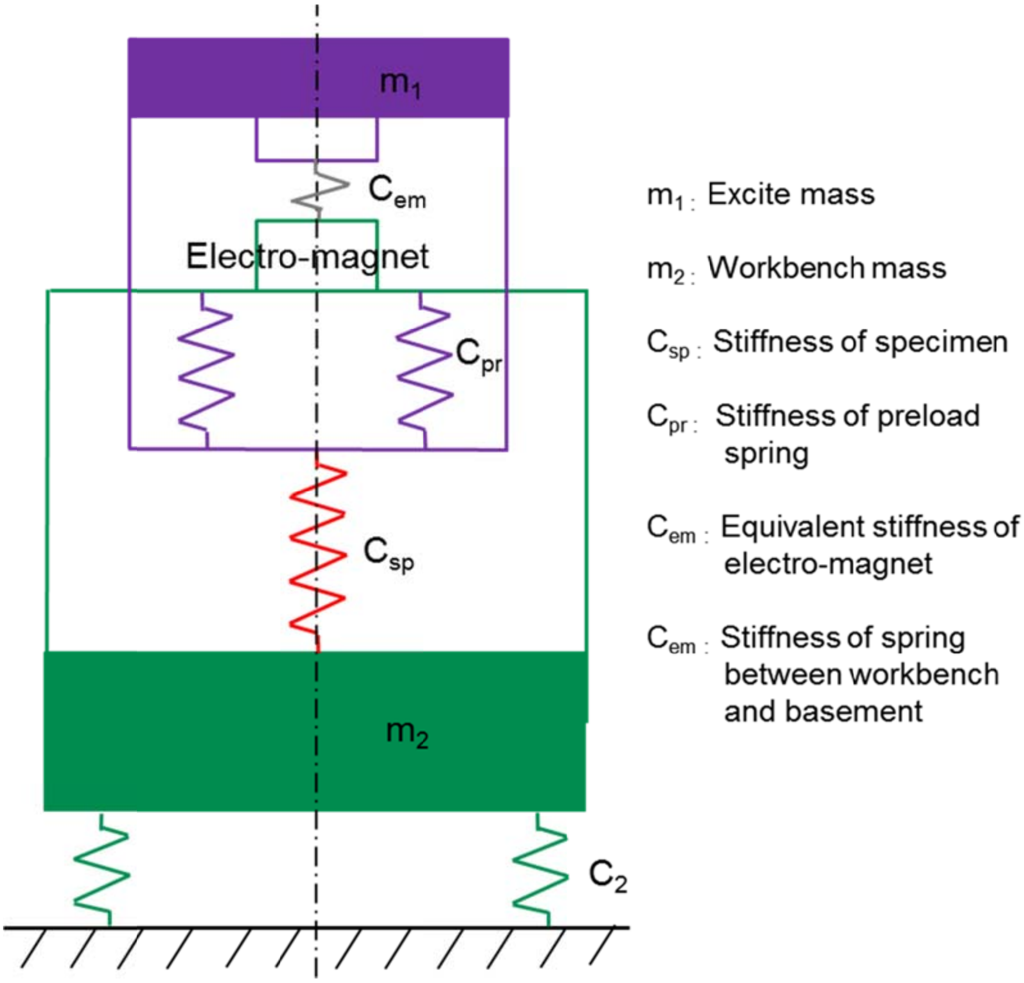

Figure 4-4: Mechanical schematic diagram of a two mass resonant testing machine

Figure 4-4 shows the schematic diagram of a two mass resonant test machine, m_1 and m_2 are the excite mass and workbench mass respectively, C_{em} is the equivalent stiffness of electro-magnet, C_{pr} is the stiffness of preload spring, C_{sp} is the stiffness of the specimen, C_2 is the stiffness of spring between workbench and basement. The natural angular frequency of the above mass-spring oscillator is [Fre-11]:

$$\omega_{1,2} = \sqrt{\left| -\frac{m_1\left(C_1+C_2\right)+m_2C_1}{2m_1m_2} \pm \sqrt{\left(\frac{m_1\left(C_1+C_2\right)+m_2C_1}{2m_1m_2}\right)^2 - \frac{C_1C_2}{m_1m_2}} \right|} \tag{4-2}$$

$$C_1 = C_{em} + C_{pr} + C_{sp} \tag{4-3}$$

The machine will run at one of the natural angular frequency (full resonance state) excited by the electro-magnet.

The stiffness of the specimen C_{sp} in this study depends on stiffness of the representative teeth pair. Dietz introduced a common mechanical model to calculate the stiffness of spline shaft-hub connection under torque and transverse force loading, as shown in Figure 4-5. The most important stiffness parameters are the contact stiffness of teeth pair in circumferential direction C, the bending stiffness of shaft teeth in circumferential direction C_{D1} and bending stiffness of hub teeth in circumferential direction C_{D2}; stiffness in radial direction C_{R1} and C_{R2} [Die-78]. For representative teeth pair specimen under pure torque, only the contact stiffness (here we give it a new name ‘local stiffness’ C_{Lo}) and bending stiffness (here we give it a new name ‘global stiffness’ C_{Gs} for shaft teeth, C_{Gh} for hub teeth) in circumferential direction are concerned, as shown in Figure 4-6, the stiffness of specimen C_{sp} can be expressed as form 4-4. The variation of local stiffness depends on the roughness and contour of contact surface, which will be gradually changed because of wear (fretting wear in this study), very small during stable phase of the test. The variation of teeth contour due to wear also slightly affects the global stiffness of teeth, but the essential change of global stiffness is brought by the abruptly occurred crack at or near teeth root of shaft or hub specimen.

$$C_{sp} = f\left(C_{Lo}, C_{Gs}, C_{Gh}\right) \tag{4-4}$$

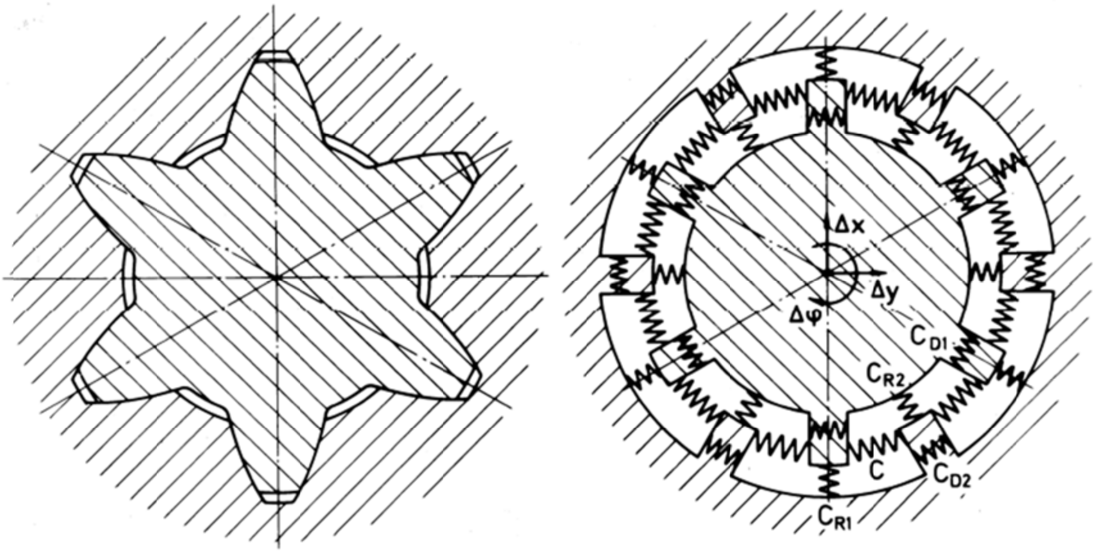

Figure 4-5: Mechanical schematic diagram of spline shaft-hub connection [Dietz-78]

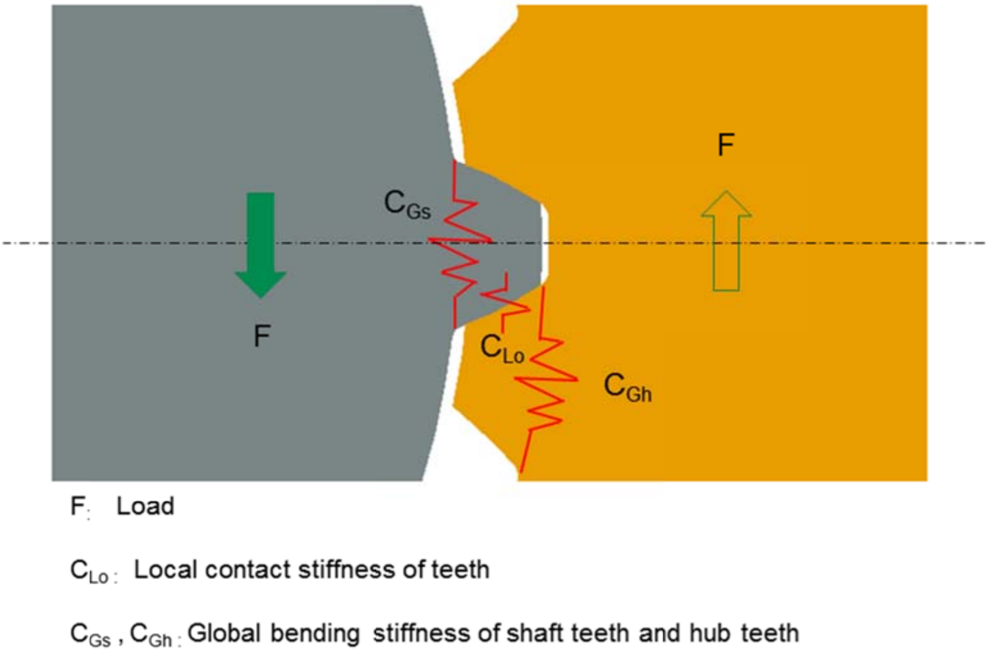

Figure 4-6: Global stiffness and local stiffness model of representative teeth pair specimen under pure torque

4.4 Structure design of the test apparatus

The concept of representative specimen and load method shown in Figure 4-1 will be realized by following design, as shown in Figure 4-7. The shaft teeth specimen is fixed in the dovetail groove of axle, which supported by two ball bearings symmetrically. Ball bearings are encapsulated in the bearing housing and lubricated by oil in order to relieve the damage of fretting. The hub teeth specimen is fixed in the dovetail groove of the basement. The alignment of the shaft teeth specimen and the hub teeth specimen is realized by adjusting the relative position of axle to the basement, as shown in Figure 4-8. The position of axle center o_2 relative to the basement can be adjusted by the rotation of eccentric bearing housing and movement of bearing housing support along the guide slot in horizontal direction. The eccentricity e between center o_1 and o_2 is 2mm and the adjustable arrange of u is ±2mm. The adjustment can be calculated with following form:

$$\begin{aligned} \Delta X &= u - e(1-\cos\theta) \\ \Delta Y &= e\sin\theta \end{aligned} \qquad (3\text{-}4)$$

Both specimens can be conveniently push in or push out from left side as well as right side of the apparatus before or after tests. The torque between shaft teeth and hub teeth specimen is created by the force F applied at the load

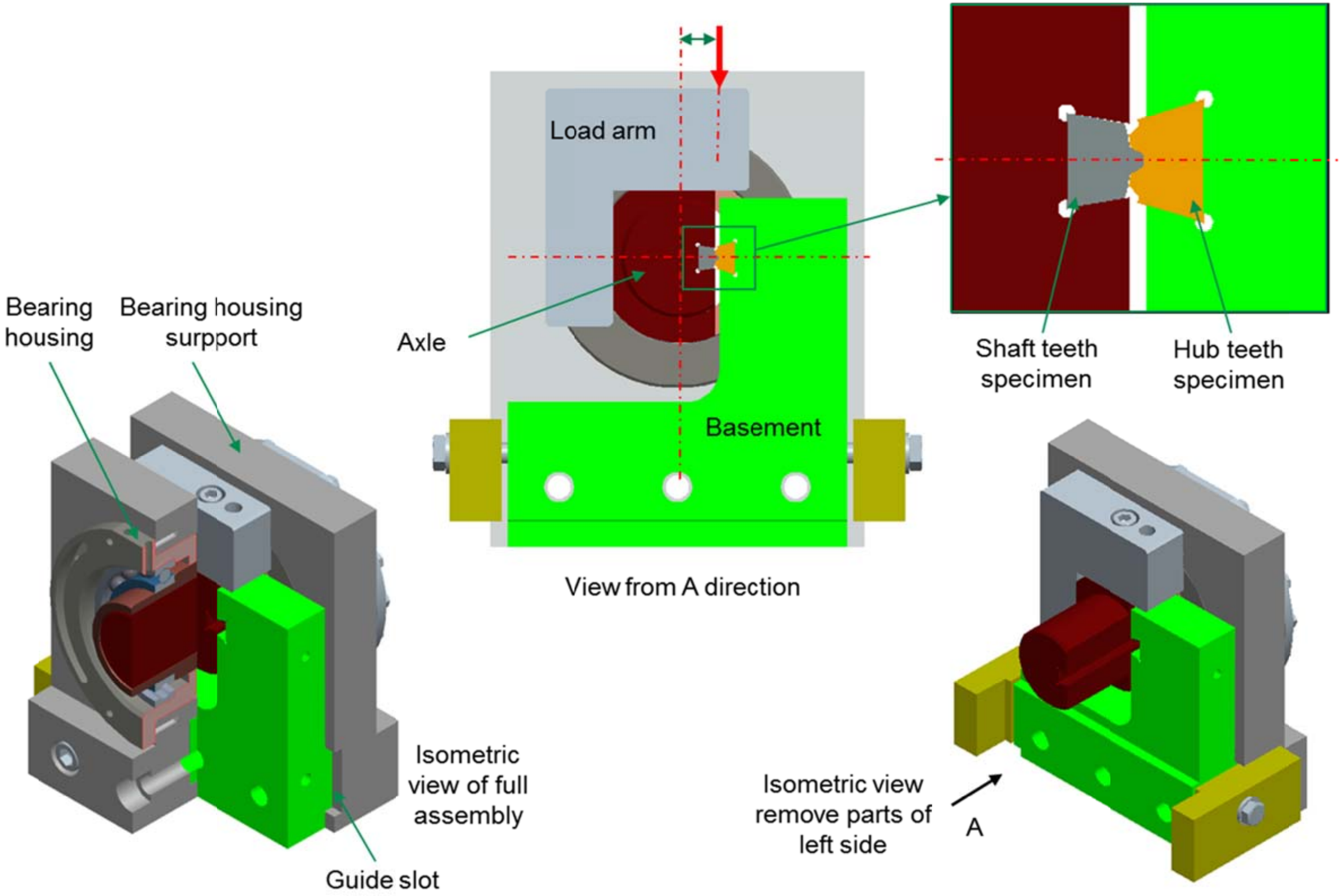

Figure 4-7: Solid model of the representative teeth pair test apparatus

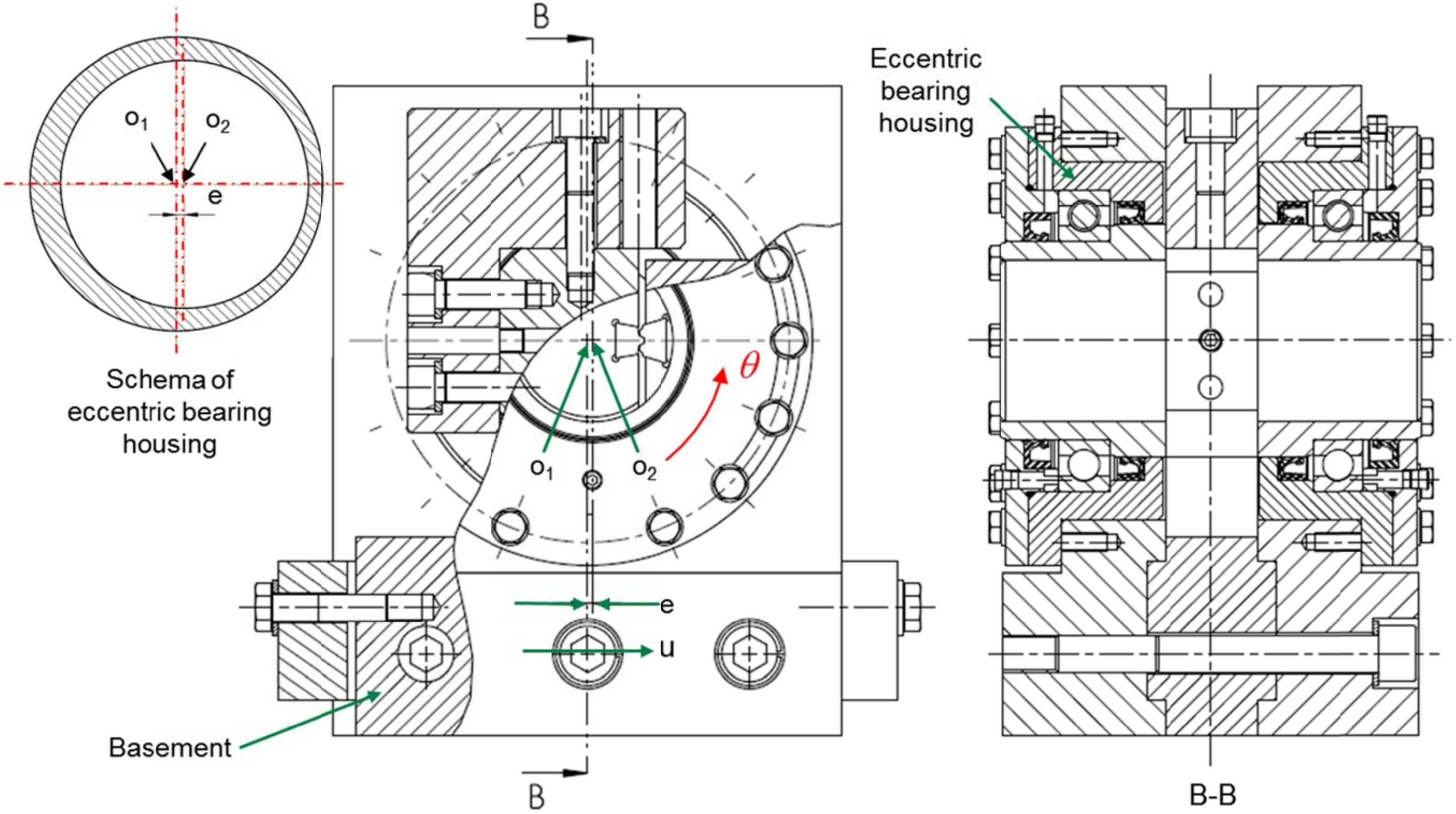

Figure 4-8: Alignment of shaft teeth and hub teeth specimens

arm, which are assembled together with the axle by screws. Dynamic load F will generate dynamic contact, consequently fretting between the shaft teeth specimen and hub teeth specimen as well as plain fatigue at teeth fillet.

Above fatigue test apparatus will be assembled between the workbench and oscillating transverse beam of the resonant fatigue test machine to execute fatigue experiments, as shown in Figure 4-9. To improve the stability and rigidity of the fatigue test apparatus, the reaction force of the rotation part (shaft teeth specimen, axle together with load arm) should be greater than zero. As analyzed in figure 4-2, when the length of moment arm L_0=20mm, F_{max}=14454N (maximal equivalent load of representative specimen corresponding to the torque T=2800Nm in spline shaft-hub connections), the reaction force F_{cx}=-2707N, F_{cy}=13687N, F_{bx}=2707N, F_{by}=776N.

Figure 4-9: Assembly of the fretting/plain fatigue test apparatus and the resonant fatigue test machine

4.5 Conclusion

Combined with a resonant fatigue test machine or a standard fatigue test machine, the fretting/plain fatigue behavior of spline teeth can be investigated more deeply and microscopically with this newly developed test apparatus. Take advantage of the resonant frequency monitoring capability of resonant fatigue test machine, the crack initiation and propagation process of spline teeth can be detected and monitored on line. As a matter of fact, this test apparatus can not only be used to investigate the fretting/plain fatigue behavior of involute spline teeth but also be used to optimize the spline teeth in structure as well as surface treatments more economically.

5 Fatigue experiments

5.1 Introduction

With the fretting/plain fatigue test apparatus developed above in chapter 4, fretting/plain fatigue experiments of representative involute spline teeth specimens will be carried out in this chapter. The possible initiated cracks (due to fretting fatigue or plain fatigue) as well as the cycle times before crack initiation will be recorded by the resonant frequency of resonant fatigue test machine, the relationship between nature frequency change and crack growth will be also investigated in order to distinguish the crack initiation period from the whole life time. Furthermore the resolution of resonant method to cracks between fretting interface will be also studied in this study. The tested specimens will be further post processed and analyzed with microscope to measure the crack or the wear scar.

5.2 Experiment design and specimen preparation

According to equation (4-1), the equivalent dynamic loads F are calculated out and listed in Table 5-1. Corresponding to different loads listed in Table 5-1, there's three levels equivalent load and with the same maximal equivalent load, the load ratio between minimal load and maximal load ($R_F=F_u/F_o$) in a cycle change from 0.8 to 0.2. Different loading levels and vibration amplitude (characterized by R_F) are expected to generate different combination of contact pressures and slip arranges. The representative specimen of shaft and hub are cut from involute spline shaft (DIN 5480 45x2x21, Material: 25MoCr4) and hub (DIN 5480 45x2x21, Material: C35) with electrical discharge wire-cutting machine respectively, as shown in Figure 5-1 and Figure 5-2. The thickness of the spline shaft teeth specimen is 12mm thick, and in order to make the spline shaft teeth flank fully contact with the spline hub teeth flank, the spline hub teeth specimen is 4mm thicker than shaft teeth specimen, that's to say which is 16mm thick. There are two kinds of surface conditions for the spline shaft teeth specimen, one is in normalized condition, and another one is in surface hardened condition. For the spline hub teeth specimen, one is in normalized condition, and another one is TiAlN coated. Microstructure of the surface hardened spline shaft teeth specimen is shown in Figure 5-3, in the case of the surface hardened specimen is martensite, in the core is pearlite, the transition zone is bainite. It is similar to the induction surface hardened gear (as shown in Figure 5-4), but the boundary of three different metallographic microstructure is not so clear due to the difference of surface hardening process.

Table 5-1: Dynamic load F

$R_F=F_u/F_o$ τ_t (MPa)		0,8	0,7	0,6	0,5	0,4	0,3	0,2
40,096	F_m(N)	2618.6	2472.5	2326.4	2180.4	2034.4	1888.6	1743.6
	F_a(N)	293.5	440.4	587.2	734	880.9	1027.8	1174.3
120,288	F_m(N)	7828.8	7392.3	6955.8	6519.2	6082.7	5646.4	5215.2
	F_a(N)	875.9	1314.4	1753.2	2192.3	2631.5	3070.5	3506.3
200,48	F_m(N)	13004	12280	11555	10830	10104	9378	8682
	F_a(N)	1450	2177	2905	3634	4364	5093	5836

Notes: 1. Spline shaft-hub connection DIN5480 45x2x30x21; 2. F_u: minimal load F, F_o: maximal load F, τ_t =T/W_t according to DIN5466 for corresponding spline shaft hub connection ; 3.Material: hub-C35, shaft-25MoCr4

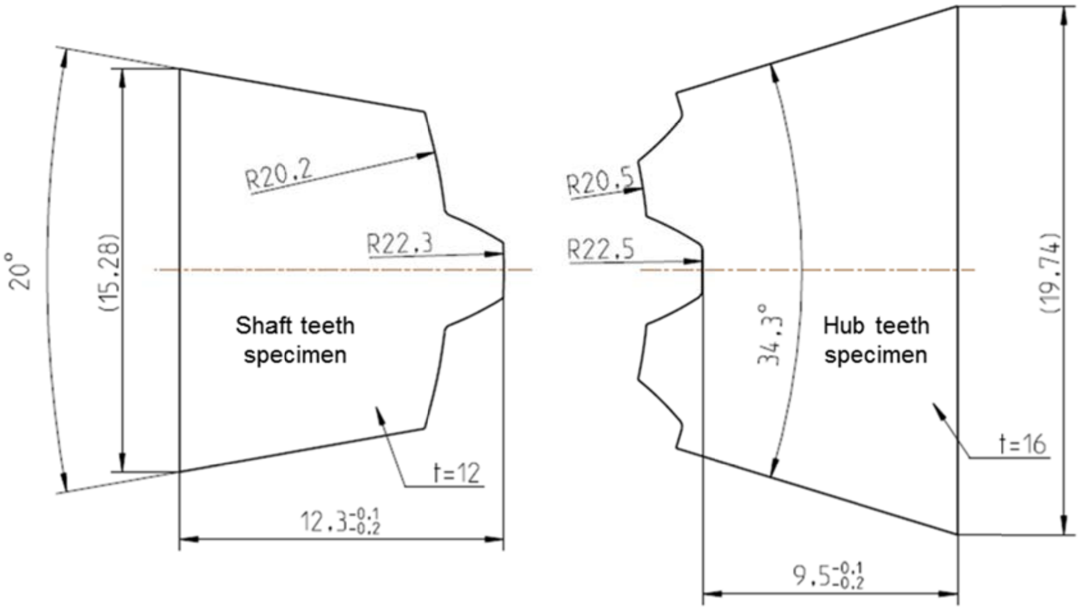

Figure 5-1: Dimension of representative specimens cut from spline shaft-hub connection DIN5480 45x2x21

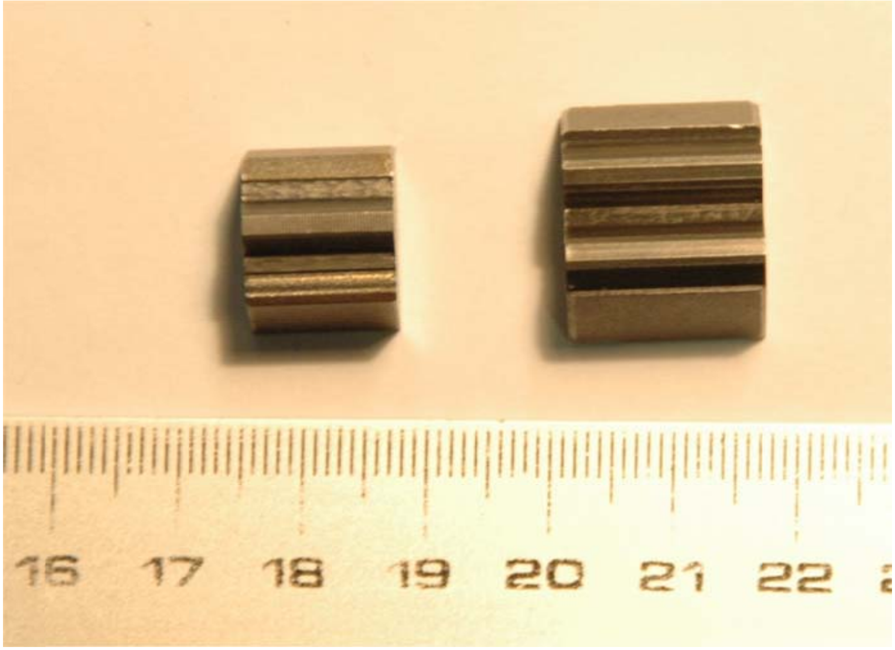

Figure 5-2: Photograph of the representative teeth pair

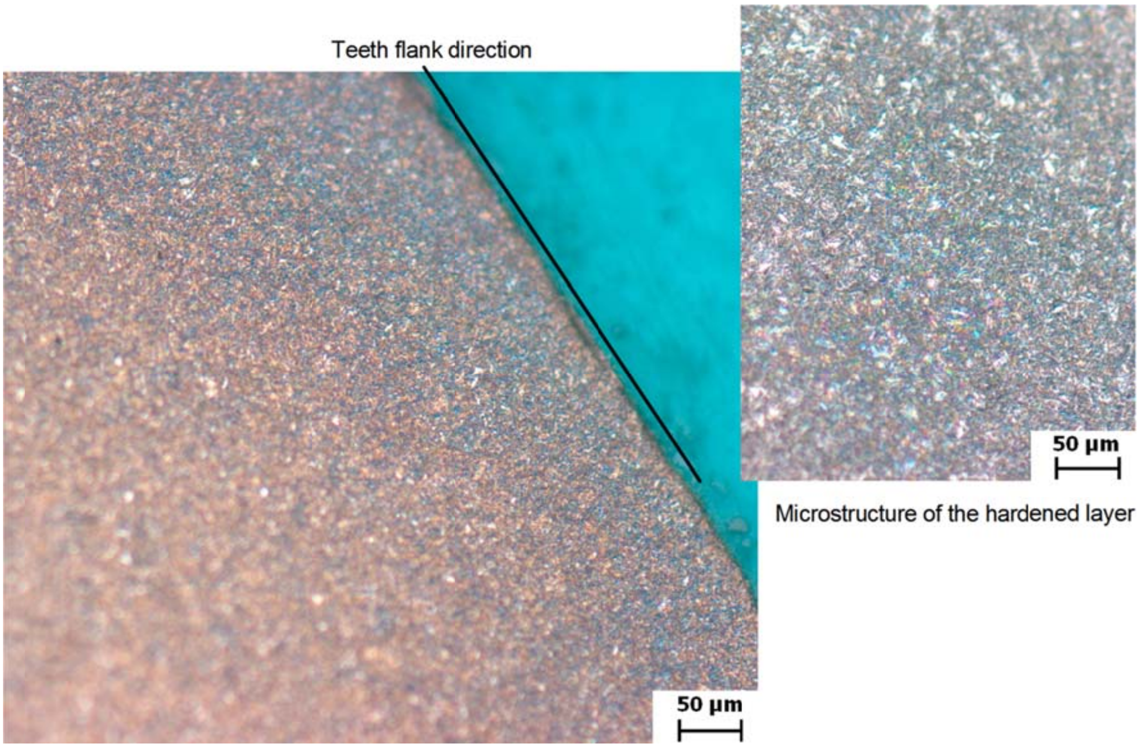

Figure 5-3: Microstructure of the surface hardened shaft teeth specimen

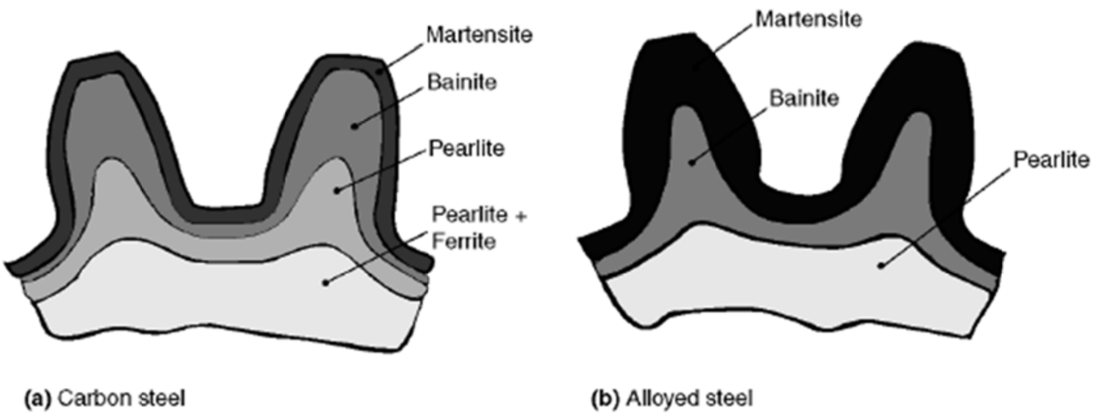

Figure 5-4: Microstructures of induction surface hardened carbon steel and alloy steel gears [Can-08]

Figure 5-5 shows the microstructure of the TiAlN coated spline hub teeth specimen. TiAlN coating have very high hardness (about 3000 $HV_{0.03}$), good thermal stability and oxidation resistance, it is often used as wear protection coating in cutting tools [Der-06].

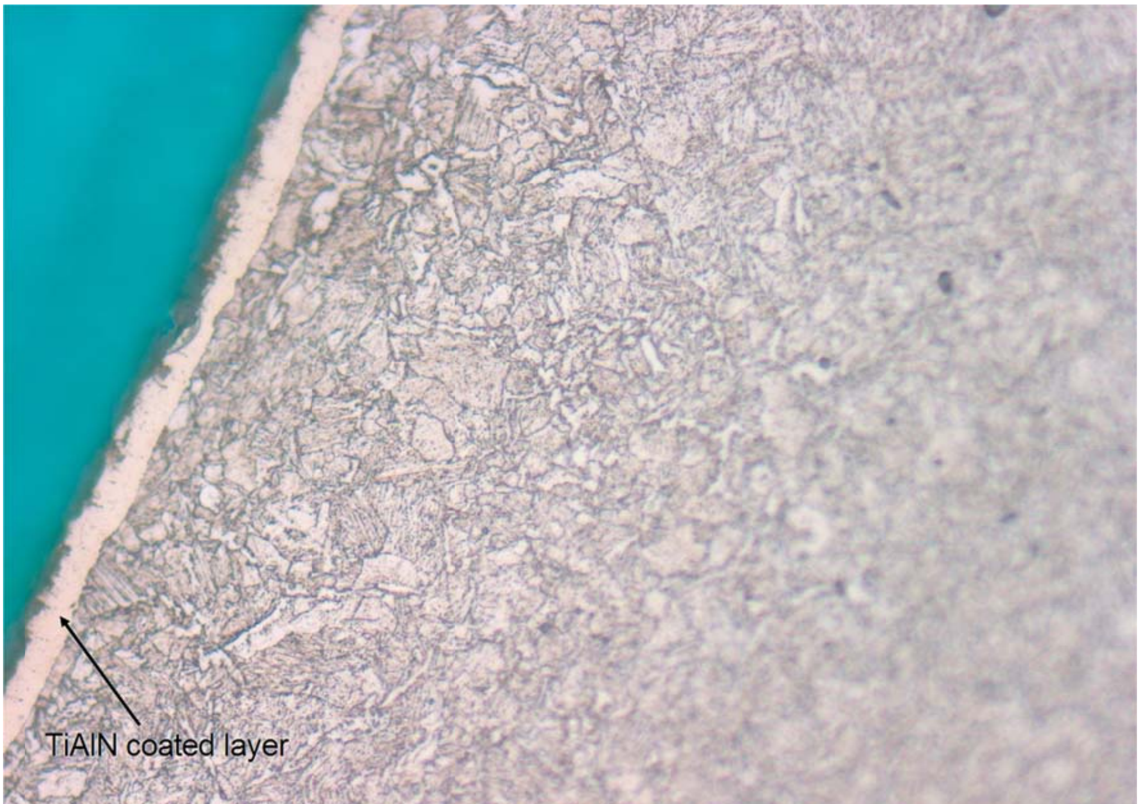

Figure 5-5: Microstructure of the surface coated spline hub teeth specimen

5.3 Analysis of experimental results

According to the FE analysis done in chapter 3, the specimens under load with higher vibration amplitude are exposed to the danger of fretting fatigue that may exceed the danger of plain fatigue at teeth fillet. At first, the specimen combination of normalized shaft teeth and normalized hub teeth will be tested under three different levels dynamic loads with the highest vibration amplitude (load ratio R=Fu/Fo=0.2). The loads and results are listed in Table 5-2

Table 5-2: Dynamic loads and results of normalized specimen

$R=F_u/F_o$ Load	0,2	0,2	0,2
Fm(N)	1743.6	5215.2	8682
Fa(N)	1174.3	3506.3	5836
Δf (Hz)	0	0.5	0.5
N_f (Cycles)	$>1\times10^7$	4.1×10^5	Plastic deformation

For the specimen under low level dynamic load, nothing happened after 1×10^7 cycles running, the specimen under high level dynamic load runs out immediately due to plastic deformation of the shaft teeth specimen. Crack initiated in the shaft teeth specimen under middle level dynamic load after 2.5×10^5 cycles running. Further running up to about 4.1×10^5 cycles, the change of resonant frequency reached 0.5Hz, which is the pre-set stop criterion of the resonant test machine. Figure 5-6 shows the resonance frequency history of this test. After fatigue test, the specimen is further analyzed by metallographic methods to characterize features of fatigue cracks. The crack occurred at the fillet of shaft teeth specimen, as shown in Figure 5-7. The direction of crack is about 30° to the vertical direction. That’s to say, for the involute spline teeth with 30° pressure angle, the direction of crack is perpendicular to the teeth flank direction approximately. Figure 5-8 shows the fretted flank surface of hub teeth, the hub teeth flank is slightly damaged by fretting, but no clear cracks initiated.

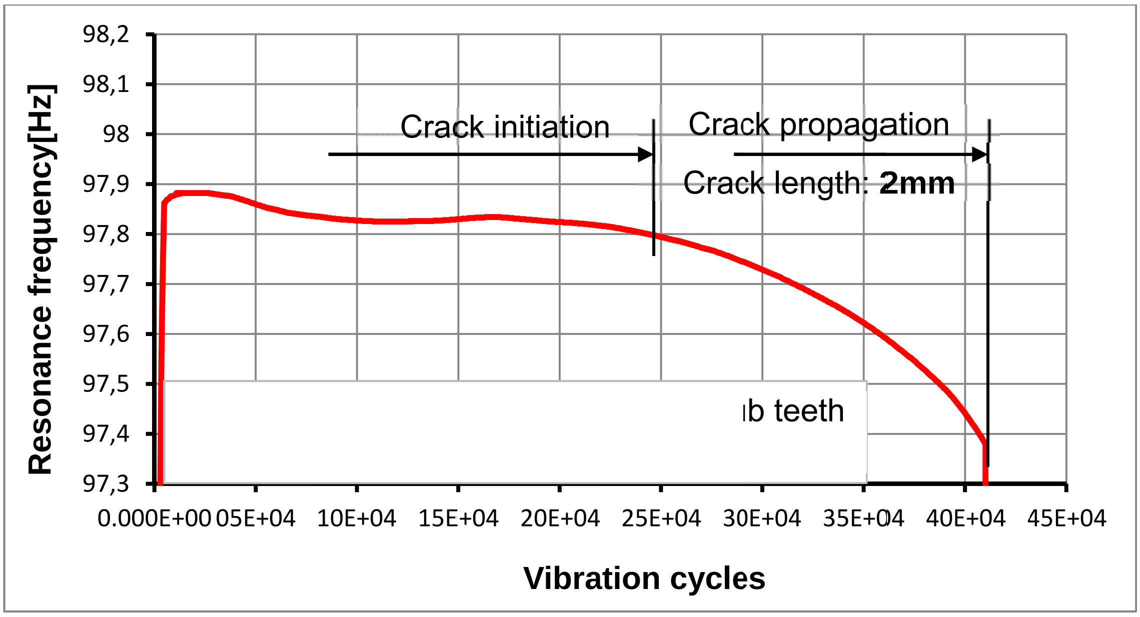

Figure 5-6: Resonance frequency history and crack growth (normalized shaft teeth+normalized hub teeth, F_m=5215.2, F_a=3506.3)

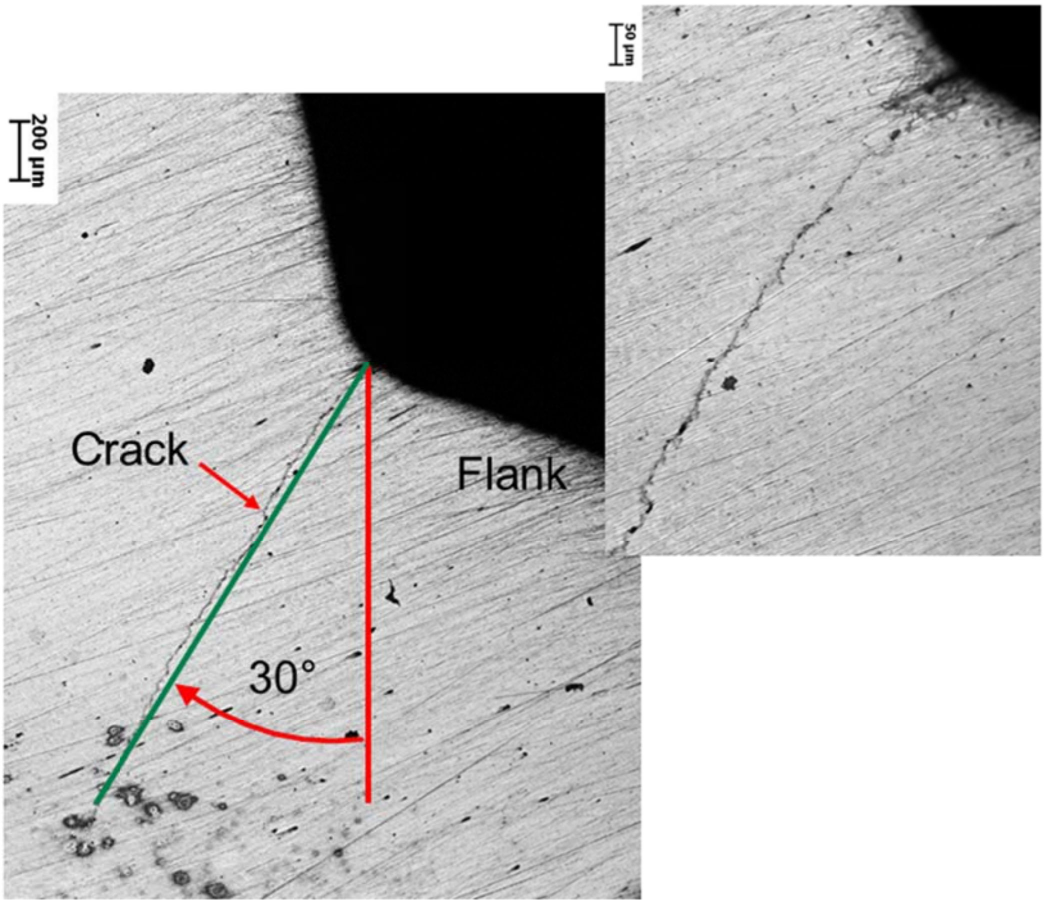

Figure 5-7: Crack at the fillet of shaft teeth specimen (normalized shaft teeth+normalized hub teeth, F_m=5215.2, F_a=3506.3)

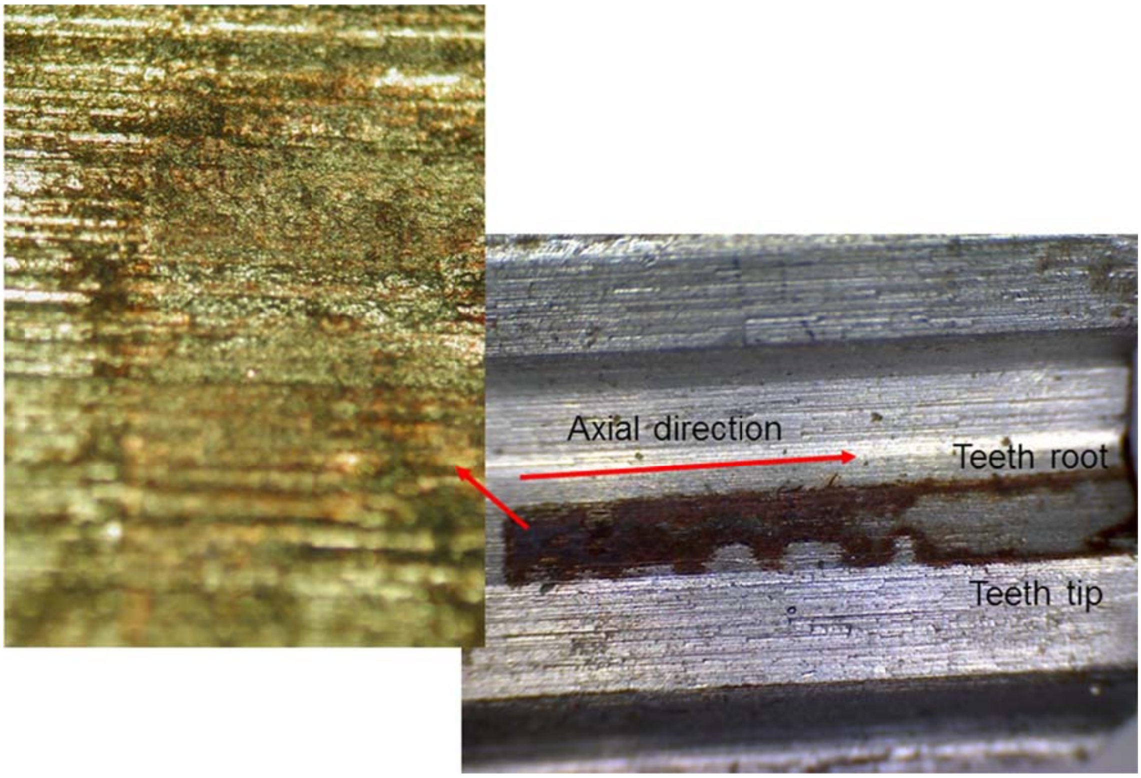

Figure 5-8: Fretted flank surface of hub teeth (normalized shaft teeth+normalized hub teeth, F_m=5215.2, F_a=3506.3)

Then, the specimen combination of surface hardened shaft teeth and normalized hub teeth will be tested under three different levels dynamic loads (with same load ratio). Because the test results of normalized shaft teeth and hub teeth showed that for the specimen under low level dynamic load, nothing happened after 1×10^7 cycles running, and the fatigue strength of the surface hardened shaft teeth are believed to be higher than normalized shaft teeth specimen. The lowest load level listed in Table 5-3 is excluded in this test round, replaced with a higher dynamic load F_m=10452.6N, F_a=6968.4N. The dynamic loads and corresponding test results are listed in Table 5-3. For the specimen under low level dynamic load, the resonant frequency changed 0.2Hz after 1×10^7 cycles running, but no clear cracks are observed under microscope. Crack initiated in the shaft teeth specimen under middle level dynamic load after 5×10^5 cycles running. Further running up to about 1.1×10^6 cycles, the change of resonant frequency reached 0.5Hz. Figure 5-9 shows the resonance frequency history of this test. The crack occurred at the fillet of shaft teeth specimen, as shown in Figure 5-10. The direction of crack is about 55° to the vertical direction. Figure 5-11 shows the fretted flank surface of hub teeth, the hub teeth flank is seriously damaged by fretting, but no clear cracks initiated.

Table 5-3: Dynamic loads and results of surface hardened shaft teeth + normalized hub teeth

$R=F_u/F_o$ Load	0,2	0,2	0,2
F_m(N)	5215.2	8682	10452.6
F_a(N)	3506.3	5836	6968.4
Δf (Hz)	0.2	0.5	0.5
N_f (Cycles)	$>1\times10^7$	1.1×10^6	<1000

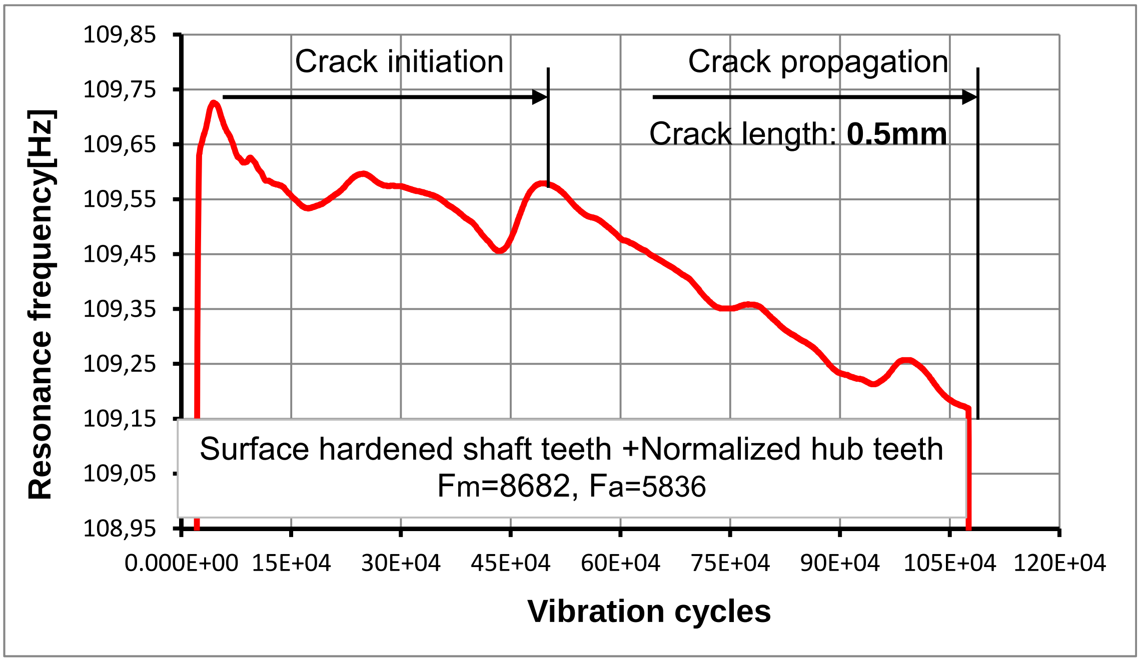

Figure 5-9: Resonance frequency history and crack initiation (surface hardened shaft teeth+normalized hub teeth, F_m=8682, F_a=5836)

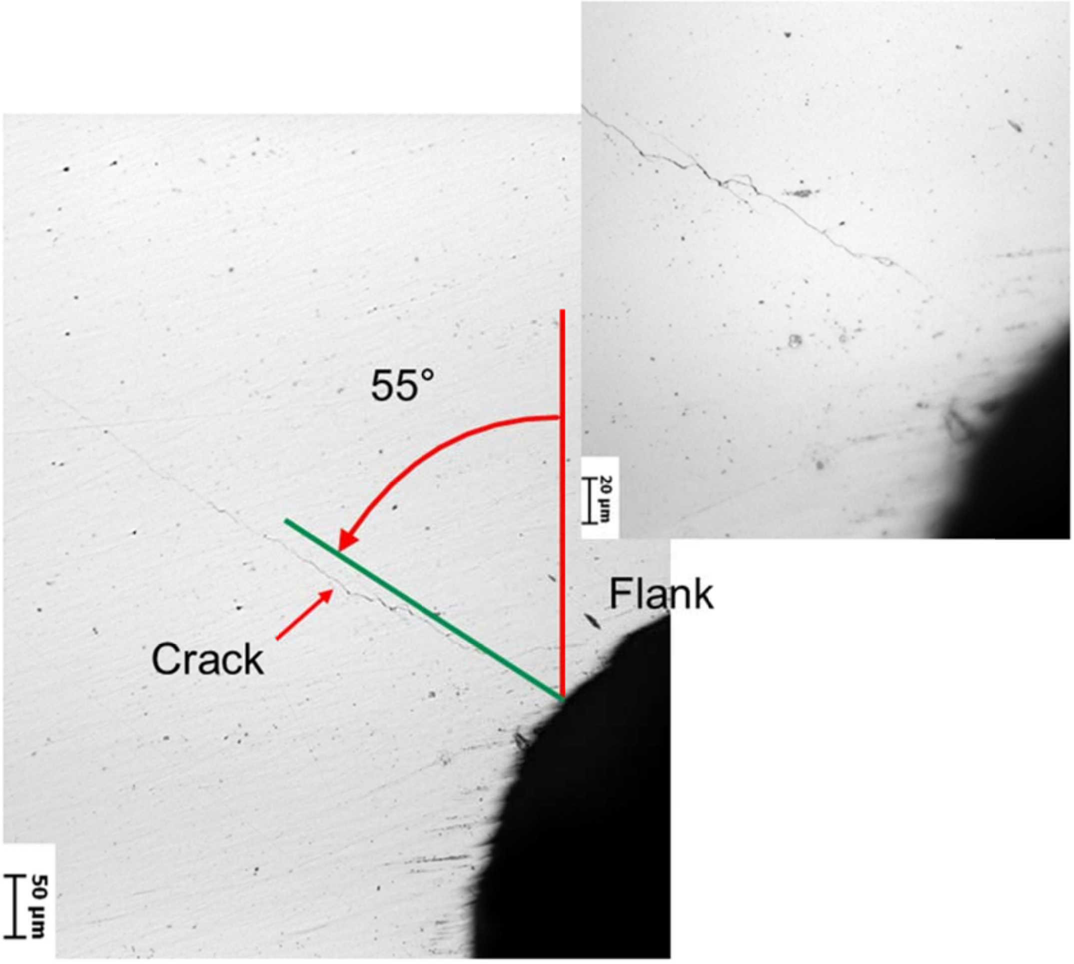

Figure 5-10: Crack at the fillet of shaft teeth specimen (surface hardened shaft teeth+normalized hub teeth, F_m=5215.2, F_a=3506.3)

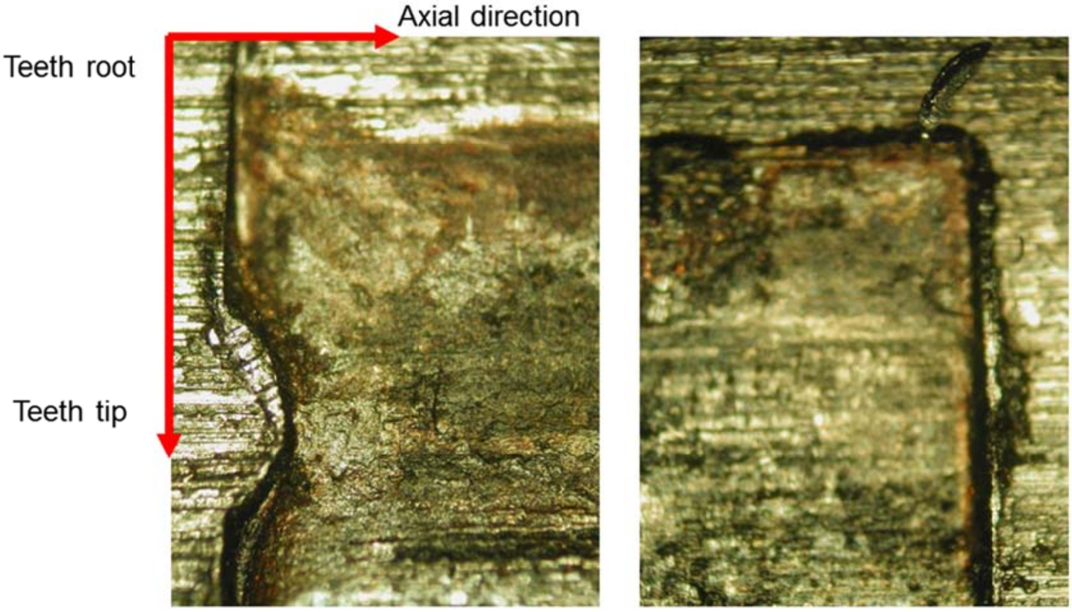

Figure 5-11: Fretted flank surface of hub teeth (surface hardened shaft teeth+normalized hub teeth, F_m=8682N, F_a=5836N)

Under high level dynamic load, brittle fracture crack happened soon after the start of test. The location of the crack is near contact edge out of contact interface. The crack is no more a fatigue crack but a brittle fracture crack due to the stress singularity near contact edge. Different to the normalized shaft teeth, there's no plastic deformation stage before fracture in the surface hardened shaft teeth.

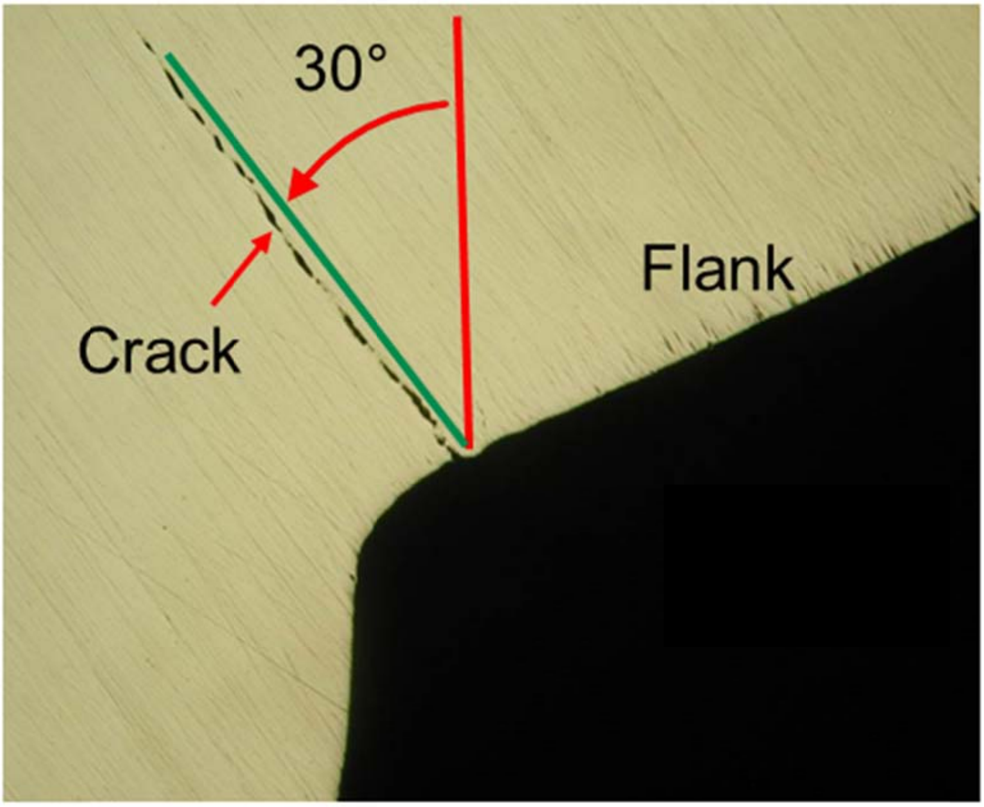

Figure 5-12: Crack near the contact edge out of contact zone in shaft teeth specimen (surface hardened shaft teeth+normalized hub teeth, F_m=10452, F_a=6968)

Table 5-4 listed the dynamic loads and results of the tested surface hardened shaft teeth and TiAIN surface coated hub teeth specimen combination. All of the specimens under three different level dynamic loads run through 10^7 cycles, no remarkable resonant frequency change happened. There's also no cracks observed under microscope after test. Even the fretting marks in the shaft teeth flank and hub teeth flank are not clear. Due to the TiAIN coated layer, the friction between hard-hard contact interfaces is greatly decreased, and the fatigue performance of them are greatly increased.

Table 5-4: Dynamic loads and results of surface hardened shaft teeth + TiAlN surface coated hub teeth

$R=F_u/F_o$ Load	0,2	0,2	0,2
F_m(N)	5215.2	8682	10452.6
F_a(N)	3506.3	5836	6968.4
Δf (Hz)	0	0	0
N_f (Cycles)	$>1\times10^7$	$>1\times10^7$	$>1\times10^7$

Above three group tests is enough to prove that the failure of the involute spline teeth is not fretting fatigue near contact edge but plain fatigue at teeth fillet dominated. So, the other dynamic loads listed in Table 5-1 will not be further tested.

5.4 Conclusion

As predicted by the fretting/plain unified prediction model, the fatigue crack will occur at the teeth fillet at first, the failure of involute spline teeth investigated here is plain fatigue crack at teeth fillet dominated. The crack orientation is close to the crack orientation predicted by the SWT parameter. For the normalized shaft teeth specimen and normalized hub teeth specimen under dynamic load F_m=5215.2, F_a=3506.3 , the crack initiation time is about $2.5\text{x}10^5$ cycles, which is close to the fatigue life predicted by the averaged SWT or FS parameter within characteristic length 0.2mm under equivalent dynamic load F_m=3113.5N; R_F=0.2 in Table 3-3.

6 Palliative measurements by structure optimization

6.1 Introduction

The simulation and experiment results above showed that the failure of studied involute spline shaft teeth are plain fatigue at teeth fillet dominated. The fillet of involute spline teeth is the critical location of structure optimization. Compared to the material engineering measurements such as surface treatment, coating, use of better materials etc., the structure optimization can improve the fatigue strength of spline teeth more economically, and is a more competent task for a mechanical engineer. Increase the radius of teeth fillet will improve the plain fatigue strength of it. But, the change or fillet radius are believed not only affect the plain fatigue at teeth fillet itself but also affect the fretting behavior near neighbored contact edge. An extreme example is that in polygon shaft-hub connection (P3C and P4C) there's no more 'weak fillet', but it was found in many researches that this kind of shaft-hub connection profile confronted with great problem of fretting fatigue, as shown in Figure 6-1 and Figure 6-2 [Zia-97, Win-01, Zia-02, Gro-07]. In another words, the failure of polygon shaft-hub connection is fretting fatigue in 'contact edge' dominated. Obviously, the purpose of structure optimization is to improve the overall fatigue life of the whole assembly. This chapter will use the fretting/plain fatigue prediction parameter developed in chapter 3 as an evaluation criterion to looking for an optimized shaft-hub connection profile that with minimized danger of fretting fatigue near contact edge and plain fatigue in fillet at the same time.

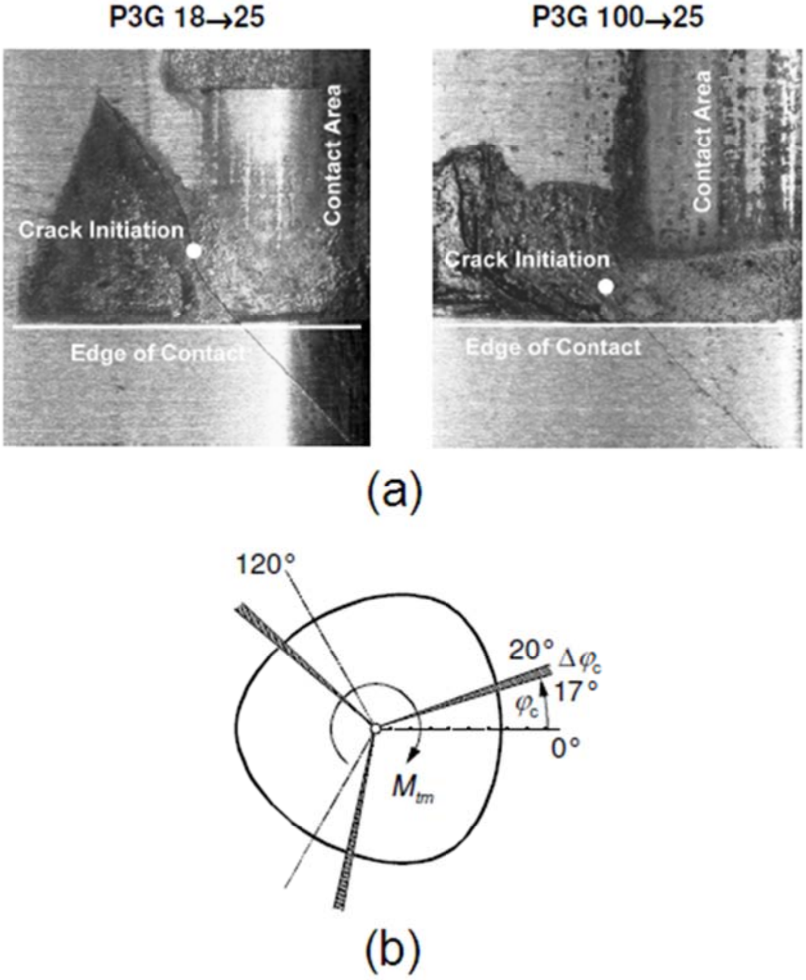

Figure 6-1: Fretting fatigue crack in P3G polygon shaft-hub connection under dynamic torsion, (a) fretting fatigue cracks in P3G shaft with different profile shapes (b) Angular ranges of the initial crack location at standardized P3G shaft. After [Gro-07]

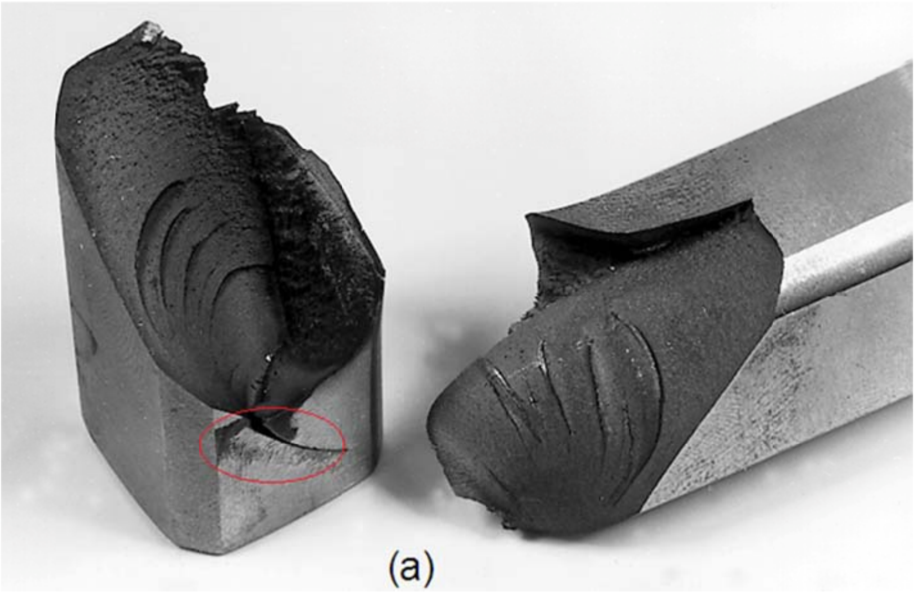

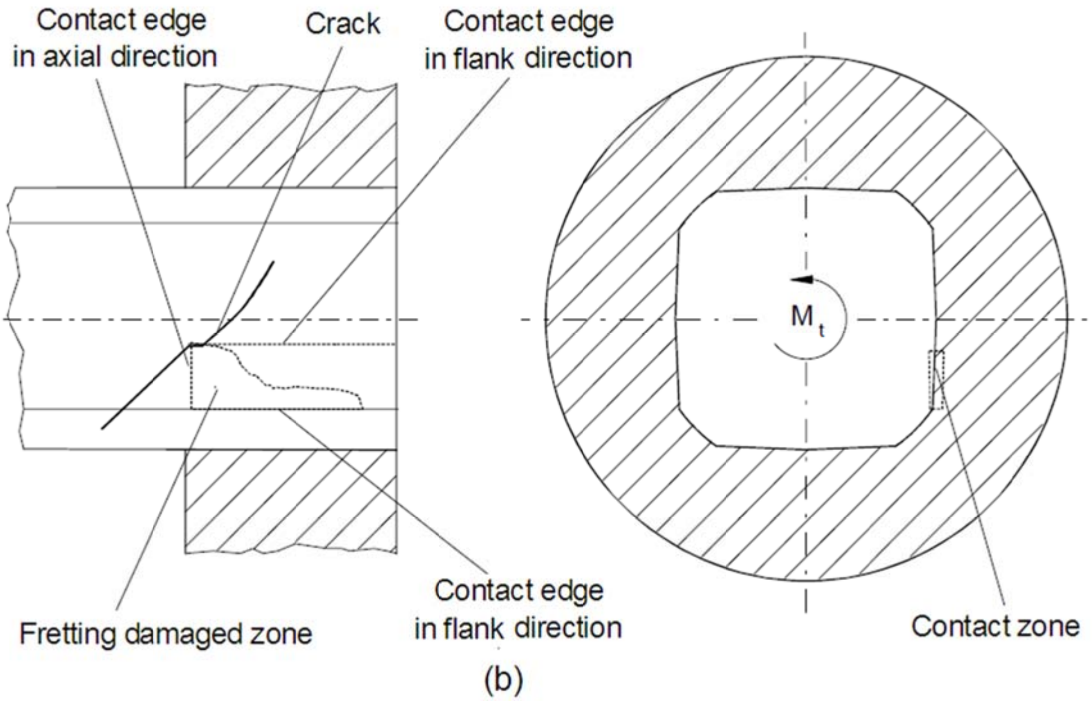

Figure 6-2: Fretting fatigue fracture of P4C polygon shaft-hub connection under dynamic torsion, (a) fretting fatigue fractured P4C shaft; (b) schematic diagram of the fretting fatigue crack initiation location. After [Win-01]

6.2 Optimization efforts in involute spline teeth

The standard spline teeth DIN 5480 45x21x2 with fillet R0.32 and rounding R0 is used as reference of comparison, the distribution of contact pressure, the fretting/plain fatigue unified prediction parameters along the spline teeth flank with different fillet radius and chamfer structure under same load are compared. The maximal value of contact pressure, the fretting/plain fatigue unified prediction parameters along spline teeth flank are quantified using percentage of the corresponding maximal value along the reference spline teeth.

Figure 6-3 showed the distribution of contact pressure along teeth flank with different fillet and chamfer design. The rounding and chamfer in teeth tip do not relieve but deteriorate the contact pressure singularity near contact edge, the maximal contact pressure will be greatly increased compared to the spline teeth without rounding or chamfer. Similar situation also observed in the fretting fatigue research of clamping element connection by T. Casper [Cas-99]. Explains to this phenomenon is that the contact length between teeth flank is decreased and the edge of teeth tip becomes stiffer due to rounding or chamfer. Increase the fillet radius will not change the distribution of contact pressure under static load. Due to stress singularity near contact edge of teeth flank, plastic deformation and consequently fracture may occur near contact edge before fatigue crack under heavy load, as showed in Figure 5-12. So, the stress singularity near contact edge of teeth flank limited the load capacity improvement of involute spline shaft-hub connections.

Figure 6-3: Distribution of contact pressure (normalized by dividing respective maximal values) along teeth flank with different fillet and chamfer structure, $F=F_m+F_a=8667.5N$.

Figure 6-4 and Figure 6-5 show the distribution of tensile crack mode K_{FDP}SWT parameter and shear crack mode K_{FDP}FS parameter along the flank of involute spline teeth that with different fillet radius respectively. It can be seen from figure 6-4 that the maximal value of K_{FDP}SWT parameter decrease with the increase of fillet radius and the danger of plain fatigue at teeth fillet is decreased, but it is still greater than the fretting fatigue danger near the contact edge. The distribution of shear mode K_{FDP}FS showed similar tendency like K_{FDP}SWT parameter, but for the teeth with fillet radius of R0.64mm, the danger of shear mode fretting fatigue near contact edge have succeed the danger of plain fatigue at teeth fillet, the fretting fatigue may become the dominant failure mechanism in this situation. Increase radius of teeth fillet do improved the overall fatigue strength of spline teeth. But the optimization domain is very constrained due to the interference with the teeth tip of the counterpart. Further increase of the fillet radius is not possible without increase the chamfer or rounding, increase chamfer or rounding will further deteriorate the stress singularity as discussed above and also decrease the fitting length of teeth flank.

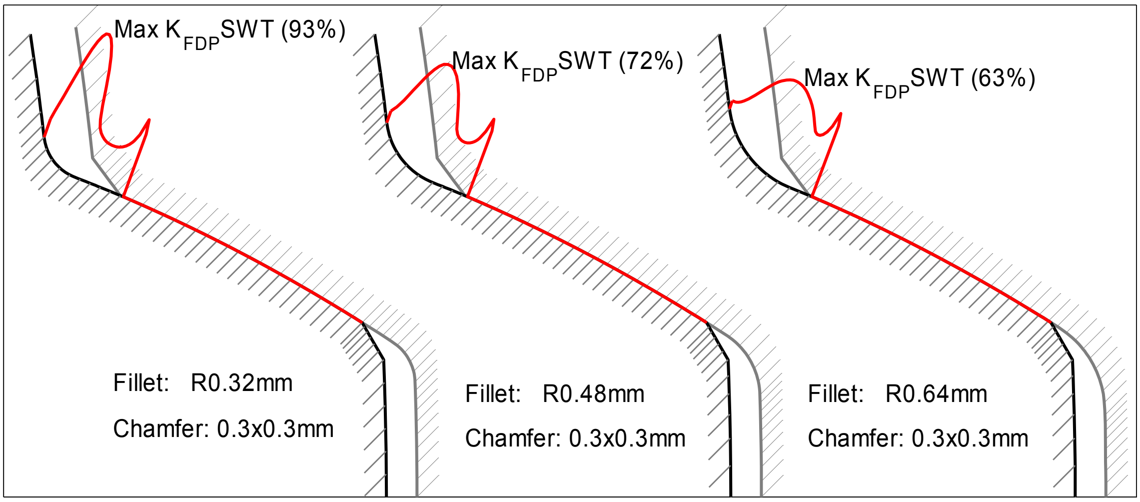

Figure 6-4: Distribution of K_{FDP}SWT parameter (normalized by dividing respective maximal values) along the flank of spline teeth with different fillet radius, F_m=5183.3N; R_F=0.2.

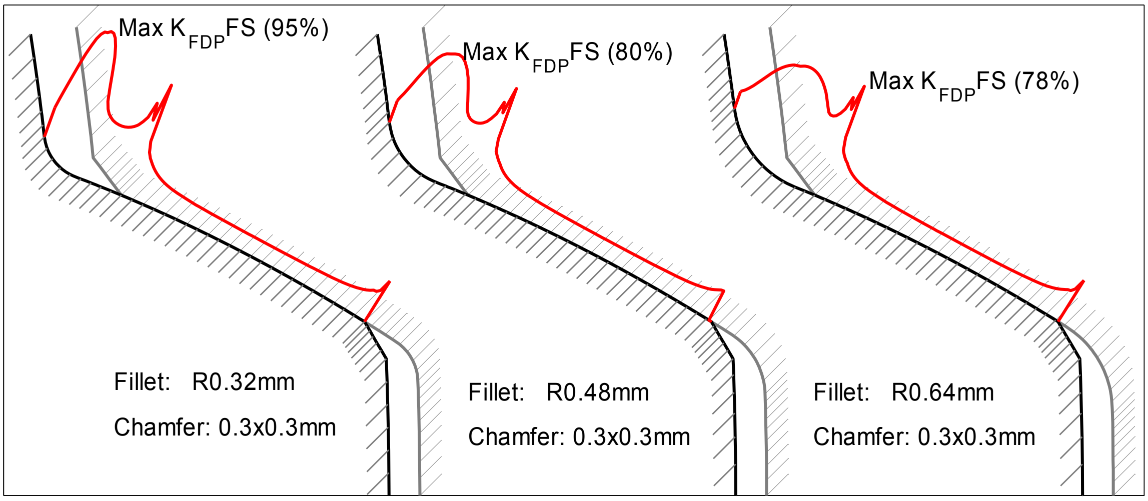

Figure 6-5: Distribution of K_{FDP}FS parameter (normalized by dividing respective maximal values) along the flank of spline teeth with different fillet radius, F_m=5183.3N; R_F=0.2.

6.3 Complex cycloid profiles

6.3.1 Complex cycloid profile developed by Ziaei, M.

The contour of the involute spline teeth is not continuous and the stress singularity near contact edge of teeth flank is inevitable. Increase the teeth fillet radius will alleviate the danger of plain fatigue strength of it, but the danger fretting fatigue near contact edge will not be alleviated and the increase of fillet radius is also limited due to the interference with the teeth tip of the counterpart. On the contrary, the polygon profile is continuous, and without problem of stress singularity and 'wick teeth fillet', but the problem of fretting fatigue will be prominent. Recently Ziaei, M. introduced a complex cycloid shaft-hub connections profile and corresponding common parameter equation, as expressed in equation (6-1):

$$\begin{aligned} x(\alpha_0) &= (R+r)\cdot cos\alpha_0 + f_{x1}(e_0)\cdot\cos(\alpha_1) + f_{x2}(e_0)\cdot\cos(\alpha_2) + f_{x3}(e_0)\cdot\cos(\alpha_3) \\ &\quad + f_{x4}(e_0)\cdot\cos(\alpha_4) \\ y(\alpha_0) &= (R+r)\cdot\sin\alpha_0 + f_{y1}(e_0)\cdot\sin(\alpha_1) + f_{y2}(e_0)\cdot\sin(\alpha_2) + f_{y3}(e_0)\cdot\sin(\alpha_3) \\ &\quad + f_{y4}(e_0)\cdot\sin(\alpha_4) \end{aligned} \tag{6-1}$$

where R is the radius of fixed circle, r is the radius of rolling circle, α_0 is the angle from the starting point to the tangential point of rolling circle and fixed circle center, e_0 is the eccentricity, $\alpha_1, \alpha_2, \alpha_3$ and α_4 are the function of α_0, f_{x1}, f_{x2}, f_{x3} and f_{x4} as well as f_{y1}, f_{y2}, f_{y3} and f_{y4} are function of eccentricity and dependent each other. This parameter equation can create complex epitrochoid, complex hypotrochoid and hybrid complex cycloid when above functions satisfy corresponding conditions [Zia-02, Zia-07]. The parameters R, r, α_0 and e_0 are originated from the simple epitrochoid or hypotrochoid, Figure 6-6 shows a simple epitrochoid and its basic parameters. In the simple epitrochoid or hypotrochoid, the eccentricity e_0 is a constant; in complex cycloid, the eccentricity e is function of e_0 and changes periodically, Figure 6-7 shows a complex epitrochoid (T00, will be mentioned in following) and its basic parameters. The common parameter equation of complex cycloid provides the possibility to look for a shaft-hub connection profile better than both involute spline and polygon shaft-hub connection profiles.

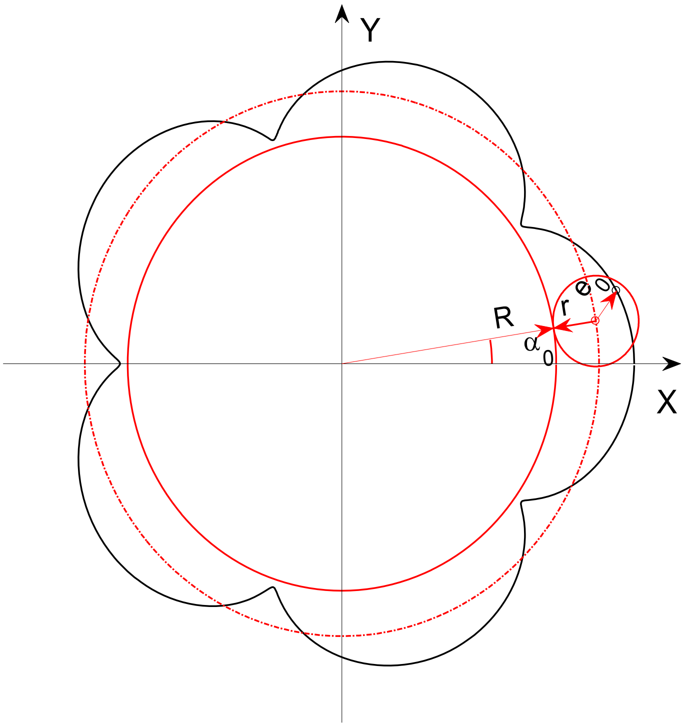

$$x(\alpha_0)=(R+r)\cos(\alpha_0)+e_0\cos((z+1)\alpha_0)$$

$$y(\alpha_0)=(R+r)\sin(\alpha_0)+e_0\sin((z+1)\alpha_0)$$

Figure 6-6: Basic parameters of epitrochoid

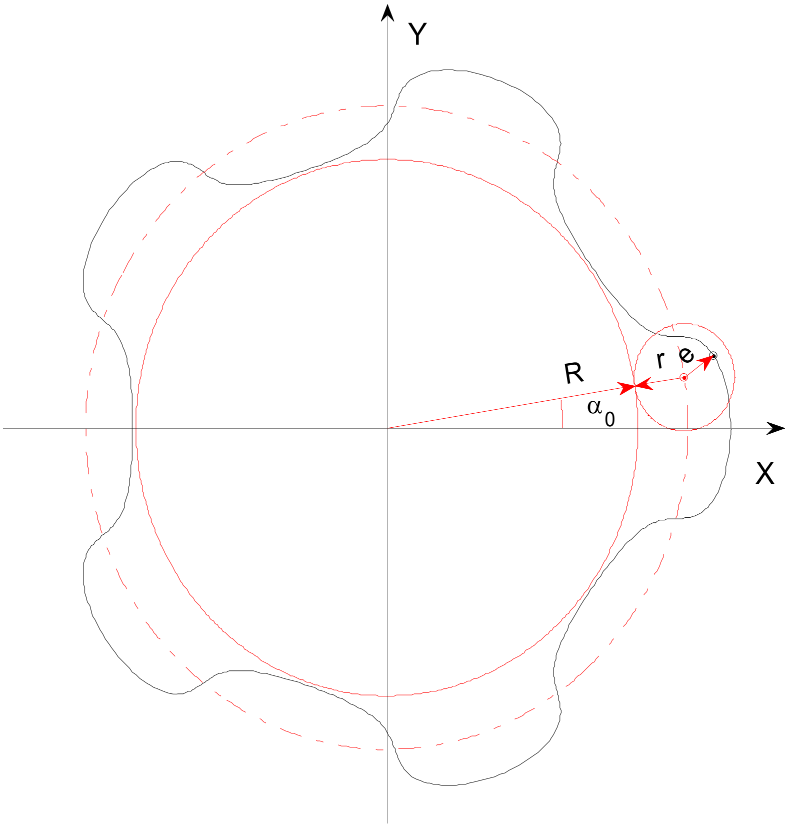

Figure 6-7: Basic parameters of a complex epitrochoid (T00)

Numerous types of complex cycloid can be generated by changing the additional eccentricities in the common complex cycloid equation (6-1), many types of complex cycloid profiles are introduced by Ziaei, M. and his colleges in the past several years, but no one is pronounced to be the best one. Here a type of complex cycloid profile(so called as T00 in [Mai-08]) is chose to compare with the involute spline SHC DIN5480 45x2x21, this profile are defined as following:

$$\begin{aligned}
x(\alpha_0) &= (R+r)\cdot cos\alpha_0 + \frac{z+1}{2}\cdot e_0\cdot\cos((z-1)\cdot\alpha_0) + \frac{z-1}{2}\cdot e_0\cdot\cos((z+1)\cdot\alpha_0)\\
&\quad -\frac{2\cdot z+1}{8}\cdot e_0\cdot\cos((2\cdot z-1)\cdot\alpha_0) + \frac{2\cdot z-1}{8}\cdot e_0\cdot\cos((2\cdot z+1)\cdot\alpha_0)\\
y(\alpha_0) &= (R+r)\cdot\sin\alpha_0 - \frac{z+1}{2}\cdot e_0\cdot\sin((z-1)\cdot\alpha_0) + \frac{z-1}{2}\cdot e_0\cdot\sin((z+1)\cdot\alpha_0)\\
&\quad +\frac{2\cdot z+1}{8}\cdot e_0\cdot\sin((2\cdot z-1)\cdot\alpha_0) + \frac{2\cdot z-1}{8}\cdot e_0\cdot\sin((2\cdot z+1)\cdot\alpha_0)
\end{aligned} \tag{6-2}$$

where $z = R/r$ is the number of teeth. To be comparable with involute spline SHC DIN5480 45x2x21, the teeth number and major diameter of complex cycloid profile are the same with DIN5480 45x2x21, changing the radius $R+r$ or eccentricity e_0 and considering the minor radius being close to the minor radius of DIN5480 45x2x21 (20.2mm), four different profiles are generated, named as T00-A (refer to DIN5480 45x2x21) ,T00-B (refer to DIN5480 45x2x21), T00-C (refer to DIN5480 45x2x21) and T00-D (refer to DIN5480 45x2x21) respectively, as shown in Figure 6-8. Because numerous profiles can be generated by the parametric equation of T00, so the text in the bracket marked the corresponding reference profile from DIN5480, and the capital letter A, B, C and D after T00 are used to differentiate the profile generated by different $R+r$ and e. Main parameters of above four complex cycloid profiles are listed in Table 6-1. Similar to the involute spline shaft-hub connections, the FE model of complex cycloid profile ‘T00-A (refer to DIN5480 45x2x21)’ is shown in figure 6-9, T00-B; T00-C and T00-D are also modeled in the same way.

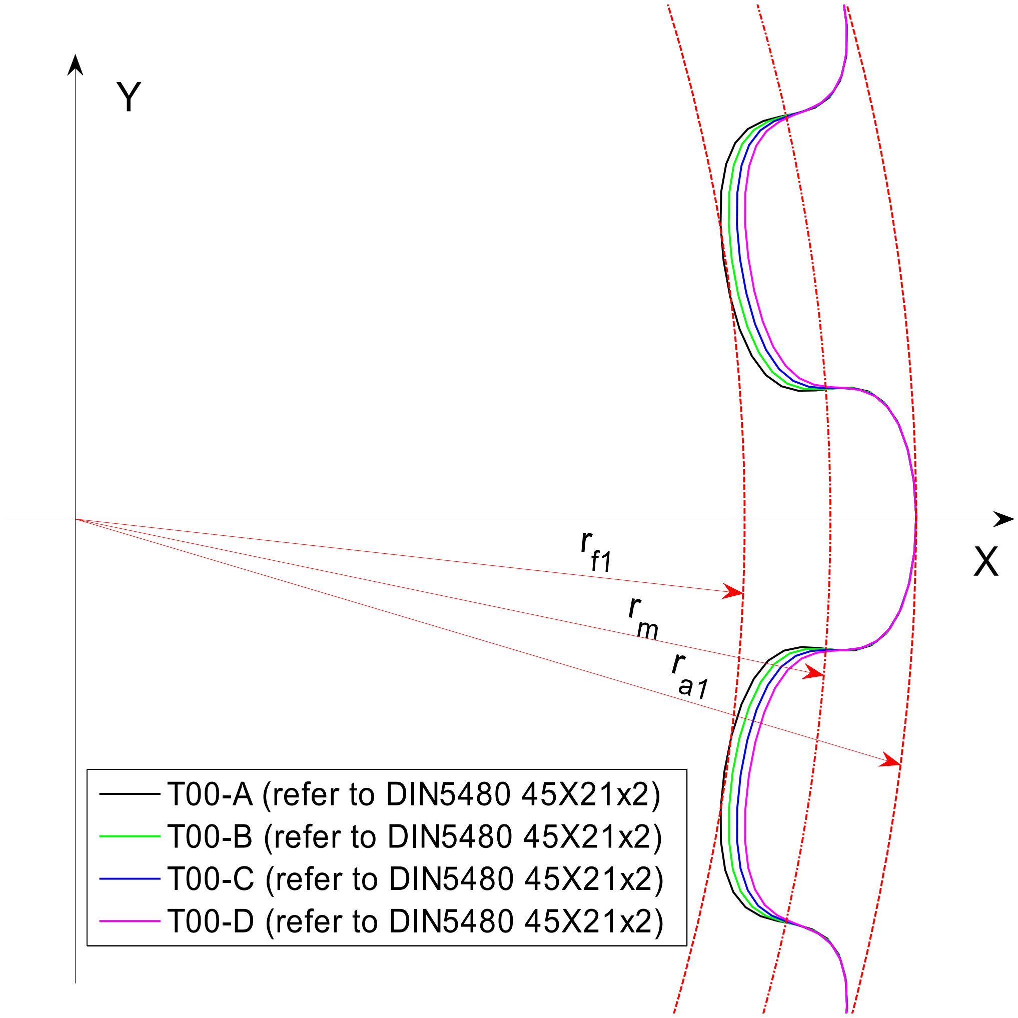

Figure 6-8: Four different T00 type profiles referred to DIN5480 45x2x21 (r_{f1}=20.2, r_{a1}=22.3, $r_m = \left(r_{a1} + r_{f1}\right)/2$ =21.25)

Table 6-1: Main parameters of complex hypotrochoid profile

Parameters / SHC profile	Radius $R+r$	Eccen-tricity e_0	Teeth number z	Major diameter r_{a1}	Minor diameter r_{f1}
T00-A (refer to DIN5480 45x2x21)	21.25	4.2/83	21	22.3	20.1747
T00-B (refer to DIN5480 45x2x21)	21.3	4/83	21	22.3	20.2759
T00-C (refer to DIN5480 45x2x21)	21.35	3.8/83	21	22.3	20.3771

T00-D (refer to DIN5480 45x2x21)	21.4	3.6/83	21	22.3	20.4783

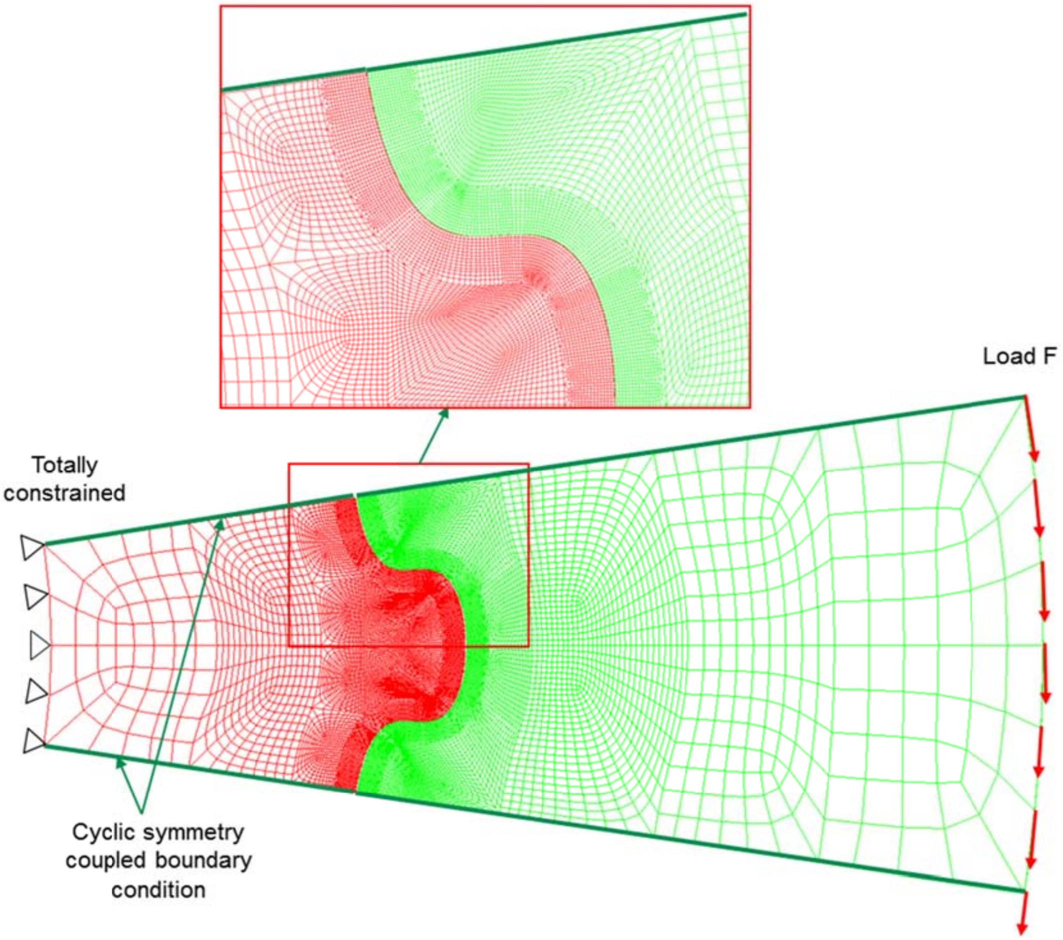

Figure 6-9: FE model of a complex cycloid profile representative teeth pair

Figure 6-10 to Figure 6-11 show the distribution of contact pressure, maximal principal stress, Von-mises stress, normal stress in tangential direction of flank and normal stress in normal direction of flank (normalized by dividing the maximal value) along the teeth flank of T00-A under static load. Compared with the involute spline teeth, the contact pressure is more averagely distributed along teeth flank; the contact pressure within the addendum and dedendum are nearly zero, that’s to say there will be small wear within the addendum and dedendum, which is good for centering between shaft and hub. Different to the involute spline teeth, the maximal principal stress and the normal stress in tangential direction of teeth flank changed from tension stress to compression stress smoothly, and not at the start of contact but in the middle of teeth flank. Distribution of contact pressure, maximal principal stress, Von-mises stress, normal stress in tangential direction of flank and normal stress in normal direction of flank along the teeth flank of Profile T00-B, T00-C and T00-D also showed similar characteristics.

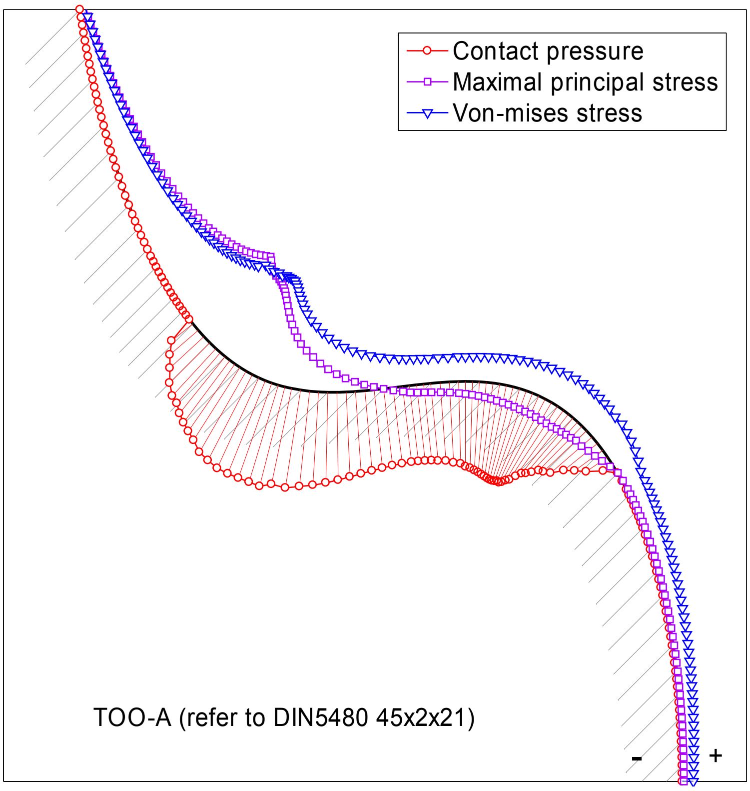

Figure 6-10: Distribution of maximal principal stress and Von-mises stress along teeth flank of T00-A (normalized by dividing respective maximal value), F=8667.5N

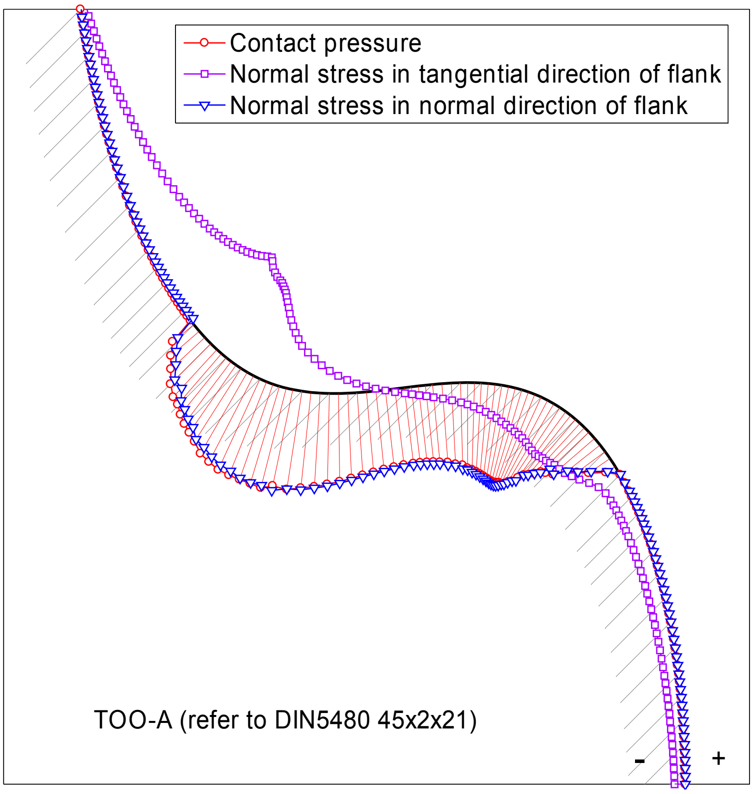

Figure 6-11: Distribution of normal stresses in tangential and normal direction of teeth flank T00-A (normalized by dividing respective maximal value), F=8667.5N

Figure 6-12 to figure 6-19 show the distributions of $K_{FDP}SWT$ and $K_{FDP}FS$ along teeth flank of profile T00-A, T00-B, T00-C and T00-D under same dynamic loads with that in involute spline teeth pair. As a comparison, the distribution of pure plain fatigue prediction parameter SWT and FS are also presented in these figures. It can be seen that the danger of tensile mode plain fatigue decreased about 20% in these four profiles compared with the reference involute spline teeth (the involute spline teeth flank with fillet R0.32 and rounding R0 are also used as reference of comparison), the danger of shear mode plain fatigue decreased about 10% in these four profiles besides T00-D. In T00-D, the maximal value of shear based FS parameter showed no difference to that in involute spline profile. But, both the tensile crack mode and shear crack mode fretting/plain fatigue unified prediction parameter in these four profiles showed no decrease but increase. The most seriously fretted location always overlaps with the location of plain fatigue at teeth ‘fillet’, the complex cycloid profiles T00-A, B, C and D are more sensitive to fretting fatigue compared with involute spline profile though the teeth root is more strength against plain fatigue.

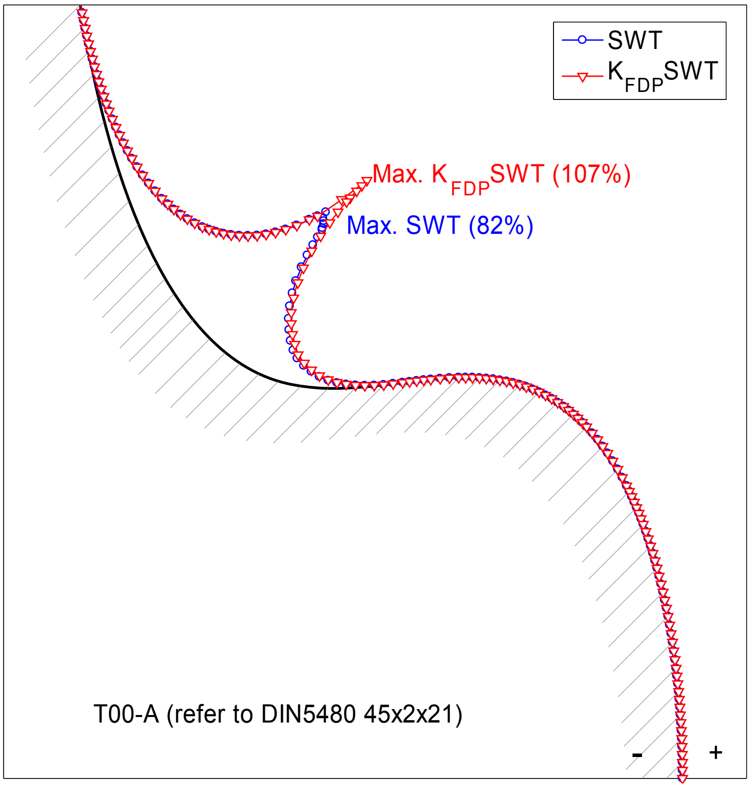

Figure 6-12 Distribution of SWT and K_{FDP}SWT parameter along teeth flank of T00-A (refer to DIN5480 45x2x21), F_m=5183.3N; R_F=0.2.

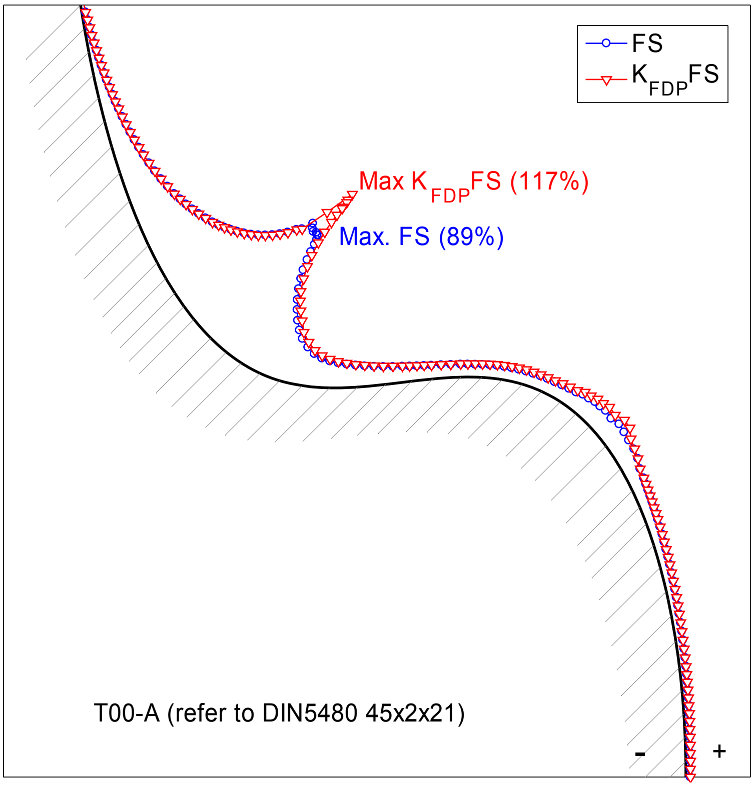

Figure 6-13: Distribution of FS and K_{FDP}FS parameter along teeth flank of T00-A (refer to DIN5480 45x2x21), F_m=5183.3N; R_F=0.2.

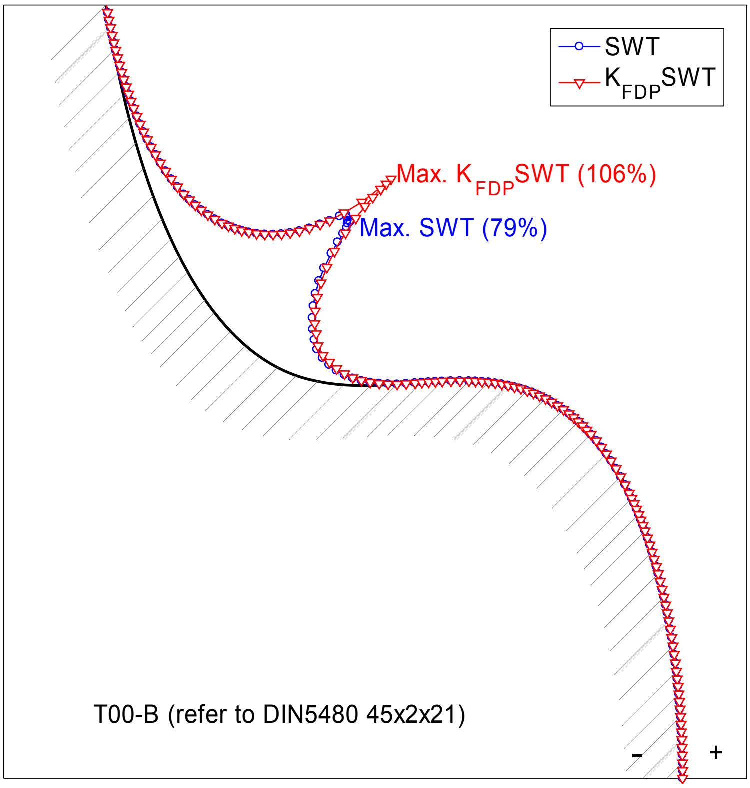

Figure 6-14: Distribution of SWT and K_{FDP}SWT parameter along teeth flank of T00-B (refer to DIN5480 45x2x21), F_m=5183.3N; R_F=0.2.

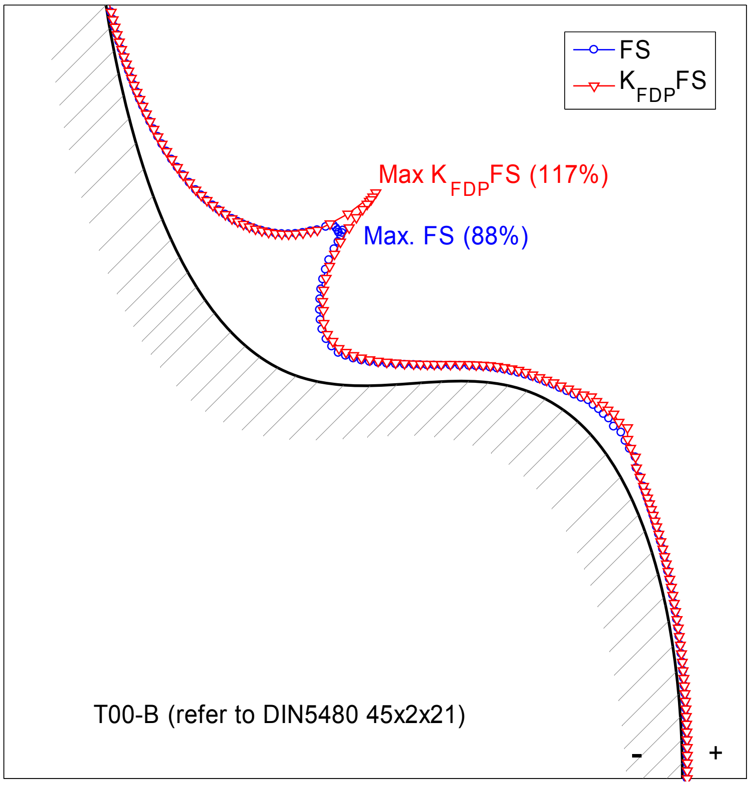

Figure 6-15: Distribution of FS and K_{FDP}FS parameter along teeth flank of T00-B (refer to DIN5480 45x2x21), F_m=5183.3N; R_F=0.2.

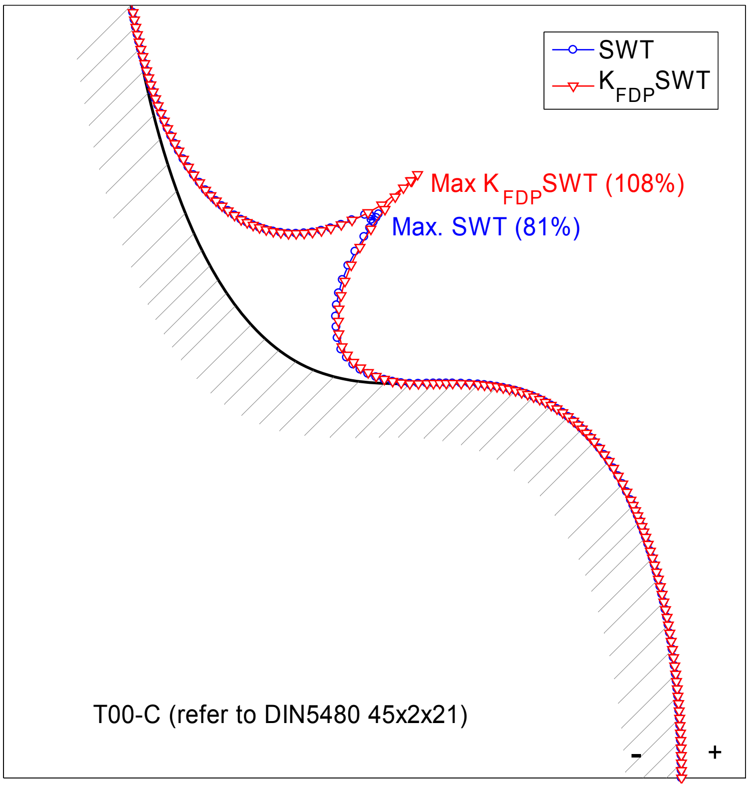

Figure 6-16: Distribution of SWT and K_{FDP}SWT parameter along teeth flank of T00-C (refer to DIN5480 45x2x21), F_m=5183.3N; R_F=0.2.

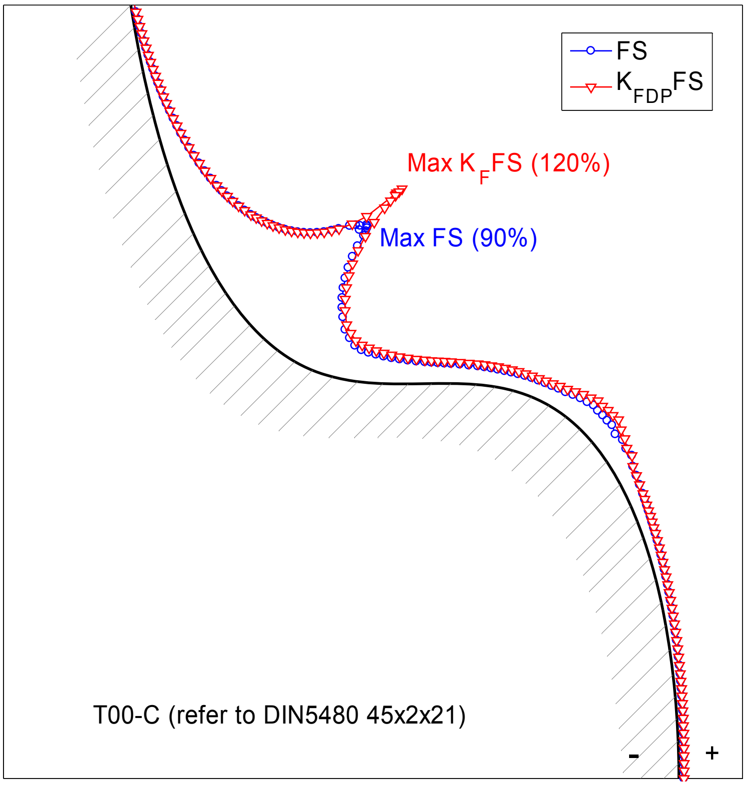

Figure 6-17: Distribution of FS and K_{FDP}FS parameter along teeth flank of T00-C (refer to DIN5480 45x2x21), F_m=5183.3N; R_F=0.2.

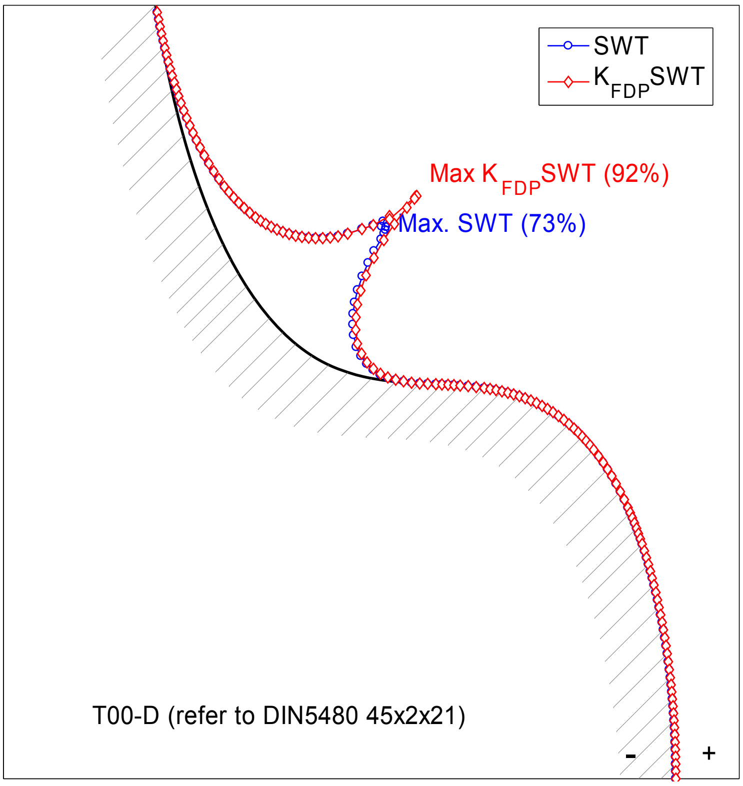

Figure 6-18: Distribution of SWT and K_{FDP}SWT parameter along teeth flank of T00-D (refer to DIN5480 45x2x21), F_m=5183.3N; R_F=0.2.

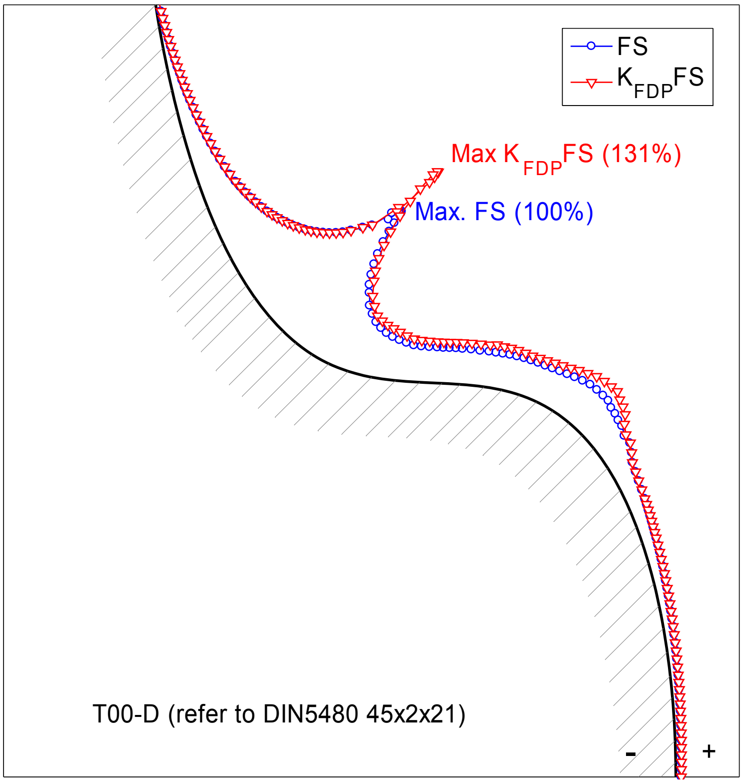

Figure 6-19: Distribution of FS and K_{FDP}FS parameter along teeth flank of T00-D (refer to DIN5480 45x2x21), F_m=5183.3N; R_F=0.2.

6.3.2 IMW complex cycloid profiles

Above analysis showed that not all the complex cycloid profiles are better than involute spline profile considering both plain and fretting fatigue performances. Though the common parameter equation introduced by Ziaei, M provided us numerous possibilities of new shaft hub connection profiles, a clearly defined and better one are still waited for. For industry application, too many possibilities means uncertainty, which makes confuse sometimes, it will be better when it can be standardized like the involute spline profiles.

Referred to the common equation introduced by Ziaei, M. [Zia-07], a new group of complex cycloid profile is introduced here, named as IMW01 profile.

$$
\begin{aligned}
x(\alpha_0) &= (R+r)\cdot cos\alpha_0 - \frac{4\cdot z}{3}\cdot e_0\cdot\cos\big((z-1)\cdot\alpha_0\big) - \frac{4\cdot z}{3}\cdot e_0\cdot\cos\big((z+1)\cdot\alpha_0\big)\\
&\quad - f_{x3}\cdot\cos\big((2\cdot z-1)\cdot\alpha_0\big) + f_{x4}\cdot\cos\big((2\cdot z+1)\cdot\alpha_0\big)\\
y(\alpha_0) &= (R+r)\cdot\sin\alpha_0 + \frac{4\cdot z}{3}\cdot e_0\cdot\sin\big((z-1)\cdot\alpha_0\big) - \frac{4\cdot z}{3}\cdot e_0\cdot\sin\big((z+1)\cdot\alpha_0\big)\\
&\quad + f_{y3}\cdot\sin\big((2\cdot z-1)\cdot\alpha_0\big) + f_{y4}\cdot\sin\big((2\cdot z+1)\cdot\alpha_0\big)\\
f_{x3} &= f_{x4} = f_{y3} = f_{y4} = \cdots,\frac{6\cdot z\cdot e_0}{10},\frac{5\cdot z\cdot e_0}{10},\frac{4\cdot z\cdot e_0}{10},\frac{3\cdot z\cdot e_0}{10},\cdots
\end{aligned}
\tag{6-3}
$$

Keep the teeth number, the major radius, minor radius and the middle radius ($R+r=(r_{a1}+r_{f1})/2$) be the same with involute spline SHC DIN5480 45x2x21, change the factor $f_{x3}, f_{x4}, f_{y3}, f_{y4}$, the pressure angle of teeth flank can be changed. Table 6-2 listed the main parameters of four IMW01 complex cycloid profiles with different factor $f_{x3}, f_{x4}, f_{y3}, f_{y4}$. With the decrease of factor $f_{x3}, f_{x4}, f_{y3}, f_{y4}$, the pressure angle will be increased.

Table 6-2: Main parameters of complex cycloid profile IMW01- IMW04

Parameters SHC profile	Radius $R+r$	Eccentricity e_0	Teeth number z	Major diameter r_{a1}	Minor diameter r_{f1}
IMW01-A, $f_{x3}=f_{x4}=f_{y3}=f_{y4}=\frac{6\cdot z\cdot e_0}{10}$	21.25	(21.25-20.2)/56	21	22.3	20.2
IMW01-B, $f_{x3}=f_{x4}=f_{y3}=f_{y4}=\frac{5\cdot z\cdot e_0}{10}$	21.25	(21.25-20.2)/56	21	22.3	20.2

IMW01-C, $f_{x3}=f_{x4}=f_{y3}=f_{y4}=\frac{4\cdot z\cdot e_0}{10}$	21.25	(21.25-20.2)/56	21	22.3	20.2
IMW01-D, $f_{x3}=f_{x4}=f_{y3}=f_{y4}=\frac{3\cdot z\cdot e_0}{10}$	21.25	(21.25-20.2)/56	21	22.3	20.2

Figure 6-20 shows the shape of these 4 profiles described by above equation and parameters. The profiles are rotated 180/21 degree around the axis clockwise in FE analysis, so that the middle line of teeth meets the X axis of the coordinate system for the unity with other profiles.

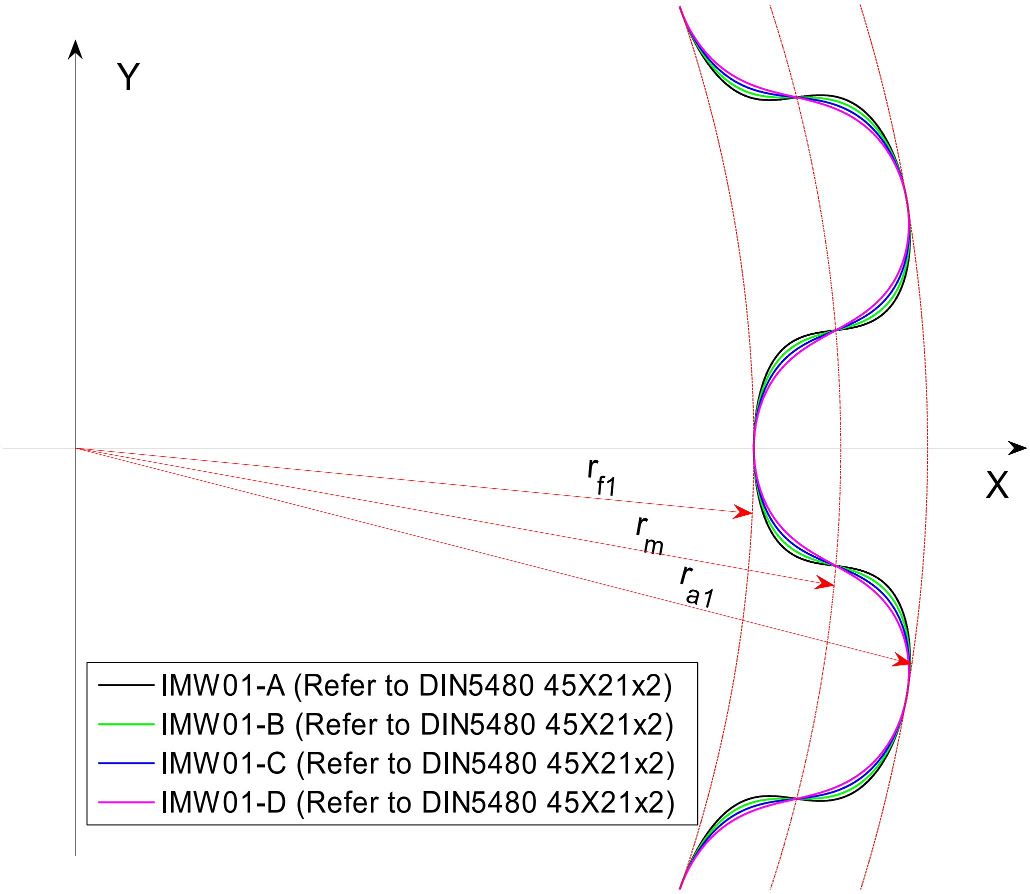

Figure 6-20: Four different IMW01 profiles referred to DIN5480 45x2x21 (r_{f1}=20.2, r_{a1}=22.3, $r_m=\left(r_{a1}+r_{f1}\right)/2$=21.25)

The distribution of contact pressure, maximal principal stress, Von-mises stress, normal stress in tangential direction of flank and normal stress in normal direction of flank (normalized by dividing the maximal value) along the teeth flank of IMW01-A under the same static load with that in involute spline teeth pair are shown in Figure 6-21 and Figure 6-22. They are similar to that in T00 profile. Figure 6-23 to figure 6-30 show the distributions of K_{FDP}SWT and K_{FDP}FS as well as SWT and FS along teeth flank of profile IMW01-A, IMW01-B, IMW01-C and IMW01-D under same dynamic loads with that in involute spline teeth pair. With the increase of pressure angle, both the maximal values of tensile mode based SWT parameter and shear based FS parameter are decreased, the maximal value of K_{FDP}SWT also decreased. But the maximal value of shear mode fretting/plain fatigue unified prediction parameter return to increase after IMW01-C profile. Considering both the tensile crack mode and shear crack mode fretting/plain fatigue unified prediction parameter, the IMW01-C is the best profile among these four profiles that with different pressure angles, the danger of tensile mode crack decreased about 30%, the danger of shear mode crack decreased about 20%. Following the same method above, every involute spline shaft-hub connection in DIN5480 can find a corresponding IMW profile that with better overall fatigue performances through pressure angle optimization. Appendix B shows the shape of some IMW profiles that with same teeth number, major radius, minor radius and middle radius with involute spline shaft hub connection in DIN5480, they are also marked with module m and teeth number z like their corresponding reference involute spline shaft-hub connections in DIN5480.

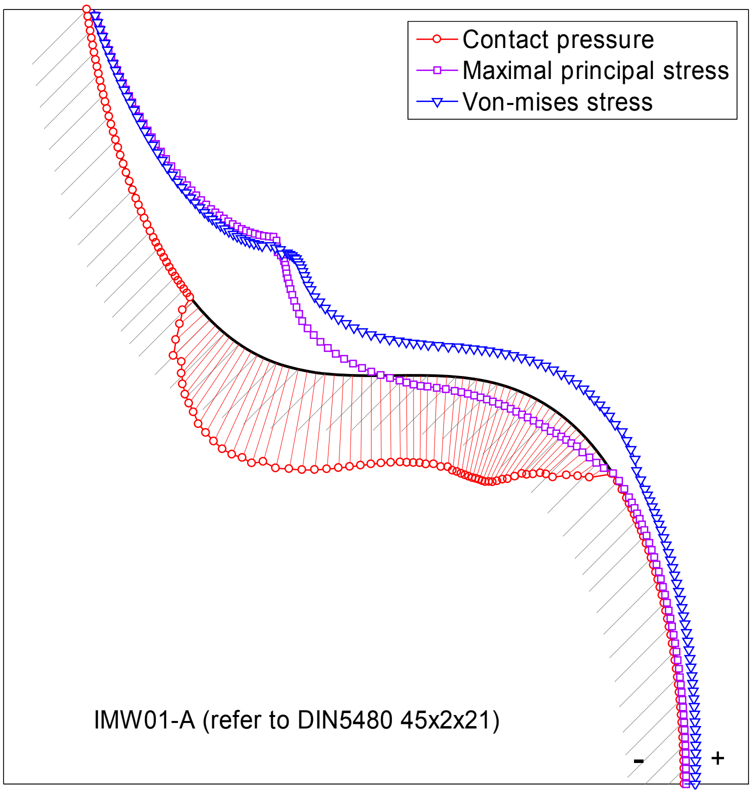

Figure 6-21: Distribution of maximal principal stress and Von-mises stress along teeth flank of IMW01-A (normalized by dividing respective maximal value), F=8667.5N

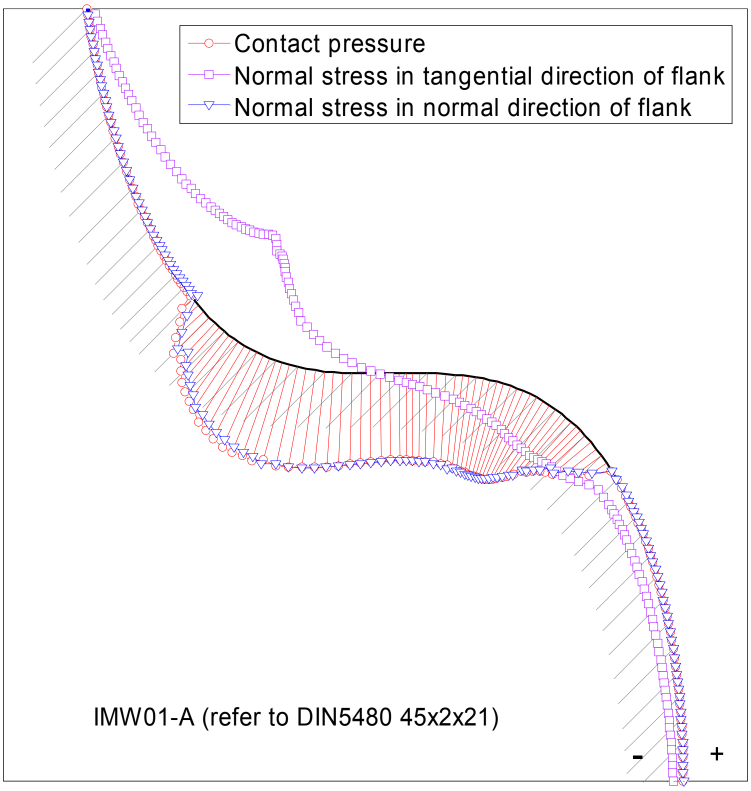

Figure 6-22: Distribution of normal stresses in tangential and normal direction of teeth flank IMW01-A (normalized by dividing respective maximal value), F=8667.5N

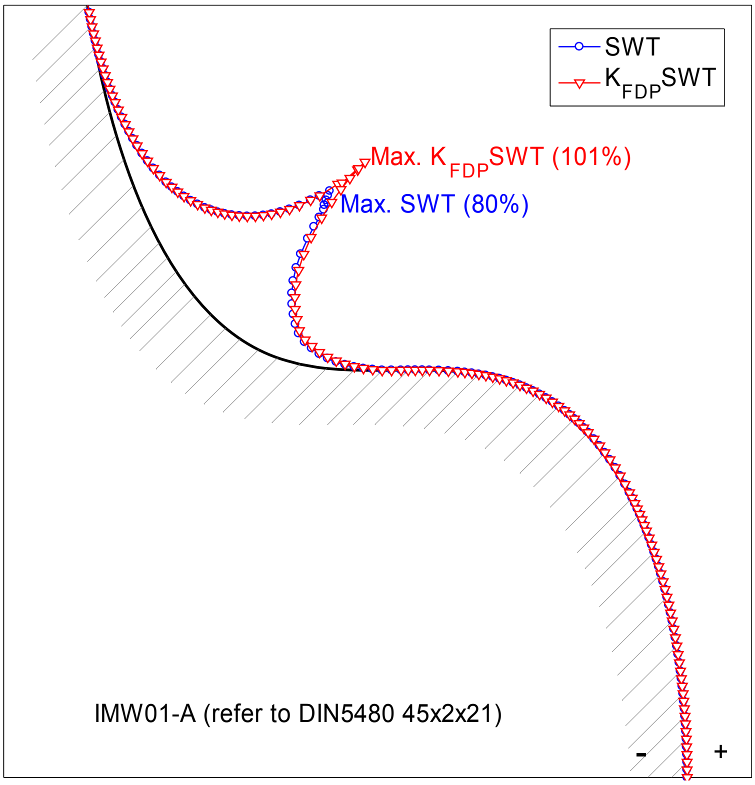

Figure 6-23: Distribution of SWT and K_{FDP}SWT parameter along teeth flank of IMW01-A (refer to DIN5480 45x2x21), F_m=5183.3N; R_F=0.2.

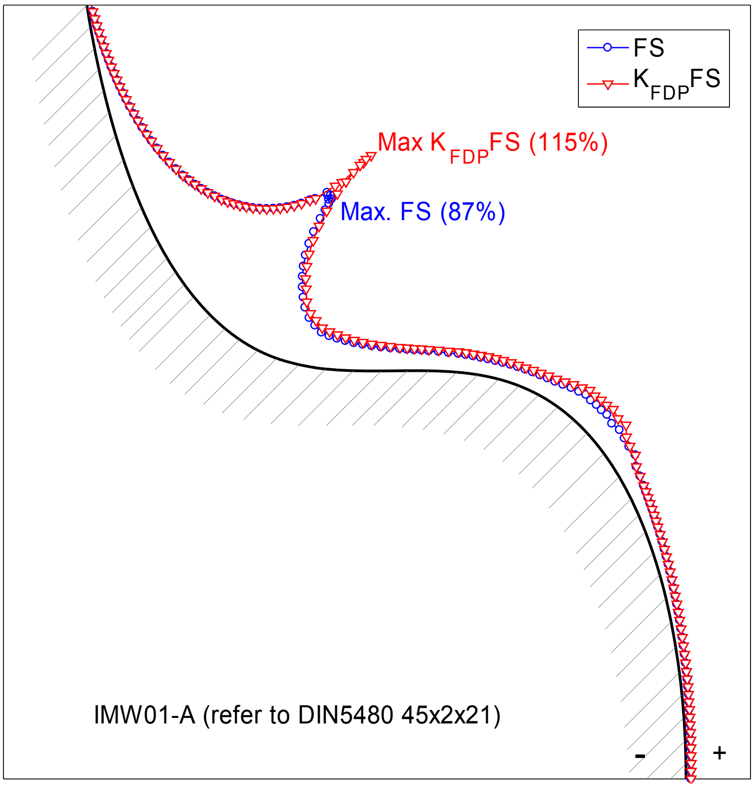

Figure 6-24: Distribution of FS and K_{FDP}FS parameter along teeth flank of IMW01-A (refer to DIN5480 45x2x21), F_m=5183.3N; R_F=0.2.

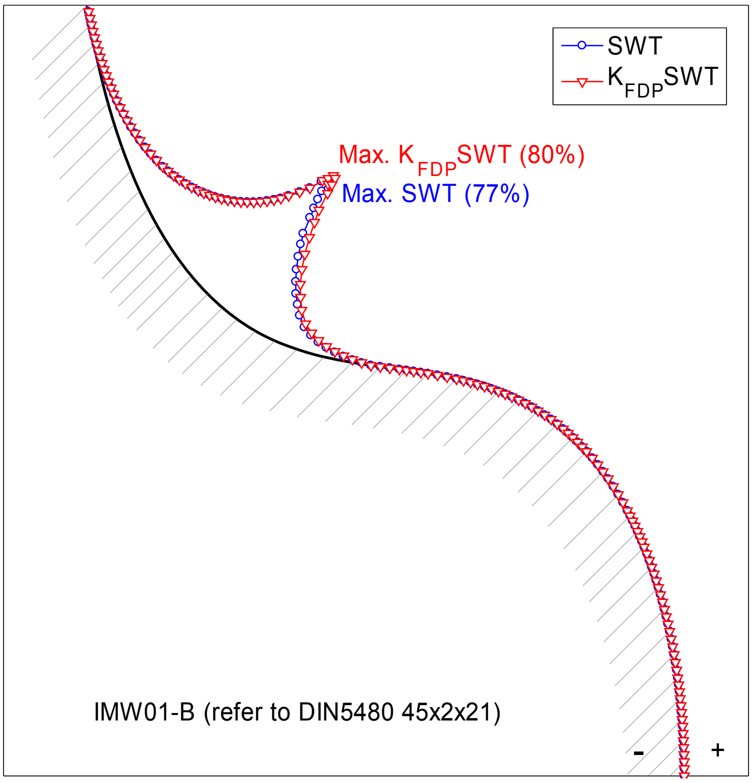

Figure 6-25: Distribution of SWT and K_{FDP}SWT parameter along teeth flank of IMW01-B (refer to DIN5480 45x2x21), F_m=5183.3N; R_F=0.2.

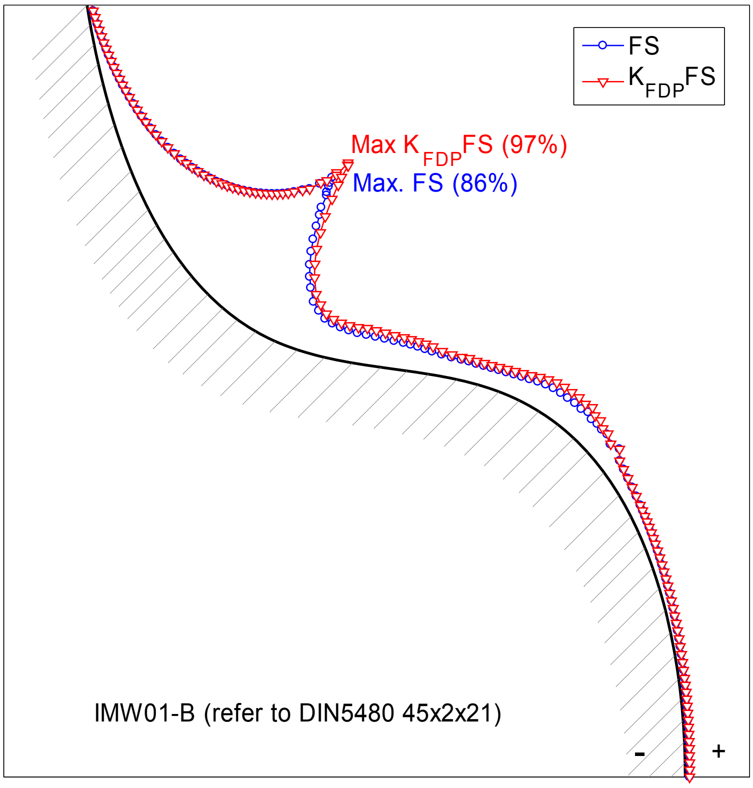

Figure 6-26: Distribution of FS and $K_{FDP}FS$ parameter along teeth flank of IMW01-B (refer to DIN5480 45x2x21), F_m=5183.3N; R_F=0.2.

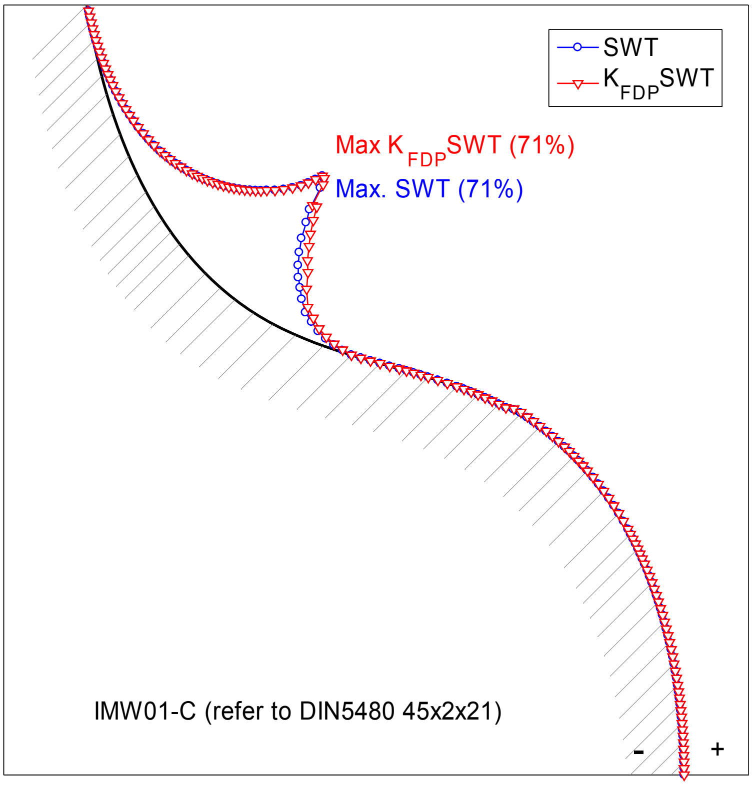

Figure 6-27: Distribution of SWT and $K_{FDP}SWT$ parameter along teeth flank of IMW01-C (refer to DIN5480 45x2x21), F_m=5183.3N; R_F=0.2.

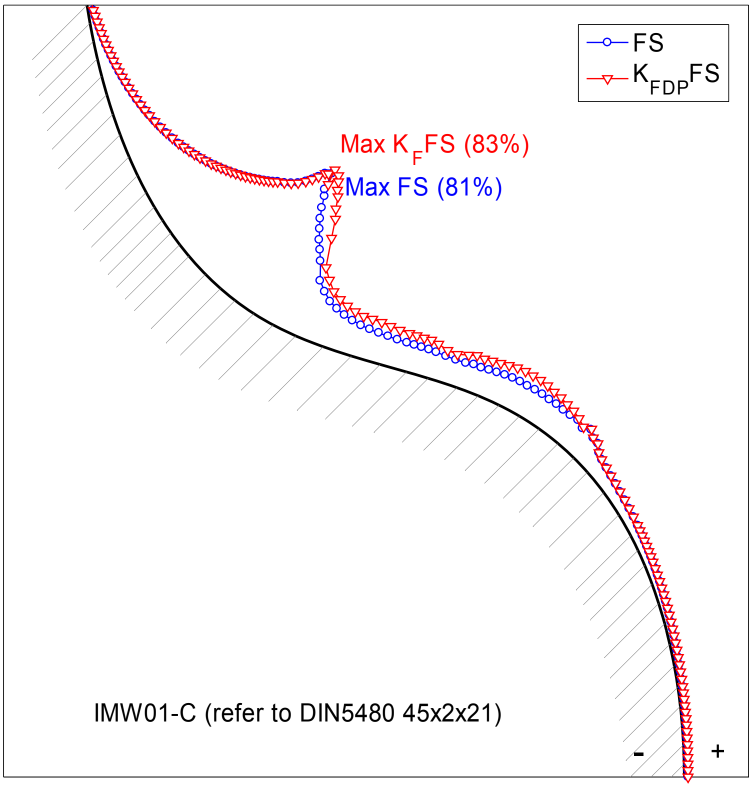

Figure 6-28: Distribution of FS and $K_{FDP}FS$ parameter along teeth flank of IMW01-C (refer to DIN5480 45x2x21), F_m=5183.3N; R_F=0.2.

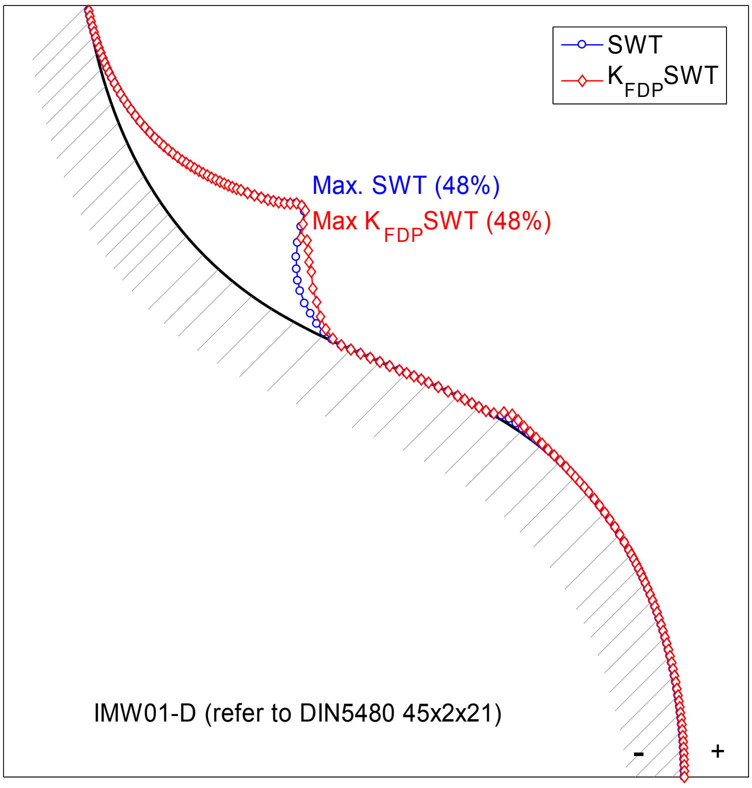

Figure 6-29: Distribution of SWT and $K_{FDP}SWT$ parameter along teeth flank of IMW01-D (refer to DIN5480 45x2x21), F_m=5183.3N; R_F=0.2.

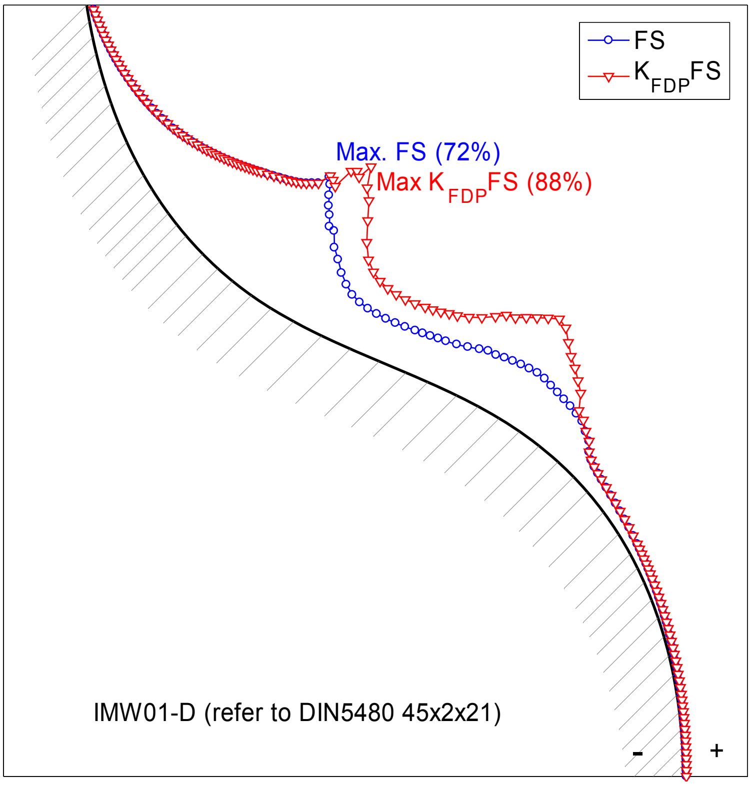

Figure 6-30: Distribution of FS and K_{FDP}FS parameter along teeth flank of IMW01-D (refer to DIN5480 45x2x21), F_m=5183.3N; R_F=0.2.

6.4 Conclusion

Theoretically, the universal parameter equation of complex cycloid profile introduced by Ziaei, M [Zia-07] provides numerous possibilities of complex cycloid shaft-hub connection profiles. The complex cycloid profiles are continuous and consequently without the problem of stress singularity, the plain fatigue strength at teeth fillet is increased. But considering the effects of fretting, not all of them are superior to the standard involute spline shaft-hub connection profile. The newly introduced IMW complex cycloid profile with optimized pressure angle showed better performances than involute spline shaft-hub connection profile evaluated by the fretting/plain fatigue unified prediction parameter, it can be also standardized conveniently refer to DIN5480.

Existing shaft-hub connection profiles have provided us many alternatives and choices. As a matter of fact, we need only a well-defined perfect one for the convenience of industry application. We should bear in the mind that the main functions of a profile shaft-hub connection are torque transmission and shaft-hub centering. To better fulfill these two functions with lower cost, some requirements of a perfect shaft-hub connection profiles are summerized as following:

(1) High capacity of transmitting both static and dynamic torque. In order to reach this aim, the shaft-hub connection profile must endure both of these problems: stress concentration and consequently plain fatigue at teeth fillet, fretting fatigue/wear within contact interface. As compared above, the strong fillet in T00 complex cycloid profiles alleviate the stress concentration at teeth fillet, but fretting also occurs at the most stressed teeth fillet, therefore increased the danger of fretting fatigue.

(2) High precision of centering shaft relative to hub. Simpler geometry of the mating surfaces can be more precisely machined and therefore be help to improve the precision of centering. For example, the external/internal cylinder mating surface in a straight spline shaft-hub connections can be more precisely and economically machined than the involute spline mating surface in an involute spline shaft-hub connections, naturally, the precision of centering is also higher.

(3) Independent function carrier of torque transmission and shaft-hub centering. With the same function carrier, these two functions will interact and weaken each other. For example, in the side fitted involute spline shaft-hub connections, the wear of teeth flank will weaken the centering of shaft and hub, therefore leads to unequal distribution of load on every tooth, which in turn aggravate the wear of teeth flank, a cycle begins; as a contrast, in diameter centered straight spline shaft-hub connections, the teeth flank bear the load and the external/internal cylinder surface center the shaft and hub, the function carriers are weakly coupled.

(4) ‘Fail safe’ principle. Shaft and hub are always the most important elements in a machine, so the ‘fail safe’ principle should be also considered in the design of a shaft-hub connection profile. For example, when a crack appeared at the fillet of a involute spline teeth, it will leads to the fracture of this teeth at first but not the whole shaft, and this remind man to take remedy measurement before catastrophic failure of the machine. But in complex cycloid profiles especially the polygon shaft-hub connections, the cracks are more likely propagate into the basic body of the shaft when it occurred and leads to the fracture of the whole shaft quickly.

7 Conclusion

7.1 Summary

In some machine connections such as railway axles, spline shaft hub connections co-exist ‘wick fillet’ and dynamic ‘contact edge’, consequently co-exists potential danger of plain fatigue and fretting fatigue. Failure of the connection depends on the competition of plain fatigue at wick fillet and fretting fatigue at contact edge. Optimization of them should consider both of the two failure mechanism at the same time.

To provide a unified evaluation criterion of fretting fatigue and plain fatigue, a fretting/plain fatigue unified prediction model is suggested an implemented in involute spline shaft-hub connection teeth in this study. It inherited the successful characteristic of existing pure fretting fatigue prediction FFDP/exFFDP models and pure plain fatigue prediction SWT/FS models, integrated the tensile mode crack dominated and shear mode crack dominated fretting/plain fatigue mechanism. Considering different microscopic crack mechanism and choose corresponding macro prediction model will improve the accuracy of fretting/plain fatigue prediction, the newly developed fretting/plain fatigue unified prediction parameter K_{FDP}SWT and K_{FDP}FS will be applied to the tensile mode crack dominated and shear mode crack dominated fretting/plain fatigue respectively. This model is based on the assumption that the tensile stress under contact surface is more benefit to initiate a fretting fatigue crack, so a design suggestion of fretting fatigue alleviate is to avoid that the contact edge located on the surface with tensile stress. Outside of the contact interface, above parameters will degenerate to the pure plain fatigue prediction parameter SWT and FS. Take advantage of the critical plane SWT and FS parameter, this model have also the ability of crack orientation prediction and fretting/plain fatigue life prediction. The failure of involute spline teeth predicted by this model is plain fatigue at teeth fillet governed.

Based on the FE analysis of spline shaft-hub connection under different dynamic torque and the modeling efforts, this study developed a fretting/plain fatigue test apparatus of representative involute spline teeth pair. Combined with a resonant fatigue test machine or a standard fatigue test machine, the fretting/plain fatigue behavior of spline teeth can be investigated more deeply and microscopically. With this newly developed test apparatus and the resonant fatigue test machine, this study investigated the fretting/ plain fatigue performance of involute spline teeth. The experimental results of the representative DIN5480 involute spline shaft-hub connection teeth showed that the failure of it is plain fatigue crack at teeth fillet dominated, which is consistent with the location predicted by the newly suggested model. The crack growth orientation at teeth fillet agree with the direction predicted by the tensile mode SWT parameter. The crack initiation and propagation recorded by the resonant frequency is close to the fatigue life predicted by the averaged SWT or FS parameter within characteristic length 0.2mm.

Polygon shaft-hub connection profile (P3C and P4C) get rid of the ‘weak fillet’ stress singularity near contact edge, on the contrary to involute spline profile their failure is fretting fatigue governed. The common parameter equation of complex cycloid profile introduced by Ziaei, M. provides a theoretically possibility to find a new shaft-hub connection profile with better fretting fatigue and plain fatigue performance at the same time. The plain fatigue performance of these shaft-hub connection profile teeth are improved compared with the standard involute spline teeth due to the more strong teeth fillet and disappear of sharp contact edge, but the most seriously fretted location often overlap with the location of plain fatigue in some complex cycloid variants such as T00 complex cycloid profile, considering the effects of fretting, not all of them are superior to the standard involute spline shaft-hub connection profile. An special IMW complex cycloid profile parameter equation is introduced in this study, after this equation, the teeth number, major radius, minor radius and the middle radius can be make the same with involute spline shaft-hub connections in DIN5480, the pressure angle can be changed smoothly. Using the fretting/plain fatigue unified prediction parameter, the fretting/plain fatigue performance of the newly developed complex cycloid profiles are evaluated and optimized. Following this method, every involute spline shaft hub connection in DIN5480 standard can find a corresponding complex cycloid profile that with better fatigue performance. So, refer to the DIN5480 standard, the new IMW profile can be also standardized conveniently.

7.2 Future works

(1) Relative fretting damage factor KFDP of different material and surface condition

The relative fretting damage factor K_{FDP} used in this study is referred to the study of Oldendorf that based on the normalized Ck45 material. Fretting fatigue is a near-surface phenomenon that occurs over a very small area with dimension comparable to the microstructure length scale. Many researches have revealed that various surface modification processes like case hardening, nitriding and carbonitriding, etc. affect the fretting fatigue performance of the contact pair greatly, not to say different materials. So, more experimental investigations should be done to determine this relative fretting damage factor of different materials in different surface treatment conditions in order to improve the accuracy of fretting/plain fatigue prediction. The investigation can be carried out in a sample fretting pad + uniaxial loaded specimen experiment configuration, through this factor, the results of simple specimen investigation can be implemented to industry applications conveniently.

(2) Looking for a ‘perfect’ shaft-hub connection profile

Improve the load capacity of shaft-hub connection is a ‘never ending story’. Currently used shaft-hub connection profiles still cannot fulfill all the requirement of a ‘perfect’ shaft-hub connection profile. Bearing in mind that the two main functions of a spline shaft-hub connection are torque transmission and shaft-hub centering, the complex cycloid profile provided us numerous shaft-hub connection profile candidates. Continuing the study of IMW profile, find a perfect one and get standardized is our future works.

Bibliography

[Ang-06] Angelika Brückner-Foit, Xinyue Huang, Numerical simulation of micro-crack initiation of martensitic steel under fatigue loading. International Journal of Fatigue, 2006(28): p. 963–971.

[ANS-10] ANSYS.Inc. ANSYS Mechanical APDL and Mechanical Applications Theory Reference, 2010.

[Ara-02] Araùjo, J.A.; Nowell, D.: The effect of rapidly varying contact stress fields on fretting fatigue. International Journal of Fatigue, 24(2002): 763-775

[Ara-04] Araùjo, J.A.; Nowell, D.; Vivacqua, R.C.: The use of multiaxial fatigue models to predict fretting fatigue life of components subjected to different contact stress fields. Fatigue & Fracture of Engineering Materials & Structures, 2004, 27(3): p. 967–978.

[Bäu-90] Baumel, A. Jr.; Seeger, T.: Materials data for cyclic loading, Supplement 1. Elsevier, Amsterdam,1990.

[Bla-91] Blanchard, P.; Colombie, C. V.; Pellerin, Fayeulle, S. et al. Material effects in fretting wear: application to iron, titanium, and aluminum alloys. Metallugical and materials transactions A,1991. 22(7):1535-1544.

[Bre-02] Brett P.Conner, Contact Fatigue: Life Prediction and Palliatives, PhD thesis, in Department of Materials Science and Engineering. 2002, Massachusetts institute of technology: Cambridge, 2002

[Can-08] Canale, L.C.F.; Mesquita, R.A.; Totten, G.E.: Failure Analysis of Heat Treated Steel Components. USA: ASM International, 2008.

[Cas-99] Casper, T.: Reibkorrosionsverhalten von Spannelementverbindungen. Dissertation RWTH Aachen, 1999.

[Che-94] Cheng, W.; Cheng, H.S. and Mura, T. et al.: Micromechanics Modeling of Crack Initiation Under Contact Fatigue. Journal of Tribology, 1994, 116(1): p. 2-8.

[Cia-01] Ciavarella M., Demelio G.: A review of analytical aspects of fretting fatigue, with extension to damage parameters, and application to dovetail joints. International Journal of Solids and Structures, 2001 (38): p. 1791-1811.

[DEA-09] DEAN HOUGHTON.:REPRESENTATIVE FRETTING FATIGUE TESTING AND PREDICTION FOR SPLINED COUPLINGS. PhD thesis, The University of Nottingham, 2009.

[Der-06] Derflinger, V.H.; Schütze, A.; Ante, M.: Mechanical and structural properties of various alloyed TiAlN-based hard coatings. Surface&Coating Technology, 200(2006):4693-4700.

[Die-78] Dietz, P.: Die Berechnung von Zahn-und keilwellen-Verbindungen. Büttelborn, Juli 1978, Selbstverlag des Verfassers.

[Die-93] Dietz, P.; Schäfer,G.; Wesolowski, K.: Zahnwellenverbindungen - Beanspruchungs- und Verschleißverhalten. Konstruktion 45 (1993) S.227-234.

[DIN 5466] Tragfähigkeitsberechnung von Zahn-und Keilwellen-Verbindungen

[Din-07] Ding, J.; Sum, W.S.; Sabesan, R.; et al.: Fretting fatigue predictions in a complex coupling. International Journal of Fatigue 2007(29): p. 1229–1244.

[Ekb-04] Ekberg, A.: Fretting fatigue of railway axles-a review of predictive methods and an outline of a finite element model. Proceedings of the Institution of Mechanical Engineers, Part F: Journal of Rail and Rapid Transit, 2004. 218(4): p. 299-316.

[Fan-92] Fan, H.; Keer, L. M. and Mura, T.: Near Surface Crack Initiation Under Contact Fatigue. Tribology Transactions, 1992, 35(1): p.121-127.

[Fat-88] FATEMI, A.; KURATH, P.: MULTIAXIAL FATIGUE LIFE PREDICTIONS UNDER THE INFLUENCE OF MEAN-STRESSES. JOURNAL OF ENGINEERING MATERIALS AND TECHNOLOGY-TRANSACTIONS OF THE ASME, 1988, 110(4): 380-388.

[Fel-97] Fellows, L.J., Nowell, D. and Hills, D.A.: On the initiation of fretting fatigue cracks. Wear, 20(1997): 120-129.

[Fou-04] Fouvry, S.; Duo, P.; Perruchaut, P.: A quantitative approach of Ti–6Al–4V fretting damage: friction wear and crack nucleation, Wear 257 (2004)916–929.

[Fou-09] Fouvry, S.; Kubiak, K.: Introduction of a fretting-fatigue mapping concept: Development of a dual crack nucleation – crack propagation approach to formalize fretting-fatigue damage. International Journal of Fatigue, 2009(31): p. 250–262.

[Fre-11] Freymann, R.: Strukturdynamik-Ein anwendungsorientiertes Lehrbuch. Springer, 2011.

[FVA-08] Daryusi, A.; Lau, P.: Profilwellen-Kerbwirkung: Ermittlung der Kerbwirkung bei Profilwellen für die praktische Getriebeberechnung von Zahnwellen. FVAForschungsheft Nr. 467, Frankfurt/Main 2008. (in German)

[Gal-06] Gallego, L., D. Nelias, and C. Jacq, A Comprehensive Method to Predict Wear and to Define the Optimum Geometry of Fretting Surfaces. Journal of Tribology, 2006. 128(3): p. 476-485.

[Gau-80] Gaul, D.J.; Duquette, D.J.: The effect of fretting and environment on fatigue crack initiation and early propagation in a quenched and tempered 4130 steel. Metallurgical transactions A. 1980, 11A (9):1555-1561.

[Glö-03] Glöggler, C.: Untersuchungen an spannungshomogenisierten und zylindrischen Pressverbindungen unter Torsionsbelastung. Dissertation, Universität Stuttgart, 2003. (in German)

[Goh-01] Goh C. -H., Wallace J. M., Neu R. W. and McDowell D. L. Polycrystal plasticity simulations of fretting fatigue. International Journal of Fatigue, 2001. 23(Supplement 1): p. 423-435.

[Gro-07] Großmann, C.: Fretting Fatigue of Shape Optimised Polygon-Shaft-Hub Connections. Doctor dissertation, Berlin University of Technology, 2007.

[He-89] He, M.J.; Ruiz, C.: Fatigue Life of Dovetail Joints: Verification of a Simple Biaxial Model. Experimental Mechanics,1989(6). p. 126–131.

[Hil-94] Hills, D.A.; Novell, D.: Mechanics of fretting fatigue. Netherlands: Kluwer Academic Publishers, 1994.

[Hil-02] Hills, D.A.; Mugadu, A.: An overview of progress in the study of fretting fatigue. JOURNAL OF STRAIN ANALYSIS, 2002, 37 (6): 591-601.

[Hil-06] Hills, D.; Novell, D.A.: Recent developments in the understanding of fretting fatigue. Engineering Fracture Mechanics. 2006, 73(2): 207-222.

[Hou-09] Houghton, D.; Wavish, P.M.; Williams, E.J.; et al.: Multiaxial fretting fatigue testing and prediction for splined couplings. International Journal of Fatigue, 2009. 31(11-12): p. 1805-1815.

[Hua-07] Hua, Q.: Überlegungen zum Lebensdauerverhalten von Zahnwellenverbindungen nach den Theorien des Reib-und des Ermüdungsverschleißes. Dissertation TU Clausthal, 2007.

[Hug-03] Hug, J. ; Runzer , V.: Prüftechnische Innovationen-Grundlage für Erfindungen in der Bauteilentwicklung. Mat.-wiss. u. Werkstofftech. 2003, 34(9): 878-882.

[Hut-05] Hutson, A.L.;Stubbs, D.: A Fretting Fatigue Crack Detection Feasibility Study Using Shear Wave Non-destructive Inspection. Experimental Mechanics, 2005.45(2):160-166.

[HYD-05] HYDE T.R., LEEN S. B.; MCCOLL, I. R. A simplified fretting test methodology for complex shaft couplings. Fatigue & Fracture of Engineering Materials & Structures, 2005. 28 (11): 1047-1067.

[Jac-07] Jacob, M.S.D.; et al., Fretting fatigue crack initiation: An experimental and theoretical study. International Journal of Fatigue, 2007, 29(7): p. 1328-1338.

[JEZ-10] N. JEZERNIK, J. Kramberger, T. LASSEN and S. GLODEˇZ. Numerical modelling of fatigue crack initiation and growth of martensitic steels. Fatigue & Fracture of Engineering Materials & Structures. 2010(00): p. 1-10.

[Jin-04] Jin, O. and Mall, S. Effects of slip on fretting behavior: experiments and analyses. Wear, 2004. 256(7-8): p. 671-684.

[Juu-01] Juuma, T.: Fretting fatigue of a shrink-fitted shaft. Doctor dissertation, University of Oulu, 2001. (in Finland)

[Klu-08] Klubberg, F.; Klopfer, I.; Berchtold, R.; et.al.: Fatigue testing of materials and components under dynamic load with superimposed static load. XXXVII CONVEGNO NAZIONALE, 10-13 SETTEMBRE 2008, UNIVERSITÀ DI ROMA “LA SAPIENZA”.

[Kon-04] KONDO, Y.; SAKAE, C.; KUBOTA, M.; et al.: Fretting fatigue limit as a short crack problem at the edge of contact. Fatigue & Fracture of Engineering Material & Structure, 2004, 27(5): 361-368.

[Lam-97] Lamacq, V.; Dubourg, M.C.; Vincent, L.: A thoeretical model for the prediction of initial growth angles and sites of fretting fatigue cracks. Tribology International, 1997, 30(6): p. 391-400.

[Lau-01] Laurent Chambon. A unified fracture mechanics approach to fretting fatigue crack growth, in Department of Aeronautics and Astronautics, Master Thesis, Massachusetts institute of technology: Cambridge, 2001.

[Lee-05a] Lee, Y.L.; Pan, J.; Barkey, M.E.: Fatigue testing and analysis (Theory and practice). Elsevier Butterworth-Heinemann, 2005.

[Lee-05b] Lee, D.H.; Goo, B.C.; Lee, C.W.; et al.: Fatigue life evaluation of press-fitted specimens by using multiaxial fatigue theory at contact edge. Key Engineering Materials, 297-300 (2005), 108-114.

[Lei-07] Leidich, E.; Vidner; J.: On the fatigue failure prediction on dynamically loaded shaft-hub connections using the critical plane approach. ATK 2007 (P.W. Gold ed.), Verlagsgruppe Mainz, Aachen 2007, 225-256. (in German)

[Lei-09] Leidich, E.; Vidner, J.; Brůžek, B.: Integral Approach for Endurance Limit Evaluation on Shrink-Fitted Assemblies. BULLETIN OF APPLIED MECHANICS, 2009. 5(18): p. 44-49.

[Lin-97] Lindley, T.C.: Fretting fatigue in engineering alloys. International Journal of Fatigue, 1997. 19(1): p. 39-49.

[Lyk-00] Lykins, C.D.; Mall, S. and Jain, V.K.: An evaluation of parameters for predicting fretting fatigue crack initiation. International Journal of Fatigue, 2000. 22(8): p. 703-716.

[Lyk-01] Lykins, C. D.; Mall, S. and Jain, V.K.: A shear stress-based parameter for fretting fatigue crack initiation. Fatigue & Fracture of Engineering Materials & Structures, 2001. 24: p. 461–473.

[Lyk-01a] Lykins, C.D.; Mall, S. and Jain, V.K.: Combined experimental-numerical investigation of fretting fatigue crack initiation. International Journal of Fatigue. 2001. 23(8): p. 703-711.

[Lyk-01b] Lykins, C. D.; MALL, S.; JAIN, V.: A shear stress-based parameter for fretting fatigue crack initiation. Fatigue & Fracture of Engineering Materials & Structures, 2001. 24: p. 461–473.

[Mal-04] Mall, S.; Namjoshi, S.A.; Porter, W.J.: Effects of microstructure on fretting fatigue crack initiation behavior of Ti-6Al-4V. Materials Science and Engineering, A 383(2004):334–340.

[Mai-08] Maiwald, A.: Numerische Untersuchungen von unrunden Profilkonturen für Welle-Nabe-Verbindungen. Masterarbeit, Westsächsischen Hochschule Zwickau, Chemnitz, 2008.

[Mur-94] Mura, T.: A theory of fatigue crack initiation. Materials Science and Engineering: A, 1994. 176(1-2): p. 61-70.

[Mad-07] Madge, J. J.; Leen, S.B.; McColl, I. R.; et al.: Contact-evolution based prediction of fretting fatigue life: Effect of slip amplitude. Wear, 2007. 262(9-10): p. 1159-1170.

[Mad-07a] Madge, J. J.; Leen, S.B.; McColl, I. R.; et al.: Contact-evolution based prediction of fretting fatigue life: Effect of slip amplitude. Wear, 2007. 262(9-10): p. 1159-1170.

[Mad-07b] Madge, J. J.; Leen, S.B.; McColl, I. R. et al Contact-evolution based prediction of fretting fatigue life: Effect of slip amplitude. Wear, 2007. 262(9-10): p. 1159-1170.

[Mad-08a] Madge, J.J.; Leen, S.B.; and Shipway, P.H.: A combined wear and crack nucleation-propagation methodology for fretting fatigue prediction. International Journal of Fatigue, 2008. 30(9): p. 1509-1528.

[Mad-08b] Madge, J.J.:Numerical modeling of the effect of fretting wear on fretting fatigue. PhD Thesis, University of Nottingham, 2008.

[Med-02] Medina, S. and Olver, A.V.: Regimes of Contact in Spline Couplings. Journal of Tribology, 2002. 124, 351-357.

[Mih-09] Mihaela Buciumeanu: Prediction of fretting fatigue life. PhD thesis, Minho University, 2002.

[Nam-02] Namjoshi, S. A.; Mall, S.; Jain, V. K.; et. al. Fretting fatigue crack initiation mechanism in Ti–6Al–4V. Fatigue & Fracture of Engineering Materials & Structures, 2002, 25(10): p. 955-964.

[Neu-00] Neu, R.W., Pape,J.A., and Swalla, D.R., “Methodologies for Linking Nucleation and Propagation Approaches for Predicting Life Under Fretting Fatigue,” Fretting Fatigue: Current Technology and Practices, ASTM STP 1367, D.W. Hoeppner, V.Chandrasekaran, and C.B. Elliott, Eds., American Society for Testing and Materials, West Conshohocken, PA,2000.

[Neu-05] Neuner, F.C. Untersuchung von mikrostrukturellen Einflussgrößen auf das Reibermüdungs-verhalten und auf die Schädigungsmechanismen von

Eisenbasislegierungen, in Technischen Fakultät. 2005, Universität Erlangen-Nürnberg: Erlangen. p.186.

[Nic-06] Nicholas, T.: High Cycle Fatigue-A Mechanics of Materials Perspective. 2006, Great Britain: Elsevier.

[Old-99] Oldendorf, U. Lastübertragungsmechanismen und Dauerhaltbarkeit von Passfeder-Verbindungen. Dissertation, TU Darmstadt, Shaker Verlag, Aachen1999.(in German)

[Old-01] Oldendorf, U.: Lebensdauerberechnung von Paßfederverbindungen. FVA-Forschungsabschlußbricht Nr.217/II , Darmstadt, 2001. (in German)

[Pet-09] Petukhov, A. N. Fretting Corrosion and Fretting Fatigue in Slow-Moving Joints of Gas-Turbine Engines and Power Units. Russian Engineering Research, 2009. 29(6): 579-582.

[Pöt-04] Pöting, S.;Traupe,M.;Hug,J.; et. al.:Variable Amplitude Loading on a Resonance Test Facility. Journal of ASTM International. 2004, 1(10):67-80.

[Pro-05] Proudhon, H.; Fouvry, S.; Buffière, J.Y.: A fretting crack initiation prediction taking into account the surface roughness and the crack nucleation process volume. International Journal of Fatigue, 2005, 27(5): p. 569-579.

[Rat-04] Ratsimba, C.H.H.; McColl, I.R.; Williams, E.J.; et al.: Measurement, analysis and prediction of fretting wear damage in a representative aeroengine spline coupling. Wear 2004(257), 1193–1206.

[Rui-84] Ruiz, C.; Boddington, P.H.B.; Chen, K.C.: An Investigation of Fatigue and Fretting in a Dovetail Joint. Experimental Mechanics, 1984(9). p. 208-217.

[Rus-84] Russenberger, Max E.: Über das Frequenz verhalten von Resonanzprüfmaschinen. Fortschrittberichte der VDI Zeitschriften, 1984.

[Sad-06] Sadeler, R. and Sengul A.B. Influence of induction hardening on fretting fatigue behaviour of AISI 1045 steel under two different contact pressures. Kovove Materialy-Metallic Materials, 2006. 44(4): p. 235-241.

[Sae-08] Saether, E., A Multiscale Method for Simulating Fracture in Polycrystalline Metals, in Virginia Polytechnic Institute and State University. 2008, Virginia Polytechnic Institute and State University: Blacksburg, Virginia. p. 213.

[Sch-95] Schäfer, G.: Der Einfluß von Oberflächenbehandlungen auf das Verschleißverhalten flankenzentrierter Zahnwellenverbindungen mit Schiebesitz, Dissertation, Technischen Universität Clausthal: Clausthal, 1995.

[Sch-09] Schijve, J.: Fatigue of Structures and Materials. 2009, Delft: Springer.

[Sha-09] Shamsaei, N. and Fatemi, A.: Effect of hardness on multiaxial fatigue behaviour and some simple approximations for steels. Fatigue & Fracture of Engineering Materials & Structures, 2009, 32(6): p. 631–646.

[Smi-70] Smith, K.N.; Watson,P. and Topper, TH.: A stress-strain function for the fatigue of metals. J.Mater. JMLSA 5, 1970: 767-778.

[Soc-87] Socie, D.: Multiaxial Fatigue Damage Models. Journal of Engineering Materials and Technology-Transactions of ASME, 1987, 109(4): 293-299.

[Ste-01] Stephens, R.I.; Fatemi, A.; Stephens, R.R.; Fuchs, H.O.: Metal fatigue in engineering (second edition). John Wiley &Sons, 2001.

[Sum-04] Sum, W.S.: FE-Based Multiaxial Fatigue Life Prediction of Spline Couplings Undergoing Fretting. PhD Thesis, University of Nottingham, 2004.

[Sum-05] Sum, W.S.; Williams, E.J. and Leen, S.B.: Finite element, critical-plane, fatigue life prediction of simple and complex contact configurations. International Journal of Fatigue, 2005. 27(4): p. 403-416.

[Tan-81] Tanaka, K. and Mura, T.: A Dislocation Model for Fatigue Crack Initiation Journal of Applied Mechanics, 1981. 48(1): p. 97-103.

[Val-07] Vallellano, C.; Dominguez, J.; Navarro, A.: Influence of R ratio and stick zone eccentricity on the prediction of the fretting fatigue limit with spherical contact. International Journal of Fatigue. 29(2007): 1208-1219.

[Vid-04] Vidner, J.; Leidich E.: Enhanced Ruiz criterion for the evaluation of crack initiation in contact subjected to fretting fatigue. International Journal of Fatigue 2007(29): p. 2040–2049.

[Vin-88] Vingsbo, O.; Soderberg, S.: On fretting wears. Wear 126 (1988) 131–147.

[Wag-09] Wagle,S.;Kato, H.: Ultrasonic detection of fretting fatigue damage at bolt joints of aluminum alloy plates. International Journal of fatigue, 2009. 31(8-9):1379-1385.

[Wag-11] Wagle,S.; Kato, H.: Real-time Measurement of Ultrasonic Waves at Bolted Joints under Fatigue Testing. Experimental Mechanics. 2011, online.

[Wav-09] WAVISH, P. M.; Houghton, D.; DING, J.; et al.: WILLIAMS ,E. J.;I. R. McCOLL.: A multiaxial fretting fatigue test for spline coupling contact. Fatigue & Fracture of Engineering Materials & Structures, 2009(32): p. 325-345.

[Wes-96] Wesolowski, K.: Dreidimensionale Beanspruchungszustände und Festigkeitsnachweis drehmomentbelasteter Zahnwellen-Verbindungen unter elastischer und teilplastischer Verformung. Dissertation, TU Clausthal, 1996. (in German)

[Win-01] Winterfeld, J.:Einflüsse der Reibdauerbeanspruchung auf die Tragfähigkeit von P4C-Welle-Nabe-Verbindungen. Dissertation, TU Berlin, 2001. (in German)

[Wri-06] Wriggers, Peter.: Computational Contact Mechanics. Springer, 2006.

[Yan-01] Yang, B. and Mall, S.: On Crack Initiation Mechanisms in Fretting Fatigue. Journal of Applied Mechanics, 2001, 68(1): p. 76-80.

[Yin-09] Yin, F. and Fatemi, A.: Fatigue behaviour and life predictions of case-hardened steels. Fatigue & Fracture of Engineering Materials & Structures, 2009, 32(1): p. 197–213.

[Zia-97] Ziaei, M.: Untersuchung der Spannungen und Verschiebungen in P4C-Welle-Nabe-Verbindungen mittels der Methode der Finiten Elemente. Dissertation, TH Darmstadt, 1997. (in German)

[Zia-02] Ziaei, M.: Analytische Untersuchungen unrunder Profilfamilien und numerische Optimierung genormter Profile für Welle-Nabe-Verbindungen. Professorial dissertation, Technical University Chemnitz, 2002. (in German)

[Zia-07] Ziaei, M.: Anpassungsfähige kontinuierliche Innen-und Außen-konturen form- und Reibschlüssige Verbindungen auf Basis der komplexen Zykloiden. 4.VDI-Fachtagung Welle-Nabe-Verbindungen 2007, VDI-Berichte 2004: 277-294.

[Zha-09] Zhang M., Neu R.W., and McDowell D.L. Microstructure-sensitive modeling: Application to fretting contacts. International Journal of Fatigue, 31(2009): p. 1397-1406.

Appendix A: Details of different fretting fatigue prediction models

Table1. Details of different fretting fatigue prediction models

Main researchers- Organization- Year	Model	Advantages and Disadvantages	Applications and Verification	Remarks
Ruiz, C. Oxford University, UK. 1984 [Rui-84, He-89]	FFDP: $FFDP = \sigma_{\tan} \cdot \tau_{fric} \cdot s$ $\sigma_{\tan}$ - maximal tangential stress τ_{fric} - contact shear stress s - slip	①one-dimensional ②can predict failure location, but not life	Dovetail joints Material:?	Frictional energy based
Oldendorf, U. TU Darmstadt, Germany 1999 [Old-99, Old-01]	exFFDP(Erweiterung des Ruiz-Chen-Kennwerts) $ErFFDP = \beta_{KC} \cdot \sigma_1$ $\beta_{KC} = \hat{\beta}_K \cdot S(\delta) \cdot S\left(\bar{P}\right) + 1$	①The experiments based empirical equation $S(\delta)$ and $S\left(\bar{P}\right)$ help to understand the threshold between fretting wear and	key–shaft–hub connection	Frictional energy based

	$\begin{cases} S(\delta)=-\frac{2}{3}\cdot e^{-0.0277\cdot\delta}\cdot\cos\left(\frac{2\pi}{50}\cdot\delta\right)+\frac{2}{3} & 0\le\delta\le 50 \\ S(\delta)=\frac{1}{2}+\frac{3}{1000}\cdot(\delta-50) & \delta>50 \end{cases}$ $\begin{cases} S\left(\bar{p}\right)=\frac{2}{10}\cdot\ln\left(\bar{p}\right) & 1\le\bar{p}\le 150 \\ S\left(\bar{p}\right)=1 & \bar{p}>150 \end{cases}$ β_{KC} - stress concentration factor of friction stress; $\hat{\beta}_K$ - maximal damage value; δ - relative slip amplitude between two contacting surfaces; $\bar{P}$ - contact pressure.	fatigue. ② $\hat{\beta}_K$ needs experimental tests, and remain unclear		
Ziaei. M. Chemnitz University of Technology, Germany. 1997 [Zia-97, Zia-02]	Modified FFDP (mFFDP): $mFFDP=W^*_{fric}\cdot\sigma_1$ σ_1 - maximal principal stress $W^*_{fric}=\int\tau_{fric}ds$ If: constant surface pressure and a straight-line slipping trajectory, then: $W^*_{fric}=2\cdot S_a\cdot\tau_{fric}$	①can predict shaft failure location, but not life ②Not valid for every type of connection, e.g. key–shaft–hub connections subjected to combined torque and bend loading.	polygon and press –fitted shaft-hub connection Material: C45	Frictional energy based

	S_a-slip amplitude			
Vidner, J. Chemnitz University of Technology, Germany. 2006 [Vid-04]	Enhanced FFDP（enFFDP）: $eFFDP = P^*_{fric} \cdot SWT$, $eFFDP = P^*_{fric} \cdot FS$ $P^*_{fric} = f_{LC} \int_{T_{LC}} \tau_{fric}(t) \cdot \dot{s} \cdot dt$ f_{LC} -load cycle frequency $SWT = \sigma_{n,\max} \cdot \varepsilon_{1,a}$ $\sigma_{n,\max}$ - maximum normal stress, $\varepsilon_{1,a}$ -maximum principal strain amplitude on the maximum principal strain amplitude plane. $FS = \gamma_{a,\max} \cdot \left(1 + k_{FS} \cdot \frac{\sigma_{n,\max}}{s_y}\right)$ k_{FS} -material constant. $\gamma_{a,\max}$ - maximum shear strain, $\sigma_{n,\max}$ - maximum normal stress, on the Maximum shear strain amplitude plane	①It remains unclear if it works in other shaft-hub connections such as spline coupling	correctly predicts both cracking sites observed on the key groove and edge of the shaft key–shaft–hub connection under combined torque and bend loading Material: C45	Frictional energy based
Lykins, C.D. Air Force Research Laboratory, Wright Patterson Air	Critical plane approach incorporating SWT criterion： $SWT = \sigma_{\max} \frac{\Delta\varepsilon}{2} = \frac{\left(\sigma_f^{'}\right)^2}{E}\left(2N_{ft}\right)^{2b} + \sigma_f^{'}\varepsilon_f^{'}\left(2N_{ft}\right)^{b+c}$	①Have shortcomings with respect to prediction of failure location. ②The value of life was gen-	①Cylinder-on-flat fretting contact Material: Ti6Al4V	Critical-plane fatigue based

Force Base, USA, 2000 [Lyk-00, Lyk-01, Sum-04, Sum-05]	$\sigma_{\max}$ - maximum normal stress $\Delta\varepsilon$ - normal strain range $\sigma_f^{'}$, b- fatigue strength coefficient and exponent $\varepsilon_f^{'}$, c- fatigue ductility coefficient and exponent	erally over-estimated.	②Aero-engine spline coupling Material: CrMoV alloy steel	
Ding, J. University of Nottingham, UK 2005 [Din-07]	Modified SWT (mSWT)： $\sigma_{n,\max}\cdot\varepsilon_{1,a}\cdot D_{fret}=\frac{\left(\sigma_f^{'}\right)^2}{E}\left(2N_f\right)^{2b}+\sigma_f^{'}\tau_f^{'}\left(2N_f\right)^{b+c}$ $D_{fret}=(1+\tau\delta)^m\left\langle 1-\frac{\tau\delta}{\left(\tau\delta\right)_{th}}\right\rangle^n$ $\sigma_{n,\max}$ - maximum normal stress $\varepsilon_{1,a}$ -maximum principal strain amplitude $\sigma_f^{'}$, b- fatigue strength coefficient and exponent $\varepsilon_f^{'}$, c- fatigue ductility coefficient and exponent τ - contact surface shear stress δ - relative slip amplitude between two contacting surfaces	①Does not include the effect of slip or wear on stresses and, therefore, the variation of $\sigma_{n,\max}\cdot\Delta\varepsilon_a$ with evolving contact geometry. ②Crack location in the axial direction, are not accurately predicted	aero-engine spline coupling Material: CrMoV alloy steel	Critical-plane fatigue based

	$m,n,(\tau\delta)_{th}$ -material constants to be determined experimentally			
Madge, J.J.; University of Nottingham, UK. 2007 [Mad-07]	Wear evoluation-SWT model : a. ABAQUS FEA of one fretting cycle, calculate σ , ε , contact pressure p(x) and slip $\delta(x)$ distributions; b. Calculate nodal wear depth $\Delta h(x)$ at each node and update FE mesh geometry $\Delta h(x)=K\cdot p(x)\cdot\delta(x)$ c. Calculate SWT parameter and cyclic damage for each element $SWT=\sigma_{\max}\frac{\Delta\varepsilon}{2}=\frac{(\sigma_f^{'})^2}{E}(2N_{ft})^{2b}+\sigma_f^{'}\varepsilon_f^{'}(2N_{ft})^{b+c}$ d. Accumulate damage in each element $W=\sum_{i=1}^{N_T}\frac{1}{N_{ft}}$ e. If accumulated damage in any element exceeded 100%, then component failed, or return to a step.	① Computationally intensive; ② Only applicable for simple configuration; ③ Gives better correlation with the test data for the higher slip amplitudes (gross slip)	Compared with the test data reported by Jin and Mall[10], Cylindrical (radius 50.8 mm) fretting pads are held in contact with a flat, uniaxially -loaded fatigue specimen (depth 3.8 mm). Material: Ti6Al4V	Critical-plane fatigue combined with Fracture mechanic
Madge, J.J. University of Nottingham, UK. 2008 [Mad-08]	Wear–nucleation–propagation model a. Wear model $\Delta h(x)=K\cdot\Delta N\cdot p(x)\cdot\delta(x)$ b. Critical plane fatigue model $SWT=\sigma_{\max}\frac{\Delta\varepsilon}{2}=\frac{(\sigma_f^{'})^2}{E}(2N_{ft})^{2b}+\sigma_f^{'}\varepsilon_f^{'}(2N_{ft})^{b+c}$	① Computationally intensive and complicate; ② Only applicable for simple configuration; □Gives better correlation with the test data for the	Cylindrical (radius 50.8 mm) fretting pads are held in contact with a flat, uniaxially -loaded fatigue specimen (depth 3.8	Critical-plane fatigue based combined with Fracture mechanic

	$W=\sum_{i=1}^{\frac{N_i}{\Delta N}}\frac{\Delta N}{N_{ft}}$ c. Fracture mechanics analysis	lower slip amplitudes (partial slip);	mm). Material: Ti6Al4V	
Houghton, D. University of Nottingham, UK. 2009 [Hou-09]	Multiaxial nucleation-propagation model: a. Identify the location and orientation of crack nucleation with the peak SWT magnitude and specify initial crack length, in this case, as the grain size. b. Assume nucleated crack is perpendicular to surface ; c. Determine modes I and II weight functions from $h_{\mathrm{I}}=\sqrt{\frac{2}{\pi a}}\frac{1}{\sqrt{1-\rho}}\left[1+\sum_{(\nu,\mu)}\frac{A_{\nu\mu}\alpha^{\mu}}{(1-\alpha)^{3/2}}(1-\rho)^{\nu+1}\right]$ and $h_{\mathrm{II}}=\sqrt{\frac{2}{\pi a}}\frac{1}{\sqrt{1-\rho}(1-\alpha)^{1/2}}\left[(1-\alpha)^{1/2}+\sum_{(\nu,\mu)}A_{\nu\mu}(1-\rho)^{\nu+1}\alpha^{\mu}\right]$ respectively. Identify local stress ranges ($\Delta\sigma_{zz}$ and $\Delta\sigma_{yz}$) via interpolation from detailed (sub-model) predicted distributions, and determine ΔK_{I} and ΔK_{II} using Eq. $\Delta K_{\mathrm{I}}=\int_0^a\Delta\sigma_{zz}(x)h_{\mathrm{I}}(x,a)\,dx$, $\Delta K_{\mathrm{II}}=\int_0^a\Delta\sigma_{yz}(x)h_{\mathrm{II}}(x,a)\,dx$ or, for short cracks, using (a + a0) in place of a in above Eq. d. Determine $\Delta K_{eff}=\sqrt{\Delta K_{\mathrm{I},\mathrm{eff}}^{2}+\Delta K_{\mathrm{II},\mathrm{eff}}^{2}}$ e. Calculate increment in crack length for a given ΔN using Eq.	① Computationally intensive and complicate ② Only applicable for simple configuration;	Multi-axial representative specimen of aero - engine spline coupling Material: CrMoV alloy steel	Critical-plane fatigue based combined with Fracture mechanic

	$\Delta a = C\left(\Delta K_{eff} - \Delta K_{th}\right)^{n} \Delta N$ f. Calculate new crack position and repeat steps c–e until a > 0.85, at which point the accumulated number of cycles is taken to correspond to N_p (number of cycles of crack propagation in linear elastic fracture mechanics).			
Lykins, C. D. Air Force Research Laboratory, Wright Patterson Air Force Base, USA, 2001[Lyk-01b, Nam-02]	Modified Shear Stress Range (MSSR): $MSSR = A\Delta\tau_{crit}^{B} + C\sigma_{\max}^{D}$ A, B, C and D are constants obtained by curve fitting $\Delta\tau_{crit} = \tau_{\max}\left(1 - R_{\tau}\right)^{m}$ $\tau_{\max}$ - maximum shear stress on the critical plane, R_{τ} -shear stress ratio on the critical plane, m - fitting parameter $\sigma_{\max}$ - maximum normal stress on the critical plane defined by shear stress range	① Predict angle of crack orientation and crack location, ② represent fretting fatigue life but cannot predict fretting fatigue life directly	Different pad geometries Material:Ti-6Al-4V	Shear stress based

Appendix B: Standardization of IMW01 profile

m=0.5,z=10

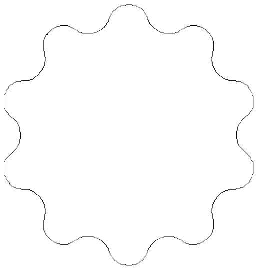

m=0.5,z=16

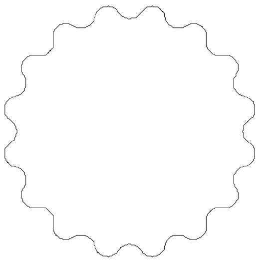

m=0.5,z=30

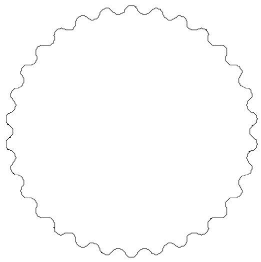

m=0.6,z=8

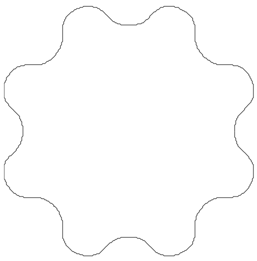

m=0.6,z=13

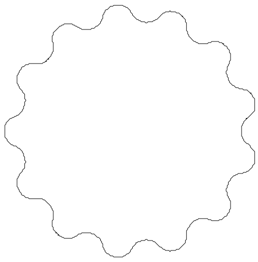

m=0.6,z=23

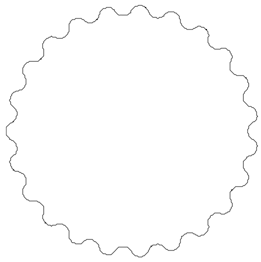

m=0.75,z=6

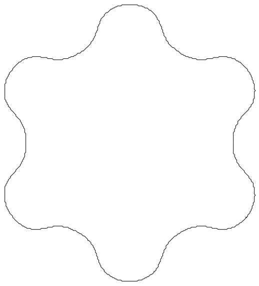

m=0.75,z=12

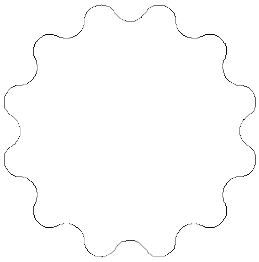

m=0.75,z=17

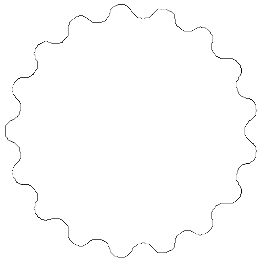

m=0.8,z=7

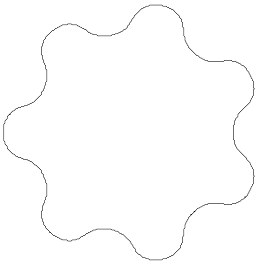

m=0.8,z=11

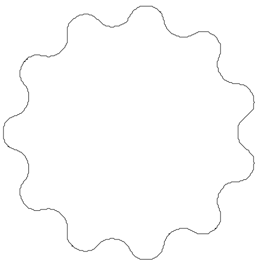

m=0.8,z=18

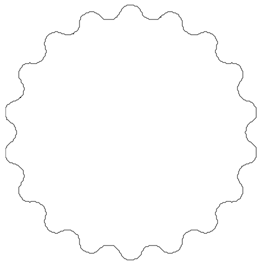

m=1,z=7

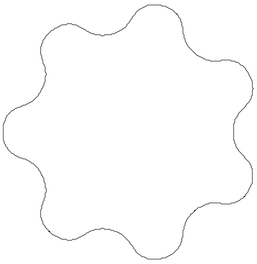

m=1,z=13

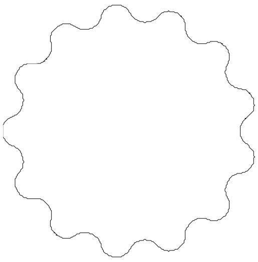

m=1,z=20

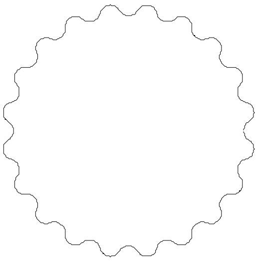

m=1.25,z=6

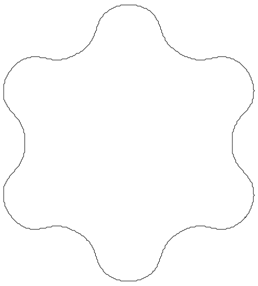

m=1.25,z=14

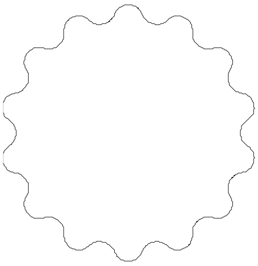

m=1.25,z=21

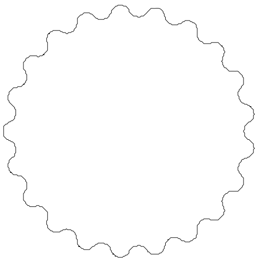

m=1.5,z=8

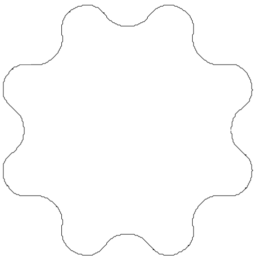

m=1.5,z=14

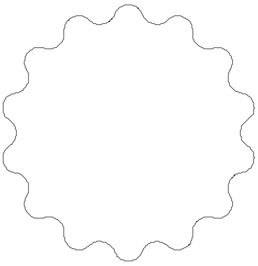

m=1.5,z=19

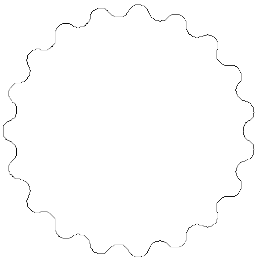

m=1.75,z=9

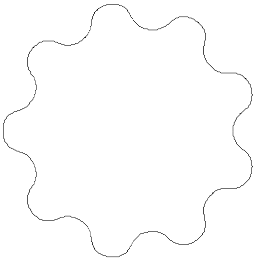

m=1.75,z=15

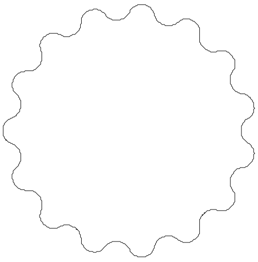

m=1.75,z=18

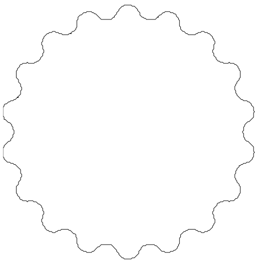

m=2,z=6

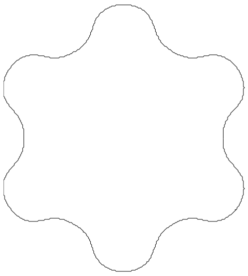

m=2,z=11

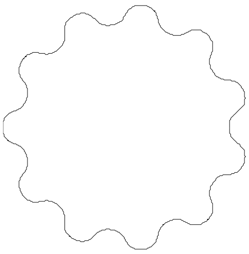

m=2,z=22

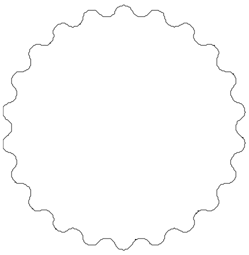

m=2.5,z=7

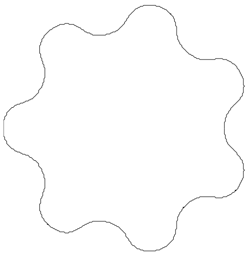

m=2.5,z=14

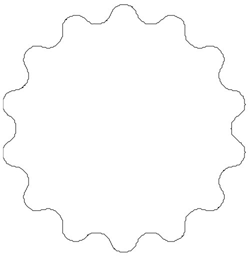

m=2.5,z=19

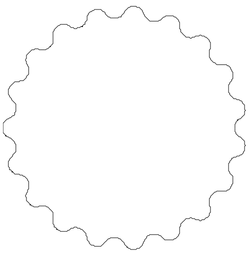

m=3,z=8

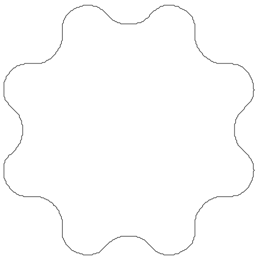

m=3,z=13

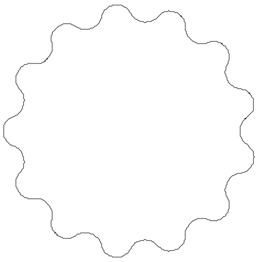

m=3,z=18

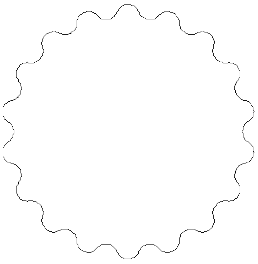

m=4,z=6

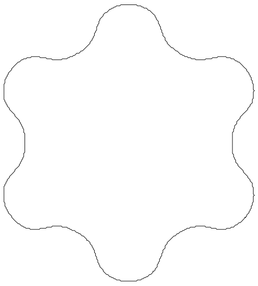

m=4,z=13

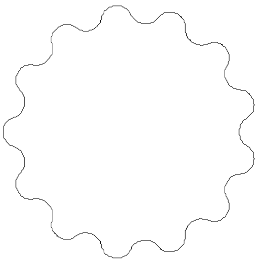

m=4,z=21

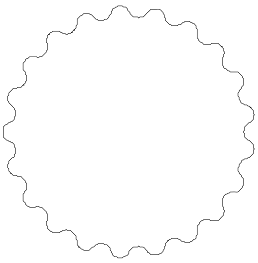

$m=5, z=9$

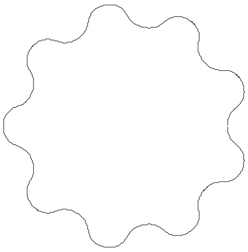

$m=5, z=15$

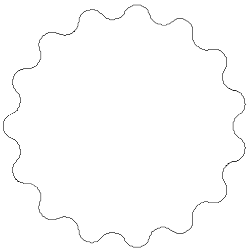

$m=5, z=24$

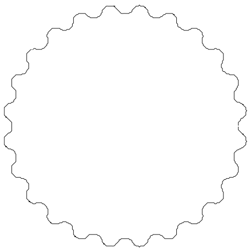

$m=6, z=7$

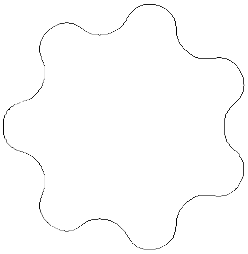

$m=6, z=14$

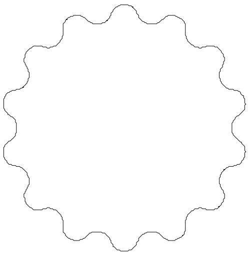

$m=6, z=25$

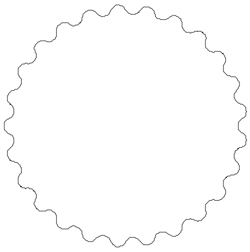

$m=8, z=11$

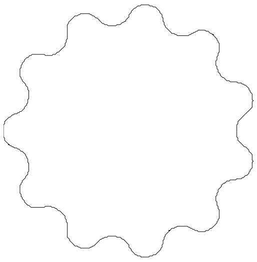

$m=8, z=17$

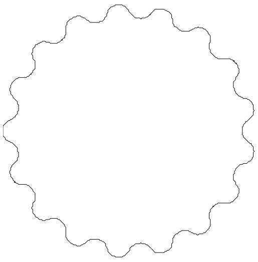

$m=8, z=26$

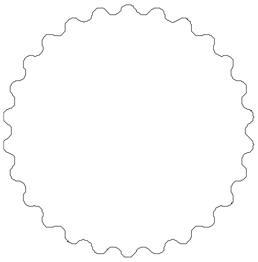

$m=10, z=8$

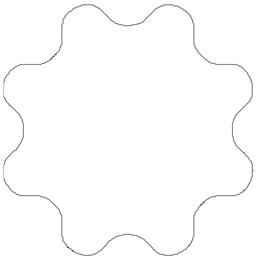

$m=10, z=15$

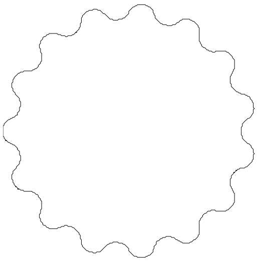

$m=10, z=32$

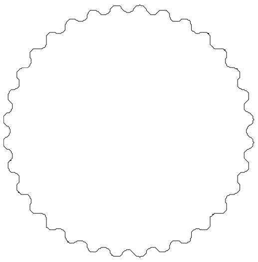

Curriculum Vitae

Personal information

Surname: Shen	Name: Longjiang
Date of birth: Sep.26th, 1979	Place of birth: Liuyang, Hunan Province, China

Education

Oct. 2008-Present	Institute of Mechanical Engineering, Clausthal University of Technology, Clausthal-Zellerfeld, Germany PhD Candidate
Sep.2007-Sep.2008	College of Mechanical and Electrical Engineering, Central South University, Changsha, China PhD Candidate
Sep.2004-Jun.2007	College of Mechanical and Electrical Engineering, Central South University, Changsha, China Master of Science in Mechanical Manufacture and Automation Thesis title: ‘‘Replication fidelity evaluation and processing parameter optimization of microlens array in injection molding’’
Sep.1998-Jun.2002	College of Mechanical and Electrical Engineering, East China Jiaotong University, Nanchang, China Bechelor of Science in Mechanical Manufacture and Automation Thesis title: ‘‘PLC control system design of automatic withdrawing machine for railway axle box bearing’’
Sep.1995-Jun.1998	The first high school of Liuyang, Liuyang, Hunan Province, China
Sep.1992-Jun.1995	Junior high school of Longfu, Longfu
Sep.1985-Jun.1992	Central elementary school of Longfu, Longfu

Job Experience

Aug.2002-Aug.2004	Bogie Business Department, CSR Zhuzhou Electric Locomotive Co., LTD. , China Manufacture engineer of railway wheelset